THE
PHYSICAL REVIEW
A Journal of Experimental and Theoretical Physics Established by E. L. Nichols in 1893

VOL. 50, NO. 8 OCTOBER 15, 1936 SECOND SERIES

The Primary Ionization of High Energy Electrons in Nitrogen and Neon

HAROLD K. SKRAMSTAD* AND DONALD H. LOUGHRIDGE, *University of Washington, Seattle, Washington*
(Received July 27, 1936)

A large expansion chamber in a magnetic field of about 400 gauss is used to study the tracks of high energy beta-rays produced by bombarding a lead screen inside the chamber by gamma-radiation from radon. Two photographs at right angles are taken, and the tracks examined by projection on to a screen in their original configuration. Measurements are made of the number of primary ions per cm of path produced in nitrogen and neon. The results in nitrogen can be expressed approximately by the relation:

$$I = 19\beta^{-1.15\pm 0.15},$$

and in neon by the relation:

$$I = 12.6\beta^{-1.35\pm 0.15},$$

where I is the primary ionization in ions per cm at normal temperature and pressure, and β is the velocity of the beta-ray in units of the velocity of light. Measurements on a few tracks in oxygen agree within experimental error with the results of Williams and Terroux. The primary ionization of the positive electrons observed is indistinguishable from the negative electrons. Comparisons are made with the theoretical calculations of Bethe, Moller, and Williams, and the agreement is satisfactory over the range of velocities used. The magnitude obtained for the primary ionization in nitrogen corresponds, on the basis of the formula obtained by hydrogen like wave functions, to an average ionization potential of 16.6 volts for the five outer electrons in the nitrogen atom, which is very near its minimum ionization potential. Theoretical calculations are made for neon, using ionization potentials for each electron calculated from critical absorption wave-lengths. The experimental results are somewhat greater than those calculated from the theory, but are as close as the somewhat arbitrary assumptions involved would allow one to expect. The variation of primary ionization with velocity checks well for values of less than 0.97, but the predicted increase for very high energies is not observed.

INTRODUCTION

VERY little experimental work has been done on measuring the primary ionization produced by high energy electrons. C. T. R. Wilson[1] in 1923, counted the number of primary ions in portions of nine different tracks, and found for fast beta-particles that the primary ionization varied from 18 to 22 ions per cm, with an average of about 20. No measurements were made on the velocities of the electrons, but they were estimated to be greater than 2×10^{10} cm per sec.

Williams and Terroux[2] in 1930, using an expansion chamber placed in a magnetic field of about 400 gauss, measured the primary ionization produced by the beta-rays from an old radium emanation tube in oxygen and hydrogen. The results of measurements of the primary ions on 108 tracks in hydrogen were shown to be expressible by the equation:

$$I = 5.2\beta^{-1.5\pm 0.2},$$

and the results on 72 tracks in oxygen by the equation:

$$I = 22\beta^{-1.1\pm 0.2},$$

* Now at National Bureau of Standards, Washington, D. C.

[1] C. T. R. Wilson, Proc. Roy. Soc. **A104**, 1, 192 (1923).

[2] E. J. Williams and F. R. Terroux, Proc. Roy. Soc. **A126**, 289 (1930).

where I is the number of primary ions per centimeter of path at normal temperature and pressure, and β is the velocity of the electron in units of the velocity of light.

From the standpoint of classical mechanics, the ionization of a molecule by an electron is regarded as a collision between two particles, the moving electron and one of those in the molecule, in which sufficient energy is given the latter to remove it entirely from the molecule. The classical theory was worked out by J. J. Thomson,[3] who obtained the following expression for the primary ionization:

$$I = 2\pi ne^4/mv^2J$$

where n is the number of electrons per unit volume, e and m the charge and mass of the electron, respectively, v the velocity of the incident electron, and J the ionization energy, or energy required to remove an electron from its atom. Williams and Terroux found that the observed primary ionization was five to six times as great as predicted by the theory, as well as showing a much smaller variation with velocity than the inverse square law.

The quantum theory has been applied to the problem by several authors. Gaunt[4] in 1927, applied the theory to distant collisions, in which case the incident particle moves essentially in a straight line. Its passage gives rise to a perturbing potential that varies in known manner with the time. His results are obtained by solving the Schrödinger equation for the atomic electron alone. The application of Gaunt's theory to primary ionization is discussed by Williams,[5] who shows that the theory gives results which are closer to the experimental facts than the classical theory, but still in considerable disagreement.

A more rigorous treatment of the problem has been made by Bethe[6] on the basis of Born's theory of collisions. As distinguished from Gaunt's theory, Bethe's treatment is statistical, not dealing with the individual electrons. He represents the atomic electrons by hydrogen-like wave functions, and assuming that the velocity of the moving electron is large compared with the Bohr orbit velocity of the atomic electrons, and is small compared with the velocity of light, finds a solution of Schrödinger's wave equation for particles in each other's field and the field of the nucleus. Bethe calculates the perturbation only as far as the first approximation, and obtains the following expression for the primary ionization of a hydrogen-like atom:

$$I = (0.285)(2ne^4/mv^2J)\log(42mv^2/J). \quad (1)$$

For the case of relativistic velocities of the moving electron, Moller[7] and Williams[8] obtain an expression which should hold for high energy electrons. The primary ionization is found to be given by:

$$I = (0.285)\frac{2\pi ne^4}{mv^2J}\left[\log\frac{42mv^2}{J} - \log\frac{1}{1-\beta^2} - \beta^2\right]^{9}. \quad (2)$$

The present work was undertaken to obtain more experimental data on the primary ionization of fast beta-particles so that comparisons could be made with the above theoretical equations.

Apparatus and Procedure

The experimental method used in the present work is briefly as follows: A large expansion chamber is placed in a magnetic field produced by two Helmholtz coils. High speed electrons produced by bombardment of a lead strip inside the chamber by gamma-radiation from radon, produce tracks which are bent into arcs of circles, and from measurements made on their radii of curvature, the energies of the electrons are computed. Two photographs are taken at right angles, and the tracks obtained are studied by replacing the film in projectors arranged so that the tracks are projected on a screen in their original size and configuration. Measurements of the primary ionization are made by counting the

[3] J. J. Thomson, Phil. Mag. **23**, 449 (1912).
[4] J. A. Gaunt, Proc. Camb. Phil. Soc. **23**, 732 (1927).
[5] E. J. Williams, Proc. Roy. Soc. **A130**, 328 (1931).
[6] H. Bethe, Ann. d. Physik **5**, 325 (1930); Zeits. f. Physik **76**, 293 (1932).
[7] C. Moller, Ann. d. Physik **14**, 531 (1932).
[8] E. J. Williams, Proc. Roy. Soc. **A135**, 108 (1932); **A139**, 163 (1933).
[9] Dr. Bethe has pointed out in conversation with one of the authors that this formula cannot be satisfactorily applied to atoms other than hydrogen, due partly to the way in which energy transferred from incident electron is divided between excitation and ionization, which varies for different atomic types. A new formula fitting each particular atom must be developed in order to experimentally check the theory.

number of ion groups per centimeter length of the images of the tracks on the screen.

The expansion chamber is ten inches in diameter, and of the diaphragm type, similar in many respects to that described by Locher.[10] The magnetic field is obtained by a pair of Helmholtz coils which surround the chamber, and produce a field of about 400 gauss, uniform to within 1.5 percent over the chamber. Arc lamps are used as a source of illumination, and the arc resistances are short-circuited at the time of expansion in order to provide sufficient illumination for photographing the very thin tracks produced by high energy electrons.

Two matched Leica cameras with $f:3.5$ lenses are used to obtain two photographs at right angles. In order to bring the entire chamber into focus, it was necessary to rebuild the cameras so as to tilt the lenses about 7° to the normal to the film, as described by Blackett.[11] Reconstruction of the tracks is accomplished by inserting the negative film in projectors arranged so that the optical system is an exact replica of that used in photographing the tracks. The general method is similar to that described by Blackett[11, 12] and others.[13, 14]

The gamma-radiation from radon tubes is used to produce the high energy electrons used in this work. A large trapezoidal-shaped block of lead 12 inches long, containing a $\frac{1}{4}$ inch hole through its center, is used to collimate the beam, and shields all parts of the chamber from the gamma-radiation by at least 10 inches of lead. The narrow beam of gamma-rays entering the chamber is filtered through about $1\frac{1}{4}$ inches of lead as well as the $\frac{3}{16}$ inch glass wall of the chamber, and strikes a lead strip placed inside the chamber, from which high energy electrons are emitted. The average energy of the tracks measured is about one million electron volts.

The direct counts of primary ions were reduced to normal temperature and pressure, and small corrections were applied to correct for the presence of water vapor in the chamber, and for the possibility of two primary ions being produced so close together as to be unresolvable.

This latter correction depends upon the size of the drops and their average distance apart, and involves more uncertainty than the other corrections applied. The average diameter of the drops determined by measurements on the film with comparator was found to be 0.4 mm. However, droplets may be resolved even when they overlap considerably, and it is assumed that the resolution of the droplets is actually limited by the resolving power of the eye, which is 0.1 mm. The correction was calculated on a pure probability basis. The probability that an electron will go at least a distance l before colliding with a molecule, denoted by $f(l)$, is given by[15]

$$f(l)=e^{-l/\lambda}$$

where λ is the "mean free path" of the electron. Letting I be the true number of ions per cm, and I_0 the observed member, we have

$$I_0=Ie^{-lI}$$

where λ has been put equal to $1/I$. The equation may be solved graphically for I as a function of I_0, using $l=0.1$ mm. The corrections are of the order of 10 percent to 15 percent in nitrogen and 7 percent to 10 percent in neon, depending on the energy of the incident electron.

The effect of the presence of water vapor in the chamber on the number of ions per cm measured was estimated from the known stopping power of water vapor and found to make an error of the order of 0.3 percent, which was neglected.[16]

Experimental Results

The results on the measurements of 100 tracks in nitrogen is shown in Fig. 1. The six points on the curve are obtained by dividing the tracks measured into six energy groups and plotting the "center of gravity" of each group. It is seen that the primary ionization decreases with increasing energy of the incident electron, apparently approaching asymptotically a constant value. In Fig. 2 are shown the same data plotted on a logarithmic scale, in order to show the variation

[10] G. L. Locher, J. O. S. A. and R. S. I. **19**, 58 (1929).
[11] P. M. S. Blackett, Proc. Roy. Soc. **A123**, 613 (1929).
[12] P. M. S. Blackett, Proc. Roy. Soc. **A102**, 294 (1922); **A103**, 62 (1923); J. Sci. Inst. **4**, 433 (1927); **6**, 184 (1929).
[13] L. F. Curtiss, Nature **123**, 529 (1929); Bur. Standards J. Research **4**, 663 (1930); **8**, 579 (1932).
[14] P. Auger, Thesis, University of Paris (1926).
[15] Jeans, *Dynamical Theory of Gases*, 3rd ed., pp. 257.
[16] F. N. D. Kurie, Rev. Sci. Inst. **3**, 655 (1932).

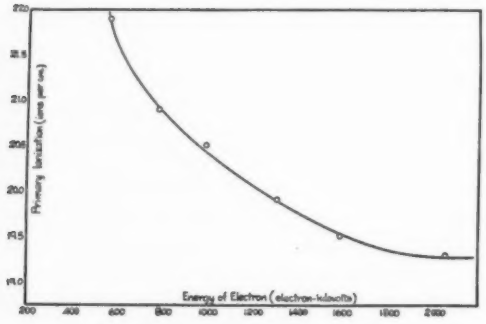

FIG. 1. Primary ionization in nitrogen.

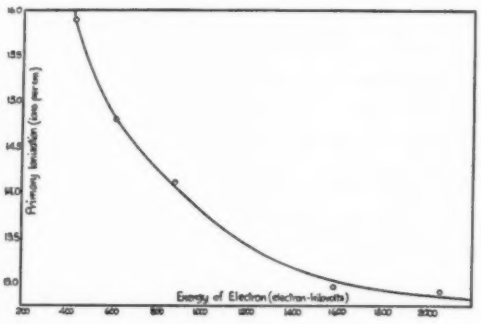

FIG. 3. Primary ionization in neon.

with velocity. If a straight line is drawn as near as possible through the experimental points, its slope shows that the primary ionization varies as the -1.15 power of the velocity, and the experimental results for nitrogen may be represented by the equation:

$$I = 19\beta^{-1.15\pm 0.15}.$$

On the same figure is plotted a theoretical curve calculated from the wave mechanical expression for primary ionization given by Eq. (2). Since the ionization potentials of the two K electrons in nitrogen is very large compared to that of the L electrons, we may assume that only the five outer electrons in the nitrogen atom are available for ionization. If the average ionization potential of these outer electrons is taken as 16.6 volts, which is very near the minimum ionization potential for the nitrogen molecule, the theoretical curve may be made to fit the observed data. The dotted curve of Fig. 2 is plotted on this basis. The ionization potentials for each electron in the nitrogen atom is not known. In general, however, the minimum ionization potentials observed correspond to that for the $2p$ electrons, and that for the $2s$ electrons is somewhat higher, which tends to make the experimental results somewhat higher than that predicted by the theory. The magnitude calculated on the classical theory is only about one-fourth that observed.

The experimental and theoretical curves have approximately the same slope over the range of velocities investigated, and agreement with variation with velocity is satisfactory. However, for values of the velocity greater than 0.97 the velocity of light, the theoretical curve shows an increase with velocity, increasing indefinitely as the velocity of the electron approaches that of light. Although the data obtained do not extend very far above this predicted minimum point, there is no indication of this increase, and observations on two or three tracks of very high energy undeflected in the magnetic field show a primary ionization approximately the same as those of the highest energy on the previous graph. The rise in the theoretical curve, however,

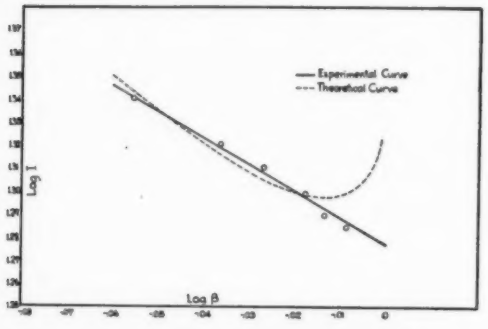

FIG. 2. Logarithmic curve for nitrogen.

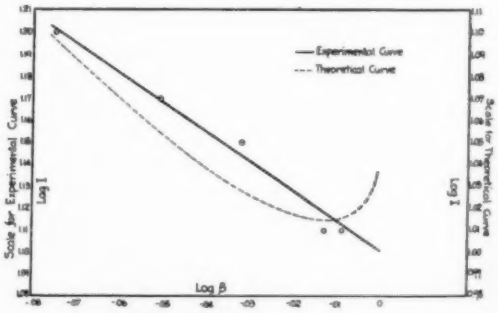

FIG. 4. Logarithmic curve for neon.

does not occur until very high energies are reached, and no conclusions can be drawn as to the existence of this increase at high energies.

The results on neon are shown in Figs. 3 and 4. The data are compiled and plotted by the same method as used for nitrogen, except that the theoretical curve is moved up vertically so that it can be plotted on the same scale as the experimental curve. The experimental results in neon may be represented by the equation:

$$I = 12.6\beta^{-1.35\pm0.15}.$$

The ionization potentials for each of the neon electrons is known from measurements on critical absorption wave-lengths, and these correspond to the molecule since neon is monatomic; and thus more accurate comparisons with theory may be made. The experimental results show that the primary ionization varies as the -1.35 power of the velocity, and is within experimental error in agreement with the theoretical predictions. As in the case of nitrogen, however, the increase at high velocities is not observed. The magnitude observed is about 12 percent higher than the calculated on the basis of the formula obtained by hydrogen-like wave functions but are as close as the somewhat arbitrary assumptions involved would allow one to expect. The observed magnitude is six times the classical value.

A few tracks in oxygen have been measured to compare the results with those of Williams and Terroux, and the values obtained check their results closely. Two or three tracks, definitely due to positive electrons, show no distinguishable difference in primary ionization from the negative electrons of similar energy on which ion counts were made. Work is now being done on measurement of the primary ionization in argon and preliminary results obtained indicate a lower value than would be expected by Bethe's formula (2). A complete account of this work will, however, be published soon.

The authors hereby wish to express their sincere thanks to Dr. N. A. Johanson, Chief of Staff of the Swedish Hospital, and to Dr. Charles B. Ward, Director of the Tumor Institute, for the use of the radon tubes used in this work, and for other facilities extended.

OCTOBER 15, 1936 PHYSICAL REVIEW VOLUME 50

Disintegration Experiments on the Separated Isotopes of Lithium

L. H. RUMBAUGH, *Bartol Research Foundation of the Franklin Institute*
AND
L. R. HAFSTAD, *Department of Terrestrial Magnetism, Carnegie Institution of Washington*

(Received August 17, 1936)

Observations made with targets of 18 micrograms of Li^6 and 200 micrograms of Li^7 under proton and deuteron bombardment have given the following results. (1) Two groups of protons with mean ranges of 25.4 cm and 29.6 cm air-equivalent are emitted by Li^6 under deuteron bombardment at 540 kv. No group of such range was found for Li^7 under similar conditions. (2) Neutrons are emitted by Li^6 under deuteron bombardment at 300 kv and above. (3) Short period beta-ray activity was observed from Li^7 under deuteron bombardment at 500 kv and above with no observable activity from Li^6 under similar conditions. (4) Gamma-rays are emitted by Li^7 under proton bombardment in the neighborhood of 450 kv and of 1000 kv, with no observable gamma-rays or neutrons emitted from Li^6 with protons of these energies.

I. INTRODUCTION

WHILE it is to be expected that the proper parent of most transmutation products may be assigned from energy considerations and mass spectrograph data, the origin of other products may be ambiguous, particularly in case a previously unknown nucleus is formed or the available energy is utilized only partially in a single process. Furthermore, certain nuclear processes in one isotope may be obscured by the products of another isotope. In these instances, the use of targets of single isotopes assumes special significance. An example of such work is that of Oliphant, Shire, and Crowther,[1] using

[1] M. L. Oliphant, E. S. Shire and B. M. Crowther, Proc. Roy. Soc. **A146**, 922 (1934).

isotopic specimens of lithium of about 5×10^{-8} grams, who showed that the correct isotopic origins had been given for the heavy particle and 30 cm proton groups which occur with proton and deuteron bombardment.

II. Apparatus and Procedure

The lithium targets used in this work were from a group of 20 isotopic specimens ranging from 10 to 200 micrograms in mass. The lithium was uniformly deposited as spots about one cm in diameter on small copper disks in a magnetic lens type of mass spectrometer.[2] A few targets were prepared as lithium chloride, but the targets chiefly used were 200 micrograms of Li^7 and 18 micrograms of Li^6 collected simultaneously and allowed to oxidize in air. Targets of Li^6 and Li^7 which were collected simultaneously and similarly handled subsequently, may be called matching targets. Wherever feasible, results with one isotope were compared with matching targets of the other to eliminate contamination effects from other elements. The isotopes were separated and collected with the mass spectrometer at the Bartol Research Foundation of the Franklin Institute.

The two-meter electrostatic generator of the Department of Terrestrial Magnetism[3] was used in the transmutation work. Voltages were read with the calibrated resistance voltmeter with which the generator is equipped. Range and neutron recoil observations were made with a linear amplifier coupled to a cathode-ray oscillograph for identifying particles, and to a dial counter through a scale-of-eight thyratron circuit. The thyratrons were usually biased to count only heavy ionizing particles near the ends of their ranges. Electrons were counted with a Geiger counter. A Lauritsen electroscope, shielded by a quarter-inch of lead, was used both with a paraffin lined chamber and with an aluminum chamber for neutron and gamma-ray measurements. The air equivalents of particle ranges were determined with graded mica foils mounted in two concentric wheels. The solid angle from the target subtended by the amplifier chamber was governed by diaphragming with a disk containing graded circular openings. All observations were made at angles between $90\pm16°$ and $90\pm7°$ with the ion beam. In general, no particular effort was made to determine absolute ranges with greater accuracy than about ±0.7 cm since the ranges of all the main groups in lithium transmutations have been measured by other workers. The range differences of associated groups are much more accurate, the chief limitation being set by the number of points determined on the number-range curves.

The atomic masses used in this work are those calculated by Bonner[4] from transmutation data.

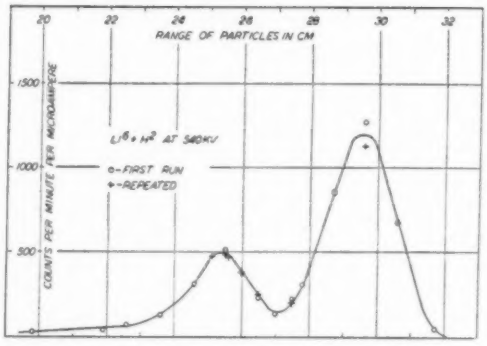

Fig. 1. Range curve for protons from Li^6+H^2.

III. Results

(a) Proton groups from ($Li+H^2$)

Deuteron bombardment of Li^6 yields two prominent proton groups differing in range by 4.2 ± 0.4 cm of air. The differential range curve plotted in Fig. 1 was obtained by biasing the thyratron counter against fast protons. It shows proton groups ending near 27.2 and 31.4 cm of air. Since the shorter group could not be obtained with matching Li^7 targets, it is not due to contamination by another element.

Li^7 targets were examined first for proton groups of 20 cm or more range. A yield curve

[2] L. H. Rumbaugh, Phys. Rev. **49**, 882 (1936); W. R. Smythe, L. H. Rumbaugh and S. S. West, Phys. Rev. **45**, 724 (1934).

[3] M. A. Tuve, L. R. Hafstad and O. Dahl, Phys. Rev. **48**, 315 (1935); L. R. Hafstad, N. P. Heydenburg and M. A. Tuve, Phys. Rev. **50**, 504 (1936).

[4] T. W. Bonner, presented at the symposium on nuclear physics, Cornell University, July 2–4, 1936. These masses closely agree with the recent mass spectrograph determinations of Bainbridge and are probably accurate to ±0.0002 mass unit. The following values are used in this work: $n^1=1.0090$; $H^1=1.0081$; $H^2=2.0147$; $He^3=3.0171$; $He^4=4.0040$; $Li^6=6.0170$; $Li^7=7.0182$; $Be^8=8.0080$; $Be^9=9.0149$.

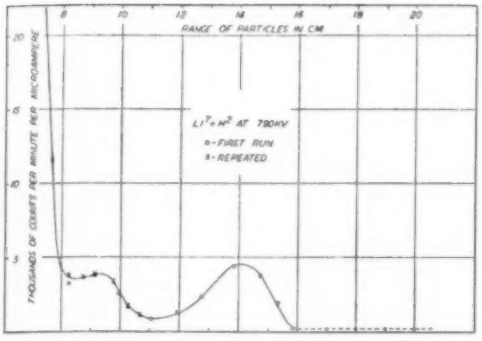

FIG. 2. Range curve for particles from Li^7+H^2.

was taken from 260 to 790 kv, using a 200-microgram target of Li^7, with the absorbing foils set at 20 cm and the thyratrons biased to count all fast protons. The yield curve obtained increased smoothly with voltage, giving no evidence for the existence of resonances. The kicks observed with the oscillograph throughout were of the heterogeneous character of neutron recoils. Next, the interval between 20 and 80 cm was explored at 790 kv and no trace of any group as strong as 20 percent of the neutron recoil background could be observed. Since no evidence for a resonance had been found, it was concluded that no proton groups of ranges greater than 20 cm are emitted by Li^7+H^2.

The Li^7 targets under deuteron bombardment at 790 kv show two weak proton groups ending at about 10.6 and 15.8 cm (Fig. 2). The strong group ending at 7.9 cm is composed of the continuous alpha-particles from Li^7. These groups were the only ones found when the region between 7 and 20 cm was investigated at three voltages; 260, 540, and 790 kv. Later in this paper it will be shown that the proton groups at 10.6 and 15.8 cm may be ascribed to contamination of the target, though no comparison with matching Li^6 targets was made, since in that case the strong 13-cm group of alpha-particles would have marked both proton groups.

(b) Alpha-particles

The five groups of alpha-particles from lithium have been studied by a number of workers since the discovery of lithium transmutation by Cockcroft and Walton. The separated isotopes, Li^6 and Li^7, have been used by Oliphant, Shire, and Crowther to show that the five groups had been attributed to the proper isotopes.[1] Three alpha-particle groups were observed in the course of the present work: one at 8.5 cm, from Li^7+H^1; another at 13 cm, for Li^6+H^2; and the continuous group ending at 7.9 cm, from Li^7+H^2. Though a short group was observed visually, the groups at 0.8 and 1.1 cm, from Li^6+H^1, were not investigated.

(c) Mass and purity of targets

The relative masses of isotopic specimens were obtained from the collector currents observed in the mass spectrometer. The absolute masses of several specimens, of weights up to one milligram, were determined by chemical methods with an accuracy of ± 2 micrograms, so that the correction to be applied to the collector currents for secondary electron emission was known. Thereafter, the masses of the isotopes deposited during any run were computed from the collector currents.

The isotopic purity of targets of Li^6 and Li^7 was found from the comparative strengths at the same voltages of the appropriate alpha-particle groups, diaphragms of different sizes necessarily being used with the amplifier chamber. The ratio Li^6/Li^7 in a Li^6 target is approximately 1000, as determined by comparing the 8.5 cm alpha-particles, produced by the reaction $Li^7+H^1=He^4+He^4$, in a Li^7 target with the same group from a Li^6 target. The ratio Li^7/Li^6 was greater than 30,000 for the Li^7 targets, the 13-cm alpha-particles from $Li^6+H^2=He^4+He^4$ being used for comparison. These alpha-particles, though only about twice as numerous as the background of large neutron recoils, in Li^7 targets, proved very useful in identifying other contamination products, since the range of the group has been carefully determined by Oliphant, Kempton, and Rutherford.[5]

The shorter proton group from Li^7 targets, Fig. 2, having a range of 10.6 ± 0.4 cm at 790 kv was attributed to the reaction $O^{16}+H^2=O^{17}+H^1$, originating in oxygen contamination. The range of this group has recently been determined as 9.2 cm at 575 kv by Cockcroft and Lewis[6] and

[5] M. L. E. Oliphant, A. R. Kempton and Lord Rutherford, Proc. Roy. Soc. **A149**, 406 (1935).
[6] J. D. Cockcroft and W. B. Lewis, Proc. Roy. Soc. **A154**, 261 (1936).

the value given agrees satisfactorily, when proper correction is made for voltage.

The other proton group has ranges of 15.8 cm at 790 kv, 14.1 cm at 540 kv and 12.7 cm at 260 kv, and so must have originated from carbon contamination giving the reaction, $C^{12}+H^2=C^{13}+H^1$. The ranges were measured with an accuracy of about ± 3 mm by reference to the underlying Li^6+H^2 alpha-particles, and closely agree with the recent determination of 13.9 cm at 560 kv by Cockcroft and Lewis.[6] Fig. 3 gives the differential range curve from this region at 540 kv. The 14.1-cm protons were about 200 times stronger than the alpha-particle group, which was picked up under the protons by biasing the thyratrons to count only alpha-particles near the ends of their ranges. At this voltage, the range of the deuterium protons should be 15.5 cm.[5, 6] Since no group of that range was observed, it was concluded that the deuterium contamination was negligible.

(d) Gamma-rays from ($Li+H^1$)

The gamma-radiation from matching targets (18 micrograms of Li^6 and 200 micrograms of Li^7), under proton bombardment, was measured with the electroscope shielded by a quarter-inch of lead. The rate of discharge of the electroscope for Li^6 and Li^7 is plotted against voltage in Fig. 4.

Both the strong resonance at 450 kv and the increase in ionization at higher voltages reported by Hafstad and Tuve[7, 8] are clearly indicated as being due to Li^7. The observations with a paraffin lined ionization chamber at about 1000 kv show no appreciable increase in ionization, suggesting that the radiation at this voltage also is predominantly of a gamma-ray nature. The discharge rate for the Li^6 target was practically indistinguishable from the zero drift of the electroscope (0.07 division per minute) both at resonance and at higher voltages, so that the small effect indicated in Fig. 4 is probably spurious.

(e) Neutrons from ($Li+H^2$)

The neutron emission by lithium under deuteron bombardment, first reported by Crane,

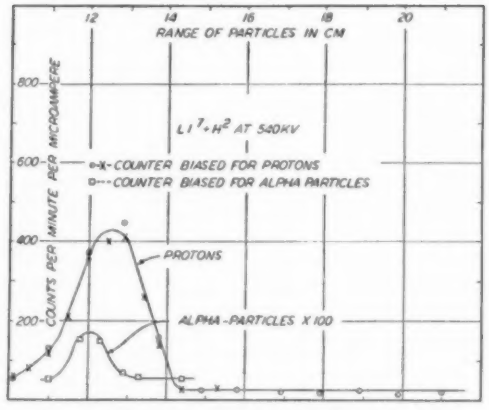

FIG. 3. Range curve for particles from Li^7+H^2.

Lauritsen, and Soltan,[9] was found to come from *both* isotopes, contrary to the results of the Cambridge investigators.[1] A 200-microgram target of Li^7 was exposed to deuterons at 540 kv and the neutron recoils produced in the shielded air-filled chamber of the amplifier were recorded. There were counted 20 ± 3 kicks per microampere per minute, of sizes equal to or greater than those produced by protons in their last 2 cm of range. The discharge rate of the shielded electroscope with a paraffin lined chamber was 11.8 divisions per minute. The ratio of the discharge rate using a paraffin lined chamber to that using an aluminum chamber was 1.7, the increased discharge rate occurring with the paraffin lining being due to proton recoils produced by the neutrons.

At the same voltage and thyratron bias, the matching 18-microgram target of Li^6 yielded 4.8 ± 0.8 amplifier kicks per microampere per minute and discharged the lined electroscope at the rate of 4.1 divisions per minute. The ratio of the paraffin lined electroscope discharge rate to that without lining was 2.3 for the 18-microgram target. A shorter observation with 35 micrograms of Li^6, used as Li^6 Cl, gave an electroscope ratio of 2.6.

It appeared impossible to account for any appreciable part of these Li^6+H^2 neutrons by contamination by Li^7 or H^2 in view of the isotopic purity and negligible deuterium contamination of the targets as discussed above. Oxygen and

[7] L. R. Hafstad and M. A. Tuve, Phys. Rev. **48**, 306 (1935).

[8] L. R. Hafstad, N. P. Heydenburg and M. A. Tuve, Phys. Rev. To appear in November 1, 1936, issue.

[9] H. R. Crane, C. C. Lauritsen, and A. Soltan, Phys. Rev. **44**, 692 (1933).

carbon were the only other elements present in amounts detectable by means of their characteristic protons. The activation function of oxygen by deuterons, as determined by Newson,[10] indicates that neutron emission does not occur below 2 Mev. Since carbon is known to emit neutrons at much lower voltages, a graphite disk was exposed to 1.3 microamperes of 540 kv deuterons as a check. The discharge rate produced in the paraffin lined electroscope was 0.07 ± 0.02 division per minute, from which the residual drift of 0.07 division per minute had to be subtracted. While this negative result was to have been expected for carbon neutrons, which are of low energy, it also served as a further check against contamination effects, particularly in those parts of the target chamber from which transmutation groups could not be emitted through the window.

As a further precaution, rough excitation curves were made for neutrons from both Li^6+H^2 and $C^{12}+H^2$, counting air recoils with results as shown by solid lines in Fig. 5. The marked difference in the curves together with the visual observation that the sizes of the deflections on the cathode-ray monitor were several times larger for Li^6 neutron recoils than for C neutron recoils, showed conclusively that the neutrons from Li^6 targets cannot be ascribed to carbon contamination.

To further test the possibility that the neutrons might be due to deuterium, a target of $P_2O_5+D_2O$ was prepared and bombarded with deuterons at 540 kv. Few neutron recoils were observable above the residual count of the detecting chamber, indicating that the neutron yield from Li^6 is large compared to that from such a target of deuterium. This evidence, together with that given in Fig. 3 which was obtained with a target that had had about four times the exposure of the Li^6 target to deuterons, appears to us to eliminate the possibility that the neutrons observed were due to deuterium contamination.

The results of Fig. 5 have a further important significance. Since the yield of neutrons from $C^{12}+H^2$ can be deduced immediately from the yield of radioactive N^{13} which is known,[7, 11]

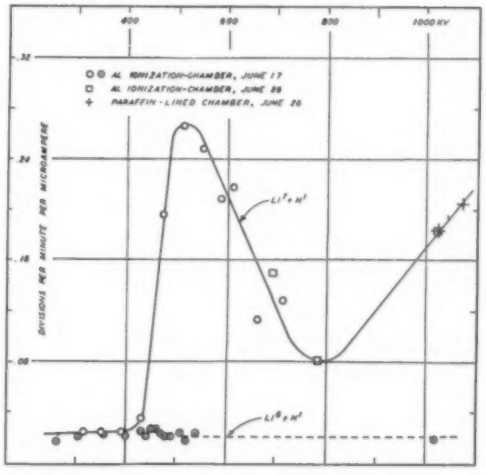

FIG. 4. Excitation curve for gamma-rays from lithium.

an estimate of the yield of neutrons from Li^6 can be obtained. As given, any comparison of the solid curves in Fig. 5 must take into account the fact that the low energy C^{12} neutrons will produce fewer air recoils with sufficient energy to be detected than the high energy Li^6 neutrons. This correction can be greatly reduced by counting recoils with an ionization chamber filled with hydrogen in which case low energy neutrons can be detected. Observed points for 810 kv, obtained with such a chamber, using a pressure of about two atmospheres of hydrogen, are shown in Fig. 5, the dotted lines showing the corresponding excitation curves obtained by adjusting the solid curves to fit the new points at 810 kv. From the intersection of these two curves one may conclude that the yield of neutrons from this 18-microgram target is equal to that from a thick carbon target at about 750 kv. The latter yield is approximately 6 neutrons per 10^8 incident particles at this voltage, and since the excitation curve for Li^6 does not drop rapidly with voltage, thick targets of Li^6 may prove to be of value in the production of neutrons with low voltage ion accelerators.

(f) Radioactivity from ($Li+H^2$)

A 0.5 second half-life beta-radioactivity induced in lithium by deuterons has been reported from the California Institute of Technology.[12]

[10] H. W. Newson, Phys. Rev. **48**, 790 (1935).
[11] S. K. Allison, Proc. Camb. Phil. Soc. **32**, 179 (1936).
[12] H. R. Crane, L. A. Delsasso, W. A. Fowler and C. C. Lauritsen, Phys. Rev. **47**, 971 (1935).

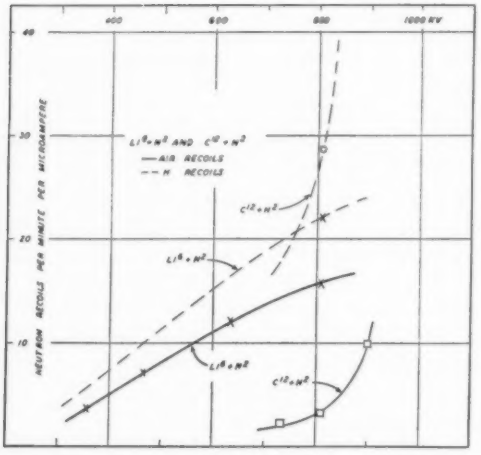

FIG. 5. Excitation curve for neutrons from Li^6+H^2 and $C^{12}+H^2$.

In the present work, the activity was observed from a semi-thick target of Li^7 in a crude but convincing manner. A Geiger counter, covered with thin aluminum equivalent to about 40 cm of air, was placed before the window of the target chamber. Counts were made while the target was exposed to deuterons for a few seconds and were continued when the deuteron beam was interrupted by a movable quartz disk. In this way, a definite and very rapidly decaying activity was observed. At 750 kv, the count was 35 to 40 per second during exposure, and 35 to 45 counts were recorded in the first 5 seconds following manual interruption of the deuteron beam. At 5 seconds, the counting rate had fallen to the background rate of about 0.4 per second. Between observations the counter was checked with the beta-rays of Ra D and E for sensitivity and sharpness of cut-off following rapid counting. The induced activity of lithium, as indicated by counting rates during exposure of the target to deuterons, showed an abrupt threshold at about 500 kv below which it could not be detected. The activation function shown in Fig. 6 was obtained with a 200-microgram target of Li^7.

A target of Li^6 gave no increase in counting rate during exposure of the target to deuterons for periods up to one minute at several voltages between 350 and 750 kv. The slight increase occurring after exposures of more than one minute was attributed to the activation of carbon in the target chamber. Because of the neutron emission for Li^6, which might be interpreted to imply a positron emission of fairly long life, a thick target of ordinary pure lithium chloride was bombarded with two microamperes of 850-kv deuterons for 2.5 hours and examined in the electroscope chamber for positron activity. The only activity detected had the half-life of activated carbon.

(g) Possibility of observing (Li^5+H^2) reactions

Brewer[13] recently has reported evidence indicating that a new isotope, Li^5, constitutes about one part in 20,000 of the lithium ion emission from thermal sources. As part of the present work, three targets were exposed in the mass five position of the magnetic lens mass spectrometer during the collection of three milligrams of the lithium isotopes. The ions fell on the collectors through windows which were opened only when Li^7 showed good focus. The best of the targets was prepared in a discontinuous run totaling 15 hours during which 1.2 milligrams of Li^7 were collected. The electrically measured background at the mass five position varied between one part in 4000 and one part in 15,000 of the Li^7 collector current. The faint deposit on the mass five target only became visible after exposure to the fumes of hydrochloric acid.

A preliminary survey with this target indicated that carbon and Li^7 were the principal contaminations and that a small amount of Li^6 was also present. If Li^5 exists,[14] its mass should be less than that of He^4+H^1. Hence, the maximum range particle to be expected from a Li^5 would be a five cm proton from the reaction $Li^5+H^2=Li^6+H^1$. If the mass is still lower, all particles may be too short in range to be detected. Furthermore, the contamination background would make the search for particles from this reaction a very difficult one. In consequence, no detailed survey of short-range particles from these targets will be made until the ratios of Li^5 to Li^6 and Li^7 have been determined in a mass spectrograph with ion sources prepared at the mass five position. If the results warrant it, the background during collection probably can be decreased by a considerable factor.

[13] A. K. Brewer, Phys. Rev. **49**, 635 (1936).
[14] W. Bleakney (private communication) has failed to observe Li^5.

IV. Discussion of Results

Proton groups from Li^6+H^2

The two proton groups found with Li^6 under deuteron bombardment are important for two reasons. (1) The shorter of these groups is doubtless the one observed by Delsasso, Fowler and Lauritsen[15] with a cloud chamber and generally attributed to the transmutation of Li^7. Calculations of the mass of Li^8 based on the range of this group therefore are wrong. (2) The emission of two line groups of protons from a single nuclear species points to the existence of two absorption or emission levels in one of the reacting nuclei. On the assumption that emission of the shorter group involves the formation of Li^7 in an excited state, the equations for the reactions may be written

$$Li^6+H^2=Li^7+H^1,$$

and $$Li^6+H^2=Li^{7*}+H^1;\quad Li^{7*}\rightarrow Li^7+h\nu$$

where $h\nu=400\pm40$ kv. A more detailed discussion, of particular interest to theorists, may be made when the two groups have been examined at a number of deuteron energies.

Mass of Li^8

The failure to observe any proton group of range greater than 8 cm from Li^7+H^2 introduces difficulties in the previous interpretation of the beta-activation of lithium by deuterons. Since the discovery of this activity at the Pasadena laboratories,[12] Knol and Veldkamp[16] have succeeded in inducing it in lithium with slow neutrons, and the present work has shown that it is derived from Li^7. It follows that the radioactive nucleus formed probably is Li^8, so the equation for the first stage of the reaction is

$$Li^7+H^2=Li^8+H^1.$$

Since by our observations the range of the protons from this reaction at 790 kv is probably less than 8 cm, the mass of Li^8 is given by

$$Li^8>Li^7+H^2-H^1-1.8\text{ Mev}$$
$$Li^8>8.022(8).$$

The mass of Li^8 also may be computed from the observed energy of 10.5 ± 1 Mev for the upper limit of the beta-spectrum[12] assuming no gamma-radiation:

$$Li^8\rightarrow Be^8+\bar{e}=Be^8+10.5\pm1\text{ Mev}$$
$$=8.019(3)\pm0.001.$$

The discrepancy between the mass values obtained in the two ways is too large to be explained by experimental error in the determination of the upper limit of the beta-spectrum, particularly since Crane, Delsasso, Fowler and Lauritsen[12] already have extended the apparent value of the limit somewhat to fit the extrapolated Konopinski-Uhlenbeck formula. It appears, therefore, that if this process does occur, then the ejection of the proton and the emission of the beta-particle must be accompanied by yet a third reaction to absorb the excess energy. This reaction probably follows the ejection of the beta-particle and may involve any of three processes:

1. $Li^8\rightarrow Be^{8*}+\bar{e}\rightarrow He^4+He^4+\bar{e}$
2. $Li^8\rightarrow Be^{8*}+\bar{e}\rightarrow He^4+He^4+\bar{e}+h\nu$
3. $Li^8\rightarrow Be^{8*}+\bar{e}\rightarrow Be^8+\bar{e}+h\nu.$

The most definite information pertaining to the formation of Li^8 is given by the activation function for Li^7+H^2 (Fig. 6), which shows that the transmutation to Li^8 with emission of a proton starts abruptly when the deuteron energy reaches 500 kv. The function seems to rise too slowly and extend over too wide a voltage range to be due to resonance in a thin

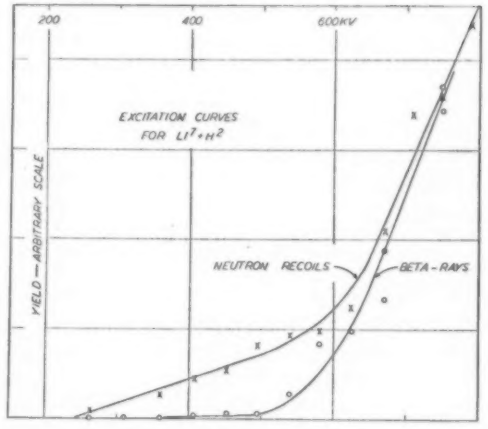

FIG. 6. Excitation curve for beta-rays and neutrons from Li^7+H^2.

[15] L. A. Delsasso, W. A. Fowler and C. C. Lauritsen, Phys. Rev. **48**, 848 (1935).
[16] K. S. Knol and J. Veldkamp, Physica **3**, 145 (1936).

target. On the other hand, the sharp threshold is totally different from that predicted by the Oppenheimer-Phillips[17] relation which requires that the experimental curve shall rise tangentially from an indefinite threshold on the voltage axis. It appears, therefore, that the processes are selective rather than endothermic below 500 kv.

Since the Oppenheimer-Phillips relation does not hold, the deuteron may be captured as a whole and the proton emitted from within the resultant Be^9 nucleus. Hence the three known transmutations of Li^7 by deuterons may be written as deuteron capture equations:

$$\text{Li}^7+\text{H}^2=\text{Be}^{9*}\begin{cases}1.\ \text{He}^4+\text{He}^4+n^1\\ 2.\ \text{Be}^8+n^1\\ 3.\ \text{Li}^8+\text{H}^1.\end{cases}$$

A plausible explanation of the form of the activation function can be given on the basis of selective reactions. Suppose that when the energy of the deuteron is below a certain critical value, $E_0\sim 500$ kv, a proton may be excited to a positive energy level *below* the top of the potential barrier for Be^9. The time necessary for the proton to penetrate the potential barrier, bringing about reaction (3), is long compared to the time for the emission of a neutron, in accordance with reactions (1) or (2), because of the relatively low binding energy of the neutron in the Be^9 nucleus and its immunity to the potential barrier. Hence, proton emission will not occur until a deuteron energy E_0 is supplied, at which protons begin to escape over the top of the potential barrier. In consequence, the transmutation to Li^8 shows an abrupt threshold at that voltage.

Existence of Li^8

The beta-activity induced in lithium by deuterons cannot be ascribed to Li^8 with certainty until a *line* group of protons is found, indicating *two-body* disintegrations and the consequent formation of Li^8. It is plausible that three-body disintegrations may occur and that one of these bodies is the radioactive one, rather than Li^8. In either case, the investigations of Knol and Veldkamp[16] with neutrons require that proton emission shall occur when deuterons are used to produce the activity.

The neutrons from Li^6; approximate mass of Be^7

Neutron emission produced from Li^6 by deuterons may be expected to originate in only two ways:

1. $\text{Li}^6+\text{H}^2=\text{He}^4+\text{He}^3+n^1+Q_1$
2. $\text{Li}^6+\text{H}^2=\text{Be}^7+n^1+Q_2$.

The first process is exothermic, since Q_1 is about 1.5 Mev on the Bonner mass scale. The maximum energy of the neutrons would be 1.3 Mev and the mean energy about 400 kv, in marked contrast to the well-known analogous reaction, $\text{Li}^7+\text{H}^2=\text{He}^4+\text{He}^4+n^1$. In the latter case the neutron energies are distributed to a maximum of 13.3 ± 0.5 Mev and the mean neutron energy is about 3.9 Mev, according to Bonner and Brubaker.[18]

The energy balance, Q_2, of the transmutation to Be^7 cannot be computed accurately since it contains the mass of the unknown nucleus, Be^7. If Be^7 is radioactive, the reaction must be $\text{Be}^7\rightarrow\text{Li}^7+e^+$, and it follows that Be^7 is heavier than Li^7 by at least two electronic masses; i.e., Q_2 is not greater than 3.162 Mev, if the possibility of positron emission by Be^7 is admitted. If such radioactivity exists, it must have a fairly long life and a low energy spectrum to have escaped detection, both in the present experiments in which it was investigated, and in the cloud chamber studies of the beta-activity of lithium by Crane, Delsasso, Fowler and Lauritsen.[12] In the latter case, positrons would have been immediately obvious because of their curvature in the magnetic field of the cloud chamber, unless their maximum energy was little greater than 0.3 Mev, the stopping power of the foil surrounding the target. Consequently, if Be^7 is a positron emitter, $Q_2\sim 2.86\pm 0.3$ Mev, possible gamma-radiation being neglected. On the other hand, Be^7 may be nonradioactive and as light as its isobar, Li^7. A close equivalence of isobaric masses has been found for H^3 and He^3 and for Be^{10} and B^{10}. If the mass of Li^7 is taken for Be^7, $Q_2\sim 4.2$ Mev.

It is clear that accurate knowledge of the

[17] J. R. Oppenheimer and M. Phillips, Phys. Rev. **48**, 500 (1935).

[18] T. W. Bonner and W. M. Brubaker, Phys. Rev. **48**, 742 (1935).

energies of the neutrons emitted from Li^6+H^2 is needed to distinguish between the two suggested values of Q_2, and thus indicate the process involved.

ACKNOWLEDGMENTS

The writers are glad to acknowledge their indebtedness to their respective Directors for support and encouragement, and to their colleagues for helpful discussion and aid in experimental work. One of us (L. H. Rumbaugh) is especially indebted to the Carnegie Institution for partial defrayal of expenses while in Washington, and to The American Philosophical Society for a grant used in perfecting the mass spectrometer.

OCTOBER 15, 1936 PHYSICAL REVIEW VOLUME 50

Gamma-Rays of Lithium and Fluorine Under Alpha-Particle Bombardment*

KARL C. SPEH, *Sloane Physics Laboratory, Yale University, New Haven, Connecticut*

(Received August 3, 1936)

The energies of the γ-rays emitted from lithium and fluorine under bombardment by polonium α-particles are determined, and their variation with the energy of the incident particles is studied. In the case of lithium no change in γ-ray energy is observed as the range of the incident α-particles is reduced from 3.9 cm to 2.5 cm. This is taken to support the view that the radiation results from excitation of the lithium nucleus without capture of the α-particle. At an incident range of 3.9 cm the γ-radiation from fluorine is shown to consist of two components. When the incident range is reduced to 3.1 cm the harder component disappears. Possible explanations are discussed, and the existence of a hitherto undetected proton group of low energy is suggested.

INTRODUCTION

IT is now generally recognized that the study of the γ-rays resulting from the bombardment of light atoms with high energy particles yields important information concerning nuclear structure. In particular, in the light of present theory the energies of these γ-ray quanta offer a direct measure of excited energy states in the nuclei responsible for their emission, and a knowledge of these energies is essential for the formulation of a quantitative theory of nuclear constitution. Accordingly, the present investigation was undertaken to measure the energy of the γ-rays thus obtained from lithium and fluorine, two of the most favorable elements for such studies. Special attention was paid to the effect on the quality of the radiation of varying the range of the incident α-particles. With a Geiger point counter for detection, the energies of the γ-rays were determined from their absorption in lead.

The existence of induced nuclear γ-rays was first demonstrated by Bothe and Becker,[1] who observed their emission from six of the light elements under intense α-particle bombardment. Subsequently Curie and Joliot,[2] Webster,[3] and others extended their results and defined more accurately the conditions of excitation. Savel[4] has recently investigated the penetrating radiations emitted in artificial disintegration, finding evidence for several different processes giving rise to accompanying γ-rays.

The γ-rays are believed to arise in the following manner. During a collision the incident α-particle is captured, a composite nucleus being formed momentarily, and subsequently one of the constituent nuclear particles is ejected. If the product nucleus is left in an excited state, a γ-ray is emitted in the subsequent return to the ground level. It may happen that the α-particle is not absorbed into the nucleus, but penetrates and then escapes again with reduced energy, the difference being spent in exciting the struck nucleus. In this case also the surplus nuclear energy is later released in the form of a γ-ray.

It is likely that some of the γ-rays from both lithium and fluorine are the result of the latter

* Part of a dissertation presented to the Faculty of the Graduate School of Yale University in candidacy for the degree of Doctor of Philosophy.

[1] W. Bothe and H. Becker, Zeits. f. Physik **66**, 289 (1930).

[2] I. Curie and F. Joliot, Comptes rendus **194**, 273 (1932); **194**, 708 (1932); **194**, 876 (1932).

[3] H. C. Webster, Proc. Roy. Soc. **A136**, 428 (1932).

[4] P. Savel, Ann. d Physik (II) **4**, 88 (1935).

process of "excitation without capture." In the case of lithium it is known that both γ-rays and neutrons are emitted under α-particle bombardment, but from all indications they are the result of two distinct processes. Savel[4] and Schnetzler[5] have shown that in shape and lower limit the γ-ray excitation curve (yield of γ-rays as a function of incident α-particle energy) does not coincide with the corresponding curve for neutron excitation. Since no other process (e.g., proton emission) has been observed in the α-particle-lithium reaction, it appears that the γ-rays must arise from excitation without capture. The neutrons observed are attributed to the reaction

$$_3Li^7+{}_2He^4\rightarrow{}_5B^{10}+{}_0n^1.$$

It will be seen that our results support this interpretation.

In the case of fluorine, disintegration protons as well as neutrons and γ-rays result from bombardment by polonium α-particles. The protons are ascribed to the reaction

$$_9F^{19}+{}_2He^4\rightarrow{}_{10}Ne^{22}+{}_1p^1;$$

and the neutrons to the reaction

$$_9F^{19}+{}_2He^4\rightarrow{}_{11}Na^{22}+{}_0n^1.$$

The radioactive sodium nucleus formed in the second of these reactions is supposed later to disintegrate with the emission of a positron. Here also Savel[4] has shown that the minimum range of α-particles exciting γ-radiation is 0.9 cm lower than that for neutron emission and 1.5 cm lower than that for proton emission. Hence it is likely that some at least of the γ-rays arise independently of either of the disintegration processes postulated above.

Other evidence indicates that γ-rays may also result from the formation of an excited product nucleus after either the proton or the neutron disintegration. Chadwick, Constable and Pollard,[6] and Chadwick and Constable[7] have shown that the protons fall into six definite groups, which may be separated into pairs of constant energy difference. Each pair is ascribed to the impact of α-particles of a certain energy, penetrating the nucleus either over the barrier or through a resonance level. The surplus energy of the reaction, including the kinetic energy of the α-particle and the mass annihilated in the transformation, may be imparted entirely to an ejected proton of long range, or it may be spent partly in exciting the nucleus and partly in ejecting a proton of short range. Thus the pairs of proton ranges are explained, and from the excited nucleus a γ-ray is expected of an energy that may be calculated from the range difference between the members of a pair.

Bonner and Mott-Smith[8] have found that the neutrons may be resolved into similar groups. From their results they predict a third γ-ray corresponding to an excited level in the product sodium nucleus.

The need for direct measurement of all the emitted γ-rays to test these expectations and perhaps to disclose unexpected components led to the present investigation.

Very recently Bothe[9] has published data on the magnetic spectrum of the photoelectrons released by the α-excited γ-rays of lithium, fluorine and beryllium from lead. His results are comparable to ours as will appear at the end of the paper.

Experimental Arrangement

The γ-rays were detected by means of a Geiger point counter. The cylindrical counting chamber was made of 0.25 cm brass, the front being 0.08 cm in thickness. The interior of the chamber was effectively 6 cm deep and 5 cm in diameter. The platinum point, distant 5 cm from the front, was a ball of diameter approximately 0.01 cm formed on a fine platinum wire. The wire was soldered to a brass rod, which threaded through a hard rubber plug closing the back of the chamber. The counter contained dry air adjusted to be at 42 or 30 cm Hg. The case was maintained at a high positive potential (2900 or 2200 volts) furnished by the voltage amplifiers developed by C. D. Bock (description not yet published). The results obtained at the two pressures were compared both with a standard

[5] K. Schnetzler, Zeits. f. Physik **95**, 302 (1935).
[6] J. Chadwick, J. E. R. Constable and E. C. Pollard, Proc. Roy. Soc. **A130**, 463 (1931).
[7] J. Chadwick and J. E. R. Constable, Proc. Roy. Soc. **A135**, 48 (1932).
[8] T. W. Bonner and L. M. Mott-Smith, Phys. Rev. **46**, 258 (1934).
[9] W. Bothe, Zeits. f. Physik **100**, 273 (1936).

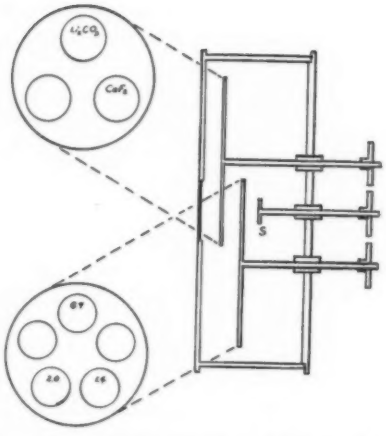

FIG. 1. Arrangement of source, mica foils, and targets. (Stopping powers of foils indicated in cm of standard air.)

radium source and with the radiators studied in the experiment, and were found to be entirely consistent. The chamber was housed in a specially cast cylindrical block which interposed a shield of five cm of lead between the counter and the background radiation of cosmic rays and stray γ-rays, cutting down their effect by 50 percent. The number of counts was independent of the voltage on the case over a range of 25 volts. With the standard source of radium (B+C) in position the response of the counter was tested by means of the inverse square law. The voltage impulses on the case were carried through a two-stage amplifier to the grid of a Thyratron, which in turn actuated a mechanical relay to record the counts.

The polonium and the materials to be bombarded were mounted in the evacuated brass box shown in Fig. 1. The source S was supported on the central brass rod; on either side of it were two brass disks, one carrying the target plates and the other mica foils of different stopping powers, laid over apertures in the brass flange. By rotating the disks a target of either Li_2CO_3 or CaF_2 could be brought before the source and a foil of the desired stopping power could be interposed. The stopping powers were determined by weighing, using the reduction factors found by Lawson.[10]

The polonium source (12 millicuries initially) was deposited on a silver button from a solution of radium (D+E+F). It was dissolved and redeposited three times. The spread in range of the α-particles was found to be unimportant. For the preparation and gift of this source I am greatly indebted to Dr. L. R. Hafstad of the Department of Terrestrial Magnetism, Carnegie Institution, Washington. The targets were prepared from suspensions of finely powdered Li_2CO_3 or CaF_2 in chloroform or alcohol, evaporated on to clean copper plates. The stopping powers of the targets were calculated and their total weights so chosen that the air equivalent was always greater than the full range of polonium α-particles.

The absorbing sheets were cut from lead tested for absence of radioactive contamination and were supported between target and counter in a small framework. A thickness of lead up to 2.5 cm could be interposed, in steps of 0.175 cm. At zero thickness there was actually interposed a thin sheet of lead (0.07 cm) in order to obtain the maximum count, considering the absorption coefficients both of the γ-rays and of the secondary electrons projected from the adjacent surface of the absorber.

The measured absorption coefficients were corrected where necessary for obliquity and scattering, and the corresponding energies of the γ-rays were estimated by means of the Klein-Nishina scattering formula and the empirical photoelectric law of L. H. Gray.[11]

EXPERIMENTAL RESULTS

A. Lithium

The absorption curves obtained from lithium are shown in Fig. 2. It is seen that the γ-rays are apparently monochromatic. Moreover, the measured absorption coefficients are the same within experimental error for three different ranges of the incident α-particle.

The values obtained appear in Table I.

B. Fluorine

The fluorine absorption curves are reproduced in Figs. 3a and 3b. When the target is bombarded by α-particles of reduced range, the induced γ-radiation is clearly monochromatic; no indication of a mixture of two or more components is

[10] R. W. Lawson, Wien. Ber. (IIa) **127**, 943 (1918).

[11] L. H. Gray, Proc. Camb. Phil. Soc. **27**, 103 (1931).

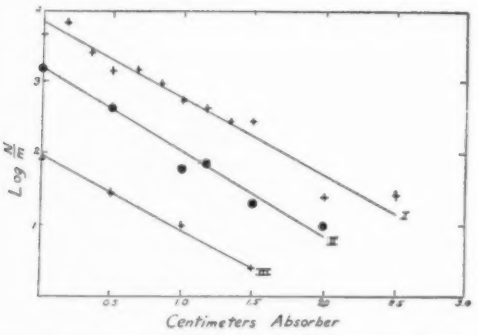

FIG. 2. Absorption of lithium γ-rays. Curve I, $R_\alpha = 3.9$ cm, curve II, $R_\alpha = 3.1$ cm., curve III, $R_\alpha = 2.5$ cm.

discernible. The absorption coefficient of the beam is 1.88 cm^{-1}, corresponding to a γ-ray energy of 0.48 ± 0.05 Mev.

The analysis of the beam resulting from the bombardment at full incident range is more complex. The points might be regarded as falling on a straight line, though on one of markedly different slope from that obtained at the reduced range. They are much more closely represented, however, by a curve which may be resolved into two straight-line components. The absolute determination of the absorption coefficients is necessarily inaccurate in such an analysis; but with this reservation we find that the beam is a mixture of two γ-rays of absorption coefficients 0.55 ± 0.1 cm^{-1} and 2.5 ± 0.7 cm^{-1}, respectively. The corresponding energies are 1.5 ± 0.2 and 0.4 ± 0.1 Mev.

Since, owing to the thickness of the fluoride layer, the atoms were effectively bombarded by α-particles of all ranges from 0 to 3.9 cm, the γ-ray observed for $R_\alpha = 3.1$ cm must have been present at the full range also. It seems likely, therefore, that the soft component of the complex beam is to be identified with the single γ-ray measured at the reduced range. This is just permissible with the probable errors given. If the proper alterations are made in the slope of both lines the energy of the hard component becomes 1.3 Mev. It is thought better, however, to retain the values originally determined, since these appear to fit the actual data more consistently.

TABLE I. *Lithium absorption.*

R_α cm	μ cm^{-1}	$h\nu$ Mev
3.9	1.07	0.71 ± 0.07
3.1	1.13	0.68 ± 0.07
2.5	1.07	0.71 ± 0.07
	Mean 1.09; 0.70	

INTERPRETATION OF RESULTS

A. Lithium

The absorption coefficient for the lithium γ-ray has never been determined under bombardment by polonium α-particles of less than the full range. The fact that the γ-ray energy does not change as the range of the α-particles is reduced below the limit of neutron excitation contributes further strong support to the notion that the γ-radiation indicates an excited level in the lithium nucleus itself rather than in the boron nucleus formed after the neutron disintegration, as has been suggested.[11]

At full incident range the γ-ray energy has been measured by Webster,[3] Savel,[4] and others. Their value of 0.5 to 0.6 Mev is somewhat lower than ours, but the discrepancy is not serious. Bothe[9] finds evidence for two components, 0.39 and 0.59 Mev. Our results do not indicate such a composite beam, but in any case the energy difference of the two components is probably insufficient to permit resolution by the absorption method at its present stage of development.

B. Fluorine

The various predictions for the energies of the γ-rays to be expected from the bombardment of fluorine have been discussed above. Quantitatively they are:

(1) 0.68 Mev from observed ranges of disintegration protons,
(2) 0.34 Mev from observed neutron energies,
(3) 1.8, 1.2 and 0.6 Mev from possible excitation of the nucleus without capture of the α-particle.

Under bombardment by α-particles of range 3.1 cm we find a γ-ray of energy 0.48 Mev. This falls between the first two energies above, and hence the γ-ray cannot be definitely associated with either of the disintegration processes, although it may well be a mixture of γ-rays from both processes. The two predicted energies of 0.34 and 0.68 Mev, even if present, are not separated enough to be resolved in experiments like these. The value of $h\nu$ observed is closer to

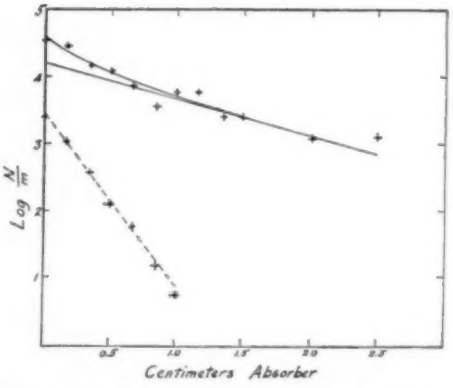

FIG. 3a. Absorption of fluorine γ-rays, $R_a = 3.9$ cm.

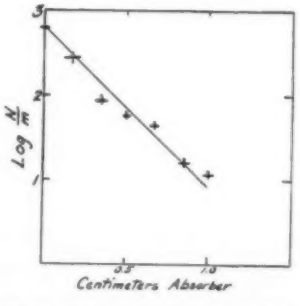

FIG. 3b. Fluorine γ-rays, $R_a = 3.1$ cm.

the value 0.6 Mev given under (3) above, but the evidence is insufficient to decide whether its presence really indicates excitation without capture. Similar remarks apply to the softer component of the radiation measured at full incident range ($h\nu = 0.4$ Mev). It can be said at present only that the soft γ-rays from fluorine lie in the right frequency region to accord with the measurements of proton and neutron groups. It is likely that γ-rays accompany both types of disintegration, giving a complex beam the mean absorption coefficient of which was measured in the present experiment.

The hard γ-ray found at the maximum incident range cannot be explained on the basis of proton or neutron groups now known. There are two alternative interpretations which may account for it: it may be a composite beam, made up of two γ-rays of energies 1.2 and 1.8 Mev in accordance with the noncapture excitation cited under (3) above, or it may represent the energy difference of two proton groups, one group accompanying the formation of the product neon nucleus in the second excited state. The first assumption is compatible with all our experimental results: a heterogeneous beam of two components separated by only 0.6 Mev in this energy region would not be resolved, and the penetrating γ-ray would disappear as soon as the energy of the α-particles was reduced appreciably below the barrier height. This is observed, as we have shown.

On the alternative assumption we may predict the existence of a proton group corresponding to a disintegration of energy change -0.5 Mev, since the lower group of each pair measured by Chadwick and Constable[7] corresponds to $Q = 1.0$ Mev, and our hypothetical group lies 1.5 Mev below this. This interpretation is equally consistent with our results. The proton group originating in such a transformation may easily have escaped detection on account of its short range.

The fact that the hard γ-ray and hence the suspected proton group vanish at 3.1 cm incident range indicates that below this energy input protons no longer acquire sufficient energy to scale the potential barrier of the neon nucleus formed. From the energy equation of the reaction for the case of protons emitted at right angles to the direction of the incident α-particle, calculation gives for the corresponding proton energy the value 2.7 Mev which may be taken as an indication of the barrier height. Henderson, Livingston and Lawrence[12] have found that the barrier height of fluorine is in excess of 1.5 Mev. Since the value for neon should be higher, the figure given is not unreasonable, although it is probably too high.

Bothe[9] similarly finds two components at the full incident range, one of 0.6 Mev and the other of energy somewhat greater than 1.1 Mev. In view of the small yields measured and the different methods used these are in good accord with the values given above.

Finally, it is a great pleasure to thank Professor Alois F. Kovarik for his constant guidance and counsel throughout the experiment, and Dr. Ernest Pollard, who suggested the problem, for

[12] M. C. Henderson, M. S. Livingston and E. O. Lawrence, Phys. Rev. **46**, 38 (1934).

many fruitful discussions and continual encouragement. I am also indebted to Mr. Howard Schultz for the design and construction of the amplifier.

Note. As this paper was being submitted, May and Vaidyanathan[13] published the results of new measurements on the ranges of disintegration protons from fluorine, from which they deduce for the *first* excited level in the product neon nucleus the value 1.5 Mev. This coincides exactly with our value for the energy of the hard γ-ray and indicates quite definitely that it is emitted by the neon nucleus. Since they give no term differences in the neon level scheme of less than 1.1 Mev, the soft γ-ray which we find ($\sim$0.5 Mev) is most probably to be ascribed to the fluorine nucleus itself, or possibly to the sodium nucleus formed after the neutron disintegration.

[13] A. N. May and R. Vaidyanathan, Proc. Roy. Soc. **A155**, 519 (1936).

OCTOBER 15, 1936 PHYSICAL REVIEW VOLUME 50

Effects of Chemical Combination on the *K* Beta Lines of 26 Fe–30 Zn

JOHN C. McDONALD,* *University of Minnesota*

(Received July 11, 1936)

The $K\beta$ lines of 26 Fe–30 Zn from the sulfides of those metals have been studied in fluorescence with a focusing crystal spectrograph of the Johansson type. The only lines showing a shift from their position in the spectra of the pure metals are the $K\beta_5$ lines of Fe and Ni. Calculation of the second ionization potential of Cu by application of Pauling's theory gave a value much too high The term values of the levels in which the $K\beta_5$ has its origin, for Fe, Co and Ni in the sulfides, were somewhat larger than in the pure metal, whereas for Cu and Zn they were about the same.

I. INTRODUCTION

VARIOUS workers in the past fifteen years have investigated the effects of chemical combination on x-ray absorption edges and line spectra. In the study of the line spectra it was soon found that consistent results, independent of target material, could be obtained best by the secondary radiation method, except in the case of refractory materials which suffered no chemical change under electron bombardment. Different apparatus, all using the principle that the substance studied must be kept cool and shielded from the direct electron beam, have been constructed and used by Alexander and Faessler,[1] Lundquist,[2] Valasek,[3] and Privault.[4] Yoshida[5] and Tanaka and Okuno[6, 7] used essentially the method of Alexander and Faessler. All these workers except Privault used a plane crystal spectrograph and photographic plate. Privault used a focusing crystal spectrograph of the Cauchois[8] type.

Valasek[3] studied the $K\alpha$ and $K\beta$ lines of S in the sulfides of 26 Fe–30 Zn and found a considerable effect due to chemical combination. Since the $K\beta$ lines might originate in crystal levels common to both ions, in which levels certain lines in the metallic spectra could possibly arise also, it was thought desirable to make a study of the $K\beta$ lines of the metals in those sulfides, particularly of the $K\beta_5$, which has its origin in the outermost levels of the atom. Since it is a quadrupole line and therefore of low intensity,[9, 10] it would be difficult to photograph it in fluorescence with a plane crystal spectrograph. For this reason a focusing crystal vacuum spectrograph constructed much like that of Johansson,[11] which gives theoretically the perfect focusing first suggested by DuMond and Kirkpatrick,[12] was built. Use of such a spectrograph in x-ray spectroscopy

* Now with The Dow Chemical Co., Midland, Michigan.

[1] Alexander and Faessler, Zeits. f. Physik **68**, 260 (1931).

[2] Lundquist, Zeits. f. Physik **77**, 778 (1932); **83**, 85 (1933).

[3] Valasek, Phys. Rev. **43**, 612 (1933); **47**, 896 (1935).

[4] Privault, Ann. de physique **5**, 280 (1936).

[5] Yoshida, Inst. Phys. Chem. Res. Tokyo **20**, 298 (1933).

[6] Tanaka and Okuno, Jap. J. Phys. **9**, 75 (1934); **10**, 1 (1935); **10**, 45 (1935).

[7] Tanaka and Okuno, Proc. Phys. Math. Soc. Jap. **17**, 540 (1935).

[8] Cauchois, J. de phys. et rad. (7) **3**, 320 (1932).

[9] Meyer, quoted in Siegbahn, *Spektroskopie der Röntgenstrahlen*, second edition (Springer, Berlin, 1931), p. 355.

[10] Williams, Phys. Rev. **44**, 146 (1933).

[11] Johansson, Zeits. f. Physik **82**, 507 (1933).

[12] DuMond and Kirkpatrick, Phys. Rev. **35**, 136 (1930).

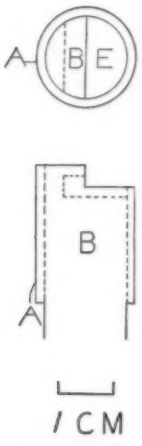

FIG. 1. Target for secondary radiation.

has not yet been reported, although Johansson did make some spectrographs with it which are reproduced in his article.

This spectrograph employs a crystal which is ground cylindrically to a radius twice that of the cylinder to which it is bent after grinding. Source of radiation, crystal and film are all placed symmetrically on a circle formed by cutting the cylinder normally with a plane. The gain in intensity over the plane crystal spectrograph is large, and it was found in practice that the focusing attainable was sufficient for accurate determination of wave-lengths of not too asymmetrical lines, so that the advantages of such an instrument for the type of work outlined above is manifest. The chief disadvantage is the lack of high resolution due to the comparatively small radius of the instrument, and the departures from perfect focusing. Another disadvantage is the greater susceptibility to breakage of the crystal, in comparison with the bent crystal of the Johann[13] type spectrograph, which may account for the lack of reports of its use in research up to this date.

II. APPARATUS

The tube was of the usual metal type, sweated into the side of the camera so that the source of radiation would lie on the focal circle, along with the crystal and film. The high voltage was applied to the filament, hence a glass insulator was

[13] Johann, Zeits. f. Physik **69**, 185 (1931).

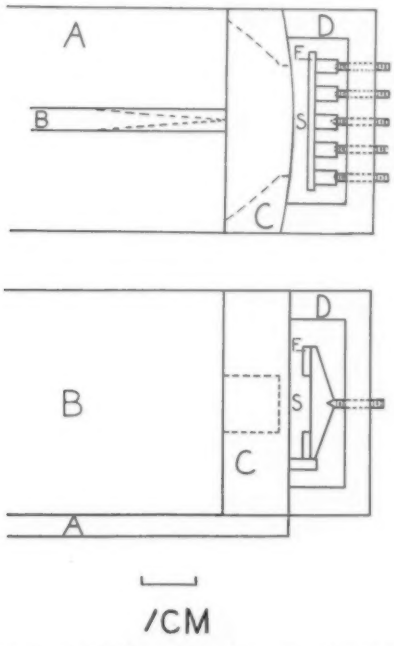

FIG. 2. Crystal holder: plan, above; elevation, below.

used in the filament assembly. In this assembly was also incorporated a piece of sylphon tubing so as to permit easy change of the location of the electron focus on the target. The construction of the target is illustrated in Fig. 1. The water-cooled portion, *B*, was surrounded by a cylinder, *A*, cut so that the primary rays caused by electrons striking at *E* could not reach the diffracting crystal. The primary rays and some scattered electrons struck the substance being studied, which was placed in the recess in *B*, and there produced secondary rays which emerged through a horizontal window covered with aluminum foil into the camera. This foil, 0.0003 in. in thickness, served to separate the high vacuum of the tube from the low vacuum of the camera, and also prevented filament light from fogging the film. It was cemented to the tube with clear glyptal lacquer.

The high vacuum was produced by a diffusion pump using Apiezon *B* oil. Apiezon grease was used on the filament and target cones; the camera cover was sealed with Lubriseal.

The crystal was of quartz, about 0.4 mm thick, ground by Bausch and Lomb to a radius of 14 in.,

FIG. 3. Typical spectrogram. From left to right, Cu $K\alpha$, Zn $K\alpha$, Cu $K\beta_1$, Zn $K\beta_1$, and Va $K\alpha$ in the first order. Enlargement about 3X. Ghost structure on long wave-length side of Zn $K\beta_1$. Zn $K\beta_{2,3}$ was visible on the original negative. Obtained from ZnS.

the radius of the focal circle being 7 in. The type of crystal holder constructed first would not give an even distribution of pressure, which resulted in the eventual destruction of the first crystal. A holder was then built along the lines of Johansson's, and is sketched in Fig. 2. *A* is the crystal arm, extending out from the inner central cone of the camera; *B* is a screen to prevent direct radiation from reaching the film, beveled in the center to make the opening to the crystal a maximum; *C* is the steel piece, cut to a 7 in. radius, against which the crystal is pressed by the screws passing through *D* and bearing against the phosphor bronze strips *F*. The opening in *C* for the radiation to strike and leave the crystal is shown with dotted lines. The crystal itself is placed in the space *S*. The four parts *A*, *B*, *C*, and *D* are fastened rigidly together with screws before the bending is begun. This apparently produced no large deformation of the cylindrical surface, as good focusing has been obtained, marred to a certain extent by the existence of easily recognizable "ghosts." The crystal was etched in 48 percent HF for 24 hours at 20°C before being bent. Both the first and second crystals purchased had corners crack off during or immediately after this operation. The second crystal cracked once after having been in place three months, the larger of the two pieces then remaining was bent and has now been in place a year without breaking. Its original dimensions were 2×3 cm, while the opening in *C* is 1×2 cm.

The film holder is provided with a plate drawn up against the film by springs; the film is thus also pressed to a cylindrical surface of 7 in. radius. This type of construction was used by Sandstrom.[14] The opening in the film holder is about 1×6 cm, permitting more than the wave-length spread allowed by the range in angle subtended at the crystal by the extended source to be photographed.

III. OPERATION

The substance to be studied was placed in the recess in the target and left there until well pumped out, before turning the power on. Most of the work was done at 25–30 kv and 5–10 milliamperes. Exposures ranged from 10 to 30 hours for the faintest lines. The crystal was set so that the central angle between its center and the center of the target was twice the Bragg angle in the second order for the $K\beta_1$ line, and the film holder was then set so that its center was as far from the crystal center as the crystal was from the target. Eastman Process film, developed in solution D–19, was used to give good contrast.

Determination of wave-lengths was carried out by the same interpolation process used by Sandstrom,[14] positions of the apparent centers of the lines being measured with a Gaertner comparator. The reference lines were nearly all $K\alpha$ lines, fairly narrow and symmetrical, so that the dis-

TABLE I. *Wave-lengths of the $K\beta_5$ line in the metals in X.U.*

	Present work	Siegbahn
26 Fe	1740.80±5	1740.80
27 Co	1605.65±5	1605.62
28 Ni	1485.58±5	1485.61
29 Cu	1378.0±2	1378.24
30 Zn	1281.7±1	1281.07
		1281.2

[14] Sandstrom, Nova Acta Reg. Soc. Sci. Upsaliensis (4) **9** (1935).

persion could be measured accurately, but many of the lines studied were wide and asymmetrical, so that the wave-lengths obtained are not those of the peak intensity. The dispersion varied somewhat from film to film, of course, due to varying shrinkage of the film, but wave-lengths of "good" lines were reproducible consistently to the accepted values. The limit of error in any determination was estimated from the spread in values obtained in measuring, and from the consistency of results from different spectrograms. All results were checked on at least two spectrograms.

An enlargement of a typical spectrogram, obtained with ZnS, is shown in Fig. 3.

As a check on the method, wave-lengths of the $K\beta_5$ were first obtained from the metals. Good results were secured except for Cu and Zn. In Cu the $K\beta_5$ line is highly asymmetrical; in Zn the $K\beta_2$ and $K\beta_5$ could not be visually resolved, because of the low resolution of the spectrograph and the closeness and high natural widths of the lines. The wave-lengths of other lines are often somewhat different from the peak values given by Bearden and Shaw,[15] but check well with the photographically determined values given by Siegbahn. When studying Ni and Zn, a Mo filament was used to eliminate the W lines which would otherwise have obscured lines being studied.

These results with the metals are listed in Table I, along with Siegbahn's values for comparison. The two values for Zn are those of the $K\beta_2$ and $K\beta_5$ peaks as determined by Bearden and Shaw.

IV. Results

The compounds studied were: FeS_2, CoS, NiS, Cu_2S, and ZnS. Pyrites and marcasite, cubic and orthorhombic crystals respectively, were the source of FeS_2. Results from both were the same. Cu_2S was studied in the form of chalcocite; ZnS, wurtzite. These minerals were ground into shape to fit into the recess in the target.

NiS and CoS were obtained by precipitation with H_2S from ammoniacal $NiCl_2$ and $CoCl_2$ solutions; they were dried in vacuo and then pressed into semi-cylindrical pills which fit into the recess. With these last two compounds it was necessary to hold the current and voltage down to 5 mills and 25 kv, otherwise they would disintegrate leaving a magnetic residue in the recess. Spectrograms obtained under that condition gave the same results as the metal.

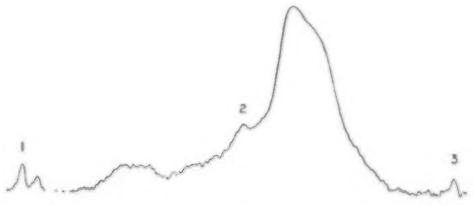

FIG. 4. Microphotometer trace showing the Ni $K\beta_5$ (designated as 2).

With the sulfides of Fe, Co, Cu and Zn no difficulty was experienced in determining wave-lengths to within the same limit of error as in the metal. With NiS, however, five spectrograms gave a mean wave-length of 1485.5 ± 2, the error thus being much larger than in the metal. Three of these films were therefore microphotometered, two traces, each at a different point, being made of each film. Four of these traces showed a definite peak for the $K\beta_5$; one of the traces is shown in Fig. 4. The Zn $K\alpha_1$ is marked 1, the Ni $K\beta_5$, 2, and the Cu $K\alpha_1$, 3. Wave-lengths of the point of inflection on the short wave-length side of 2 and of the two peaks of 2 were determined by measuring the trace in a two way Société Genêvoise measuring engine and then applying the same interpolation process used on the originals. The point of inflection appeared on two traces as a peak, and the long wave-length component appeared on one trace as a point of inflection. The values found checked within ± 0.1 X.U., but because of possible systematic errors in the microphotometer the limit of error was set at ± 0.2 X.U.

A microphotometer trace of a spectrogram taken with Cu_2S is reproduced in Fig. 5. The lines marked 1 and 3 are the comparison lines Ti $K\alpha_1$ in the first order, and Zn $K\alpha_1$ in the second order; 2 is the Cu $K\beta_5$. The mean peak wave-length from several traces was 1378.2 ± 2, checking with the known peak wave-length in the metal.

A line believed to be the same as the $K\beta_5'$ of Yoshida[8] was observed with Cu_2S at 1381.0 ± 2; the $K\beta''$ was obtained with CoS at 1610.1 ± 2. The rest of the results are contained in Table II,

[15] Bearden and Shaw, Phys. Rev. **48**, 18 (1935).

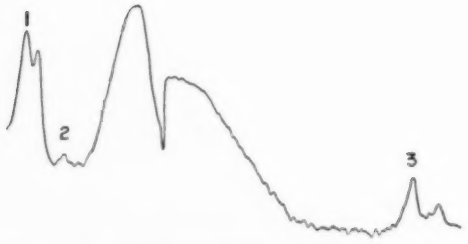

FIG. 5. Microphotometer trace showing the Cu $K\beta_5$ (designated as 2).

the corresponding values given by Siegbahn for the metals being listed for comparison.

V. DISCUSSION

Previous work on the effects of chemical combination on emission spectra has been done chiefly on elements of lower atomic number.

Karlsson,[16] using a concave mica crystal in the Johann manner, with direct bombardment, studied the $K\alpha$ and $K\beta$ lines of the metals in refractory compounds of 12 Mg, 13 Al, and 14 Si. A considerable effect of chemical combination was evident.

The $K\alpha$ lines of sulfur have been studied by Faessler,[17] Lundquist,[2, 18] Valasek,[3] and Parratt.[19] The general effect noticed was a shift to longer wave-length in the sulfides and to shorter wave-length in the sulfates. Parratt followed the disintegration of compounds under direct bombardment by noting the change in the $K\alpha$ pattern.

Lundquist[2] found a shift to shorter wave-length of the $K\alpha$ lines of 17 Cl when in chemical combination.

Valasek[3] studied the $K\beta$ pattern of 16 S in the sulfides of this research and in the sulfides of the alkali earths; he also measured the shifts of the $K\beta_1$ of 19 K and 17 Cl in the potassium halides and alkali chlorides. Lundquist,[20] however, with primary radiation, found no shift in the $K\beta_1$ and $K\beta''$ of 19 K, possibly due to the change of each compound to the oxide, similarly to what Wetterblad[21] found with 20 Ca.

Shifts in the $K\beta_5$ have been reported by Wetterblad[21] in 20 Ca and 25 Mn, and by Yoshida[5] in 22 Ti, 24 Cr, and 25 Mn. Yoshida also reported no shift in the $K\beta_5$ of Co in Co_3O_4, and no shift in the $K\beta_1$ of Ti, Cr, Mn, and Co within a limit of error of ± 0.3 X.U. Privault,[4] on the other hand, reported no shift in either the $K\beta_1$ or the $K\beta_5$ in Cr and Mn.

Within a limit of error of ± 0.2 X.U., Tanaka and Okuno[6, 7] found shifts in both the $K\beta_1$ and $K\beta'$ of Cr, Mn and Fe in various compounds, which shifts had a total range of 0.7 X.U. In particular, in FeS_2, where a direct comparison with the results of the present research may be made, they found a wave-length of 1753.43 for the $K\beta_1$, and reported the $K\beta'$ as a band. While the present results did not show the $K\beta'$ as a sharp line, nevertheless it was distinct from the $K\beta_1$ and measurable with, for this research, a rather large limit of error. That the cause of the discrepancy does not lie in a possible reduction of the FeS_2 to Fe is shown by the fact that the $K\beta_5$ has shifted. Possibly either their compounds or those of the author were sufficiently impure to account for the difference in the results.

Shearer,[22] with primary radiation and the same spectrograph Karlsson used, found no shift or change in the $L\alpha$ and $L\beta$ of Ni from the oxide and sulfide of nickel. His limit of error was of about the same order as the effects reported here for the $K\beta_5$ of Ni, which may account for his results. However, since NiS decomposes so easily, as was demonstrated in the present work, it would seem more probable that his NiS decomposed as soon as the power was turned on, thus giving him the spectrum of the pure metal.

Roseberry and Bearden,[23] using primary radiation with a double crystal spectrometer, found no

TABLE II. *Wave-lengths in X.U. of the Kβ lines of 26 Fe–30 Zn in their sulfides.* The first column under each heading gives the results of the present work in the sulfides, the second column gives Siegbahn's values for the metal.

	$K\beta'$		$K\beta_1$		$K\beta_5$	
26 Fe	1756.6±2	1756.46	1752.99±5	1753.01	1741.3±1	1740.80
27 Co	1620.1±1	1620.11	1617.42±5	1617.44	1605.7±1	1605.62
28 Ni		1499.10	1497.01±5	1497.05	1485.4±2 1485.9±2 1486.6±2	1485.61
29 Cu				1389.35	1377.9±2	
30 Zn			1292.52±5	1292.55	1281.7±1	

[16] Karlsson (Flemberg), Zeits. f. Physik **88**, 76 (1934); **96**, 172 (1935).
[17] Faessler, Zeits. f. Physik **72**, 374 (1931).
[18] Lundquist, Zeits. f. Physik **89**, 274 (1934).
[19] Parratt, Phys. Rev. **49**, 14 (1936).
[20] Lundquist, Zeits. f. Physik **33**, 901 (1925).
[21] Wetterblad, Zeits. f. Physik **42**, 603 (1927).
[22] Shearer, Phil. Mag. **20**, 133 (1935).
[23] Roseberry and Bearden, Phys. Rev. **50**, 204 (1936).

effect on the width, intensity or asymmetry of the $K\beta_5$ lines of the metals in the oxides of Ti, Cr, Mn, Fe, and Zn. Unfortunately they made no wave-length determinations, so no attempt at a comparison between their work and this is possible.

Attempts to explain theoretically these effects have been made by Wentzel,[24] Stelling,[25] Aoyama, Kimura and Nishina[26] and Pauling.[27] The theory of Pauling was applied with considerable success by Valasek[3] to a calculation of the second ionization potential of K, and the electron affinity of the Cl ion, but with no success to a calculation of the electron affinity of the S ion. A similar attempt can be made to calculate the second ionization potential of Cu from the present results.

According to Pauling, the term value $h\nu$ of an electron in an ion of an ionic lattice bears the following relationship to the term value $h\nu_0$ in the free ion:

$$h\nu_0 = h\nu - (\pm e\varphi - E_c)$$

where φ is the lattice potential as determined from Madelung's formula or the Born cycle, $+\varphi$ being used for negative ions and $-\varphi$ for positive ions; $E_c = -0.8 \times 6.43 \times 10^6 \kappa$ volts, where κ is the volume specific diamagnetic susceptibility. Of the compounds studied, the only one given by Wyckoff[28] as forming an ionic crystal is Cu_2S. It has the same structure as CaF_2. The constants of the Madelung formula, $\varphi = Ae/r$, as given by Sherman[29] and Wyckoff are:

$$A = 11.64 \qquad r = 5.59.$$

TABLE III. *Term values of the outermost electrons of 26 Fe–30 Zn in their sulfides.*

	K_∞	$K\beta_5$	ν/R-compounds	ν/R-pure metal
26 Fe	1738.9	1741.3	0.73	0.4
27 Co	1602.9	1605.7	1.01	0.5
28 Ni	1483.1	1485.4	0.95	0.7
		1485.9	1.15	
		1486.6	1.44	
29 Cu	1376.8	1377.9	0.58	0.4
30 Zn	1280.1	1281.7	0.90	0.9

The value of the mass susceptibility is taken from the International Critical Tables and is -0.18×10^{-6} c.g.s. units. The density of Cu_2S is 5.6 g/cc. Using these constants we find $(-e\varphi - E_c) = (-29.6 - 5.2)$ volts. The term value of the levels in which the $K\beta_5$ line has its origin may be obtained from the wave-length of the $K\beta_5$ and the K edge as measured by Lindh[30] for CuS. Presumably the edge would be in about the same position as in Cu_2S, within a difference not significant to this problem at least. This edge is at 1376.8 X.U., giving $h\nu$, the term value of the outermost electrons of the Cu ion in Cu_2S, as 7.9 volts, so that the second ionization potential of Cu would be $7.9 - (-34.8)$ volts, or 42.7 volts. Sherman[29] lists it at 20 volts, so the theory is seen to break down completely in this application. Evidently some term, not important in the potassium halides or the alkali chlorides but important in Cu_2S, is missing from the formula. This ought not be a term to take care of polarization, however, for the lattice potentials as determined by the Madelung formula and by the Born cycle differ by but 11 percent, whereas the $e\varphi$ term of our formula would have to be decreased to a fourth of its present value to bring about agreement.

The ν/R values in Rydberg units of the outermost terms of the metals in the sulfides are listed in Table III, together with the corresponding term values for the pure metals, taken from Siegbahn. Again it is true that the edges in the actual compounds studied have not been measured, but since the edge does not change much for all compounds in which the metal has the same valence, the average of De Boer's[31] values for Co^{2+} have been taken, and those of Lindh[30] for Ni^{2+} and Zn^{2+}. For lack of anything better, Lindh's[30, 32] data for FeS and CuS have been used in the case of iron, and copper.

Table III shows that the average binding of the outermost electrons in Cu and Zn in their sulfides is about the same as in the pure metal, whereas in the other three elements it is somewhat greater. The average bindings of the corresponding electrons in S in the sulfides, when calculated from the data of Valasek[3] and Lindh,[32]

[24] Wentzel, Naturwiss. **104**, 64 (1922).
[25] Stelling, Diss. Lund (1927).
[26] Aoyama, Kimura and Nishina, Zeits. f. Physik **44**, 810 (1927).
[27] Pauling, Phys. Rev. **34**, 954 (1929).
[28] Wyckoff, *Structure of Crystals* (Chemical Catalog Co., New York, 1931).
[29] Sherman, Chem. Rev. **11**, 93 (1932).
[30] Lindh, Zeits. f. Physik **63**, 106 (1930).
[31] De Boer, Arch. Neerl. Sc. (3A) 10, 101 (1927).
[32] Lindh, *Handbuch der Exptl. Physik* XXIV, 2. Teil, p. 291. (Ak. Verlagsg. M. B. H., Leipzig, 1930).

are much less, showing that the $K\beta_5$ of the metals and the $K\beta_1$ of S do not have their origin in levels in the lattice common to both atoms. In addition, in the cases of Co, Cu and Zn, the multiplicity observed by Valasek in the S lines does not have its counterpart in the corresponding line of the metals.

ACKNOWLEDGMENTS

The writer wishes to acknowledge his indebtedness to Dr. Joseph Valasek, who suggested the problem, and whose advice and criticism have been invaluable in the carrying out of the research; and to Mr. Christian Dane, machinist, for his careful construction of the apparatus.

OCTOBER 15, 1936 PHYSICAL REVIEW VOLUME 50

The Ultraviolet Absorption Spectrum of Ammonia

III. The Absorption Spectra of the Deuteroammonias. A Note on Rydberg Series in Ammonia

A. B. F. DUNCAN, *Department of Chemistry, Brown University*

(Received June 22, 1936)

The absorption spectrum of mixtures of ND_3, ND_2H, and NDH_2 has been obtained from 2200 to 800A in a normal incidence vacuum spectrograph with a dispersion of about 8.5A/mm. The spectrum above 1675A (the end of the first electronic transition) is made up of very diffuse bands. Below 1675 all the bands are sharp. Two electronic transitions are found between 1675 and 1220A. Each electronic transition is accompanied by many vibrational transitions. Relatively long v' progressions are found for each of the molecules. Evidence for a fourth electronic state below 1220A was found, but no analysis of the bands could be made. Only one excited state frequency appears for each molecule. This is most probably the parallel deformation frequency, which is also the only frequency found for ammonia in the ultraviolet. The numerical values of the frequencies were calculated from ammonia frequencies in corresponding excited states considering changes in mass alone, and agreed with experiment. The electronic terms for the excited states were also calculated. A discussion is given of a possible Rydberg series in ammonia.

THE absorption spectrum of ammonia has been photographed[1] in the region between 2300 and 850A, with a dispersion of 8.5A/mm. Part of the spectrum between 1620 and 1450A was recently studied[2] with much higher dispersion (1.3A/mm) and the rotational structure resolved and analyzed.

The present experiments were made with a sample of ND_3 gas given us by Professor H. S. Taylor of Princeton University and prepared in his laboratory. A preliminary report has been made on this work.[3] The sample, received in a glass bulb provided with an inner seal, was connected to the vacuum spectrograph through two small volumes separated by stopcocks. By use of these calibrated volumes the pressure of heavy ammonia was varied from 0.014 to 0.70 mm in the spectrograph, which was cut off from the pumps during exposures. At lower pressures no absorption could be observed, and no additional bands appeared between 0.28 and 0.70 mm pressure. The light source was the Lyman continuum operated as described previously.[4] The exposure times were ten seconds to two minutes on Hilger Schumann plates. These plates do not give as good contrast in our experience as Eastman III-O oiled with Nujol, but they were about twenty times as fast, and we wished to avoid as far as possible exchange reactions of ND_3 in the spectrograph. Several photographs of pure NH_3 were made on each plate at corresponding pressures for visual comparisons of intensity, and as a general check on the accuracy of measurement.

The measurement of ammonia bands on these plates agreed within experimental error with previous work. All bands reported here have been measured on at least two photographs, some on as many as twelve. The accuracy of measurement is considered to be 5–15 cm^{-1} for

[1] A. B. F. Duncan, Phys. Rev. **47**, 822 (1935).
[2] A. B. F. Duncan and G. R. Harrison, Phys. Rev. **49**, 211 (1936).
[3] A. B. F. Duncan, Phys. Rev. **47**, 886 (1935).
[4] Noyes, Duncan and Manning, J. Chem. Phys. **2**, 717 (1934).

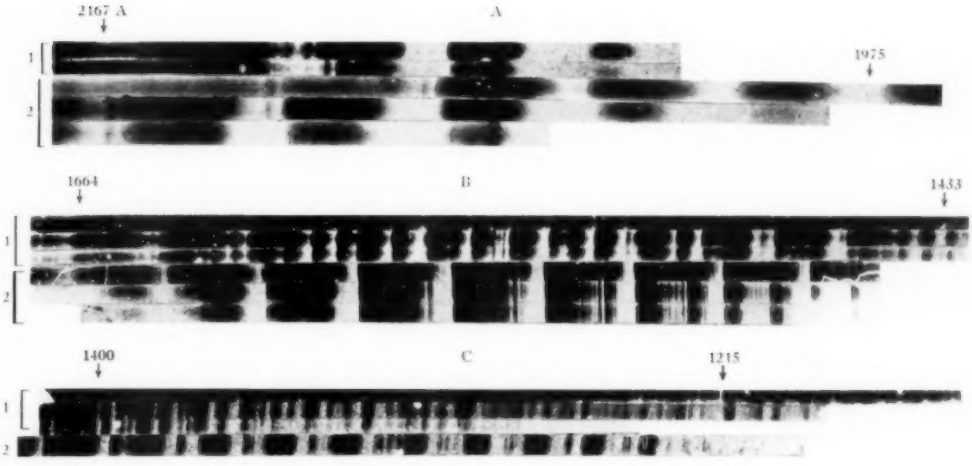

FIG. 1. A(1) ND_3, etc. 0.3, 0.5 mm. (2) NH_3, 0.4, 0.7, 1.0 mm; B(1) ND_3, etc. 0.1, 0.2, 0.5 mm, (2) NH_3, 0.2, 0.4, 0.5 mm; C(1) NH_3, etc. 0.02, 0.04, 0.07 mm, (2) NH_3, 0.01 mm.

sharp bands, and 20–50 cm^{-1} for the diffuse bands.

The general appearance of the spectra is shown in Fig. 1, which was made from enlarged reproductions (about ten diameters) of parts of representative plates. Parts of the ammonia spectrum are included for comparison.

The spectrum appears much too complicated to be due solely to ND_3, whose spectrum should not be unlike that of NH_3. Accordingly the presence of ND_2H and NDH_2 was suspected. This is confirmed by a detailed study of the spectrum. Whether these molecules were formed by exchange with hydrogen compounds in the spectrograph is not known, and the errors caused by contact with wax and stopcock grease cannot be avoided in any case, since we have been unable to operate the set up with an outside absorption column.

The data obtained in the region 1664–1248A are the most complete and certainly the most accurate. Two electronic transitions occur in this region, called those to the second and third electronic states.

Results and Discussion

The first electronic transition (2167–1675A)

The bands here are mostly of the predissociation type. The first part of this region has been studied by Benedict.[5] In ammonia the bands could be arranged satisfactorily in a progression in spite of the predissociation. In the present case it would not be safe to try this, due to the presence of at least three kinds of molecules, for an observed absorption maximum may be due merely to a coincidence of the weaker parts of several bands. The bands, or rather absorption maxima are given in Table I.

The origin of the system is taken to be 46,167 ± 30 cm^{-1}. The maximum of intensity for the whole system is at about 51,000 cm^{-1}. As Fig. 1 (A) shows the bands above 2100A have some structure. 46,167 does not reproduce well, but appears single headed on the plates. The next three bands are narrow, but weak. The next six bands have fairly sharp edges and all six appear associated in some way. Of these, the strongest is

TABLE I. *Bands between 2167 and 1675A.*

46167	47932	54061
46479	48202	54880
46583	48764	55735
46742	49562	57357
46999	50496	57931
47039	51280	58265
47102	51547	58737
47197	52167	59108
47292	52582	59769
47402	53131	59985

[5] W. S. Benedict, Phys. Rev. **47**, 641 (1935).

TABLE II. *Bands of second electronic transition.*

v	NDH_2 calc.	NDH_2 obs.	ND_2H calc.	ND_2H obs.	ND_3 calc.	ND_3 obs.
0	60113	60133	60083	60081	60071	60081
1	60992	60974	60892	60911	60795	60792
2	61883	61869	61710	61690	61525	61516
3	62788	62788	62538	62533	62263	62255
4	63706	63715	63375	63368	63007	63005
5	64636	64641	64221	64223	63757	(63765)*
6	65580	65586	65076	65080	64515	64521
7	66536	66533	65941	65947	65279	65287
8	67506	67513	66815	66821	66049	66047
9	68488	68481	67698	67699	66827	(66821)
10			68590	68582	67611	(—)
11			69492	69486	68401	68411
12					69199	69187
13					70003	70027
14					70814	70850

* Obscured by NDH_2 63,715.

47,197. All the bands following have no structure at the lowest pressure, and the centers are given.

The second electronic transition (1664–1412)

All the bands belonging to this transition are sharp, and at the low dispersion used show heads on the ultraviolet side. In spite of the somewhat complicated appearance of the spectrum it was possible to pick out by inspection two upper state progressions on the basis of appearance and intensities of the bands. They fit the following formulas, obtained from a least squares solution:

$$\nu_{NDH_2}=60{,}133+872n+6.48n^2, \quad (n=0,\ 1,\ 2,\ 3\cdots), \quad (1)$$

$$\nu_{ND_2H}=60{,}083+804n+4.64n^2 \quad (n=0,\ 1,\ 2,\ \cdots). \quad (2)$$

All the remaining bands then fitted into a third series represented by

$$\nu_{ND_3}=60{,}071+721n+3.33n^2, \quad (3)$$

except one weak band, 64,003, which is probably due to NH_3 since a strong band in the spectrum of the latter is at 64,017. Here this band has about 0.01 the intensity of neighboring bands. The bands represented by these formulas are considered due to the molecules NDH_2, ND_2H and ND_3. The observed frequencies together with those calculated by Eqs. (1)–(3) are given in Table II.

It is evident that only one frequency appears for each molecule, which in each case corresponds to the lowest fundamental frequency of the molecule. The normal state values of these frequencies are known from recent work[6] to be (taking the mean of the double frequencies) 746.5 (ND_3), 813 (ND_2H), 884 (NDH_2) and 950 (NH_3). If we assume simple ratios between normal state and excited state frequencies such as

$$\omega''_{ND_2}/\omega''_{NH_2}=\omega'_{ND_2}/\omega'_{NH_2}$$

we may estimate the excited state frequencies for the heavy ammonias from the previously found frequencies of NH_3. The results for this electronic state are given in Table III.

This calculation gives us some confidence both in regard to the assignment of the bands and in the simple dependence of the frequencies on the masses alone, implied in the above calculation. It follows that the excitation of an electron in these four molecules has at least no large specific effect on the frequencies of vibration. Such a calculation should be based on infinitesimal frequencies rather than on those observed which are of finite amplitude. The agreement in spite of this fact must be due to the fact that the anharmonic corrections are all of the same order of magnitude.

The frequencies of the pure electronic transitions in the isotopic molecules are of some interest, but to be rigorous we must know the zero point energies for both states. Since only one of the four (six in the case of ND_2H and NDH_2) frequencies appears in the excited states for each molecule, this energy cannot be determined. If the assumption is made that the absent vibration frequencies are unchanged in the excited states, the zero point energies due to them cancel and we may write Eqs. (1)–(3) in the form

$$\nu=\nu_e+\omega_1'(v'+\tfrac{1}{2})+x_1'\omega_1'(v'+\tfrac{1}{2})^2 -\omega_1''/2-x_1''\omega_1''/4$$

TABLE III. *Estimated and observed excited state frequencies for the heavy ammonias.*

M	Ratio $\omega''_M/\omega''_{NH_3}$	$\omega'_{calc.}$	$\omega'_{obs.}$
NH_3	1		936
ND_3	0.78579	736	721
ND_2H	0.85579	801	804
NDH_2	0.93053	871	872

[6] E. F. Barker and M. Migeotte, Phys. Rev. **47**, 702 (1935).

TABLE IV. *Bands of third electronic transition.*

	NDH_2		ND_2H		ND_3	
v	calc.	obs.	calc.	obs.	calc.	obs.
0	69768	69786	69764	69786	69791	69786
1	70614	70609	70546	70528	70485	(—)
2	71480	71466	71344	71345	71192	71201
3	72364	72337	72156	72152	71915	71918
4	73268	73252	72982	72976	72653	72656
5	74190	74201	73824	73811	73406	73379
6	75132	75167	74680	74682	74174	(74201)*
7	76092	76110	75550	75548	74957	74923
8	77071	77052	76435	76449	75755	75776
9	78070	78059	77335	77327	76568	76555
10	79087	79064			77332	(77327)**
11	80123	80112				
12	81179	81223 (?)				

* Used also for NDH_2.
** Used also for ND_2H.

x_1'' is not known but $x_1''\omega_1''/4$ is probably small. The equations are then

$$\nu_{NH_3}=60{,}135+936(v'+\tfrac{1}{2})+7.22(v'+\tfrac{1}{2})^2-475, \quad (4)$$

$$\nu_{NDH_2}=60{,}117+866(v'+\tfrac{1}{2})+6.48(v'+\tfrac{1}{2})^2-442, \quad (5)$$

$$\nu_{ND_2H}=60{,}087+800(v'+\tfrac{1}{2})+4.64(v'+\tfrac{1}{2})^2-407, \quad (6)$$

$$\nu_{ND_3}=60{,}083+717(v'+\tfrac{1}{2})+3.33(v'+\tfrac{1}{2})^2-373. \quad (7)$$

This gives a spread of 52 cm^{-1} in the electronic terms of the four molecules which may probably be attributed mainly to error in the assumption made above in regard to the zero point energies.

The maxima of intensity in the progressions occurs for ND_2H and NDH_2 at $v'=6$ and for ND_3 at $v'=6$ or 7. The intensities of corresponding bands of ND_2H and NDH_2 appear very nearly equal. The bands of ND_3 appear to have about $\frac{2}{3}$ the intensity of the others. Whether this is due to the composition of the sample would have to be determined by measuring the absorption coefficients of pure isotopic samples.

The third electronic transition (1433–1248A)

Bands belonging to this transition are also sharp and are more crowded together since the vibrational frequencies are smaller. The electronic transition as a whole is much stronger than the one preceding. The intensity is about equal to that of the first electronic transition as judged by the values of the pressure at which corresponding bands first appear. The same is true of the corresponding transitions of ammonia.

TABLE V. *Bands below 1220A.* In the bands marked *V* the *red* edge was measured. In the other cases the ultraviolet edge was measured.

82017 ?	83764	85732
82111 ?	83980	86272
82361	84078	86613
82806	84391 *V*	86798
83186	84838 *V*	87483
83480 *V*	85406	

Three progressions are also found here, belonging to the three molecules NDH_2, ND_2H, and ND_3. A few of the strongest ammonia bands also appear weakly in this region. *All* the bands not positively identified with NH_3 fit one of these three formulas:

$$\nu_{NDH_2}=69{,}786+837n+9.50n^2, \quad (8)$$

$$\nu_{ND_2H}=69{,}764+775n+7.32n^2, \quad (9)$$

$$\nu_{ND_3}=69{,}791+686n+7.50n^2. \quad (10)$$

The observed bands are given in Table IV, where the agreement with the above formulas may be seen. The frequencies for this state were calculated from the normal state ratios in Table III and are 840, 772 and 709 for NDH_2, ND_2H and ND_3, which are to be compared to the values in Eqs. (8)–(10). Here again the agreement is good for NDH_2 and ND_2H. The above equations may be written in the form of Eqs. (4)–(7) in order to compare the pure electronic terms. With NH_3 for comparison they are:

$$\nu_{NH_3}=69{,}769+902.5(v'+\tfrac{1}{2})+9.04(v'+\tfrac{1}{2})^2-475, \quad (11)$$

$$\nu_{NDH_2}=69{,}794+827.5(v'+\tfrac{1}{2})+9.50(v'+\tfrac{1}{2})^2-442, \quad (12)$$

$$\nu_{ND_2H}=69{,}785+768.0(v'+\tfrac{1}{2})+7.32(v'+\tfrac{1}{2})^2-407, \quad (13)$$

$$\nu_{ND_3}=69{,}823+678.5(v'+\tfrac{1}{2})+7.50(v'+\tfrac{1}{2})^2-373. \quad (14)$$

There is here again a spread of 54 cm^{-1} between the terms of NH_3 and ND_3, but the order of the terms is reversed, i.e., $\nu_e(ND_3)>\nu_e(NH_3)$.

The maximum of intensity in any one progression is rather difficult to determine due to some overlapping of the bands, but appears to occur at $v'=5$–7 for all the molecules. The

bands of NDH_2 are noticeably stronger than those of ND_2H in this region, and the latter are stronger than those of ND_3, though the difference between the latter two is not very great. The intensity decreases rapidly on the ultraviolet side of the maximum for all three molecules though the NDH_2 bands could be followed to 80,122 cm^{-1}.

In the region 78,000–82,000 cm^{-1} emission lines in the source are troublesome and often reversed. This probably explains the failure to observe additional bands in this particular region. No way of removing these lines is possible with this source, since they are due to C, and to Si and O from the glass.

The spectrum below 1220A

A list of these bands is given in Table V. Three (marked *V*) are different from all other bands of this spectrum in being shaded to the ultraviolet. The emission lines here are not troublesome but the bands overlap considerably. This is thought to be due to the beginning of a fourth excited electronic state corresponding to the ammonia state with origin 82,857 cm^{-1}. Since strong continuous absorption begins just below 87,000 the existence of progressions could not be established because of too few members. Obviously higher dispersion is needed to resolve the structure in this region. The existence of a discrete band at 87,483 cm^{-1} shows that the ionization potential is probably larger than a value calculated from this figure.

A Note on Rydberg Series in Ammonia

The analysis of the spectra of the heavy ammonias has confirmed all our previous analysis of the spectrum of NH_3. In particular a doubt previously expressed[7] about the independent existence of the second electronic state has been removed. However, if the electron in all these states is a nearly nonbonding $[2a_1]$ electron,[8] these electronic states should fit into a Rydberg series. The writer tried without success to fit the *electronic* terms of the four states into a series, the values used being 46,157, 60,135, 69,769 and 82,857. No two of these values will fit even approximately into a series which converges at the correct ionization potential, taken as 11.3 ev.

Using, however, the maxima of intensity in the four states we have the values 52,501, 65,025, 77,628, and 84,872. It can now be shown that the first, third and fourth of these fit reasonably well in a Rydberg series which converges at about 11.5 ev. The equation for the series is

$$\nu = 93{,}380 - R/(n-0.362)^2 \quad n = 2, 3, 4$$

and the calculated values are 52,480, 77,611, and 85,088. The differences between these values are 25,131 and 7477 cm^{-1} which may be compared with the differences 20,349 and 6190 between 3*s*, 4*s*, and 5*s* in the normal nitrogen atom. This analogy is not stressed however, and may even be wrong.

If this series has a reality, a difficulty is raised concerning the second electronic state, which does not fit into the series. It cannot be regarded as a continuation of the first electronic transition with origin at 46,157 cm^{-1}. The bands are definitely parallel (from the rotational analysis) and so the selection rules (electronic times vibration) give for this state A_1 if the normal state is taken as $^1A_1$. The transition $A_1 \rightarrow E$ is not consistent with definitely parallel bands. The first electronic transition has been considered by Mulliken to be to an $^1A_1$ state and if the series is real the third and fourth are also to $^1A_1$ states. So we have apparently an extra A_1 not related to the other excited $^1A_1$ states. Possibly the transition is to a $^3A_1$ state corresponding to the $^1A_1$ state with origin 69,769, following a suggestion of Mulliken.[8] The transition is much weaker than 69,765 as might be expected from a transition involving a change of multiplicity.

The writer expresses his gratitude to Professor H. S. Taylor for the sample of heavy ammonia, and to the Warren fund of the American Academy of Arts and Sciences for financial aid during the progress of this work.

[7] Reference 1, page 827.
[8] R. S. Mulliken, J. Chem. Phys. **3**, 506 (1935).

Optical Absorption by the Alkali Halides

J. C. SLATER AND W. SHOCKLEY, *Massachusetts Institute of Technology, Cambridge, Massachusetts*

(Received August 12, 1936)

The relations are investigated between three types of theory for explaining absorption of light by ionic crystals: absorption by independent atoms or ions, absorption according to Frenkel's excitation waves, and absorption according to energy bands and lattice functions, as used in the theory of metals. It is shown that each method leads to a set of unperturbed wave functions, which are related to each other by linear combinations, and that no one set is correct at the actual distance of separation in the crystal. Instead, combinations must be used, leading both to continuous absorption as in the energy bands, and to one or two discrete lines in connection with each continuum, as in absorption by independent atoms or in excitation waves. These conclusions are compared with experiment, explaining in a general way the sharp structure observed both in the near and far ultraviolet absorption spectra of these crystals. The discussion deals throughout with the undistorted crystal, leaving out of account the new absorption bands which are known to appear in these crystals after considerable illumination, resulting from the deposition of free alkali in the crystal.

THE electronic energy levels in the alkali halides have been the subject of much study in recent years. Experimentally, Hilsch and Pohl[1] and students of Pohl have made elaborate studies of the ultraviolet absorptions of these crystals, and also of the photochemical processes resulting from the absorption of light, including blackening of the crystal by deposit of free alkali, and subsequent photoconductivity when the crystal is illuminated with visible light. More recently, Smith[2] and O'Bryan[3] have studied the absorption of a few of the crystals further in the ultraviolet. On the theoretical side, Hilsch and Pohl[1] have proposed a simple theory giving the position of the first ultraviolet absorption edge in terms of the lattice spacing, the ionization potential of the alkali, and the electron affinity of the halogen, following an earlier and less satisfactory theory of Wolf and Herzfeld.[4] Frenkel[5] has discussed the general problem of the absorption of light by crystals, though without detailed application to these particular crystals. von Hippel,[6] in a paper which is now in proof, has carried further the type of argument used by Wolf and Herzfeld, Hilsch and Pohl, coming in some particulars to results in agreement with the present paper. Very recently Ewing and Seitz[7] have applied to LiF, and Shockley[8] to NaCl, the general type of theoretical analysis which has been used with success for the energy bands in metals. A number of other workers have contributed to the field, additional references being given in the paper of von Hippel.

Three different points of view are found among the references just mentioned. The first might be called the atomic method, in which excitation is supposed to be an act confined to a single atom or ion. This method makes close connections with the well-known electrostatic theory of ionic crystals, and is the simplest mathematically and the easiest to understand. It has been used by Hilsch and Pohl, Wolf and Herzfeld, and von Hippel. The second method is that of excitation waves, in which the excited electron is no longer localized on a particular atom or ion, but is allowed to wander through the crystal. This has been employed by Frenkel. Third is the method of lattice functions, in which each electron of the crystal is supposed to be in a modulated wave traveling through the crystal, as in the theory of metals. The method has been applied to insulators by Wilson[9] and others, and is that used by Ewing and Seitz and Shockley. It is the purpose of the present paper to investigate the relationships of these three methods, and to see which is

[1] Hilsch and Pohl, Zeits. f. Physik **59**, 812 (1930).
[2] A. Smith, Phys. Rev. **44**, 520 (1933).
[3] H. M. O'Bryan, Phys. Rev. **49**, 944 (1936).
[4] Wolf and Herzfeld, *Handbuch der Physik* (1928), Vol. XX, p. 632.
[5] J. Frenkel, Phys. Rev. **37**, 17 (1931); **37**, 1276 (1931); Phys. Zeits. Sowjetunion **9**, 158 (1936).
[6] A. von Hippel, Zeits. f. Physik, in press. The writers are greatly indebted to Professor von Hippel for the privilege of seeing this paper before publication.
[7] Ewing and Seitz, Phys. Rev. this issue. The writers are greatly indebted to Dr. Seitz for the privilege of seeing this paper before publication.
[8] W. Shockley, Phys. Rev. this issue.
[9] A. H. Wilson, Proc. Roy. Soc. **A133**, 458 (1931); **A134**, 277 (1931).

most applicable to the actual problem. If the atomic method or the method of excitation waves is supplemented by admitting polar, or ionized, states as well as states of pure atomic excitation, it is found that the three methods represent three different sets of unperturbed wave functions, of which the correct wave functions are linear combinations. The relations between the functions are exhibited, approximations to the solution of the perturbation problem are set up, and it is shown that no one of the methods correctly represents the real state of affairs, but that two types of energy level are simultaneously present, discrete levels like those of the atomic method and a continuum as with lattice functions, agreeing with the observation of continuous absorption with sharp structure.

One feature will be entirely neglected in the present discussion, the motion of the nuclei, which we shall assume to be held in their equilibrium positions. It has been pointed out by several of the writers just quoted that excitation or ionization within the crystal will change the interatomic forces, setting the nuclei into oscillation, and that after this oscillation dies down, the excited energy level will be stabilized in such a way that the electron will not return to its normal position. In the resulting distorted position of the nuclei and electrons, the absorption frequencies will be different from those for a normal crystal. These questions are closely tied up with the mobility of the excited electrons, the blackening of the crystal by exposure to light, and the electrical conductivity of crystals illuminated by the proper wave-lengths. We shall avoid all these questions of the distorted state of the excited crystal, discussing only absorption by the normal, unblackened crystal.

Lattice Energy Levels

We begin with the method of lattice functions and energy levels, the method of Bloch. Consider a periodic lattice containing two types of ions, as an alkali halide. There are three types of energy level for an electron moving in such a potential field: for low energy, one type of wave function is concentrated around ions of one type, and has energy levels roughly like the energy levels of that ion; a second type is concentrated around ions of the second type; the third type of wave function, found at high energy, is shared between ions of both types. In general, the electrons normally present in an alkali halide crystal are of the first two types, while the third type is met in the excited states. We consider first the normal state and the energy levels normally occupied. For example, in NaCl, which we may consider as built up of Na^+ and Cl^- ions, each sodium ion contains two $1s$, two $2s$, and six $2p$ electrons, while each chlorine contains two $1s$, two $2s$, six $2p$, two $3s$ and six $3p$. Corresponding for instance to each level of a single sodium ion, there will be a band of levels in the crystal, containing as many discrete levels as there are sodium ions in the crystal. This band will be of zero width in energy as long as the ions are far apart, but as they are pushed together the band will broaden. Even at the actual distance of separation, however, the sodium ions are far enough apart in proportion to the size of the ions so that the broadening is comparatively small. Except for one fact, which we shall mention immediately, we could then derive the energy levels in such a lattice, as a function of lattice spacing, by taking the energy levels in the various ions at infinite separation, and assuming those to broaden somewhat as the ions became squeezed as they are in the crystal.

The fact which we have just mentioned, one which makes ionic crystals essentially different from metals, is that the ions are charged. In a metallic crystal, where each atom is electrically neutral, it is convenient to adjust the arbitrary zero of potential, at each lattice spacing, so that the tightly bound x-ray energy levels are independent of lattice spacing.[10] This demands that the potential in the immediate neighborhood of each nucleus (which we can adjust at will) be independent of lattice spacing. Such an adjustment is impossible in ionic crystals, for there is a difference of potential between the positive and negative ions which is a function of the distance, so that if the potential of one type of ion is made constant, that of the other type will change with lattice spacing. The most symmetrical assumption to make in this case is that the potential in the neighborhood of a positive ion, which will be negative on account of the predominantly negative charge of its neighbors, decreases as much

[10] J. C. Slater, Rev. Mod. Phys. **6**, 209 (1934); J. C. Slater and H. M. Krutter, Phys. Rev. **47**, 559 (1935).

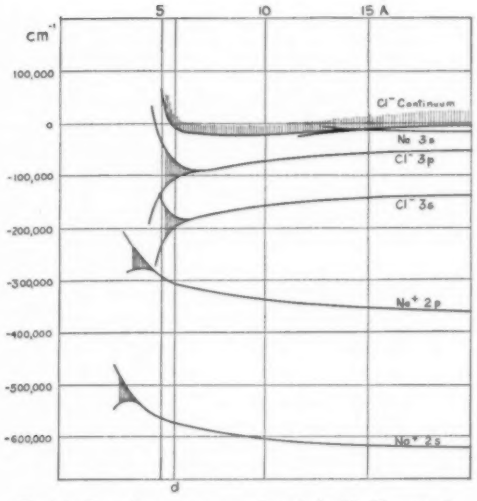

FIG. 1. One-electron energy bands in NaCl crystal.

with decreasing lattice spacing as the potential in the neighborhood of a negative ion increases. By the Coulomb law, both these variations will be inversely proportional to the lattice spacing, and we can easily get the constant of proportionality from the Madelung constant for the crystal. Thus the energy levels of an electron in this potential field will increase (on account of the negative charge of the electron) inversely proportional to the lattice spacing for those energy levels connected with positive ions, and will decrease at the same rate for negative ions, then broadening out as the ions begin to overlap, as described in the preceding paragraph.

In Fig. 1 some of these energy levels, the $2s$ and $2p$ levels of the sodium ion, the $3s$ and $3p$ of the chlorine ion, are sketched for NaCl, as a function of lattice spacing. This figure was constructed in the following manner. In the first place, the asymptotic energies were found at infinite separation from the empirical spectral terms; for the energy in a one-electron problem is an approximation to the ionization potential connected with removing the electron in question from an atom or ion. Thus the asymptotic value of Cl^- $3p$ is taken to be the negative of the energy necessary to remove a $3p$ electron from the chlorine ion, or of the electron affinity, about 30,400 cm^{-1}.[11] The value of Cl^- $3s$ differs from this by the energy necessary to raise a $3s$ to a $3p$ state in neutral chlorine. (This, as a matter of fact, has not been observed; but the corresponding energy in Cl^+ is about 94,000 cm^{-1}, in Cl^{++} about 99,000, and in Cl^{+++} about 103,000, from which we may assume that in Cl it is about 89,000 cm^{-1}, with a probable error of perhaps 8000 cm^{-1}, or about a volt.) The asymptotic value of Na^+ $2p$ is minus the energy required to remove a $2p$ electron from the sodium ion, and similarly for $2s$, the values being 381,000 and 644,000 cm^{-1}, respectively. Knowing the asymptotic energies at infinite separations, we can then add or subtract, as the case may be, the energy $3.495\ e^2/d$, where 3.495 is the appropriate Madelung number to give the electrostatic energy, d is the distance between like atoms along the axis. Expressing energies in cm^{-1}, lattice spacing in Angstroms, this becomes approximately $(405{,}000\ cm^{-1})/d$. The resulting lines represent the energy bands of zero width in the lattice. At small distances, we then allow these bands to be broadened in a plausible way. For the Cl^- $3p$ band, Shockley[8] has found the breadth at the lattice spacing of 5.63 angstroms to be approximately 35,000 cm^{-1}, the spreading being largely above rather than below the line derived from Madelung's constant. For Cl^- $3s$, the overlapping of orbits is less, so that the spreading will not start until somewhat smaller lattice spacings. The sodium bands will broaden for much the same reason as in a sodium crystal, on account of the interaction of neighboring sodiums; we have accordingly assumed the same amount of broadening of these bands that there would be in the sodium crystal with the same sodium-sodium distance. Aside from these pieces of information, the pattern of the broadened bands at small distances is merely sketched in a suggestive way, not the result of calculation.

Next, we consider the excited levels. We must first notice that, though these levels can be indicated on the same diagram as the occupied ones, a different potential field must be used to determine them. Thus for an occupied level, using an argument based on the Hartree or Fock method of approximation, the ion on which the electron is found must be assumed to lack an electron by way of compensation, though the other sodium and chlorine ions have their usual single charges. For an unoccupied state, however,

[11] Mayer and Helmholz, Zeits. f. Physik **75**, 29 (1932).

it cannot be assumed that the ion on which the electron in question happens to be found lacks an electron. If we take an atomic view of the process of excitation, an electron after excitation soon travels to another ion, eventually going to quite a different part of the crystal, finding itself on ions which have their normal charges. At large distances, then, the excited sodium-like levels will approximate those of an electron in the field of a singly charged sodium ion; that is, they will be the levels of neutral sodium. The first excited state will be the $3s$ of sodium, whose energy is given by the negative of the ionization potential, about 41,400 cm^{-1}. As the distance decreases, this energy level will rise on account of a Madelung term, broadening as atoms overlap, much as the $3s$ levels in a lattice of sodium atoms, so that at the normal distance of separation the band will be very broad, much broader than the occupied bands in the crystal.

Another feature complicates this situation, however. We have considered only excited states of sodium, not of chlorine. This is correct at large distance, for the chlorine problem in question is an electron in the field of a negative chlorine ion, which has no discrete stationary states. Of course, however, it has continuous energy levels, beginning at the energy zero at infinite separation. We consider how the bottom of this continuum changes with lattice spacing. At first sight, we might think the energy would decrease with a Madelung term, as with electrons bound to chlorine. This will not be the case, since the wave function connected with the continuum is distributed over space, and part of the charge is near chlorines, part near sodiums. As the distance decreases, the potential energy of the electron will decrease when it happens to be near a chlorine ion, increase when it is near sodium, compared to the value at infinite separation. The result will be to a first approximation no change in energy with distance, the opposing tendencies canceling. To a higher approximation, the decrease of potential energy near the chlorines will tend to concentrate the charge there, making its wave function resemble a discrete chlorine function more than at infinite separation, so that there will be some decrease of energy with distance, though not as much as for a pure chlorine level. Now it is evident from Fig. 1 that the resulting level will cross the first excited sodium level, at about the distance of separation where the sodium level begins to split up (roughly $d=15$A). There will then be an interaction of the two types of level, the resulting lower level having a wave function with appreciable charge on both chlorine and sodium ions, behaving around a chlorine like the lowest member of the continuum, around the sodium like a $3s$ electron. The level will broaden, but will neither rise as much as a sodium level would, nor fall as much as a chlorine level. A hypothetical form for the broadened level is indicated in Fig. 1.

Optical Absorption Frequencies

The energy levels of Fig. 1 may be used to investigate the optical absorption frequencies of the crystal. As always with one-electron energy levels, we may interpret an absorption as a transition of an electron from one of the lower, occupied levels to one of the higher, unoccupied ones, the energy difference in the diagram giving the absorption frequency. Thus we may expect an absorption in the near ultraviolet when a chlorine $3p$ electron is raised to the excited states; a shorter wave-length for chlorine $3s$; still shorter for sodium $2p$; and one in the very far ultraviolet for sodium $2s$. The near ultraviolet absorption should start at a frequency equal to the smallest interval between $3p$ and excited bands (roughly 60,000 cm^{-1}), with a continuum on the short wave-length side. The band is observed to start at about 1750A (57,000 cm^{-1}), and to come to a sharp peak at something less than 1600A (62,500 cm^{-1}). The chlorine $3s$ absorption should be expected at about 170,000 cm^{-1} (590A), the sodium $2p$ at 290,000 cm^{-1} (345A), and sodium $2s$ at 550,000 cm^{-1} (181A). The observed absorptions resemble those predicted by the theory, but are different in detail. Thus though the near ultraviolet absorption comes at about the right place, sharp lines as well as continuous absorption are found by Hilsch and Pohl.[1] Smith finds absorption all through the region around 600A, but with pronounced peaks about 550A, 650A, and a smaller one at 900A. O'Bryan observes a fairly sharp band at 372A, rather than a broader continuum, and Smith finds a similar sharp absorption peak at about the same place. In general, more structure

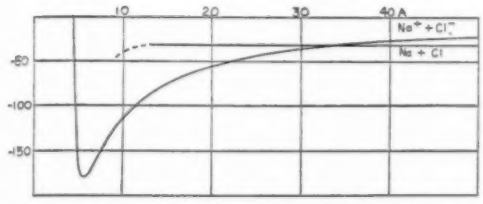

FIG. 2. Total energy of NaCl crystal, in ionic and atomic states, in kcal. per g mol.

and sharp lines are found in the absorption than the theory would suggest. We shall examine the discrepancies in the next section, showing that the method of lattice functions is only partly applicable to the problem, and that a correct solution must be obtained by considering the energy levels of the crystal as a whole. The picture of Fig. 1 remains, however, correct enough to be very suggestive. In regard to the near ultraviolet absorption, we may note an interesting approximation which we may make for the frequency of the limit. The bottom of the continuum of excited levels has risen, at the actual lattice space, about as far above the sodium $3s$ level as the top of the chlorine $3p$ is above the Madelung energy. Thus approximately the excitation energy is equal to the chlorine electron affinity, plus the Madelung energy, minus the sodium ionization potential, or numerically $30{,}400+72{,}000-41{,}400=61{,}000$ cm^{-1}. This simple approximation, already suggested on somewhat different grounds by Hilsch and Pohl, gives surprisingly good results for the absorption limits of all the alkali halides.

Energy Levels of the Crystal as a Whole: Normal State

As a next step, instead of considering lattice functions and one-electron energies, we shall examine the energy levels of the crystal as a whole as a function of lattice spacing. The energy in the normal electronic state has been discussed in a well-known way by Born and others.[12] Starting at infinite separation from the state composed of sodium and chlorine ions, the energy decreases by the amount $-3.495\ e^2/d$ per molecule, until a lattice spacing near the normal value is reached, when a repulsive term, often approximated by a formula a/d^n, where a is a constant, n a high exponent, rather suddenly sets in, resulting in a minimum of the curve. It is to be noted that the ionic state is not the lowest energy at infinite separation. Instead, the state of neutral atoms is lower, by an amount equal to the difference between the ionization potential of sodium and the electron affinity of chlorine, per molecule. This is shown in Fig. 2, in which it is seen that the ionic and atomic states have energy levels which cross at a large value of d, about 35A. It is closely connected with the fact that the lattice energies of Na $3s$ and Cl^- $3p$ cross at large distances (beyond the range of Fig. 1), so that electrons from chlorine ions can be transferred to sodium ions at large distance with liberation of energy. For all our purposes, however, we may confine ourselves to distances less than this value, so that we may regard the normal state as being formed of ions.

Next, we consider excited states in which one electron is excited, the only kind which will have appreciable optical transition probabilities from the normal state. On the scale of Fig. 2, these energy levels as functions of distance will be indistinguishable from the normal state, for the energy of Fig. 2 is the energy of all N molecules of the crystal, whereas the energy of only one molecule changes on excitation, making a change in energy of the order of $1/N$ of the value of Fig. 2. To get a quantity which can be plotted, we must take the energy difference between normal and excited states, regarded as a function of lattice spacing, giving the frequency of optical absorption by the crystal. Excitation can take place in several ways: either a sodium or a chlorine electron can be excited, and it can find a resting place in an excited state of the ion in which it was originally located, or in another ion of the same or opposite sign.

Sodium Excitation

Let us take up the various sorts of excitation in detail, now making use of an atomic point of view, localizing the electrons on definite ions. First, we consider the case of excitation of a sodium electron, in particular the removal of a $2p$ electron from a sodium ion, the electron going into a $3s$ state either on the same or another sodium ion. At infinite lattice spacing, the two processes, roughly equivalent to excitation and

[12] See for example Wolf and Herzfeld, reference 4.

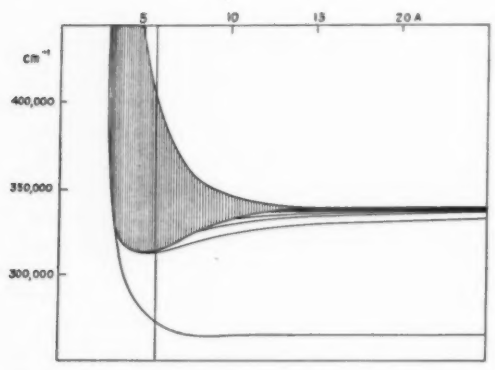

FIG. 3. Optical absorption from Na $2p$ level to lowest excited level, in NaCl.

ionization, are quite distinct. The excitation of a sodium ion to the state $2p^5 3s$ requires about 265,000 cm^{-1}, while the removal of a $2p$ electron requires about 381,000 cm^{-1}, of which about 41,500 cm^{-1} is regained when the ionized electron attaches itself to another ion to produce a neutral atom, leaving a net energy of excitation of 339,500 cm^{-1}. At finite separation, however, the ionized state splits up; for if the removed electron is attached to an ion at distance D from the ion it has left, the necessary work is less than 339,500 cm^{-1} by the electrostatic energy e^2/D, which would have to be expended to remove the electron the additional distance from D to infinity. Now D can have only certain definite values, for it is the distance from one sodium to another in the lattice. Thus it can have the values $(d/2)(n_1^2+n_2^2+n_3^2)^{\frac{1}{2}}$, where n_1, n_2, n_3 are three integers giving the relative positions of the two sodiums, and where the sum $n_1+n_2+n_3$ must be even. We thus have a discrete set of levels, approaching the value 339,500 cm^{-1} as a limit. In Fig. 3 for distances greater than 15A we show some of these levels as a function of d. At large distances, the levels involving ionization cluster together, far above the level involving only excitation, but as we approach the actual lattice spacing the spread of the ionized levels is considerable.

As we approach the actual distance of separation, it no longer is possible to localize electrons on the ions, so that the method of discussion we have just used becomes inapplicable. On the other hand, the method of lattice functions, discussed in the earlier sections, becomes increasingly appropriate. For the removal of a sodium $2p$ electron to an excited level, which we are now considering, we should take the energy difference, from Fig. 1, between the corresponding levels. Since the sodium $2p$ level is not appreciably split up at this distance, the continuum of absorption frequencies on the method of lattice functions will have the same form as the continuum of excited levels but with the Madelung functon of the sodium $2p$ subtracted off. The resulting continuum is shown for small distances in Fig. 3.

We now meet the problem of correlating the two methods of approximation to the excited states, the method of atomic excitation or ionization to neighboring ions for large distances, the method of lattice functions and energy bands at small distances. Quite without calculation, we should expect that in regions where the total splitting given by the lattice model was small compared with the separations of the various ionized or excited states, the method of atomic excitation would give the correct levels, while with very wide energy bands in the lattice model, that model would give correct results. With this in mind, the various discrete levels of the atomic and ionic method have been merged into the lattice energy band of Fig. 3 at small distances, indicating a plausible construction for the excited energy levels at intermediate distances. The relations between the two methods, however, are so important that we examine them in more detail in the next section, reserving the more mathematical parts of the discussion for the Appendix.

CORRELATION OF LATTICE AND ATOMIC WAVE FUNCTIONS

In a general way, the method of lattice functions is analogous to the method of molecular orbitals, and that of atomic excitation to that of Heitler and London, in molecular problems. The inclusion of both atomic excitation and ionization corresponds to the inclusion of both nonpolar and polar states in Heitler and London's method. As one of the authors has pointed out on several occasions,[13] the two methods are then equivalent. The wave functions formed from molecular orbi-

[13] J. C. Slater, Phys. Rev. **35**, 509 (1930); **41**, 255 (1932).

tals can be written as linear combinations of those formed from nonpolar and polar Heitler and London functions, and *vice versa*. A correct treatment of the secular equation from either point of view will then lead to the same energy levels, though an incomplete or first order perturbation treatment will not. Let us consider first the nature of the wave functions in this problem, starting with the method of lattice functions.

The properties of single lattice functions are well known from the theory of metals.[14] Each function behaves like an atomic function near each atom, but is multiplied by exp $i(\mathbf{k}\cdot\mathbf{R})$ going from one atom to another a vector distance $\mathbf{R}$ away, where $\mathbf{k}$ is a vector analogous to the momentum of a plane wave. Corresponding to a single atomic wave function, there are as many lattice functions as there are atoms in the crystal, having different vectors $\mathbf{k}$. A filled band, then, contains one electron per atom of each spin, with the $\mathbf{k}$'s so arranged that there are as many positive as negative, and the vector sum of all $\mathbf{k}$'s is zero. This is the situation of the electrons in the normal state of an ionic lattice, where all energy bands are filled or entirely empty.

If one electron is excited, in our particular case, the band of $2p$ electrons lacks one wave function, the $3s$ band has just one occupied function. For simplicity, we neglect orbital and spin degeneracy in describing the situation. Then there are N^2 excited states, with different energies; for the electron could be removed from any one of the N $2p$ states, going into any one of the N $3s$ states. Each excited state is characterized by a value of the vector sum $\mathbf{K}=\mathbf{k}_q-\mathbf{k}_p$, where $\mathbf{k}_p$ is the momentum of the removed $2p$ electron, $\mathbf{k}_q$ of the $3s$, and of the N^2 states there will be N with each possible value $\mathbf{K}$. This quantity $\mathbf{K}$ has great importance, on account of certain selection principles. In the first place, by optical excitation by light of wave-length λ, the transition probability is zero except to states of one particular $\mathbf{K}$ value, equal to $2\pi/\lambda$, and pointing in the direction of the wave normal. On account of the long optical wave-lengths, this $\mathbf{K}$ value is almost zero, so that we need consider only the excited state of $\mathbf{K}=0$. In the second place, when we use our lattice functions as the basis of a perturbation calculation, we find that the matrix component of the perturbing energy between states of different $\mathbf{K}$ values is always zero. Thus in all our work we can separate off the states of a particular $\mathbf{K}$, and treat them entirely by themselves, as if the others did not exist.

For each stationary state, we form an antisymmetric wave function for the electrons of the whole crystal, one for the normal state, N^2 for the excited states, and set up the matrix components of energy between the various approximate wave functions. First, we consider the diagonal matrix components for the excited states. Subtracting the diagonal energy of the normal state from that of the excited state, to get the excitation energy, we find just the difference between the one-electron energies of the $3s$ and $2p$ electrons of appropriate $\mathbf{k}$ values, in the lattice energy bands, as indicated by the shaded band of Fig. 3. At infinite separation this band shrinks to the single level corresponding to ionization of one sodium ion, attachment of the electron to another ion at infinite distance. For with the lattice functions, each electron is uniformly distributed over all the atoms. The removed $2p$ electron, and the $3s$, are equally and independently likely to be found on any one of the N atoms, so that the chance that they are on neighboring atoms, decreasing the energy appreciably on that account, is negligible. As far as diagonal energy is concerned, in other words, the method of lattice functions takes no account of the possibility of excitation, or of ionization and removal to nearby atoms.

It must not be supposed, however, that because individual lattice states are poor approximations to the actual states at large distances, they cannot be used as a starting point for a perturbation calculation. Instead, we can find the nondiagonal terms of the energy, which not only are different from zero between states of the same $\mathbf{K}$ value, but remain important at large lattice spaces. It is easy at large distances to solve the perturbation problem exactly, and to find the correct linear combinations of lattice functions, which may be easily described. In the first place, we may take all the lattice functions, with all their N^2 combinations of values of $\mathbf{k}_p$ and $\mathbf{k}_q$, multiply each one by the simple coefficient $(1/N)$ exp $i(\mathbf{k}_p\cdot\mathbf{R}_m-\mathbf{k}_q\cdot\mathbf{R}_n)$, where $\mathbf{R}_m$ and $\mathbf{R}_n$

[14] For instance, J. C. Slater, Rev. Mod. Phys. **6**, 209 (1934).

are the vector positions of two particular sodium atoms in the lattice, and add. The result is similar to the well-known process of building up a wave packet out of plane waves, forming a localized disturbance. It gives a wave function in which there is one electron on each atom except that with position $\mathbf{R}_m$, which has no electron, and that at $\mathbf{R}_n$, which has an extra electron, in a $3s$ state. In other words, its wave function is precisely the atomic function which we have discussed previously. When we compute the diagonal energy of such a wave function, we find that it is just the value plotted in Fig. 3 at large distances. In particular, for $\mathbf{R}_m = \mathbf{R}_n$, a $2p$ electron is merely excited to a $3s$ state in the same atom. The nondiagonal energy component between two such atomic states at large distances is zero, so that these states form the correct solution of the problem.

The atomic functions, with a $2p$ electron missing from the atom at $\mathbf{R}_m$, and present as a $3s$ on that at $\mathbf{R}_n$, are correct solutions at large distance, but they are degenerate. The energy depends only on the vector distance $\mathbf{R}_m - \mathbf{R}_n$ (whose magnitude was previoulsy called D), not on $\mathbf{R}_m$ and $\mathbf{R}_n$ separately. In other words, any atom of the crystal may be excited or ionized, so that there are N states of the same energy, corresponding to each value of $\mathbf{R}_m - \mathbf{R}_n$. Any linear combinations of these N states of the same energy would be legitimate functions at large distances, but one particular set of combinations has the property of being appropriate for smaller distances as well, that set in which each function is characterized by a particular value of the same vector $\mathbf{K}$ which we have mentioned above. Such a function represents a sort of wave of excitation or ionization, traveling along with a wave number $\mathbf{K}$. These waves of excitation have been described by Frenkel, though without making this connection with the lattice functions, and without discussing the waves of ionization (the case $\mathbf{R}_m - \mathbf{R}_n \neq 0$). For most purposes there is no great advantage in using them, and we may use the atomic functions instead.

If we could now solve our perturbation problem for intermediate distances, as we can for large distances, we should find exactly how the levels at large and small distances were connected. This unfortunately cannot be done. As the atoms begin to overlap, nondiagonal matrix components of energy appear between two atomic states, or two excitation wave states, in which the excited electrons are situated on neighboring atoms. By a second-order perturbation calculation we can see that, as the continuum of lattice energy levels begins to broaden out, the excitation state will be somewhat depressed by the action of neighboring states, while the ionized states will be pushed almost equally from above and below, and will be practically unaffected until the lattice energy band is decidedly broad. As we approach the observed distance, however, this perturbation calculation becomes inaccurate. Using an approximate model, it has been possible to follow the behavior of the excitation state, and to show that this gradually merges into the bottom of the continuum, though at the actual lattice spacing it will still be distinct. The ionization states will also merge into the continuum, at larger distances, though it has been impossible to work this out in detail. At any distance, most of the levels will form practically a continuum, with a few discrete levels at the bottom, the number of discrete levels decreasing as the lattice spacing decreases. The levels in Fig. 3 have been drawn for intermediate distances according to these principles, the position of the lowest, excitation level being given approximately by our calculation.

Before considering the agreement with experiment, we must examine not only the position of the excited levels, but also the transition probabilities to them. At large distances, we can see without calculation that the probability of transition to an ionized state is zero, the only transitions being to the excited state. For the transition probability involves the matrix component of electric current between the normal and excited states, the wave functions of these states do not overlap if they correspond to having electrons on different atoms, and the matrix component and transition probability are correspondingly zero. Thus the lowest level takes all the transition probability at large distances. At small distances where the lattice functions are correct, on the other hand, the matrix components are of the same order of magnitude for all the possible transitions in the band. By making the proper transformation, we can calculate the matrix com-

ponents corresponding to the excitation and ionization waves at large distances, in terms of the lattice components. We find, as we should expect, that the particular combination of lattice functions corresponding to the excitation wave then acquires the whole transition probability, the other combinations losing their probabilities. But now at the actual distance of separation, neither the excitation and ionization waves, nor the lattice functions, form the correct wave functions, but combinations of them, so that the transition probabilities will be intermediate between these limiting cases. From Fig. 3, we see that the excitation wave will still be far removed from the continuum at the actual distance, so that we may expect that it will still have the larger part of the transition probability; but it will have lost part of its intensity to the continuum, which will have a total intensity to make up for the intensity lost by the discrete line. It is possible that the next line, corresponding to ionization and attachment of the electron to the nearest neighbor, may still be slightly separated from the continuum, and that it may have an appreciable intensity, since at small distances the wave function of an excited atom may appreciably overlap that of the nearest neighbor. Thus there will be one, perhaps two, discrete lines, then a continuum, and the relative intensities cannot be well estimated.

From Fig. 3, we should then expect a sharp line absorption in NaCl corresponding to 271,000 cm^{-1} (369A), perhaps another sharp line at about 312,000 (320A), and a continuum beginning at just about that point, toward the ultraviolet. O'Bryan[3] observes an absorption band at 372A, but has not observed further bands, perhaps because they have not enough intensity. For the lithium salts, however, he observes more detail. The corresponding sharp line transitions in lithium should be at about 476,000 cm^{-1} (210A). O'Bryan observes in LiCl a sharp line at 204A (490,000 cm^{-1}), another at 192A (520,000 cm^{-1}), and continuous absorption beyond that, as we should expect. For the potassium crystals, one should expect an absorption at about 165,000 cm^{-1} (605A), and Smith observes absorption at about 540A in KCl, 510A in KI, which may be the corresponding bands. Both the observations and the theory thus seem to agree in demanding excitation waves for the lowest excited states, merging then into something much like the lattice states forming a continuum, though further experimental evidence would be very desirable.

We have been considering the transition from the sodium $2p$ state to the first excited state, which is largely like sodium $3s$, but has some of the properties of an excited chlorine state. The discussion of transitions from other sodium states, as $2s$, would proceed in a very similar way, with similar structure in the absorption band, further in the ultraviolet, as is seen most easily from Fig. 2. In connection with the excited states, we have spoken only of the lowest band, but should remember that the sodium $3p$, $3d$, $4s$-levels at large distances will all split into lattice bands at smaller distances, becoming mixed up with chlorine bands, and resulting in a continuum of great complexity. This continuum will have concentrations of density at some energies, deficiencies at others, and the resulting continuous absorption will show maxima and minima which may be striking, and which may give the effect of further sharp lines. Taken in connection with the sharp line structure already described, we see that the absorption spectrum can have a very complicated appearance, one very difficult to work out in detail.

Chlorine Excitation

Next, we consider the near ultraviolet absorption, in which a chlorine $3p$ electron is excited to the same lattice level as before. The excited level at large distances would correspond to the removal of an electron from the chlorine, and its attachment to a sodium, and would have no probability of occurrence on account of non-overlapping wave functions. At small distances, however, we have seen that the excited level acquires some of the properties of an excited chlorine state, and has a large probability of transition from the normal state. We can now proceed as before to find the excited levels at large and small distances. At large distances, the required energy is the electron affinity of chlorine, minus the ionization potential of sodium, plus a Madelung term. This term is different from what it was before, for the potential energy of an electron near a sodium ion is greater than that near

a chlorine by $2(3.495)e^2/d$, so that this term appears in the Madelung energy. In addition, if the sodium is only a distance D from the a chlorine, there is the same negative contribution $-e^2/D$ as before, so that the total excitation energy is (electron affinity) $-$ (ionization potential) $+2(3.495)e^2/d-e^2/D$. As before, D can have an infinite number of values, depending on how far the electron is removed from the chlorine, but now the set of D values will be different from before, starting with the distance from a chlorine to its nearest sodium neighbor $(d/2)$, and so on. The resulting sharp levels at large distance are drawn in Fig. 4. The levels become negative at large distances, as can also be seen from Fig. 1, and as would be expected from Fig. 2, from the fact that the atomic state rather than the ionic is the stable one at large distances, and that the process now being contemplated is one in which a chlorine and sodium ion exchange electrons to become neutralized.

At the actual lattice spacing, von Hippel[6] has essentially used the discrete levels we have just described, and has tried to correlate them with the observed structure in the absorption band. It is hardly possible that this is correct, for at these smaller distances the lattice method becomes reasonable, and entirely changes the situation. In Fig. 4 we have drawn the absorption continuum to be expected from the lattice method, remembering that the broadening now comes both from the normal, chlorine $3p$ lattice state and the excited state. For a given $\mathbf{K}$ value this

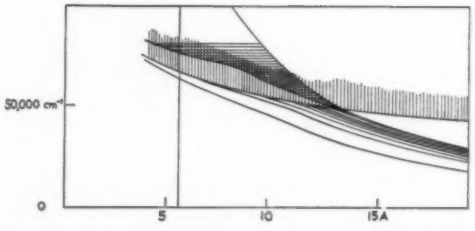

FIG. 4. Optical absorption from Cl $3p$ level to lowest excited level, in NaCl.

becomes a perfectly definite band, with N excited levels, as before. It is now easy to draw the interpolated levels, much as we have done in Fig. 3. In this case, there is nothing like the excited state in the sodium-sodium transition, simply a continuous absorption edge at large distances, lying well above the discrete levels, and merging with the continuum we have drawn at smaller distances. As far as agreement with experiment is concerned, we have already seen that the absorption edge comes at about the right place, and it is plain that it should be expected to show structure. The observations of Hilsch and Pohl on sodium chloride do not extend far enough into the ultraviolet to show much of this structure, though for some of the alkali halides a great deal is observed. It appears at any rate that the present type of theory, involving both sharp line and continuous absorption, is the correct sort to explain the details, but more elaborate calculation is probably necessary to work them out in specific cases.

APPENDIX

Consider a lattice of N atoms, each normally having one electron, all of the same spin. Assume the wave function of an electron about one of the nuclei, in the absence of the other nuclei, is $u(\mathbf{r}-\mathbf{R})$ for the normal state, $v(\mathbf{r}-\mathbf{R})$ for the only excited state we shall consider, where $\mathbf{r}$ is the coordinate of the electron, $\mathbf{R}$ of the nucleus. These functions are assumed to be normalized to unity. Then Bloch's approximation to a modulated one-electron function for the normal state is $(1/(N)^{\frac{1}{2}})\sum_s \exp(i(\mathbf{k}\cdot\mathbf{R}_s))u(\mathbf{r}-\mathbf{R}_s)$, where $\mathbf{k}$ is a momentum-like vector. The factor $1/(N)^{\frac{1}{2}}$ takes care of normalization if the wave functions u of different atoms do not overlap, but there are small corrections, which we shall neglect, on account of normalization at smaller distances. There are N values $\mathbf{k}_1\cdots\mathbf{k}_N$ corresponding to the N Bloch functions in a completed band. Similar Bloch functions can be set up for an excited electron, using v instead of u. Next we can set up antisymmetric functions of the electron coordinates, to represent the state of the whole crystal. If we have the normal state, with no excited electrons, the antisymmetric function, which we may call $B(0)$, is the determinant

$$B(0)=(1/(N)^{\frac{1}{2}}!)\,|(1/(N)^{\frac{1}{2}})\sum_s \exp(i(\mathbf{k}_f\cdot\mathbf{R}_s))u(\mathbf{r}_g-\mathbf{R}_s)|,$$

the elements of the determinant corresponding to all N values of f and g. This state is likewise approximately normalized. For an excited state with one electron excited, we may imagine that the one-electron function with $\mathbf{k}_p$ is missing, and is replaced by a one-electron function formed from the excited function v, with momentum $\mathbf{k}_q$. This function, which we call $B(p,q)$, is the determinant formed just like $B(0)$, but with terms

$$(1/(N)^{\frac{1}{2}})\sum_s \exp i(\mathbf{k}_q\cdot\mathbf{R}_s)v(\mathbf{r}_g-\mathbf{R}_s)$$

in place of

$$(1/(N)^{\frac{1}{2}})\sum_s \exp i(\mathbf{k}_p\cdot\mathbf{R}_s)u(\mathbf{r}_g-\mathbf{R}_s)$$

in the pth row. There will be N^2 states $B(p, q)$, since either of the indices p, q can take on any one of N values.

Next, consider functions built up in the atomic way from the u's and v's. The normal state corresponds to having one electron in state u about each nucleus, and its antisymmetric wave function, which we may call $A(0)$, is

$$A(0)=(1/(N)^{\frac{1}{2}}!)\,|u(\mathbf{r}_f-\mathbf{R}_g)|,$$

which again is normalized at large lattice spacings. By making suitable combinations of rows in the determinant, it is easily shown that $A(0)=B(0)$, so that the normal state is identical in the atomic or the lattice method. The excited states in the atomic method are set up by assuming the electron to be removed from the mth atom, and to be present in an excited state in the nth atom. The corresponding function $A(m, n)$ is a determinant like the preceding one, but with the terms $u(\mathbf{r}_f-\mathbf{R}_m)$ missing, and replaced by $v(\mathbf{r}_f-\mathbf{R}_n)$. In particular, if $m=n$, the state is one with the mth atom excited, while if $m\neq n$, the mth atom is positively ionized, the nth negatively. Again there are N^2 excited states, corresponding to all N values of m and n separately.

Each term in the expansion of the function $A(m, n)$ is a product of $(N-1)$ factors u, and one factor v; one of the nuclei, the mth, has no electron, and another, the nth, has two, one in state u and the other v. Similarly each term in the expansion of $B(p, q)$ is a product of $(N-1)$ factors u, and one factor v. It is not obvious that in the expansion the only terms are those with all nuclei but two occupied by one electron each, one of the remaining ones with two, and the final one with none, but this is actually the case on account of the antisymmetry, and the resulting application of the exclusion principle: no two functions u can be found on the same nucleus, so that the only possible doubling up of electrons on atoms is the single case of a function v and a function u on the same atom. The complete set of functions $A(m, n)$ thus involve the same terms as the set $B(p, q)$, and since each set is normalized and orthogonal at large distances of separation, it is obvious that one set can be derived from the other by a unitary transformation. Thus we must have $A(m, n)=\sum_{p, q}C(m, n;\ p, q)B(p, q)$. To find the coefficients C, we may multiply by $B^*(p', q')$ and integrate over the electron coordinates. Then by the normalization and orthogonality of the B's,

$$C(m, n;\ p, q)=\int A(m, n)B^*(p, q)d\tau.$$

We must now find the integral above, which is the integral of a product of two determinants. Consider the integral of a typical term of the determinant A, multiplied by the diagonal term of B^*. This is

$$\begin{aligned}1/(N!(N^N)^{\frac{1}{2}})\int\cdots\int & u(\mathbf{r}_a-\mathbf{R}_1)u(\mathbf{r}_b-\mathbf{R}_2)\\ &\cdot u(\mathbf{r}_i-\mathbf{R}_{m-1})v(\mathbf{r}_j-\mathbf{R}_n)u(\mathbf{r}_k-\mathbf{R}_{m+1})\\ &\cdot u(\mathbf{r}_z-\mathbf{R}_N)\{\sum_{s_1}\exp -i(\mathbf{k}_1\cdot\mathbf{R}_{s1})u(\mathbf{r}_1-\mathbf{R}_{s1})\}\cdots\\ \{\sum_{s_{p-1}}&\exp -i(\mathbf{k}_{p-1}\cdot\mathbf{R}_{s(p-1)})u(\mathbf{r}_{p-1}-\mathbf{R}_{s(p-1)})\}\\ \{\sum_{s_p}&\exp -i(\mathbf{k}_q\cdot\mathbf{R}_{sp})v(\mathbf{r}_p-\mathbf{R}_{sp})\}\\ \{\sum_{s_{p+1}}&\exp -i(\mathbf{k}_{p+1}\cdot\mathbf{R}_{s(p+1)})u(\mathbf{r}_{p+1}-\mathbf{R}_{s(p+1)})\}\cdots\\ \{\sum_{s_N}&\exp -i(\mathbf{k}_N\cdot\mathbf{R}_N)u(\mathbf{r}_N-\mathbf{R}_N)\}d\tau_1\cdots d\tau_N,\end{aligned}$$

where $ab\cdots ijk\cdots z$ form a typical permutation of the indices $1\,2\cdots N$. The integral over the ath electron has as an integrand $u(\mathbf{r}_a-\mathbf{R}_1)\sum_s \exp -i(\mathbf{k}_a\cdot\mathbf{R}_s)u(\mathbf{r}_a-\mathbf{R}_s)$ (unless a happens to equal p). If we neglect the lack of orthogonality of u's belonging to different atoms, the only term of this summation giving an integral different from zero is that for $s=1$, which integrates to $\exp -i(\mathbf{k}_a\cdot\mathbf{R}_1)$. With certain exceptions, the terms all integrate in similar ways, giving $\exp -i(\mathbf{k}_b\cdot\mathbf{R}_2)$, $\cdots$ $\exp -i(\mathbf{k}_z\cdot\mathbf{R}_N)$. The exceptional terms are the following: If $a=p$, on account of the orthogonality of the u's and v's, the integral over the ath electron gives zero, and the whole integral vanishes. The same thing holds if b, c, or any of the indices except j, is equal to p. Thus the only terms of the product which do not integrate to zero are those with $j=p$. If $j=p$, so that the integral does not vanish, then for the jth electron we must integrate $v(\mathbf{r}_j-\mathbf{R}_n)\sum_s \exp -i(\mathbf{k}_q\cdot\mathbf{R}_{sp})v(\mathbf{r}_p-\mathbf{R}_{sp})$. The only term different from zero is for $s_p=n$, giving $\exp -i(\mathbf{k}_q\cdot\mathbf{R}_n)$.

When we take all terms corresponding to all permutations $a\cdots z$, we see that except for the exceptional terms mentioned just above, the result could be written as a determinant, $(1/N!)\,|\exp -i(\mathbf{k}_f\cdot\mathbf{R}_g)/(N)^{\frac{1}{2}}|$, where f and g take on all values. The same result is obtained on multiplying the determinant $A(m, n)$ with each of the $N!$ terms of the determinant $B^*(p, q)$, so that the result is just $N!$ times as great, cancelling the factor $N!$ in the denominator. This determinant is just the determinant of the coefficients of expansion from the atomic functions $u(\mathbf{r}-\mathbf{R}_g)$ to the Bloch one-electron functions $(1/(N)^{\frac{1}{2}})\sum_s \exp i(\mathbf{k}_f\cdot\mathbf{R}_s)u(\mathbf{r}-\mathbf{R}_s)$, and since both sets of functions to our approximation are normalized and orthogonal, the transformation from one set of functions to the other is a unitary transformation, so that the determinant of coefficients is of unit magnitude, and may be set equal to $\exp i\theta$. This shows immediately that $|\int A(0)B^*(0)d\tau|=1$, as it should. But now on account of our exceptional terms, the integral has a different value in our case. It is easily seen that it is now the determinant of terms $(\exp -i(\mathbf{k}_f\cdot\mathbf{R}_g))/(N)^{\frac{1}{2}}$, in which all terms of the row $f=p$, and of the column $g=m$, are set equal to zero, except the term $f=p$, $g=m$, which equals $(\exp -i(\mathbf{k}_q\cdot\mathbf{R}_n)/(N)^{\frac{1}{2}})$. The result is then equal to $(\exp -i(\mathbf{k}_q\cdot\mathbf{R}_n))/(N)^{\frac{1}{2}}$ times the minor of the determinant $|\exp -i(\mathbf{k}_f\cdot\mathbf{R}_g)/(N)^{\frac{1}{2}}|$ corresponding to $f=p$, $g=m$. But the minor corresponding to a certain term in the determinant of coefficients of a unitary transformation equals the complex conjugate of the term itself, multiplied by the value of the determinant, so that finally the coefficient in question is given by

$$C(m, n;\ p, q)=(1/N)\exp i(\mathbf{k}_p\cdot\mathbf{R}_m-\mathbf{k}_q\cdot\mathbf{R}_n)\exp i\theta.$$

The factor $\exp i\theta$ is a phase factor which we shall henceforth neglect, since it is the same for all functions.

We now see that we can write an atomic function as

$$A(m, n)=1/N\sum_{p, q}\exp i(\mathbf{k}_p\cdot\mathbf{R}_m-\mathbf{k}_q\cdot\mathbf{R}_n)B(p, q).$$

We can rearrange the double summation, so as to sum first over all values of p and q for which $\mathbf{k}_q-\mathbf{k}_p=\mathbf{K}$ is constant. Thus

$$A(m, n)=\sum_{\mathbf{K}}\frac{\exp -i(\mathbf{K}\cdot\mathbf{R}_n)}{(N)^{\frac{1}{2}}}\sum_{\mathbf{k}}\frac{\exp i(\mathbf{k}\cdot\mathbf{R})}{(N)^{\frac{1}{2}}}B(\mathbf{k}-\mathbf{K},\ \mathbf{k}),$$

where we have used the relation

$$\mathbf{k}_p\cdot\mathbf{R}_m-\mathbf{k}_q\cdot\mathbf{R}_n=-(\mathbf{k}_q-\mathbf{k}_p)\cdot\mathbf{R}_n+\mathbf{k}_q\cdot(\mathbf{R}_m-\mathbf{R}_n)=-\mathbf{K}\cdot\mathbf{R}_n+\mathbf{k}\cdot\mathbf{R},$$

setting $\mathbf{k}_q=\mathbf{k}$, $\mathbf{R}_m-\mathbf{R}_n=\mathbf{R}$.

Now we can form the function

$$E(\mathbf{K},\mathbf{R})=\sum_{\substack{\mathbf{R}_n\\ \mathbf{R}=\text{const.}}}\frac{\exp i(\mathbf{K}\cdot\mathbf{R}_n)}{(N)^{\frac{1}{2}}}A(m,n),$$

an excitation or ionization wave of momentum vector $\mathbf{K}$, corresponding to an electron in each atom being removed to the atom distant by the vector displacement $\mathbf{R}$. This is given by

$$E(\mathbf{K},\mathbf{R})=\sum_{\mathbf{K}',\mathbf{k}}\frac{\exp i(\mathbf{k}\cdot\mathbf{R})}{(N)^{\frac{1}{2}}}B(\mathbf{k}-\mathbf{K}',\mathbf{k})\sum_{\mathbf{R}_n}\frac{\exp i(\mathbf{K}-\mathbf{K}')\cdot\mathbf{R}_n}{N}.$$

But by the properties of the reciprocal lattice,

$$\sum_{\mathbf{R}_n}\exp i(\mathbf{K}-\mathbf{K}')\cdot\mathbf{R}_n=0 \text{ if } \mathbf{K}-\mathbf{K}'\neq 0,\ =N \text{ if } \mathbf{K}-\mathbf{K}'=0.$$

Thus

$$E(\mathbf{K},\mathbf{R})=\sum_{\mathbf{k}}\frac{\exp i(\mathbf{k}\cdot\mathbf{R})}{(N)^{\frac{1}{2}}}B(\mathbf{k}-\mathbf{K},\mathbf{k}),$$

so that, as stated in the text, this excitation function is equal, except for the factor $(\exp -i(\mathbf{K}\cdot\mathbf{R}_n))/(N)^{\frac{1}{2}}$, to the same summation over Bloch functions which we should carry out to get an atomic function, with the exception that the summation is to be carried out only for terms of a given $\mathbf{K}$ value.

Now that we have exhibited the transformation coefficients between the Bloch functions B, the atomic functions A, and the excitation wave functions E, we shall find matrix components of the energy. We shall do this for the atomic functions, using the transformation theory to get matrix components between the other types of functions. We must make more precise assumptions than previously about the energy. We assume that the N electrons move in a potential field $U(\mathbf{r})$, which can be written as a sum of potentials from each nucleus: $U(\mathbf{r})=\sum_s V(\mathbf{r}-\mathbf{R}_s)$, in which $\mathbf{R}_s$ is the vector coordinate of the sth nucleus, and $V(\mathbf{r})$ is the potential of a singly charged positive ion, reducing to $-2/r$ in atomic units, at large values of r, but behaving differently for small r, as the nucleus is no longer well shielded by the electrons of the core. Since our problem is that of N electrons moving in this field, it is plain that the electrons will on the average cancel this nuclear charge, so that an electron at a given point of the lattice will be acted on only by its near neighbors. Then, in atomic units the energy operator is

$$H=-\sum_i\nabla_i^2+\sum_{\substack{\text{pairs}\\ i,j}}\frac{2}{|\mathbf{r}_i-\mathbf{r}_j|}+\sum_i U(\mathbf{r}_i)+\sum_{\substack{\text{pairs}\\ s,i}}\frac{2}{|\mathbf{R}_s-\mathbf{R}_i|},$$

where the first term is the kinetic energy, the second the mutual potential energy of the electrons, the third the potential energy of the electrons in the fields of the cores of the atoms, and the last the mutual energy of the positive ions. Now we allow H to operate on one of the terms in the expansion of the determinant forming an atomic function $A(m,n)$. We assume that the individual factors satisfy equations

$$(-\nabla^2+V(\mathbf{r}-\mathbf{R}_s))u(\mathbf{r}-\mathbf{R}_s)=Eu(\mathbf{r}-\mathbf{R}_s),$$
$$(-\nabla^2+V(\mathbf{r}-\mathbf{R}_s))v(\mathbf{r}-\mathbf{R}_s)=E'v(\mathbf{r}-\mathbf{R}_s).$$

Then we have

$$Hu(\mathbf{r}_1-\mathbf{R}_1)\cdots u(\mathbf{r}_{m-1}-\mathbf{R}_{m-1})v(\mathbf{r}_m-\mathbf{R}_n)u(\mathbf{r}_{m+1}-\mathbf{R}_{m+1})\cdot u(\mathbf{r}_N-\mathbf{R}_N)=\{((N-1)E+E')+\sum_{\substack{\text{pairs}\\ i,j}}\frac{2}{|\mathbf{r}_i-\mathbf{r}_j|}+\sum_{i\neq}(U(\mathbf{r}_i)-V(\mathbf{r}_i-\mathbf{R}_i))+(U(\mathbf{r}_m)-V(\mathbf{r}_m-\mathbf{R}_n))+\sum_{\substack{\text{pairs}\\ s,i}}\frac{2}{|\mathbf{R}_s-\mathbf{R}_i|}\}u(\mathbf{r}_1-\mathbf{R}_1)\cdot u(\mathbf{r}_N-\mathbf{R}_N).$$

First we shall find the diagonal component of the energy matrix. As a first step, we multiply $Hu(\mathbf{r}_1-\mathbf{R}_1)\cdots$ by the same combination of u's and v's already written, and integrate over the electron coordinates. In doing this, the repulsive potential terms between pairs of electrons and pairs of nuclei in general cancel the attractive terms between nuclei and electrons, so that except for a few special terms the result is simply $(N-1)E+E'$. The special terms arise because the mth electron is on the nth nucleus instead of the mth. The interaction terms between the mth electron and other electrons then integrate, if the distributions of charge are spherically symmetrical and nonoverlapping, to

$$\sum_{s\neq m,n}\frac{2}{|\mathbf{R}_n-\mathbf{R}_s|}+\int\int\frac{2}{|\mathbf{r}_m-\mathbf{r}_n|}v^*(\mathbf{r}_m-\mathbf{R}_n)v(\mathbf{r}_m-\mathbf{R}_n)\times u^*(\mathbf{r}_n-\mathbf{R}_n)u(\mathbf{r}_n-\mathbf{R}_n)d\tau_n d\tau_m,$$

where the last term represents the interaction between the normal and excited electrons on the nth nucleus, instead of to $\sum_{s\neq m}\frac{2}{|\mathbf{R}_m-\mathbf{R}_s|}$ as we should otherwise have had. But the interaction terms between the mth electron and the nuclei become $\sum_{s\neq n}\frac{-2}{|\mathbf{R}_n-\mathbf{R}_s|}$, where we use the value of V appropriate at large distances, so that the net result is $-\frac{2}{|\mathbf{R}_m-\mathbf{R}_n|}$ + the integral written above. Next, we multiply $Hu(\mathbf{r}_1-\mathbf{R}_1)\cdots$ by any other terms which do not integrate to zero. We shall assume that the distance of separation of atoms is great enough so that the unexcited wave functions u do not overlap at all (as for instance the $2p$ in sodium), while the excited functions v overlap only between nearest neighbors. Then the only other function by which we may integrate to get a nonvanishing integral is that in which the two electrons on the nth atom are interchanged, and this gives an integral similar to that above, but with interchange of electrons. The net result is then, in an obvious notation,

$$(mn/H/mn)=(N-1)E+E'+\int\int\frac{2}{|\mathbf{r}_m-\mathbf{r}_n|}\times v^*(\mathbf{r}_m-\mathbf{R}_n)v(\mathbf{r}_m-\mathbf{R}_n)u^*(\mathbf{r}_n-\mathbf{R}_n)u(\mathbf{r}_n-\mathbf{R}_n)d\tau_n d\tau_m+\int\int\frac{2}{|\mathbf{r}_m-\mathbf{r}_n|}v^*(\mathbf{r}_n-\mathbf{R}_n)v(\mathbf{r}_m-\mathbf{R}_n)u^*(\mathbf{r}_m-\mathbf{R}_n)\times u(\mathbf{r}_n-\mathbf{R}_n)d\tau_n d\tau_m-\frac{2}{|\mathbf{R}_m-\mathbf{R}_n|}.$$

If we refer to the normal state as the zero of energy, we see that $E=0$, so that the energy of excitation is $E'-E$ plus the integrals and the Coulomb term. Now the integrals are just

the Coulomb and exchange interaction between the two electrons on the negative nth ion, so that they, taken together with $E'-E$, give the best approximation we can make with these wave functions to the energy of the negative ion, referred to the normal state of the neutral atom as zero. If we let this be ϵ_1, we have

$$(mn/H/mn)=\epsilon_1-\frac{2}{|\mathbf{R}_m-\mathbf{R}_n|},$$

as stated in the text. The situation is quite different, however, in the special case $m=n$, where the electron is only excited, and not removed to another atom. Here all the Coulomb terms cancel, and there is no exchange integral, since no atom has more than one electron. We then have

$$(mn/H/mn)=(N-1)E+E'=\epsilon_0,$$

where ϵ_0 is the energy required to excite a single atom without ionization, a decidedly smaller value than ϵ_1.

We are now ready to find nondiagonal terms of the energy matrix. With the assumptions we have made, the only nonvanishing terms are those in which the excited electron only changes from one state to the other, and changes only from its position on the nth atom to one of the next neighbors n'. The only contribution comes from multiplying $Hu(\mathbf{r}_1-\mathbf{R}_1)\cdots$, as before, with the identical function except for the exchange of $v(\mathbf{r}_m-\mathbf{R}_n')$ in place of $v(\mathbf{r}_m-\mathbf{R}_n)$. We make the crude approximation that the orthogonality integral $\int v^*(\mathbf{r}_m-\mathbf{R}_n)v(\mathbf{r}_m-\mathbf{R}_n')d\tau$ can be neglected. (It is somewhat more complicated, but not difficult, to carry through the calculations without making this assumption; no essential change in the conclusions is brought about thereby.) Then we have

$$(mn/H/mn')=\int\{U(\mathbf{r}_m)-V(\mathbf{r}_m-\mathbf{R}_n)+\sum_{j\neq m}\int\frac{2}{|\mathbf{r}_m-\mathbf{r}_j|}u^*(\mathbf{r}_j-\mathbf{R}_j)u(\mathbf{r}_j-\mathbf{R}_j)d\tau_j\}v^*(\mathbf{r}_m-\mathbf{R}_n')v(\mathbf{r}_m-\mathbf{R}_n)d\tau_n.$$

Now $U(\mathbf{r}_m)$ plus the summation represents the potential of an electron in the field of the nuclei and of one electron per atom on every atom but the mth; that is, it is the potential in which we may assume the mth electron to be moving. The integral is then the sort met in Bloch's theory, and we may let

$$(mn/H/mn')=\beta(m, n, n').$$

So long as the nth atom is not very near the mth, the quantity β will really not depend on m, n, or n', but will be a constant. The nondiagonal term β becomes large only when the atoms overlap each other. Thus, at large distances the energy is diagonal with respect to the atomic functions, so that they form a solution of the problem, which becomes less and less accurate as the overlapping becomes greater.

By the transformation theory we can at once find the matrix components of the energy with respect to the other types of wave functions. Using the excitation waves, we find that there is no component of energy between waves of different K value; but that with the same K value, the diagonal energy, between states with the same value of $\mathbf{R}=\mathbf{R}_m-\mathbf{R}_n$, is the same as the energy of the atomic state with the same m and n values; while the nondiagonal energy between two states having the same m, but with n and n' in the two states, where $\mathbf{R}_n$ and $\mathbf{R}_n'$ represent neighbors, is $\exp i(\mathbf{K}\cdot(\mathbf{R}_n'-\mathbf{R}_n))\beta(m, n, n')$. Using Bloch waves, the diagonal energy is

$$\left\{(1-1/N)\epsilon_1+(1/N)\epsilon_0-1/N\sum_m\frac{2}{|\mathbf{R}_0-\mathbf{R}_m|}\right\}+\sum_{\substack{\text{nearest}\\ \text{neighbors}}}\exp -i(\mathbf{k}_q\cdot(\mathbf{R}_n-\mathbf{R}_n'))\bar{\beta}.$$

Here the first bracket represents the center of gravity of the band of lattice energy levels, and the second term gives the spreading, according to the usual Bloch formula. The center of gravity arises because there is one chance out of N that an electron may be just excited (energy ϵ_0), and $N-1$ chances out of N that it is ionized (energy ϵ_1), with an average electrostatic term between ions given by the summation. In the term giving the spreading, the quantity $\bar{\beta}$ is the average of β over all values of m, for a fixed n and n'. The nondiagonal energy with the Bloch functions is

$$1/N(\epsilon_0-\epsilon_1)+1/N\sum_m\exp i(\mathbf{k}_q-\mathbf{k}_q')\cdot(\mathbf{R}_m-\mathbf{R}_0)\left\{\frac{2}{|\mathbf{R}_m-\mathbf{R}_0|}+\sum_{n'}\exp i\mathbf{k}_q'\cdot(\mathbf{R}_0-\mathbf{R}_n')\beta(m, 0, n')\right\}$$

if $\mathbf{k}_q-\mathbf{k}_q'=\mathbf{k}_p-\mathbf{k}_p'=0$ otherwise. Here the first term is independent of distance, so that it becomes very important at large distances, where the energy band becomes narrow. It is the nondiagonal term responsible for splitting off the excited from the ionized states at large distances, and the summations, which fall off inversely with the lattice spacing, are responsible for the splitting up of the various ionized states.

Since there are nondiagonal components of the energy in each system of functions we have examined, no one of these sets forms a solution of Schrödinger's equation. We must instead form linear combinations, which will reduce to atomic or excitation functions at large lattice spacing, and will approach the lattice functions at small distances, without however quite reaching them until the energy band becomes of infinite width. The perturbation problem is too difficult to solve exactly, and we shall adopt approximate and schematic methods. For considerable distances of separation we can use second order perturbation theory, starting with atomic or excitation functions. Each level will be repelled by those levels obtained from it by letting its excited atom be displaced to one of its nearest neighbors, a small number of levels. The repulsion from one of these levels will be β^2 divided by the energy difference between the original level and that resulting from the displaced atom. In the first place, the whole effect is proportional to the square of β, or the square of the breadth of the lattice energy band, so that it is small. Further, for the ionized as opposed to the excited bands, opposite displacements of the electron will make opposite changes in the unperturbed energy, so that the various terms in the second order change in the energy will tend to cancel. Ionized bands, then, will have the values given by the atomic functions even when the energy bands are appreciably split up. The excited level, however, will be depressed, since all other states with which it interacts lie higher than it does.

Actually, however, we are interested in distances of separation too small for this second order perturbation to be satisfactory. It is not practicable to apply conventional perturbation theory to the Bloch functions, for they form a continuum, and the nondiagonal energy is larger than the energy differences between unperturbed functions. We shall try to investigate the behavior of the excited atomic level in this region, however, by adopting a simplified model. We take a one-dimensional lattice, so that each atom has only two nearest neighbors. Furthermore, we neglect the electrostatic interaction terms, so that we cannot expect to get correct information regarding the ionized levels. Starting with atomic functions, then, we assume the diagonal energy to be ϵ_1 for ionized states, ϵ_0 for the excited state, and we assume the nondiagonal energy to be β (a constant) between two states differing by a displacement of the excited electron to one of its two nearest neighbors. With this simplified model, we can solve the perturbation problem exactly, in the following manner.

Consider a linear crystal having N atoms, and repeated periodically, so that wave functions must satisfy periodic boundary conditions. Then there are N^2 excited states. It is most convenient to take these as the $E(\mathbf{K}, \mathbf{R})$ functions for these form N noncombining sets according to the value of $\mathbf{K}$. For convenience we shall take the zero of energy as the excitation energy ϵ_1. Then the diagonal matrix elements are $\epsilon=\epsilon_0-\epsilon_1$ for $\mathbf{R}=0$, and zero otherwise. The nondiagonal elements may be made real by using the function $F(\mathbf{R}) = \exp i(\mathbf{K}\cdot\mathbf{R})E(\mathbf{K}, \mathbf{R})$. These elements are then β for states with $\mathbf{R}$ differing by one lattice constant, zero otherwise. It is most convenient to number the states by the number of atoms the excited electron is separated from the ion, thus getting $F(0)$, $F(1)$, $\cdots F(N-1)$. If λ is an eigenvalue of the perturbation problem, and $\phi=a_0F_0+a_1F_1+\cdots a_{N-1}F(N-1)$ is the eigenfunction, the equation $H\phi=\lambda\phi$ gives

$$\begin{aligned}(\lambda-\epsilon)a_0&=\beta(a_{N-1}+a_1)\\ \lambda a_1&=\beta(a_0+a_2)\\ &\cdots\cdots\cdots\\ \lambda a_{N-1}&=\beta(a_{N-2}+a_0)\end{aligned}$$

From the symmetry of the equations, it is seen that the solutions will be of two types: Odd, $a_r=-a_{N-r}$; even, $a_r=a_{N-r}$. The odd type leads to solutions of the form $a_r=\sin\alpha\, r$, where the range of distinct values of α is from 0 to π. The allowed values of α are thus $2\pi l/N$ where $l=1, 2, \cdots$, the largest integer $<N/2$. The values of λ are $2\beta\cos\alpha$. The even type solutions are of the form $a_r=\cos\alpha(r-N/2)$ with eigenvalues $\lambda=2\beta\cos\alpha$. These values of a_r satisfy all equations save the first which gives the condition

$$(\lambda-\epsilon)\cos N\alpha/2=2\beta\cos(1-N/2)\alpha.$$

Hence, we get the equation for α, $\epsilon/2\beta=-\sin\alpha\tan(N\alpha/2)$. For $E=0$, this gives the same allowed α values and energy spectrum as the odd type. However, for $\epsilon\neq0$ one of the roots in the range $0\leq\alpha\leq\pi$ is lost and it is necessary to use complex values of α of the form $0+i\gamma$ or $\pi+i\gamma$ to find it. Since the number of atoms is very large the values of $-\sin(i\gamma)\tan(i\gamma N/2)$ and $-\sin(\pi+i\gamma)\tan((\pi+i\gamma)N/2)$ may be simplified to $\sinh\gamma$ and $-\sinh\gamma$. The form of the curve for this function for the various values of α is shown in Fig. 5. The allowed values of α are given by its intersections with a horizontal line whose ordinate is $\epsilon/2\beta$. The corresponding energies are $2\beta\cos\alpha$. The values of $\cos\alpha=\lambda/2\beta$ are also plotted. It is seen that the allowed values of α form a continuum with one separated state whose energy is given by $2\beta\cosh\gamma=2\beta(1+\sinh^2\gamma)^{\frac{1}{2}}=((2\beta)^2+\epsilon^2)^{\frac{1}{2}}$. It is clearly this state which becomes the excitation wave for large distances, $\epsilon\gg2\beta$, while the continuum is composed of the ionization waves. The energy spectrum of the continuum itself is almost independent of ϵ, the maximum shift in any level due to changes in ϵ being equal to the energy spacing in the continuum.

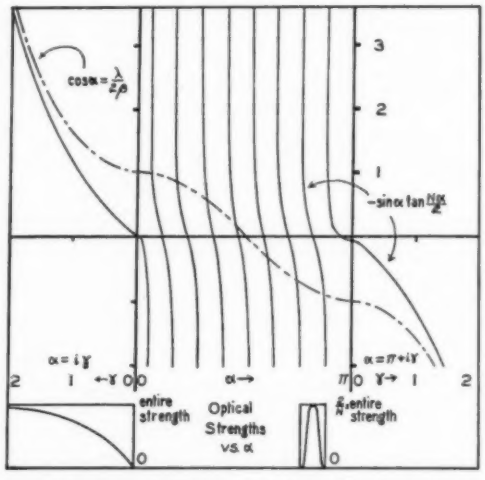

FIG. 5. Diagram for illustrating one-dimensional model. Abscissae of intersections of a horizontal line at ordinate $\epsilon/2\beta$ (where ϵ is energy difference between excitation and ionization energy at infinity, and 2β is width of Bloch band) and the curve $-\sin\alpha\tan N\alpha/2$ give values of α for the even states. The dotted curve gives energy λ, divided by 2β, as function of α. Lower diagrams give optical strength as function of α, the right-hand one for one of the states of the continuum, the left-hand one for the excitation state.

We can use the solution given above to estimate the relative strengths of light absorption from the normal state to the various excited states. As was shown in the text, there is no matrix component for electric current between the normal state and the ionization waves, the entire optical strength being concentrated in the excitation wave. If the optical strength of the excitation wave is taken as unity, then the optical strength of one of the new eigenfunctions $\phi=a_0F_0+a_1F_1+\cdots$ is given by $|a_0|^2/\Sigma|a_i|^2$. From the unitary property of the transformation to principal axes, it follows that the sum of these is always unity. The optical strength is seen to be zero for the odd states. For the even states with α real it is $\cos^2(\alpha N/2)/\sum_{r=0}^{N}\cos^2\alpha(r-N/2)\doteq2\cos^2(\alpha N/2)/N$. For the separated state, for which α is complex, the strength is $\cosh^2(\gamma N/2)/\sum_{r=0}^{N}\cosh^2\times\gamma(r-N/2)\doteq\tanh\gamma$. For the case of large separation,

$\epsilon_0-\epsilon_1=\epsilon\gg\beta$, we see that γ is large and $\tanh\gamma\doteq 1$. Hence the separated state is almost pure excitation wave and contains almost all the optical strength. For the states in the continuum $\tanh(\alpha N/2)$ must be large compared with unity so that $\cos(\alpha N/2)\ll 1$ and the strengths of these states are small. The figure shows how the strengths depend upon the values of α. It is seen that even for the case where separation of the single state from the continuum is only 5 percent of the width of the continuum, it still possesses 40 percent of the optical strength.

OCTOBER 15, 1936 PHYSICAL REVIEW VOLUME 50

The Infrared Absorption of Hydrogen Chloride in Nonionizing Solvents

DUDLEY WILLIAMS,* *Department of Physics, University of North Carolina, Chapel Hill, North Carolina*

(Received August 3, 1936)

The infrared absorption of hydrogen chloride in four nonionizing solvents has been measured. In every solution studied the HCl fundamental vibrational frequency was found to be lower than for the gas. The variation in frequency was found to increase regularly with dipole moment of solvent when the solvents employed were of the same chemical nature. Solvents of the benzene type were used, and it was found that the displacement of the 3.4μ band approached no limiting value even when a solvent of dipole moment 4.20×10^{-18} e.s.u. was used. The results obtained were attributed to the combined effects of dipole interaction and the formation of complexes.

THE infrared absorption spectrum of hydrogen chloride has been studied by a number of investigators, and the fundamental vibrational-rotational band has been observed at 3.46μ while the first harmonic has been found to appear at 1.76μ.[1] The rotational structure of both bands has been carefully studied. It has been of interest to determine the effects exerted upon the HCl molecules by neighboring units. Shearin[2] has studied the spectrum of solid HCl and reports the appearance of the fundamental at 3.74μ in this crystal with a series of broad rotational lines equally spaced about a zero line. In the case of solutions, Plyler and Williams[3] have found the fundamental HCl frequency in benzene to be only slightly lower than in the gas but have reported their inability to detect any absorption arising from HCl molecules in aqueous solution, attributing the latter result to the high degree of dissociation of HCl in this solvent. Working with the Raman spectra of solutions of HCl in silicon tetrachloride, chloroform, sulphur dioxide, ethyl bromide, and acetyl chloride, West and Arthur[4] found that the vibrational frequency of the solute decreased with increasing dipole moment of solvent. These authors report that with solvents of low dipole moment the decrease in frequency is proportional to the dipole moment of the solvent. However, it appears that in the case of the solvents used by these authors there is a limiting variation in vibrational frequency of about 89 cm^{-1} produced by a solvent of moment 1.63×10^{-18} e.s.u., beyond which further increase in dipole moment is without effect. The solvent of highest dipole moment used in this study was acetyl chloride of moment 2.70×10^{-18} e.s.u. Subsequent infrared studies by West and Edwards[5] on the effects of the same solvents on the harmonic near 1.76μ yielded results in agreement with the Raman work.

It was the purpose of the present investigation to determine the effects of another type of organic solvent on the HCl vibrational frequency in order to test the generality of the results obtained with the solvents mentioned above. It was desirable to use as solvents a series of compounds having similar chemical structures and having a wide range of dipole moments. Benzene, chlorobenzene, nitrobenzene, and *m*-nitrotoluene have dipole moments varying from zero in benzene to 4.20×10^{-18} e.s.u. in *m*-nitrotoluene and do not react chemically with HCl. The effects of these solvents on the HCl vibrational frequency was studied.

A Hilger infrared spectrometer with a fluorite

* Now at the University of Florida.

[1] W. Burmeister, Verh. d. D. Phys. Ges. **15**, 589 (1913); E. von Bahr, Verh. d. D. Phys. Ges. **15**, 1154 (1913); H. M. Randall and E. S. Imes, Phys. Rev. **15**, 152 (1920); E. S. Imes, Astrophys. J. **50**, 25 (1919).

[2] P. E. Shearin, Phys. Rev. **48**, 299 (1935).

[3] E. K. Plyler and D. Williams, Phys. Rev. **49**, 215 (1936).

[4] W. West and P. Arthur, J. Chem. Phys. **2**, 215 (1934).

[5] W. West and R. T. Edwards, Phys. Rev. **49**, 405 (1936).

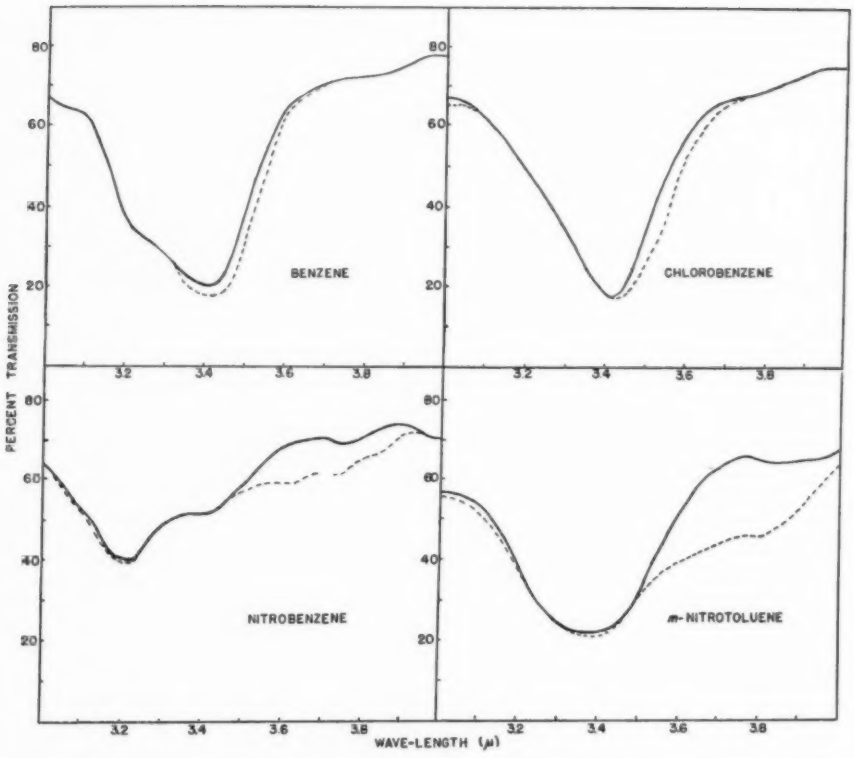

FIG. 1. The percentage transmission of aromatic solvents and HCl solutions from 3.0μ to 4.0μ.

prism was used as a resolving instrument. The effective slit width was 0.03μ in the 3μ region and 0.02μ near 4μ. The absorption cells were prepared by separating fluorite windows by mica washers of known thickness, the thickness of the absorbing layers of the liquids being 0.06 mm. Every effort was made to keep the fluorite windows as dry as possible in order to preclude the possibility of ionization by small amounts of adsorbed water. The windows were kept in a desiccator with P_2O_5 for several hours before being used.

The benzene and nitrobenzene were Baker's chemically pure compounds, and the chemically pure chlorobenzene and *m*-nitrotoluene used were obtained from Eastman. After being kept over suitable drying agents for several days these liquids were distilled. The boiling points of the samples used were in close agreement with the accepted values, a high degree of purity being indicated in this manner. In preparing the solutions the hydrogen chloride was passed through three drying towers containing concentrated sulphuric acid before entering the solvent. Owing to the low solubility of the gas, it was found advisable to use saturated solutions.

The spectra of the solutions were studied with special care in the region between 3.0μ and 4.0μ, since it seemed improbable that the fundamental band would be shifted very far from its normal position at 3.46μ. Special attention was also given the spectra of the solutions in the neighborhood of characteristic solvent bands in order to observe possible changes in the spectra of the solvent produced by the dissolved gas.

In Fig. 1 are shown the results obtained with the four solutions and the corresponding solvents in the region between 3.0μ and 4.0μ. The transmissions of the solvents are given by the solid curves, while those of the solutions are indicated by the dotted curves at all places where they differ from the solvent transmission. The fact

that the transmission curves of solvent and solution coincide in most spectral regions indicates accurate matching of cell thicknesses. It will be observed that in the case of benzene the principal difference between solvent and solution transmission occurs near 3.45μ, a result in agreement with the previous study.[3] In the chlorobenzene, nitrobenzene, and *m*-nitrotoluene plots the major differences occur at longer wave-lengths (3.5μ, 3.6μ, and 3.7μ, respectively). In the case of chlorobenzene a minor difference occurs near 3.0μ. This variation may arise from a small amount of some reaction product. At wave-lengths shorter than 2.9μ the chlorobenzene curves coincide once more. The major differences listed are attributed to the absorption of the molecules of the solute, since characteristic solvent bands in other spectral regions were apparently unaffected by the presence of the HCl. There was some difficulty in measuring the HCl absorption in benzene and in chlorobenzene owing to the proximity of solvent bands. However, the results given in Fig. 1 were repeated a number of times, and the additional absorption observed is too great to be attributed to apparent shifts of solvent band with variations in cell thickness of the type observed by Barnes in his studies of benzene.[6]

In order to gain accurate information concerning the exact spectral positions of the absorption bands produced by the HCl in solution, curves were plotted showing the ratios of solution transmissions to solvent transmissions. Band positions obtained from ratio curves of this type are accurate for the dilute solutions used in the present work, the localizations of maxima being accurate to 0.03μ. The ratio curves are given in Fig. 2. As one may readily see from this figure, the HCl absorption maxima appear as follows: in benzene at 3.47μ, in chlorobenzene at 3.52μ, in nitrobenzene at 3.68μ, and in *m*-nitrotoluene at 3.75μ. The differences in the intensities of the absorption bands as revealed by the ratio curves are due primarily to differences in concentration. As the dipole moment of the solvent is increased, the absorption maximum produced by the HCl present is shifted to longer wave-lengths. Although no generalizations can be made from a study involving only four aromatic solvents, it appears that in the case of the solutions studied variations in wave-length of the HCl maxima from the maximum gaseous absorption can be expressed in terms of the first and second powers of the dipole moments of the solvents.

In Table I are given the solvents, their dipole moments, the variations in wave numbers of the frequency of the solute from the frequency of gaseous HCl, and the relative absorption coefficients of HCl in the various solvents. It will be noted that the frequency shifts caused by nitrobenzene and *m*-nitrotoluene are greater than the limiting value found by West and Arthur[4] for the solutions investigated in their Raman work. In computing the relative absorption coefficients it was assumed that the coefficient in any solution is directly proportional to the HCl concentration, and the values given in the table are for solutions of equal concentration. The low value of the coefficient in nitrobenzene and in *m*-nitrotoluene is probably due to a slight dissociation of HCl in these solvents.[7] In all the solutions the absorption coefficients are greater than the coefficient of gaseous hydrogen chloride.

The results obtained in this study show that the HCl vibrational frequency varies in a manner

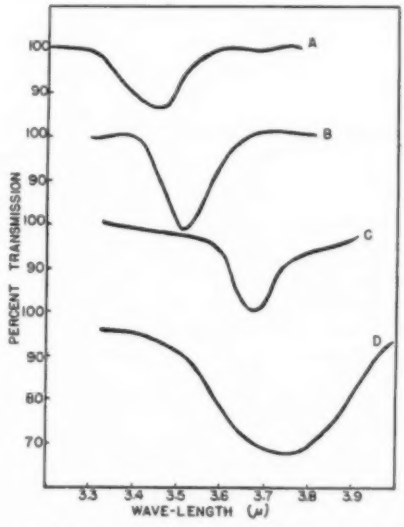

FIG. 2. The ratios of HCl solution transmission to solvent transmission: A. Benzene; B. Chlorobenzene; C. Nitrobenzene; D. *m*-Nitrotoluene.

[6] R. R. Barnes, Phys. Rev. **36**, 296 (1930).

[7] C. P. Wright, D. M. Murray-Rust and Harry Hartley, J. Chem. Soc. 199 (1931).

TABLE I. *Deviation of position of maximum absorption in solutions of HCl in various solvents.*

Solvent	Dipole moment* e.s.u.$\times 10^{18}$	Variation of HCl maximum	Relative absorption coefficients
Benzene	0.08	10 cm^{-1}	2.19
Chlorobenzene	1.52	40	2.71
Nitrobenzene	3.90	170	1.00
m-Nitro-toluene	4.20	200	1.09

*Values from P. Debye, *Polar Molecules* (Chemical Catalog Co., 1928).

depending upon the dipole moment of the solvent. The diminution of the vibrational frequency with increasing moment of solvent indicates a decrease in the effective binding force between the hydrogen and chlorine nuclei. It is possible that HCl in a polar liquid is in a state of incipient dissociation, the effect recognized by Nernst and Thomson in their early correlation between ionizing power and dielectric constant of solvents. On this hypothesis, the decrease of the effective force constants is due solely to dipole interactions. However, the changes in vibrational frequency produced by aromatic solvents are greater than those predicted by West and Arthur[4] on the basis of results obtained with solvents of another type. This indicates that the chemical nature of the solvent is also an important factor in determining the state in which HCl exists in solution. Fairbrother[8] in his studies of dipole moments finds that the moment of HCl apparently increases from 1.08×10^{-18} e.s.u. in the gaseous state to 1.30×10^{-18} e.s.u. in benzene solution, while the solvent ethyl bromide leaves the HCl moment unchanged. It is thus probable that dissolved HCl enters into associational complexes with certain solvents but remains unassociated with others. The formation of complexes would greatly modify the spectra of both solvent and solute, but changes in the spectrum of the solvent would be difficult to observe because of the masking effect of the vastly greater number of undistorted absorbing units. It is probable that both dipole interaction and the formation of complexes are involved in producing the observed effects.

The writer wishes to express his appreciation to Dr. E. K. Plyler for the use of his laboratory facilities and for his discussion of the manuscript and to Miss Estelle McClees and Mr. G. C. Kyker for their assistance in certain parts of the experimental work.

[8] F. Fairbrother, J. Chem. Soc. **43** (1932); J. Chem. Soc. 1541 (1933).

OCTOBER 15, 1936 PHYSICAL REVIEW VOLUME 50

A Mass-Spectrographic Analysis of the Ions Produced in HCl Under Electron Impact

ALFRED O. NIER AND ELMO E. HANSON, *Department of Physics, University of Minnesota, Minneapolis, Minnesota*

(Received July 13, 1936)

An investigation has been made by a mass spectrograph of the ions formed in HCl under electron impact. The following ions were observed: HCl^+, HCl^{2+}, H^+, Cl^+, Cl^{2+}, Cl^{3+}, Cl^{4+}, Cl^{5+}, and Cl^-. When He and Ne were used as calibrating gases, the following appearance potentials were determined: HCl^+, 12.9 ± 0.2 volts; HCl^{2+}, 35.7 ± 1.0; H^+, 18.6 ± 0.3 and 28.4 ± 0.3; Cl^+, 17.2 ± 0.5 and 21.2 ± 0.5; Cl^{2+}, 45.7 ± 0.3; Cl^{3+}, approximately 160; Cl^-, approximately 1.6 volts. The efficiency of ionization curves were of the usual form. From the ratio of the peak heights of HCl^{35} to HCl^{37} the abundance ratio Cl^{35}/Cl^{37} was found to be 3.07 ± 0.03. Cl^{39} if present was less than 1/20,000 of Cl^{35}.

INTRODUCTION

IT is the purpose of this paper to present the results of a mass-spectrographic study of the ions formed in HCl under electron impact and to correlate these results as far as possible with other available data.

The mass spectrograph used in the investigation was the same as that employed by Tate, Smith, and Vaughan.[1] It should be recalled that in this apparatus the ions are formed in a homogeneous beam of electrons of controlled energy and are subsequently analyzed by a 180° magnetic analyzer. The analyzed ion current is

[1] Tate, Smith, and Vaughan, Phys. Rev. **48**, 525 (1935).

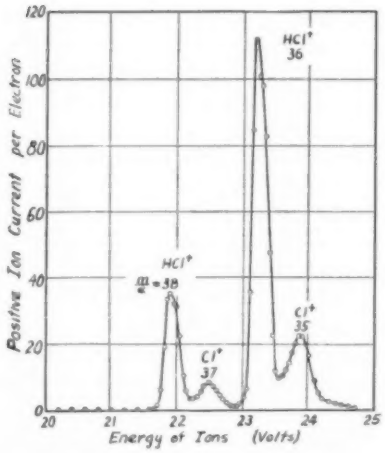

FIG. 1. Typical mass spectrum found in the region of HCl^+. Accelerating voltage applied to electrons, 100 volts. Magnetic field, 1175 gauss.

measured by a vacuum tube amplifier described by Distad and Williams.[2] As the mass spectrograph is designed primarily for the study of polyatomic gases, a differential pumping system is employed to prevent thermal dissociation products formed around the hot filament from diffusing into the ionizing region.

After the apparatus was baked out for several days at a temperature of 400°C, the only impurities which remained were a negligible amount of water vapor and carbon monoxide. The HCl was then permitted to flow into the tube through a capillary leak. The combined rate of leak and pumping speed were such that the pressure in the tube was less than 10^{-4} mm Hg. Liquid air was used on the traps between the mass spectrograph and the mercury diffusion pumps.

Mass Spectra

Fig. 1 shows a typical mass spectrum found in the region of HCl^+. It is seen that peaks are present for m/e values 38, 37, 36, and 35 corresponding to the ions $(H^1Cl^{37})^+$, $(Cl^{37})^+$, $(H^1Cl^{35})^+$, and $(Cl^{35})^+$, respectively. From Fig. 2 it is seen that the ions HCl^{2+} and Cl^{2+} are present. This figure shows also the isotopes of neon which was present in the apparatus as a calibrating gas. Fig. 3 shows the mass spectrum in the neighborhood of H^+. The trailing to the left of the peak is

[2] Distad and Williams, Rev. Sci. Inst. **5**, 289 (1934).

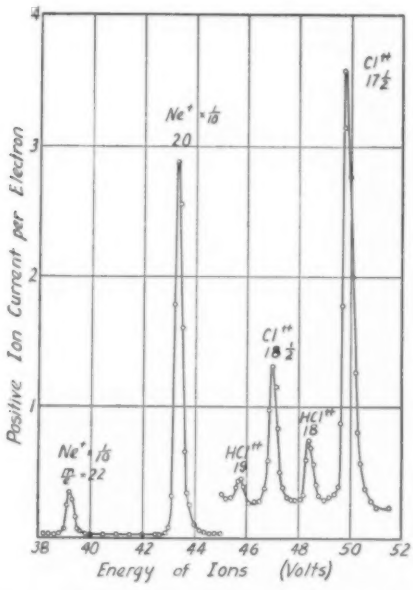

FIG. 2. Typical mass spectrum found in the region of $(HCl)^{2+}$. Accelerating voltage applied to electrons, 100 volts. Magnetic field, 1175 gauss.

due to the considerable amount of kinetic energy given the H^+ ion in the dissociation process.

In addition to the above mentioned ions, Cl^{3+}, Cl^{4+}, Cl^{5+}, and Cl^- were observed. A search was made for Cl_2^+, H_2^+, HCl^{3+}, H^-, and HCl^-, but no trace could be found of these ions.

Efficiencies of Ionization

In Figs. 4, 5, and 6 are shown curves for the relative efficiencies of formation of the more abundant ions as a function of electron energy.

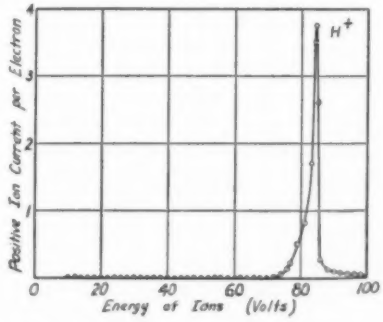

FIG. 3. Typical mass spectrum found about H^+. Accelerating voltage applied to electrons, 100 volts. Magnetic field, 400 gauss.

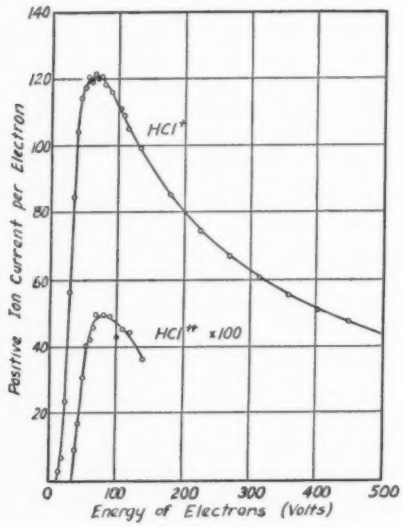

FIG. 4. Efficiency of formation of $(HCl)^+$ and $(HCl)^{2+}$ as a function of electron energy. HCl^{2+} curve carried out to only 140 volts.

The ordinates of these graphs have all been reduced to the same pressure and electron current. It is to be observed that the positive ion curves are of the usual form. The efficiency curve of Fig. 6 for Cl^- is similar in shape to the curves found for negative ions in H_2O,[3,4] CO,[4,5] NO,[4] and O_2.[4,6] In order to identify definitely the negative ions fomed in HCl, Cl_2 was admitted to the apparatus as a calibrating gas. It is known that when Cl_2 is bombarded by electrons of the proper energy, Cl^- ions are formed. As the ions formed in HCl had exactly the same m/e as those found in Cl_2, it was definitely established that they were Cl^- ions.

Ionization Potentials and Probable Processes of Ionization

In Table I is given a list of all the ions observed, the appearance potentials of the more abundant ones, the probable processes of formation, and the theoretical minimum electron energy required to form the ions by the assumed processes.

While the ionization potential measurements were being made, HCl, He, and Ne were present together in the apparatus. The appearance potentials of HCl were determined in reference to the ionization potentials of the calibration gases, Ne and He.

The calculated minimum energy of formation was obtained by using a heat of dissociation of HCl of 4.42 volts.[7] The energy levels of the Cl atom are taken from Bacher and Goudsmit.[8]

The appearance potential of HCl^+, 12.9 ± 0.2 volts, is in agreement with Barton's[9] value of 13.3 ± 1.5 volts.

The group of H^+ ions with the appearance potential of 18.6 ± 0.3 volts may be correlated with a dissociation process in which the chlorine atom remains unexcited. The minimum energy required for such a process would be $4.42(D_{HCl})+13.54(\text{I.P. of H})=17.96$ volts. The fact that the observed appearance potential is slightly higher than this calculated minimum indicates that the molecule must dissociate with some kinetic energy.

The group of H^+ ions with the appearance potential of 28.4 ± 0.3 volts may be ascribed to a process in which dissociation takes place with excitation of the chlorine atom. The lowest excited level in the chlorine atom is 8.89 volts

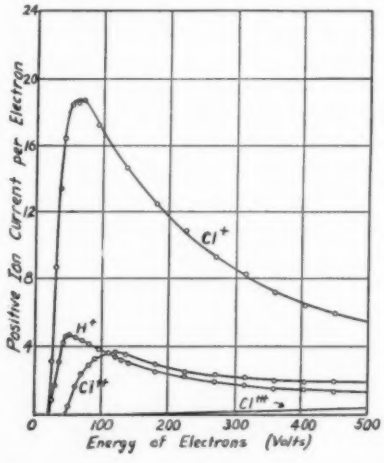

FIG. 5. Efficiency of formation of H^+, Cl^+, Cl^{2+}, and Cl^{3+} as a function of electron energy.

[3] Lozier, Phys. Rev. **36**, 1417 (1930).
[4] Tate and Smith, Phys. Rev. **39**, 270 (1932).
[5] Tate and Lozier, Phys. Rev. **39**, 254 (1932).
[6] Lozier, Phys. Rev. **46**, 268 (1934).
[7] Landolt-Börnstein **2**, 1489 (1923); Frank, Trans. Faraday Soc. **2**, 536 (1926).
[8] Bacher and Goudsmit, *Atomic Energy States* (McGraw-Hill Book Company, New York).
[9] Barton, Phys. Rev. **30**, 614 (1927).

above the ground state. Thus, the minimum energy required to form $H^+ + Cl$ (excited) would be $4.42(D_{HCl}) + 13.54(\text{I.P. of H}) + 8.89 = 26.85$ volts. The discrepancy between this value and the observed appearance potential may be explained either in one or both of two ways: (1) The dissociation takes place with a large amount of kinetic energy, or (2) The chlorine atom is excited to some higher level or levels than the one considered.[10]

The group of Cl^+ ions with the lower appearance potential is probably formed by a dissociation into H (normal) $+ Cl^+$ (normal). The calculated minimum energy required for this process is within experimental error equal to the observed appearance potential.

It has not been possible to correlate definitely the second group of Cl^+ ions with any known process. Neither the hydrogen atom nor the Cl^+ ion can be excited since this would require an appearance potential larger than the one observed. A possibility that suggests itself is that the lower group of Cl^+ ions come from the stable $HCl^+(^2\Pi)$ potential energy curve, while the second group arises from the corresponding repulsive curve. The difference in the appearance potentials is a measure of the difference in the kinetic energy given the dissociation products by the two processes. The fact that r_e for HCl (normal) is nearly equal to r_e for $HCl^+(^2\Pi)$[11] militates against this explanation. Another possible explanation is that both groups of Cl^+ ions arise from repulsive potential energy curves and that the second group comes from a higher or steeper curve. Such unstable potential curves might exist for each of the triplet states of $Cl^+(^3P)$.[12]

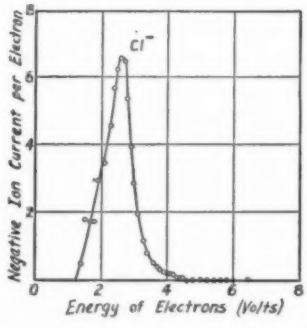

FIG. 6. Efficiency of formation of Cl^- as a function of electron energy.

TABLE I. *Summary of experimental results.*

Ion observed	Appearance potential (volts)	Probable process	Calculated minimum energy required (volts)
HCl^+	12.9±0.2	$HCl \rightarrow HCl^+$	
HCl^{2+}	35.7±1.0	$HCl \rightarrow HCl^{2+}$	
H^+	18.6±0.3	$HCl \rightarrow H^+ + Cl$	17.96
	28.4±0.3	$HCl \rightarrow H^+ + Cl(^4P)$	26.85
Cl^+	17.2±0.5	$HCl \rightarrow H + Cl^+$	17.38
	21.3±0.5	$HCl \rightarrow H + Cl^+$	
Cl^{2+}	45.7±0.3		
Cl^{3+}	160 (approximately)		
Cl^{4+}			
Cl^{6+}			
Cl^-	1.2 (approximately)	$HCl \rightarrow H + Cl^-$	0.7

It should be noted that in Barton's work on HCl[9] the formation of H^+ and Cl^+ ions was a function of the water vapor present in the experimental tube. This made it uncertain whether these ions were formed by simple collisions between electrons and HCl molecules. In the present work, since the tube could be baked out, only a minute trace of water vapor was present, while the HCl gas was dry.[13] The fact that no H_2^+ or Cl_2^+ ions were observed showed that dissociation products were not getting into the ionizing region and that the H^+ and Cl^+ ions did not come from H_2 and Cl_2 molecules respectively. Barton's failure to observe some of the ions found in this work may be easily explained by the fact that his apparatus was not so sensitive as that used here.

ISOTOPE RATIO

From the ratio of the peak heights of HCl^{35} to HCl^{37} the abundance ratio of the chlorine isotopes was calculated to be $Cl^{35}/Cl^{37} = 3.07 \pm 0.03$. The value for this ratio as calculated from the atomic weight is 3.10. This may be regarded as a very satisfactory check. Kallman

[10] Two other possibilities of excitation of Cl exist: it could be in either the ^3P state or in the $^4P^0$ state. (See reference 8.)

[11] Jevons, *Report on Band Spectra of Diatomic Molecules* (The Physical Society, London).

[12] Mulliken, Rev. Mod. Phys. **4**, 6 (1932).

[13] As a second precaution to insure dryness of the gas, CO_2 snow was kept on a trap in the gas reservoir.

and Lazareff[14] found the ratio to be 3.24. Aston[15] found values between 3.0 and 3.1.

Becker,[16] Hettner and Bohme,[17] and Kallman and Lazareff[14] have given evidence for the existence of Cl^{39}. On the other hand, Ashley and Jenkins,[18] and Hardy and Sutherland[19] have been unable to find Cl^{39}. From the present investigation it is concluded that Cl^{39}, if present, exists to less than 1 part in 20,000 compared to Cl^{35}.

The writers wish to express their appreciation to Professor John T. Tate for his interest and advice in connection with this experiment. The HCl gas was furnished by D. L. Fuller, C. P. Roe, and R. E. Peck of the School of Chemistry, University of Minnesota.

[14] Kallman and Lazareff, Zeits. f. Physik **80**, 237 (1933).
[15] Aston, *Mass Spectra and Isotopes* (Longmans, Green & Co., New York).
[16] Becker, Zeits. f. Physik **59**, 583 (1930).
[17] Hettner and Bohme, Zeits. f. Physik **72**, 95 (1931).
[18] Ashley and Jenkins, Phys. Rev. **37**, 1712 (1931).
[19] Hardy and Sutherland, Phys. Rev. **41**, 471 (1932).

OCTOBER 15, 1936 PHYSICAL REVIEW VOLUME 50

Collisions of Alpha-Particles with Sulphur Nuclei*

ROBERT L. ANTHONY, *Sloane Physics Laboratory, Yale University, New Haven, Connecticut*
(Received July 20, 1936)

More than 700,000 thorium C and C′ alpha-particle tracks have been photographed with a stereoscopic camera in a Wilson chamber filled with a mixture of hydrogen sulphide and hydrogen. A range-velocity curve for sulphur recoil atoms has been constructed by plotting the measured ranges (reduced to standard air) against the calculated velocities for 60 selected alpha-particle sulphur collisions. This curve is discussed and compared with the results of other workers. A possible relationship has been noted between the range-velocity curves of atoms having similar electronic configurations. No collisions indicating possible sulphur disintegrations were observed. Several low energy collisions were noted which were apparently lacking in coplanarity, but this effect is explained as being due to small deflections suffered by the recoil nucleus shortly after the collision. The calculated distances of closest approach are compared with the radius of the sulphur nucleus as given by Pollard and Brasefield. The methods of measurement and calculation employed have been checked by applying them to collisions with protons.

I. INTRODUCTION

SINCE the pioneer experiments of Blackett and others, the Wilson cloud chamber has become of great importance in the study of nuclear reactions. No accurate interpretation of the energy changes in these reactions can be made, however, unless it is possible to deduce the velocities of the recoiling particles from their observed ranges. The relationship expressing the velocity as a function of the range of the particle cannot as yet be obtained from theory for heavy nuclei owing to the complexity of these atoms, and the construction of such a curve is of necessity an experimental problem.[1] Previous experiments by Blackett,[2] Blackett and Lees,[3] Feather,[4] and Eaton[5] have established such curves for several elements. However, it is important that such information be extended as far as possible in order that a general empirical relationship may be established which will apply to all atoms.

The element sulphur was selected in this work for the following reasons:

First, a stable gaseous compound of sulphur, hydrogen sulphide, can be obtained, enabling this element to be studied conveniently in the cloud chamber, and the form of the range-velocity curve can therefore be determined.

Second, in addition to increasing the general information on the subject of range-velocity curves the form of the sulphur curve is of particular interest in the study of the following nuclear reaction

* Part of a dissertation presented to the Faculty of the Graduate School of Yale University in candidacy for the degree of Doctor of Philosophy.
[1] Calculations made by W. E. Duncanson, Proc. Camb. Phil. Soc. **30**, 102 (1933–34), and by G. Mano, J. de phys. et rad. [7] **5**, 628 (1934), using the theoretical expressions of Bethe and Bloch, have yielded results in good agreement with experiment for the range-velocity relations of alpha-particles and protons of moderately high energies. Unfortunately, however, the assumptions made in the derivation of these formulae preclude their application to particles having the low energies considered here.
[2] P. M. S. Blackett, Proc. Roy. Soc. **A102**, 294 (1922); **A103**, 62 (1933).
[3] P. M. S. Blackett and D. S. Lees, Proc. Roy. Soc. **A134**, 658 (1932).
[4] N. Feather, Proc. Roy. Soc. **A141**, 194 (1933).
[5] W. W. Eaton, Phys. Rev. **48**, 921 (1935).

$$_{15}P^{31}+{}_{2}He^{4}\rightarrow{}_{16}S^{34}+{}_{1}H^{1}$$

giving a proton and the $_{16}S^{34}$ nucleus, an isotope of $_{16}S^{32}$. This reaction has been shown to take place by counting experiments when phosphorus is bombarded with thorium C′ alpha-particles. (The range-velocity curve determined experimentally in this work is for $_{16}S^{32}$, whereas the nucleus obtained in the above reaction is $_{16}S^{34}$. However, to a first approximation this curve may be taken as representing also the range-velocity relation for any such $_{16}S^{34}$ nucleus, the actual error involved in this procedure being as yet unknown, but certainly small.)

Third, since disintegration protons are known to appear when sulphur is bombarded with thorium C′ alpha-particles, there was a small but finite probability that a disintegration of a sulphur nucleus might be observed during the course of this work. The importance of observing such an event in the cloud chamber is readily seen when we consider the fact that only with the cloud chamber can we observe all of the particles resulting from a single nuclear process of this type along with their respective ranges and directions of emission.

II. Experimental Arrangements and Analysis of the Tracks

Since the chamber was to be used primarily for the study of range-velocity relations of heavy nuclei, it was deemed advisable to make it large in diameter and capable of operation at any pressure below 76 cm. The use of a large diameter chamber and operation at a pressure sufficiently low to make the ranges of the thorium C′ alpha-particles in the chamber comparable to the diameter enables relatively long recoil tracks to be obtained. The accuracy of the measurements made upon the forks may thus be increased. This is especially important when studying the collisions of alpha-particles with heavy nuclei since the velocity which a heavy nucleus attains when struck by an alpha-particle is comparatively small, and its range in air at normal pressure and at a temperature of 15°C (hereafter designated as its reduced air range) is therefore short.

The internal diameter of the chamber was accordingly made slightly greater than 20 cm, and the chamber was so constructed as to be possible of operation at any pressure between the extreme limits of 0 and 2 atmospheres. The chamber is of the sylphon type and follows the general design of Dahl, Hafstad and Tuve.[6] The agency for producing the sudden expansion is a piston operated by compressed air. The adjustment of the expansion ratio is made by means of stops threaded on to the drive shaft connecting the piston to the sylphon. This adjustment is entirely independent of the pressure of the gas used in the chamber. Variations in atmospheric pressure do not affect either the expansion ratio or the pressure of the gas in the chamber.

The illumination is provided by a pair of carbon arcs placed on opposite sides of the chamber. The arcs are operated in series from the 220 volt d.c. line. The shorting out of a large resistance in series with the arcs at the time of the expansion permits a current of about 40 amperes to flow through the arcs for a short interval of time and produces very intense illumination.

The camera used in this work is of the Kurie type.[7] The essential features of this type of camera are briefly as follows. By means of an appropriate mirror and prism system this camera is made equivalent to two cameras taking two simultaneous pictures along lines of sight at right angles to each other. By inclining the film planes slightly to the plane of the lens (accomplished by means of a special film wedge) the mid-plane of the chamber is made conjugate to both images. Thus the whole illuminated region of the chamber may be kept in sharp focus for each image. The operation of the camera is entirely automatic, a small d.c. motor serving to drive the film forward between expansions. The lens used is a Bausch and Lomb "Micro-Tessar" of 32 mm focal length, and the shutter is a Wollensak "Betax" (automatic). A flexible cable release attached to the armature of a small electromagnet opens the shutter at the appropriate moment in each cycle of operations.

The source of alpha-particles is a small monel metal button upon which thorium active deposit has been collected. This source is mounted outside the chamber and separated from the

[6] O. Dahl, L. R. Hafstad and M. A. Tuve, Rev. Sci. Inst. **4**, 373 (1933).
[7] F. N. D. Kurie, Rev. Sci. Inst. **3**, 655 (1932).

chamber by means of a piece of mica waxed over a series of five 1-mm diameter holes. The space between the source and the mica window is evacuated in order to insure that no loss in the energy of the alpha-particles occurs before they enter the mica. The stopping power of the mica window used was 0.8 cm air equivalent (determined by weighing). Thus the residual reduced air ranges of the thorium C and C′ alpha-particles in the chamber were 3.99 cm and 7.82 cm, respectively.

The stopping power of the gas mixture in the chamber relative to standard air was computed at all times since the relative proportions of the hydrogen sulphide, hydrogen, and water vapor present in the chamber were always known. This method of determining the stopping power of the gas mixture was preferred to a direct comparison of the measured ranges in the chamber with those to be expected in standard air, since it was found that the direct comparison involved a small error as a result of the vertical spread of the beam of alpha-particles from the source. This vertical spread had the effect of making the average alpha-particle range in the chamber appear to be shorter than the true range when this average range was determined by measurements made upon any single reprojection print, the difference in stopping powers as determined by the two methods amounting to about three percent. This effect was not, however, a source of error in the measurements made upon any single collision when the collision had been properly recombined.

Photographs were taken on 100-foot reels of Eastman "Super X" panchromatic grayback film. The individual pictures were examined visually by passing the film over a specially constructed light box. Reprojection of the images is accomplished by replacing the film in the camera and illuminating the film from above. The methods and apparatus used for recombining the forks and the analysis of the reprojection prints have been thoroughly described by Eaton[5] and need not be discussed here.

III. Results

A little more than 10,000 stereoscopic pictures were taken of alpha-particle tracks in a gas mixture of hydrogen sulphide and hydrogen. A rough estimate of the average number of alpha-particle tracks on each picture yields the value of 70 tracks per expansion, making a total of 700,000 alpha-particle tracks photographed. Of this total number approximately 65 percent, or 455,000, were of the longer range type while the remaining 35 percent, or 245,000 were of the shorter range variety. Over 200 collisions of alpha-particles with sulphur nuclei were reprojected and examined. Approximately 50 of these were rejected in the measuring-up process, and from the remaining number 60 were selected as being suitable for a range-velocity curve. Fig. 1 shows the plot of the ranges of the recoil sulphur nuclei (reduced to standard air) against their computed velocities. The dotted curve, drawn in for comparison, is the range-velocity curve for argon as given by Blackett and Lees. It is seen that for ranges of the recoil nuclei greater than 1 mm the argon curve falls below the sulphur curve. This is to be expected on the basis of the formula proposed by Blackett and Lees

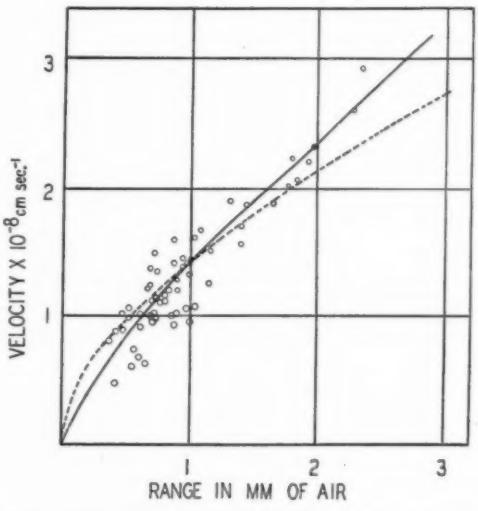

FIG. 1. Range-velocity curve for sulphur recoil atoms. Dotted curve is curve for argon atoms as given by Blackett and Lees.

$$R = kmZ^{-\frac{1}{2}}f(v).$$

Here R is the range of the recoil atom, m its mass, Z its atomic number, and v its velocity. $f(v)$ is a function of the velocity alone, and k is a constant. If this formula applies we see that for the case of argon and sulphur nuclei of the same velocity we should have

$$R_S/R_A=(m_S/m_A)(Z_A/Z_S)^{\frac{1}{2}}$$

where R_S, m_S and Z_S are the range, mass, and atomic number respectively of the sulphur atom, and R_A, m_A, and Z_A are the corresponding quantities for the argon atom. Since $m_S=32$, $m_A=39.9$, $Z_S=16$, and $z_A=18$ we have

$$R_S/R_A=0.85.$$

Hence, for the same velocity the sulphur atom should have a shorter reduced air range than the argon atom, and the sulphur range-velocity curve should lie above the argon curve. The fact that the two curves cross at about 1 mm range may have no real significance. Blackett and Lees had available Gurney's data[8] on the variation of the stopping power of argon with the range of the alpha-particles and were therefore able to correct the reduced air ranges of the recoil argon nuclei in the short range region. Since no data exist on this variation in hydrogen sulphide or even in sulphur, it could only be hoped that these variations in the case of hydrogen and sulphur (assumed to be opposite in direction) would partially balance out. The form of the sulphur curve below 1 mm range may, therefore, be slightly incorrect. However, exactly the same effect was noted by Eaton when he compared his neon curve with Feather's fluorine curve, the two curves crossing in the low range region.

If we compare the ratios of the ranges as measured from the curves in Fig. 1 for four selected values of the velocity we obtain Table I. The value of the ratio is seen to decrease steadily as higher velocity points are selected, whereas the formula predicts a value of 0.85 for all cases.

TABLE I.

Velocity (10^{-8} cm/sec.)	1.6	2.0	2.4	2.6
Ratio R_S/R_A	0.95	0.90	0.85	0.80

TABLE II.

Velocity (10^{-8} cm/sec.)	1.0	1.5	2.0	3.0
Ratio R_S/R_O	1.18	1.14	1.16	1.16

TABLE III.

Velocity (10^{-8} cm/sec.)	1.0	1.5	2.0	2.5
Ratio R_A/R_{N_e}	1.07	1.07	1.07	1.07

[8] R. W. Gurney, Proc. Roy. Soc. **A107**, 340 (1925).

Since the two curves are obviously not similar, this discrepancy between the measured ratios and the predicted value might have been expected.

If we compare the sulphur curve with the oxygen curve of Blackett and Lees (not shown), a marked similarity between the forms of the two curves is noted. Comparing the ratios of the ranges for four selected velocity points we obtain Table II. The ratio is seen to remain constant within the limits of measurement showing that for this case, at least, $R_S=K_Sf(v)$ and $R_O=K_Of(v)$ where the K's are undetermined constants. That is, the unknown function of the velocity is the same for each curve. Here the formula of Blackett and Lees predicts a value of 1.41 for the ratio of R_S to R_O, and this is definitely too high. The constancy of this ratio in the case of sulphur and oxygen suggested the possibility that the unknown function of the velocity upon which the range of the recoil atom depends might be the same for atoms of similar electronic configurations, for elements in the same column in the periodic table. Eaton's neon curve was accordingly compared with the argon curve of Blackett and Lees. Again, a decided similarity between the forms of the two curves was noted. For four different velocity points the following ratios in Table III were obtained. The ratio is seen to remain constant here also. For this case the predicted value is 1.35 and is again too high. In each of these two cases the comparison of the two curves was somewhat rough, and the agreement of the range ratios for the case of argon and neon may not be quite as good as that given above. The curves for argon and neon were also compared with the helium curve (alpha-particle range-velocity curve). In general, the range ratios were not as constant as in the preceding two examples. However, for ranges greater than 1 mm the agreement between the individual ratios was fair.

The reduced air ranges of the recoil sulphur nuclei in the four highest energy collisions obtained were 2.35, 2.28, 1.97, and 1.93 mm respectively, while the corresponding velocities were 2.92, 2.61, 2.32, and 2.22×10^8 cm/sec. It is interesting to note that the angle ϕ for the recoil alpha-particle in each of these four cases was appreciably greater than 90°, the four values being 117.5°, 109.0°, 126.9° and 100.4°.

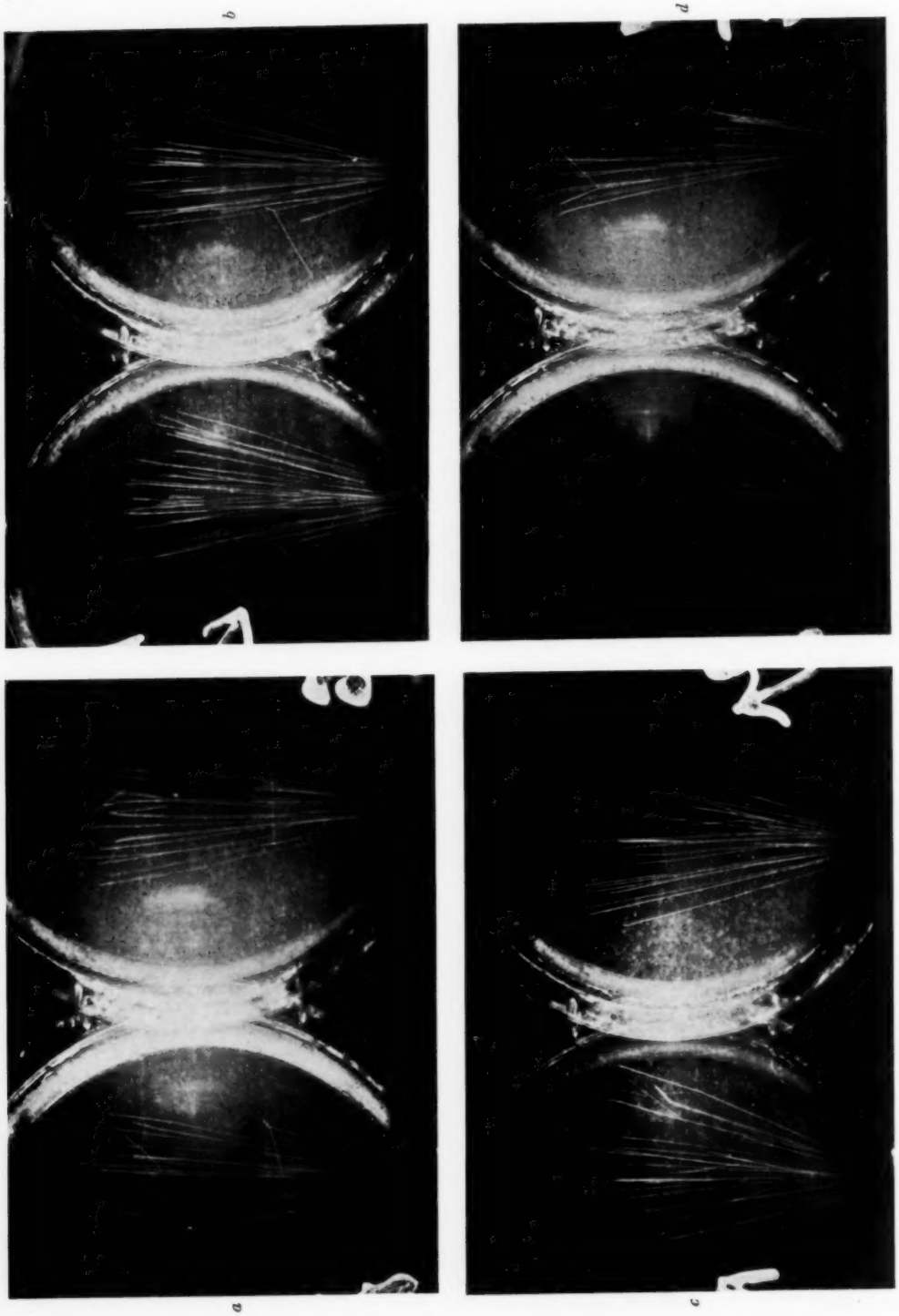

FIG. 2. *a*, *b*, Cloud chamber photographs of collisions between α-particles and sulphur nuclei. *c*, *d*, Typical photographs of collisions between α-particles and protons.

The distances of closest approach of the alpha-particles to the sulphur nuclei were calculated for these four collisions, on the assumption that the inverse square law of force held, and were found to range from 11.9 to 22.6×10^{-13} cm. It is of interest to compare these values with the value 5.4×10^{-13} cm for the radius of the sulphur nucleus as given by Pollard and Brasefield.[9] The two highest energy collisions observed with sulphur nuclei are shown in Fig. 2 (*a*) and (*b*).

No disintegrations of sulphur nuclei were observed. Several low energy collisions were noted which were apparently not coplanar, but these were collisions in which the ranges of the recoil sulphur nuclei were so short that very little reliance could be placed in the measurements made upon them. In the examination of a large number of collisions the same effect previously noted by Eaton[5] was frequently observed, namely, that when near the end of the range the recoil atom frequently gives rise to a track showing a decided curvature due to a series of small collisions. It therefore seems probable that the apparent lack of coplanarity in a small number of low energy collisions was due to this cause, the "curving" of the recoil atom out of the plane of the collision making a complete recombination of the fork impossible.

Since the chamber was filled with a mixture of hydrogen sulphide and hydrogen an appreciable fraction of the collisions observed were with protons, the majority of these being examined merely to insure that the proton tracks could not be the result of sulphur disintegrations. However, measurements were made upon several of these and the results were compared with the proton range-velocity curve of Blackett and Lees as a check upon the accuracy of the methods of measurement employed in this work. This plot is shown in Fig. 3. Examples of two typical proton collisions are shown in Fig. 2 (*c*) and (*d*). Fig. 2 (*c*) shows a proton being ejected out of the chamber as a result of a collision with an alpha-particle.

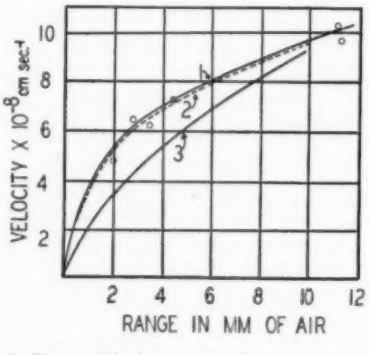

FIG. 3. Range-velocity curves for protons. Curve 1, protons in 50 percent H_2S+50 percent air; curve 2, protons in air; curve 3, α-particles in air.

[9] C. J. Brasefield and E. C. Pollard, Phys. Rev. **50**, 296 (1936).

IV. Discussion and Conclusion

In the comparison and use of range-velocity curves in their present form, it is well to bear in mind the following points.

First, in obtaining the reduced air ranges of the recoil nuclei the assumption is made that the stopping power of the gas mixture is the same for the recoil atom as for the alpha-particle. This is, at best, a somewhat doubtful procedure, although for higher energies than those considered here this assumption is valid as has been shown by the theoretical work of Bethe and Bloch.

Second, the assumption is made that the variation of the stopping power with the range of the particle is the same for both the alpha-particle and the recoil atom. There is no more justification for this assumption than for the first.

Third, the possible small variations in the form of the range-velocity curve for a given type of atom in different gas mixtures containing different elements are not usually considered.

Finally, attention should be called to the spread of the experimental points from which any range-velocity curve is obtained. The straggling of the alpha-particles introduces a small error into the determination of the velocities of the recoil atoms. Also, the straggling of the recoil atoms, which according to Blackett's estimate may be as high as 15 percent, introduces an appreciable error into the determination of the ranges of the recoil atoms. These two combined effects of straggling, according to Eaton, probably account for the greater portion of the spread of the points on most range-velocity curves, the remaining errors being errors inherent in the methods of analysis used.

It is hardly wise to attempt to draw any conconclusions from the above two comparisons, that

of sulphur with oxygen, and argon with neon. However, if any significance can be attached to them, it would seem that a satisfactory range-velocity relation must take into consideration the electronic configuration of the recoiling atom, at least in the low energy regions where we cannot consider the recoil particle to be a nucleus stripped of all outer electrons. If this be true, it should lead to a regularity in the forms of the range-velocity curves for the various atoms corresponding to their positions in the periodic table, as has been suggested by Feather. In any event, the simple empirical formula of Blackett and Lees has been shown definitely to be invalid, not only in this work but also in the earlier work of Feather and of Eaton.

In conclusion, it is a pleasure to thank Professor A. F. Kovarik for his constant advice and encouragement throughout the course of this work, Dr. F. N. D. Kurie for the camera castings and a blue-print of his latest design, and Dr. E. C. Pollard for much helpful advice.

OCTOBER 15, 1936 PHYSICAL REVIEW VOLUME 50

The Relative Abundance of the Isotopes in Mn, Cb, Pd, Pt, Ir, Rh and Co

MILO B. SAMPSON AND WALKER BLEAKNEY, *Palmer Physical Laboratory, Princeton University, Princeton, N. J.*

(Received August 3, 1936)

Using a new type of ion source, the abundances of the isotopes of Pd, Ir and Pt were measured and the atomic weights deduced from these values. The atomic weight of Ir was found to be quite different from the chemical value. The analysis of Mn and Cb confirmed the simple nature of these elements to a higher degree than known before. Evidence for the existence of Rh^{101} present to one part in 1300 of Rh^{103} was obtained. Likewise Co^{57}, present to one part in 600 of Co^{59}, was found.

INTRODUCTION

IT is only recently that the isotopic analysis of the last few remaining elements has been determined. Dempster[1] has given some results on Pt, Ir, Rh and Pd but has made no quantitative measurements of abundances. A more thorough search for isotopes of rhodium is of particular interest in view of the fact that it emits β-rays of two periods (44 sec. and 3.9 min., half lives) on irradiation with slow neutrons.[2] Since a knowledge of the relative abundances of isotopes in many other elements is desirable in view of the intensive study now in vogue of nuclear disintegration by various bombarding particles, it seemed worth while to re-examine some of the elements which may be studied by our method.

Apparatus

The apparatus used was the 180° permanent magnet mass spectrograph described in a previous paper.[3] The arrangement was the same except for the ion source, which is shown in Fig. 1. The substance to be analyzed was vaporized from a furnace of tungsten foil W. The ions were produced in the molecular jet by collisions with electrons entering from the opposite side of G_2. G_2 is made of tantalum, the top and bottom being covered with platinum gauze. A small potential of about 1 volt was applied between G_2 and S_1 to draw the ions out. S_1 is a double slit, the two being placed 5 mm apart to prevent the high field between S_1 and S_2 from reaching into the ionization space and producing a velocity spread of the ion beam. The same system of focusing and deflecting the ion beam onto the entrance slit of the mass spectrograph was again applied. The electrons were emitted from a 7.5-mil tungsten filament F. A potential of 45 volts was applied between F and G_1 and a variable potential between G_1 and G_2. For the production of multiply charged ions the total electron accelerating voltage was about 300 volts. The furnace W was made of 1-mil tungsten or tantalum foil, folded into a V shape. The ends of the foil were spot welded to heavy nickel leads. R is a tantalum radiation

[1] Dempster, Proc. Am. Phil. Soc. **75**, 755 (1935); Nature **136**, 909 (1935).
[2] Fermi *et al.*, Proc. Roy. Soc. **A146**, 483 (1934).
[3] Sampson and Bleakney, Phys. Rev. **50**, 456 (1936).

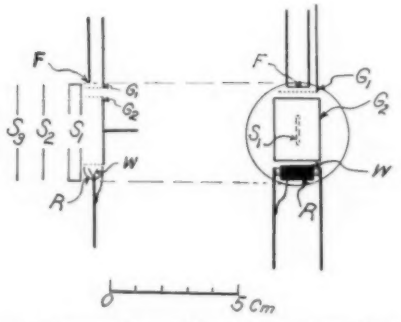

FIG. 1. Ion source. Ions produced by collisions of electrons from filament F, with vapor jet from tungsten furnace W. Slits S_1, S_2 and S_3 are 1.5 mm by 1 cm.

shield supported by one of the current leads, the whole structure being mounted on a ground glass joint to facilitate renewal of the furnace W or its contents. The furnace was heated by a suitably insulated low voltage transformer.

This type of ion source was found to work very well for nearly all the elements tried, giving a reasonably steady source of ions for some time, depending on the rate of vaporization. Multiply charged ions were produced quite effectively with this arrangement, which is particularly advantageous because the isotopes may be examined in several different "orders." The resolution for the higher masses is also greatly improved by using the multiply charged ions.

Palladium

Pure palladium metal was vaporized from the tungsten furnace giving very steady ion beams in several orders. The six isotopes given by Dempster[1] were confirmed and their abundances measured. The ion currents used were not sufficiently great to show any additional isotopes that might have been present in very small amounts. One of the plots taken for palladium is shown in Fig. 2. The mean values for eight measurements on the abundances are given below. The accuracy is believed to be about one part in one hundred.

Mass number	102	104	105	106	108	110
Percent abundance	0.8	9.3	22.6	27.2	26.8	13.5

The atomic weight of palladium, calculated by assuming a packing fraction of -6 and reducing to the chemical scale, is 106.6 from these measurements. The chemical value[4] is 106.7.

[4] Baxter, Hönigschmid and Le Beau, J. Am. Chem. Soc. **58**, 541 (1936).

Iridium

Dempster[5] has shown iridium to consist of two isotopes of mass numbers 191 and 193, the latter being somewhat more abundant. Venkatesachar and Sibaiya[6] have given the ratio of 193 to 191 as roughly 2 : 1 from their work on the hyperfine structure, and deduce an atomic weight of 192.4. Abundance measurements on iridium were made both for the singly and doubly charged ions. A plot of the Ir^{++} ions is shown in Fig. 3. Masses 191 and 193 were found to comprise 38.5 and 61.5 percent respectively of the total ion current. The packing fraction has not been measured but from Aston's curve the masses of iridium must be nearly integral. The atomic

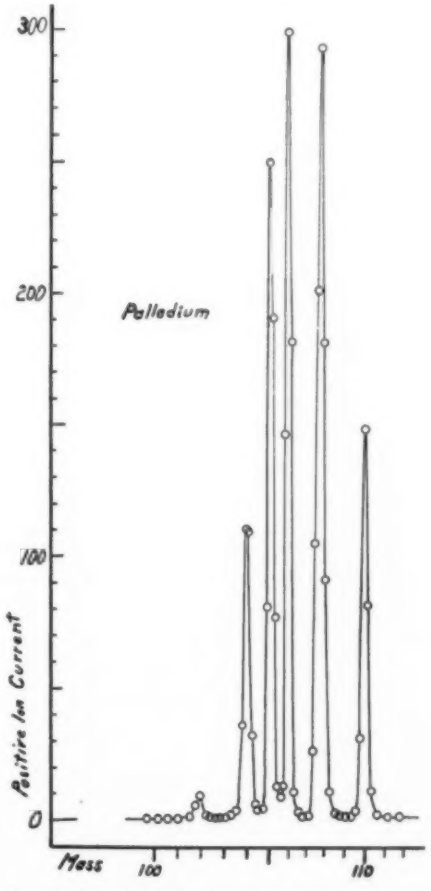

FIG. 2. Plot of singly charged palladium isotopes.

[5] Dempster, Nature **136**, 902 (1935).
[6] Venkatesachar and Sibaiya, Proc. Ind. Acad. Sci. **2**, 203 (1935).

weight of 192.2 thereby deduced is in very poor agreement with the chemical value[4] of 193.1. It seems fairly certain that the value now in use is too high.

Platinum

Abundance measurements made on the platinum isotopes confirmed the isotopes given by Dempster. Doubly, triply and quadruply charged ions were readily produced. The abundances* given below are the average of four measurements, none of which deviated more than one part in 100 from the mean for the abundance of any one isotope.

Mass number	192	194	195	196	198
Percent abundance	0.8	30.2	35.3	26.6	7.2

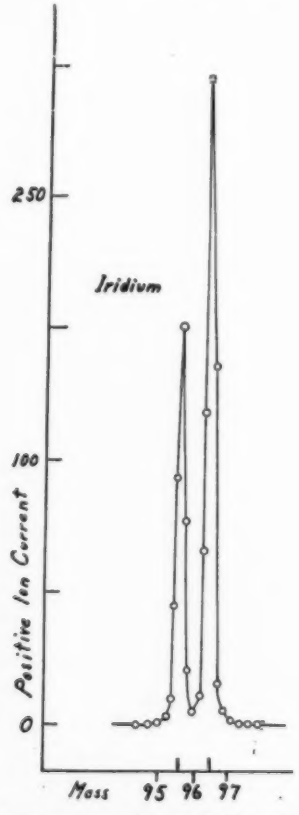

FIG. 3. Mass-spectrum plot of doubly charged iridium isotopes. Peaks at mass numbers 95.5 and 96.5 correspond to masses 191 and 193, respectively.

* Recently Kopfermann and Krebs, Zeits. f. Physik **101**, 193 (1936), have found abundances in rough agreement with those presented here.

If we assume a packing fraction of 0.5 from Aston's curve the atomic weight corrected to the chemical scale comes out to be 195.23 which is identical with the chemical value.

Columbium

This element was found to be very difficult to volatilize. A peak of 400 units at mass 93 was obtained however, confirming Aston's observation.[7] No peaks appeared at mass numbers 91 and 95. No isotope of either of these masses is therefore present to a greater extent than 1 part in 400 of mass 93.

Manganese

Very large ion currents of this element were easily obtained in the three orders Mn^{+}, Mn^{++}, Mn^{+++}. No isotope of either mass 53 or 57 was found to as much as one part in 15,000 of Mn^{55}.

Rhodium

Rhodium was tried in the hope of discovering an additional isotope, which would explain the presence of the two periods of artificial radioactive decay observed for this element.

Pure rhodium metal was vaporized from a tungsten furnace. Considerable trouble was experienced with this element because of the high temperatures (*ca.* 2500°C) necessary to vaporize the metal in sufficient quantities. The tungsten foils burned out very readily and results were only obtained after a large number of trials. Large peaks were obtained but were not sufficiently constant to give accurate values of their magnitudes. With a peak of 13,000 units at mass 103 one of 10 units at mass 101 was also observed. No isotope of mass 105 was found although 1 in 1000 of mass 103 would have been observable. The 101 peak maintained a reasonably constant ratio to the 103 peak under all experimental conditions. As no peak was observed at mass 102 the possibility of its being a ruthenium impurity of this mass is eliminated. With doubly charged ions of rhodium, peaks were observed at mass numbers 50.5 and 51.5 bearing the same ratio as for the singly charged ions. The ratio of the 103 to the 101 peak was concluded to be about 1300. The possibility of the 101 peak being due to a multiply charged

[7] Aston. *Mass Spectra and Isotopes* (Arnold, 1933).

mercury ion is improbable since no peak was observed at this position except when the one due to Rh^{103} was more than 1000 units high and no other mercury isotopes were observed. It seems reasonably sure that these data represent a new isotope of rhodium. If we assume a packing fraction of -6, the atomic weight of rhodium comes out to be 102.89, in fair agreement with the chemical value of 102.91.

Cobalt

Metallic cobalt was first tried and gave indications of an isotope of cobalt of mass 57 in addition to the one at 59. An impurity peak at mass 57 due to some vapor contamination in the tube was observed, so to get around this difficulty anhydrous cobalt chloride was tried with a tantalum furnace. $CoCl^+$ ions were found at masses 92 ($Co^{57}Cl^{35}$), 94 ($Co^{57}Cl^{37}$, $Co^{59}Cl^{35}$) and 96 ($Co^{59}Cl^{37}$) in relatively large intensities. An average run gave the following results.

Mass number	92	94	96
Height of peak	4	2400	740 cm

These results agree with the known abundances of the two chlorine isotopes and it is concluded that Co^{57} is present to 1 part in 600 of Co^{59}. Since no peaks were observed due to a mass 56, the possibility of an iron impurity is eliminated. Results on the irradiation of cobalt with slow neutrons lend support to this analysis.[8]

A grant from the Penrose fund of the American Philosophical Society aided us greatly in this research.

[8] Sampson, Ridenour and Bleakney, Phys. Rev. **50**, 382 (1936).

OCTOBER 15, 1936 PHYSICAL REVIEW VOLUME 50

Positive and Negative Thermionic Emission from Tungsten

H. B. Wahlin and L. V. Whitney, *University of Wisconsin, Madison, Wisconsin*

(Received August 10, 1936)

The positive and negative thermionic emission and the rate of evaporation of neutral atoms have been studied for well outgassed tungsten. To fix a reliable temperature scale the spectral emissivity for $\lambda=0.669\mu$ has been determined for a cylinder heated in a vacuum. The emissivity has been found to be a constant and equal to 0.46 from 1200°K–2200°K. A determination of the heat of evaporation of neutral atoms gave a value of 8.44 ev. The electron work function was found to be 4.55 ev with an A of 75 amp./cm²/degree² until the filament was heated to a temperature of 3100°K, after which the work function was 4.63 ev and the value of A was 212. The average positive ion work function was 11.93 ev. This value closes the thermionic cycle if Russell's value of 8.1 for the ionization potential is used.

Introduction

THE positive ion work function of tungsten has been determined by Smith[1] and by Moon[2] with results which are far from agreement. Thus Smith found a value of 6.44 ev, and Moon a series of values between 10 and 11 ev. The discrepancy in these results led the writers to undertake the experiments described below in order to determine if, with improved technique, more consistent values could be obtained.

Smith has shown that the following relation should hold:

$$H+I=\varphi_{0-}+\varphi_{0+} \qquad (1)$$

where H is the heat of evaporation of neutral atoms, I the ionization potential, φ_{0+} the positive ion work function, and φ_{0-} that of the electrons.

Of these quantities φ_{0-} is the only one which is known with any degree of certainty. Smith assumes a value of 7.1 volts for the ionization potential and Russell[3] estimates it to be 8.1 volts. Jones, Langmuir and McKay[4] calculated the heat of evaporation to be 8.33 ev, but their calculations are based on evaporation data obtained at a time when vacuum conditions had not been developed to the present extent, so this value is somewhat questionable. Further-

[1] L. P. Smith, Phys. Rev. **35**, 381 (1930).
[2] P. B. Moon, Proc. Camb. Phil. Soc. **28**, 490 (1932).
[3] H. N. Russell, Astrophys. J. **70**, 11 (1929).
[4] Jones, Langmuir and McKay, Phys. Rev. **30**, 201 (1927).

more, accurate determinations of three of the above quantities require that a reliable temperature scale for tungsten be known.

Because of these uncertainties it was decided to determine the emissivity, the heat of evaporation, the electron work function, and the positive ion work function.

The Temperature Scale

Since the use of a disappearing filament optical pyrometer for measuring temperatures requires that the emissivity of the material whose temperature is to be measured be known, it is essential that this quantity be determined under conditions as nearly identical as possible with those under which the temperature is measured. Worthing[5] has measured the emissivity of tungsten in an inert gas atmosphere, but recent results obtained by Whitney[6] on other metals makes it doubtful whether these results are applicable to an outgassed tungsten filament in a vacuum.

The spectral emissivity (for $\lambda=0.669\mu$) was therefore measured, using an outgassed tungsten cylinder heated at a pressure of the order of 10^{-7} mm. The cylinder was made by bending a flat strip of the metal approximately 1 cm wide, 7.5 cm long, and 0.05 mm thick, into a cylinder 3 mm in diameter. A hole 0.45 mm in diameter was drilled through the cylinder wall and the radiation from this acted as a reliable black body source. The cylinder was mounted in a Pyrex bulb connected to a vacuum system and fitted with a flat Pyrex observing window. The bulb was evacuated and baked at a temperature of 400°C for 7 days, and the cylinder heat treated to a final temperature of 2000°K for 700 hours, the final pressure being 10^{-7} mm.

At the end of this time the true and apparent temperatures were determined in the temperature range from 2000°K to 1200°K by matching the pyrometer alternately with the radiation from the hole and the outside of the cylinder. The emissivity calculated from this was a constant and equal to 0.46. When the temperature was raised to 2100°K the emissivity dropped to a value of 0.43 but with heat treatment for about two hours at this temperature it rose to 0.46 and remained at this value for all lower temperatures. A similar effect was observed when the temperature was raised from 2100° to 2200°.

These results are not in agreement with the values found by Worthing. He found that the emissivity decreased with increasing temperatures. Whether or not this is due to the fact that his determinations were made in an inert gas atmosphere the writers cannot say. That the disagreement is not due to a difference in the pyrometer calibration is indicated by the fact that Worthing's results on platinum were checked.

In all the following work the constant value 0.46 has been used in computing the true temperatures.

The Heat of Evaporation

In this determination the loss of weight method was used. Two filaments of the metal 0.3 mm in diameter and 20 cm long were mounted in Pyrex bulbs which were fitted with flat windows for temperature observations and which were sealed to a vacuum system consisting of a liquid-air trap, two air-cooled mercury pumps in series, and a forepump. The bulbs were baked at a temperature of 400°C for times ranging from 150 hours for the earlier specimens to 24 hours for the later ones. During this baking the temperature of the filaments was raised to a final value of 2000°K. The furnaces were then removed and the heat treatment of the filament continued for at least six hours. One filament was then turned off and the temperature of the other raised to a predetermined value such that the evaporation became appreciable. During this heating the pressure in the system remained at 10^{-6} mm or better as measured with a McLeod gauge. During the evaporation the temperature of the filament was checked at frequent intervals

Table I. *Mass loss from tungsten in filament grams per cm² per sec. and calculated heat of evaporation in calories.*

Temp. °K	m	H_0
3120	2.36×10^{-6}	194,000
3070	1.53×10^{-6}	193,000
3015	7.50×10^{-7}	194,000
2950	3.58×10^{-7}	195,000
2900	2.00×10^{-7}	195,000
2850	1.02×10^{-7}	195,000
2800	5.90×10^{-8}	195,000
	Average	194,600

[5] A. G. Worthing, Phys. Rev. **10**, 377 (1917).
[6] L. V. Whitney, Phys. Rev. **48**, 458 (1935).

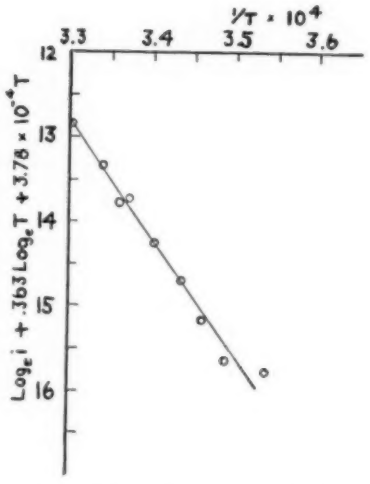

FIG. 1. Richardson plot for positive ion emission.

with an optical pyrometer. After the filament had been kept at the high temperatures for a specified time, both filaments were removed and the mass of equal lengths (12 cm) of the central portions were compared using a microbalance. Knowing the mass loss, the time of evaporation, and the area, the heat of evaporation can be found from the equation giving the relation between this quantity and known experimental quantities. Such an equation has been developed by JLM, *viz.*:

$$H_0/T = 44.51 - 1.66 \log_{10} T - 4.577 \log_{10} m - 0.00075T - 80/T.$$

Table I lists the temperatures, the mass loss (m) in grams per cm² per second and the heat of evaporation calculated from the above equation.

The average heat of evaporation in electron volts is then 8.44, which is in good agreement with the value (8.33) found by JLM.

The possible error involved in the determination of the heat of evaporation is rather large when the pyrometric method is used in measuring the temperature, since the emissivity varies for a time after the filament has been raised to a high temperature. A considerable error is thus possible in the measurement of the higher temperatures because at these temperatures the time necessary for the emissivity to reach a steady value may be comparable to the total time of heating. For this reason the low temperature values given above should be given more weight.

THE ELECTRON WORK FUNCTION

A U-shaped filament of tungsten 0.3 mm in diameter was mounted in a single guard ring tube connected to a vacuum system. The baking and heat treatment, as well as the experimental tube, have been described in earlier papers on Cb[7] and Mo[8] except in one respect. The guard ring and collector, in addition to being heated by electron bombardment before the tube was assembled, were also alternately heated by induction and baked after being mounted in place and after the filament had been given a considerable heat treatment.

The filament after being heat treated for 1200 hours up to a temperature of 2300°K gave a reproducible electron work function (determined from a Richardson plot) of 4.55 ev with A of 75 amp./cm²/degree². After the filament had been flashed at a temperature of 3100°K the value rose to 4.63 ev with an A of 212.

The first value is in good agreement with the accepted one for a polycrystalline tungsten filament. The value found after flashing is unexplained but may be due to recrystallization.

THE POSITIVE ION WORK FUNCTION

When steady conditions, as indicated by a reproducible electron work function, had been reached, the temperature was increased and the positive ion current measured with a high sensitivity galvanometer as a function of the temperature. Fig. 1 shows a Richardson plot of one set of data using the positive ion equation derived by Smith, *viz.*:

$$\log_e i + 0.363 \log_e T + 3.78 \times 10^{-4} T = (\varphi_{0+}/kT) + B.$$

In this plot the points to the right have been given less weight since they represent galvanometer deflections of a few mm only so that the error in measuring the current was appreciable. Three filaments gave values of 11.9, 11.8 and 12.1 ev for φ_{0+}. These values are all higher than those obtained by Smith and Moon. This is probably due to the extreme precautions taken to remove alkaline impurities from the metal parts and the glass walls of the tube by alternate baking and induction heating. The

[7] Wahlin and Sordahl, Phys. Rev. **45**, 886 (1934).
[8] Wahlin and Reynolds, Phys. Rev. **48**, 751 (1935).

writers found that long baking alone was not sufficient to remove such contamination. In fact, without the induction heating it was possible to get a positive ion current leaving the outside of the collector and guard ring which was comparable with the metallic ion current which was to be measured. Some such effect may account for the lower values found by Smith and Moon.

While the accuracy in the determination of φ_{0+} is not as great as is desired, it is questionable whether due to the variable emissivity discussed above greater precision would have much significance.

Discussion of Results

Eq. (1) establishes a relation between the quantities determined in the foregoing sections and the ionization potential. If we take Russell's value for this quantity, the left side of the equation equals 16.54, and if a value of 4.6 ev be taken for φ_{0-} the right side is 16.53 ev. The writers feel however that the possible error is so large that such a close check is of no significance. The value of 4.6 ev for φ_{0-} is chosen as the weighted mean of 4.55 and 4.63. Either of the values would of course close the cycle well within the limits of error.

It is questionable furthermore if the cycle should close when observations are made on a polycrystalline surface. If one assumes, for example, that the thermionic surface is made up of two crystal faces of equal area but with a difference in the work function of 0.2 ev, the low work function surface would contribute 80 percent of the electron emission at a temperature of 1500°K. This is on the assumption that the A of Richardson's equation is the same for both surfaces. While this is probably not true, it still seems probable that the measured φ_{0-} will be closer to the value for the low work function face than to that of the other.

If the positive ion equation is written in the form

$$i_+ = Bf(T) \exp(-11{,}600)(I + H - \varphi_{0-})/T$$

one sees immediately that the greater positive ion emission comes from the surface with the high value of φ_{0-} assuming that the rate of evaporation of neutral atoms from the two surfaces is the same. The cycle should accordingly fail to close by an amount somewhat less than the difference in the work functions of the two surfaces. The failure of the cycle to close in the work on Mo mentioned above is probably partly due to such an effect.

In conclusion, the writers wish to express their appreciation to Mr. George Sears for his assistance in the emissivity determinations, and to the Wisconsin Alumni Research Foundation whose support made the above work possible.

OCTOBER 15, 1936 PHYSICAL REVIEW VOLUME 50

The Production and Absorption of Thermal Energy Neutrons

George A. Fink, *Pupin Physics Laboratories, Columbia University, New York, New York*

(Received August 13, 1936)

From measurements of the number of neutrons reduced to thermal energies in successive cylindrical layers of water the rate of absorption of the thermal energy neutrons in the water, corrected for the rate of production, was calculated. The total number of neutrons emitted from a Rn–Be source was estimated to be of the order of 15,000/sec./mc. Similar experiments with C, Al, Cu, Fe and SiO_2 were performed, in each case some slowing down of the neutrons from the source being observed. The angular distribution of slow neutrons emerging from the surface of paraffin spheres was found to be more concentrated along the normal than a cosine law distribution. A description is given of the construction of a source arrangement concentrating the slow neutrons coming from it into a roughly collimated beam. Measurement of the absorption of neutrons having slightly greater than thermal energy proved that Hg is nearly transparent while Rh and Ag showed less absorption than for thermal neutrons. Experiments with a neutron source cooled to liquid-air temperature show increased absorption for H, Li, B, Rh, Ag, I, Gd and Hg and practically no change for Sm and Cd. The construction and operation of mechanical velocity selectors for slow neutrons is discussed and results are given showing that the neutrons from the source used were in thermal equilibrium with it.

Introduction

FERMI and his collaborators[1] found that the radioactivity induced in some elements such as Ag and Rh was enormously increased when a source of neutrons was surrounded by a hydrogen-containing material. The nuclear reactions thus enhanced were found to be those in which the active product is an isotope of the irradiated element formed by radiative capture. They observed that the "slow" neutrons producing the intense activity were not only strongly absorbed in the activated elements but also in others such as Cd and Hg which do not become active. Fermi explains this effect by assuming that the neutrons were slowed down by elastic collisions with protons and then because of their slower motion past the nuclei in the absorber were more likely to be captured. Since the proton mass is approximately the same as the neutron mass, a neutron can lose nearly all of its energy in a single central impact, and on the average will lose about half its energy in one impact.[1, 2] A neutron with an energy of some millions of electron volts can be brought into the thermal energy region by about 25 collisions.

Westcott and Bjerge,[3] using the radioactivity induced in Ag, and Dunning and his colleagues,[4] using an ionization chamber as the detector, have experimented with Rn–Be neutron sources in spheres of water and paraffin. While the number of "fast" neutrons detected by proton recoil decreases steadily with increase in radius, about 50 percent in a sphere of 10 cm radius, the "slow" neutrons which produce the activity of Ag and the disintegration of Li in a Li-lined chamber increase to a maximum for a paraffin sphere of about 10 cm radius and for larger spheres decrease at a rate about equal to that of the fast neutrons. The number of slow neutrons obtained with only 3 to 4 cm of paraffin around the source is too great to be ascribed to the slowing down to thermal energies of neutrons that started with energy of the order of 1 Mev or higher because the radius of the paraffin sphere is of the order of magnitude of a single mean free path of such neutrons. This is in agreement with the experiments of Dunning[5] and Auger[6] which indicate that a Rn–Be source emits many neutrons having energies less than the maximum, perhaps less than 0.1 Mev. Bonner and Brubaker[7] showed that the neutrons producing increased activity in indium had energies of less than 0.03 Mev.

Attempts to demonstrate that these "slow" neutrons actually had thermal energies by finding an effect of the temperature of the material through which they passed on the properties of the neutrons were at first unsuccessful,[1, 8] but later definite effects were found.[9–11] That some neutrons have thermal velocities was definitely shown by experiments with rotating disks by Fermi and his associates[12] and by Frisch and Sorenson.[13] In this laboratory a direct measurement with a mechanical velocity selector proved that those neutrons coming from a block of paraffin that can be absorbed by ½ mm of Cd are in approximate thermal equilibrium with the paraffin.[14] Rasetti and his collaborators have also done another type of rotating disk experiment further confirming thermal velocities.[15] These thermal energy neutrons form the "*C*" group of selectively absorbed neutrons of Fermi and Amaldi.[16]

Experimental

(A) Production and absorption of thermal energy neutrons in water and paraffin

When spheres or cylinders of hydrogenous materials are used to slow down neutrons emitted from centrally placed Rn–Be sources, the number of slow neutrons emerging depends on two factors,

[1] Amaldi, d'Agostino, Fermi, Pontecorvo, Rasetti and Segrè, Ricerca Scient. **2**, 282, 380 (1934); Proc. Roy. Soc. **A149**, 522 (1935).
[2] Condon and Breit, Phys. Rev. **49**, 229 (1936).
[3] Westcott and Bjerge, Proc. Camb. Phil. Soc. **31**, 145 (1935).
[4] Dunning, Pegram, Fink and Mitchell, Phys. Rev. **48**, 265 (1935).
[5] Dunning, Phys. Rev. **45**, 586 (1934).
[6] Auger, Comptes rendus **196**, 170 (1933).
[7] Brubaker and Bonner, Phys. Rev. **48**, 470 (1935).
[8] Dunning, Pegram, Fink and Mitchell, Phys. Rev. **47**, 796 (1935).
[9] Moon and Tillman, Proc. Roy. Soc. **A153**, 476 (1936).
[10] Lukirski and Zareva, C. R. de l'acad. sc. U.R.S.S. **3**, 393 (1935).
[11] Westcott and Niewodniczanski, Proc. Camb. Phil. Soc. **31**, 617 (1935).
[12] Amaldi, d'Agostino, Fermi, Pontecorvo, Segrè, Ricerca Scient. **6**, No. 1 (1935).
[13] Frisch and Sorenson, Nature **136**, 258 (1935).
[14] Rasetti, Segrè, Fink, Dunning and Pegram, Phys. Rev. **49**, 104 (1936).
[15] Dunning, Pegram, Fink, Mitchell and Segrè, Phys. Rev. **48**, 704 (1935).
[16] Amaldi and Fermi, Ricerca Scient. **6**, No. 2 (1935).

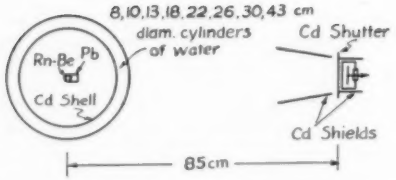

FIG. 1. Experimental arrangement for measurement of production of "slow" neutrons in cylindrical layers of water.

(1) the conversion of faster neutrons into "slow" neutrons, by which we mean those that disintegrate Li and B and are strongly absorbed in Cd, and (2) the absorption of the slow neutrons by the material. In order to separate these two factors and find the true rate of absorption by capture we have observed the numbers of slow neutrons coming from successive cylindrical layers of water surrounding Cd cylinders filled with water.[17] The experimental arrangement is shown in Fig. 1 and the results in Fig. 2 reduced to a source strength of about 325 mc. Both the inside Cd shell and the outer vessel containing the water were cylinders with heights equal to their diameters. The detector used was an 8-cm diameter Li-lined ionization chamber and the linear amplifier-Thyratron recorder system described previously.[4] The upper curve in Fig. 2 gives the numbers when no Cd was inside the water cylinder, while the others are for inner Cd shells of radii 3.8, 6.5, 9, 11 and 15 cm as given by the abscissas of their endpoints on the lower curve which represents the numbers of neutrons counted when the ionization chamber was covered by a screen of $\frac{1}{2}$ mm Cd.

The curves show that the rate of production of slow neutrons per cm increase of radius at 12 cm from the source is still about half of what it was at 6 cm. The fast neutrons from which the slow ones are produced decrease at about the same rate, indicating that approximate equilibrium between fast and slow neutrons has been reached, as is also shown by the fact that the ratio of fast to slow neutrons remains nearly constant as both decrease beyond 10 cm radius. It is estimated that in the layers used the actual rate of production of slow neutrons is twice the observed rate since about half of the slow neutrons "produced" (brought into the energy range where they are strongly absorbed by Cd) will diffuse inward and be captured by the Cd inside the water layer. On this basis the rate of production of slow neutrons per cm increase in radius was calculated from the data shown in Fig. 2 and the results are given in Fig. 3, curve number 1.

At 12 cm radius the number of slow neutrons emerging from a sphere or cylinder has begun to decrease although slow neutrons are still being produced. This must mean that the slow neutrons are being absorbed in the paraffin or water, presumably by the hydrogen with the formation of deuterium. Lea[18] and others have observed gamma-rays attributed to this capture process. To calculate the true absorption per cm increase of radius of the paraffin we must correct the apparent absorption coefficient that would be obtained from the measured rate of decrease of emergent slow neutrons by subtracting the rate at which slow neutrons are being produced from the fast neutrons present. The mean corrected rate of absorption is 0.35 per cm increase in radius, giving a half-value thickness of 2 cm. The corrected rates of absorption at different radii are in fair agreement, the probable error being estimated at about 25 percent. From this half-value thickness for absorption and the half-value thickness of 2.8 mm and cross section of 35×10^{-24} cm² found for scattering in paraffin[4] we calculate that a slow neutron makes on the average about 150 elastic impacts before being captured and the absorption cross section of the proton is about 20×10^{-26} cm². This cross section is larger than the value of 3.0 to 8.3×10^{-26} cm² found by

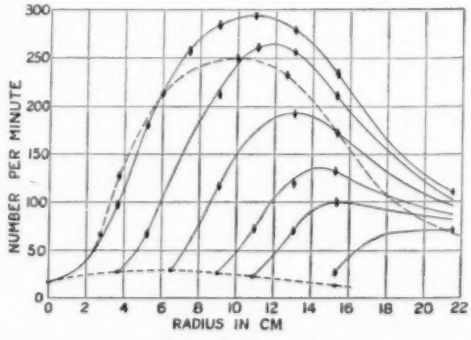

FIG. 2. Curves showing the production of slow neutrons in cylindrical layers of water.

[17] Fink, Dunning, Pegram and Segrè, Phys. Rev. **49**, 199 (1936).

[18] Lea, Nature **133**, 24 (1934).

Kikuchi, Husimi and Aoki[19] who compared the intensities of gamma-radiation produced by neutrons absorbed in water and in a solution of Cd but smaller than the latest value given by Amaldi and Fermi, 31×10^{-26} cm^2.[20] Our distance for half-absorption is between that found by Westcott and Bjerge[3] (1.5 cm H_2O) and that found by Preiswerk and von Halban[21] (2.5 cm paraffin).

Knowing the rate of production of slow neutrons per cm as a function of the radius, one can calculate the total number produced out to a given radius, or the number that would come from a sphere of that radius if there were no absorption. The results of such a calculation are shown in Fig. 3 where curve 1 gives the number produced per cm increase in radius, curve 2 the number observed from spheres, and curve 3 the total produced out to a given radius. Curve 3 extrapolated goes to nearly 8000 neutrons counted per minute per millicurie of radon using the whole solid angle around the source, or 140/sec./mc. Now the only neutrons which can be detected by a B or Li-lined ion chamber are those which are captured in the lining near enough to the surface for one of the ionizing particles produced by the resulting disintegration to emerge from the chamber lining into the air in the chamber. From the ranges of the particles and the absorption coefficient of Li for slow neutrons we estimate an upper limit for the sensitivity of the chamber used in this work to be 1.6 percent with 1 percent more probable since the ionizing particles must emerge from the chamber lining with a considerable fraction of their initial range if they are to be detected above the background of gamma-ray ionization and tube noise. With the detection efficiency taken as one percent a count of 140/sec./mc means that approximately 14,000 neutrons are emitted per second by a one millicurie radon plus Be source, in rough agreement with Jaeckel[22] who found ~10,000/sec./mc, Paneth and Loleit[23] who found >3000/sec./mc and Amaldi and Fermi[20] who found 30,000/sec./mc.

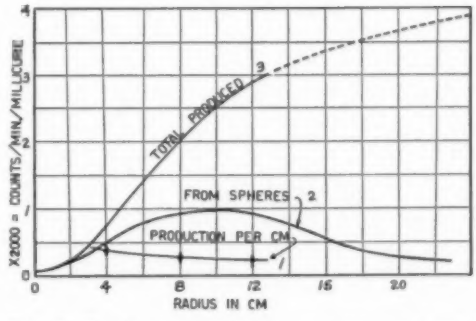

FIG. 3. Total number of slow neutrons produced in spheres of paraffin, number emerging from spheres, and rate of production per cm increase of radius.

(B) Production and absorption of slow neutrons in other materials

Similar experiments have been performed on the absorption and production of thermal energy neutrons in other materials: C,[24] Al, Pb, Fe, SiO_2, Cu. Counts were taken with each material in a set of standard arrangements as follows: 1, no absorber around a paraffin cylinder 8.8 cm diam., and 10 cm long, no Cd in front of ionization chamber; 2, same as 1 with Cd in front of chamber; 3, Cd around paraffin and absorbing material around it in a 22 cm diameter can filled to a height equal to its diameter, no Cd on chamber; 4, same as 3 with Cd on chamber; 5, absorbing material around paraffin without Cd between them, no Cd on chamber; 6, same as 5 with Cd on chamber. The results are plotted in Fig. 4 in a manner similar to Fig. 2 along with a curve for paraffin cylinders from Fig. 2. The data for arrangements 3, 4, 6 are replotted in Fig. 5 on a larger scale so that the small differences can be seen. In every case there seems to be a small number of slow neutrons produced in the material surrounding the paraffin and Cd, indicated by the count for set-up 3 being higher than that for set-up 4. A comparison of the counts in arrangement 5 with that in 1 shows that in Al, SiO_2, C and Pb slowing down overbalances absorption. Even for the relatively light nuclei Al, Si, O and C, and certainly in the case of Pb which is much heavier and yet produces more slow neutrons, the results indicate the high probability of inelastic collisions with nuclei and the necessity for introducing a nuclear model

[19] Kikuchi, Husimi and Aoki, Nature **137**, 30 (1936).
[20] E. Amaldi and E. Fermi, Ricerca Scient. **1**, No. 11–12 (1936).
[21] Preiswerk and von Halban, Nature **136**, 951 (1935).
[22] Jaeckel, Zeits. f. Physik **91**, 493 (1934).
[23] Paneth and Loleit, Nature **136**, 950 (1935).
[24] Fink, Dunning and Pegram, Phys. Rev. **49**, 340 (1936).

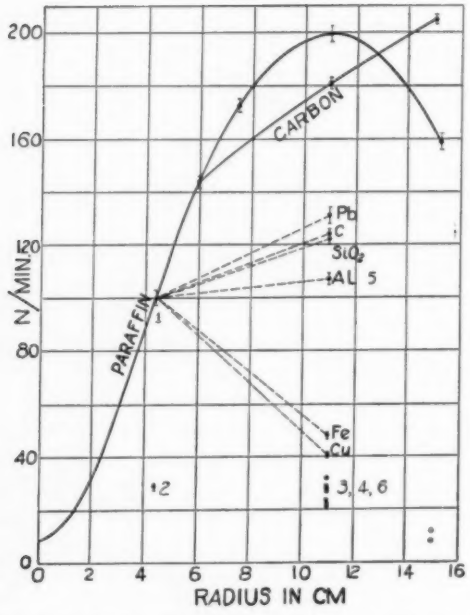

FIG. 4. Production and absorption of slow neutrons in Pb, C, SiO_2, Al, Fe and Cu.

such as that of Bohr such that the neutron remains in the nucleus a relatively long time and hence may lose considerable amounts of energy before emerging. Fleischmann[25] and Fermi and others have also observed phenomena indicating inelastic collisions in Pb.

The upper curve marked carbon shows that by surrounding a 6 cm radius paraffin cylinder with carbon more slow neutrons may be obtained than from any size of paraffin sphere.

(C) Angular distribution of neutrons from the surface of a sphere

To measure the number of neutrons coming from the surface of a paraffin sphere at a chosen angle, the following method was used. Sheet Cd disks and rings were placed between the sphere and ionization chamber so that slow neutrons could reach the chamber from only one zone of the sphere at a time. The fast neutron count with Cd in front of the chamber was subtracted from the count from each zone. The relative numbers of slow neutrons from the zones divided by the areas of the zones are plotted against the angles of the zones to get the arcs in Fig. 6. Smooth angular distribution curves are drawn through points on these arcs dividing the zones into two approximately equal areas. On each diagram is drawn a circle representing for comparison the cosine law distribution expected if the neutrons are emitted from the *surface* uniformly in all directions. The neutron distribution is seen to be more concentrated along the normal to the surface. This may be explained by a filtering process in the surface layers of the sphere. A slow neutron starting out from a point inside the surface of a sphere a distance of the order of a mean free path will have a better chance of emerging without collision if it starts out in the direction of the normal than if it started out in any other direction where it must penetrate a greater thickness of material to escape. The experimental angular distributions here given are quite similar to the theoretical angular distribution derived by Fermi,[26] especially in the case of the 12.5 cm sphere where the number of zones and other experimental conditions were better.

(D) Design and test of a source arrangement to produce a beam of neutrons concentrated in one direction.

To produce an intense collimated beam of slow neutrons a special arrangement of scattering material around the source was developed. Its cross section is shown to the left in Fig. 8. Growth curves such as those in Fig. 2 show a maximum (number of neutrons per unit solid angle) from a sphere or cylinder of approximately 10 cm radius

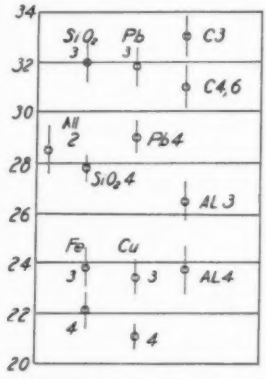

FIG. 5. Points in lower right hand corner of Fig. 4 replotted on larger scale.

[25] Fleischmann, Zeits. f. Physik **97**, 242, 265 (1935).

[26] Amaldi and Fermi, Ricerca Scient. May 1936.

but the number emitted per unit area at the surface of the sphere is a maximum at about 4 cm. This high density of slow neutrons near the source is also shown by the curves in Fig. 7 which give the numbers of neutrons counted from a 22 cm diameter cylinder of water with the source in different positions along a diameter of the cylinder through its center. The number emerging is seen to be a maximum when the source is about 3 cm from the side of the cylinder toward the ionization chamber. The density per unit area of the surface of the cylinder when the source is 3 cm from it is greater than the density at the surface of a 4 cm radius sphere because the added material behind the source scatters back many of the neutrons that leave the small sphere with high velocity. A further increase is obtained by putting paraffin around the beam from the source to the chamber which is similar to the effect of the paraffin tubes used for "canalization" of neutrons by Szilard and Chalmers.[27] Neutrons coming from the paraffin surface near the source in directions that do not go through the opening of the tube are partly scattered back and the density near the source is increased. Some of the neutrons thus scattered back will after a few more impacts emerge down the tube in a useful direction. The direct beam of fast neutrons that have made few collisions since leaving the source is scattered away from the chamber by a plug of copper and paraffin which also serves to reduce the intensity of the gamma-ray ionization in the chamber.

The intensity of the slow neutron beam from this device, commonly known in this laboratory as a "howitzer," is more than six times as great as that from a sphere of the same diameter

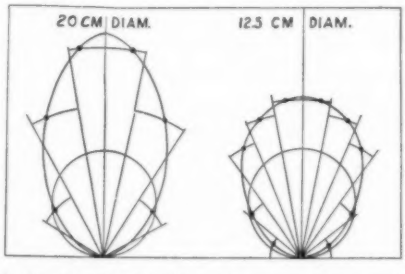

FIG. 6. Angular distribution of neutrons from surface of paraffin spheres.

[27] Hopwood and Chalmers, Nature **135**, 341 (1935).

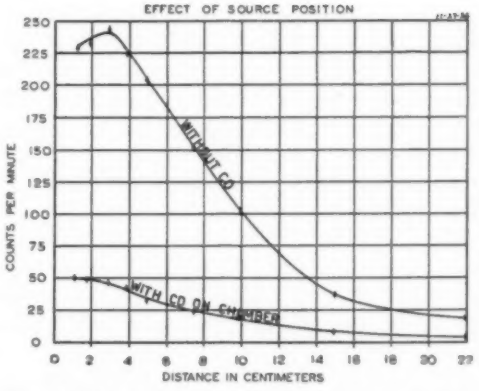

FIG. 7. Effect of change of position of source in cylinder of water on number of neutrons coming out on one side.

as the opening of the howitzer with the source at the same distance from the detector. This slow neutron intensity is 5 times that from the optimum size of sphere although the total intensity is only 4.5 times as great because of a smaller fraction of fast neutrons. The fraction of the neutrons from the howitzer that are not absorbed by Cd is about six percent while 11 to 19 percent of those from spheres are not absorbed. This lower background is an advantage for many purposes, especially for the velocity selector described below. The degree of collimation obtained is indicated by the fact that the intensity 20° off the axis is only 60 percent of that on the axis.

(E) Absorption of neutrons of slightly more than thermal energy

The absorption of several materials for those neutrons that pass through Cd but after a few impacts in a layer of paraffin are absorbable in Cd was measured with the experimental arrangement shown in Fig. 8. A sheet of Cd was placed over the opening of the howitzer source placed near an 8 cm diameter ionization chamber. A disk of paraffin 6 mm thick and 14.5 cm diameter was placed between the source and chamber. Counts were then taken; 1, without a Cd screen in front of the chamber, 2, with a Cd screen in front of the chamber, 3 and 4, same as 1 and 2, respectively, but with an absorber between the howitzer and paraffin. The difference 1–2 is the number of slow neutrons produced in the paraffin from the neutrons that passed through the Cd on

the source and 3–4 is the number produced from neutrons passing through both Cd and the other absorber. The ratio 3–4/1–2 is the fraction transmitted through the absorber, of those Cd-penetrating neutrons which after passing through the paraffin are absorbable by Cd. The results are given in Table I. It will be noticed that the transmission of Ag+Rh is less than the product of the transmissions of Ag and Rh, indicating selective absorption by these elements of certain energy regions slightly above the thermal range although the difference is barely larger than the experimental error. Recently Ag and Rh[28] have been shown to exhibit the phenomenon of resonance capture for neutrons having energies of 2 to 3 and 1 to 1.2 ev. The Ag and Rh absorbers show absorption cross sections for these higher energy neutrons. That Rh shows a greater fraction of its thermal energy cross section than does Ag agrees with the fact since found that Rh has a broader resonance at lower energy as mentioned above. More striking is the almost complete transparency of the HgO sample which absorbed 51 percent of thermal energy neutrons.

This in connection with the temperature effect which is about the same as that for Ag, Rh, Li and B, indicated that if mercury has any resonance it must be in the thermal region and broad enough so that the slope of the cross-section-velocity curve in that region is not much different from that for Ag.

(F) The effect of temperature on neutron absorption

As mentioned in the introduction the concept of neutrons coming into thermal equilibrium with matter led to attempts to demonstrate an effect of the temperature of the scattering material on the properties of the scattered neutrons. Fermi and his associates[1] found no difference, to within two percent, of the activity of Rh placed near a source in cylinders of hydrocarbons having at 20° and 200°C the same density and atomic composition. Using a more favorable arrangement with a thinner layer of material cooled to liquid air temperature, Moon and Tillman[9] observed a definite increase of the activity induced in Ag at the lower temperature. Lukirsky and Zareva[10] tried various thicknesses

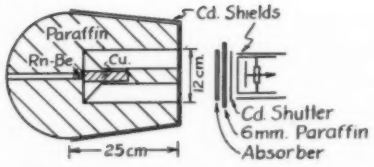

FIG. 8. Arrangement for absorption measurements with neutrons of slightly greater than thermal energy.

of cooled paraffin and showed that with large thicknesses absorption in the paraffin masked the effect of lowering the neutron velocity range. The change in number of neutrons was separated from the change in their effectiveness in producing activation by Westcott and Niewodniczanski[11] who measured the absorption of several materials including the detecting substance at each temperature and also went down to liquid hydrogen temperature with increased effects.

The first experiments in this laboratory[8] performed to show an effect of the temperature of the material through which neutrons passed on their absorption in Cd gave a negative result which is now understandable since a rotating disk experiment[14] has shown that the absorption of Cd is nearly constant throughout the thermal region. Further experiments on the absorption of Cd and other elements have now been performed.[29] In these experiments the "cold" neutron beam was taken out of the top of a small "howitzer" weighing 2400 grams cooled to liquid air temperature in a wide-mouthed Dewar flask covered with only a single thickness of paper. Table II gives the results in terms of nuclear absorption cross sections for neutrons coming from the source at room temperature and liquid air temperature. Large changes in absorption are found in every case except those of Cd and Sm. The results for Cu and Ag are in substantial agreement with other observers using artificial radioactivity as the detector of slow neutrons.

TABLE I. *Data on absorption of neutrons.*

Absorber	Ag	Rh	HgO	Rh+Ag
Fraction transmitted	0.791	0.686	0.981	0.483
Stan. dev.	0.037	0.035	0.051	0.028
Cross section	20±4	86±12	12±33	$\times 10^{-24}$ cm²
C neutron transmission	0.519	0.596	0.487	
C neutron cross section	56	128	450	$\times 10^{-24}$ cm²

[28] Goldsmith and Rasetti, Phys. Rev. **50**, 328 (1936).

[29] Powers, Fink and Pegram, Phys. Rev. **49**, 650 (1936).

(G) Mechanical velocity selectors for slow neutrons

Previous work in this laboratory with a mechanical velocity selector[15] had shown that the distribution of velocities of neutrons coming from a block of paraffin is approximately Maxwellian. An improved velocity selector with higher resolution and higher velocity range has now been built and tested. The principal features of its construction are illustrated in Fig. 9 which is diagrammatic and not drawn to scale. It is mounted with vertical shaft so that the velocity distribution curve may be determined for a cold source of the type described in the previous section as well as for a source at room temperature. The shaft is made shorter to regain some of the intensity lost by going to higher resolution. To cover the same velocity range with the short shaft a larger number of sectors was put on each disk, 90 in place of 50. Higher disk speeds were made possible by using steel sectors plated with Cd in place of pure Cd which is mechanically weak and flows under a small stress, less than one thousand pounds per square inch. The phase of the fixed sectors at one end may be varied with respect to that of the other by rotating the casing which carries the fixed Cd sectors at the upper end. The ratio of closed to open space on the rotating Cd sector disks of the old velocity selector is 1 to 1 while on the new one the ratio is 3 to 1. The open space is then one-quarter of the total in place of one-half. The relative resolving power of the two selectors may best be judged from their velocity transmission curves, calculated as follows from the geometry of the fixed and moving sector systems.

TABLE II. *Absorption of neutrons at room temperature and liquid-air temperature.*

Absorber	Capture cross section ($\times 10^{-24}$ cm^2) Room temperature source	Liquid-air temperature source	% Increase
H (paraffin)	38±3	48±3	26
Li (LiF)	72±3	86±3	20
B (Pyrex)	540±20	715±20	32
Rh	130±5	175±6	35
Ag	56±2	77±3	20
Cd	2900±100	3100±200	7
I	14±1	17±2	21
Sm (Sm_2O_7)	4600±100	4400±100	−4
Gd ($Gd_2(C_2O_4)_3$ 10 H_2O)	22000±1000	31000±1000	41
Hg (HgO)	445±25	605±25	36

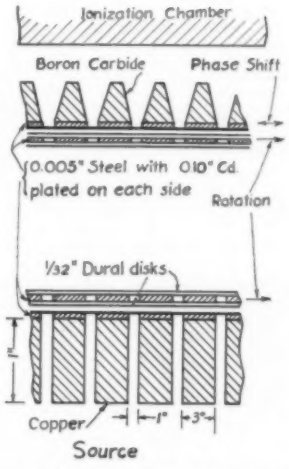

FIG. 9. Diagram of shutter systems of new velocity selector.

The probability of a neutron getting through the selector is the product of the fractions of the area that are open at each end of the velocity selector. These fractions are equal in the case of what may be called the "in phase" adjustment in which the shutter system at one end reaches its maximum opening at the same time as the system at the other end. As the shaft of the velocity selector is rotated the fraction open at each end F, and its square, which is the instantaneous probability W of a neutron getting through, vary as shown in Figs. 10A, E and B, F for the 1 to 1 and 3 to 1 ratio. The average probability $\overline{W}$ of a neutron passing through when the shaft is revolving slowly and uniformly is of course the average ordinate of the instantaneous probability curve.

Now consider a beam of neutrons of a single velocity V incident upon the selector when the disk is revolving at a speed of the order of 1000 r.p.m. The probability W is now the product of the fractional area open at the source end at the time of incidence and the fraction open at the detector end at a time d/V later where d is the distance between the ends of the selector. In this time the disks have turned through an angle $d/V \times$r.p.m./$60 \times 360°$. If this angle is 3.6° in the case of the selector with 50 sectors or 2° in the case of the one with 90 sectors the disks turn from the open to the closed position in the time taken for a neutron to travel the length of the shaft, 54 cm in the first case and 25.7 cm in the second. We then have maximum cut-off and the

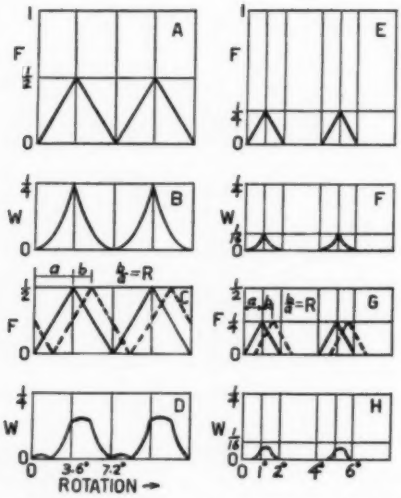

FIG. 10. Diagrams illustrating operation of velocity selectors.

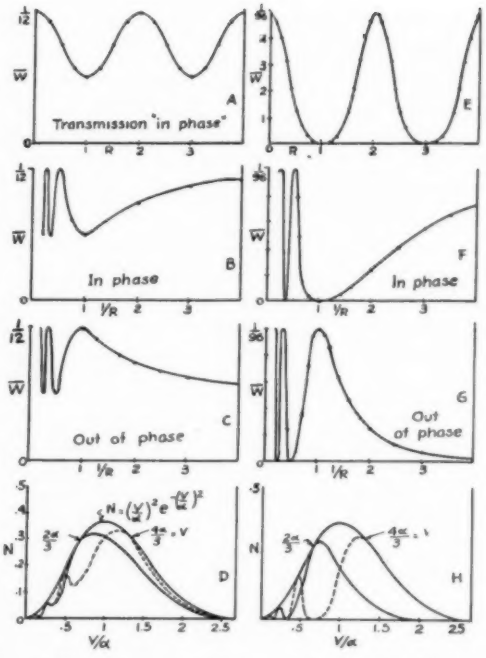

FIG. 11. Velocity-transmission curves for velocity selectors.

necessary rotational speeds are: r.p.m. $= V/54 \times 60/100 = V(\text{cm/sec.})/90$ and r.p.m. $= V/25.7 \times 60/180 = V/79$. The linear velocity thus related to the rotational speed of the shaft and disks we may call the "velocity" of the selector. The transmission of the selector may then be calculated as a function of the ratio R = selector velocity/neutron velocity. This ratio determines the shift of one curve with respect to the other in Figs. 10C and 10G. The product of corresponding ordinates of the curves in 10C and 10G is plotted in Figs. 10D and 10H to get the instantaneous transmission curves for a particular value of R. The average ordinates of such curves for various values of R are plotted against R in Figs. 11A and 11E. It will be noted that the 1 to 1 selector at most only cuts off half of the neutrons of a fixed velocity while the 3 to 1 selector cuts off completely neutrons of one velocity. The transmission may also be plotted as a function of $1/R$ = neutron velocity/selector velocity as in Figs. 11B and 11F marked "in phase." Figs. 11C and 11G are the corresponding curves for the "out of phase" condition. The two sets of curves are complementary in that one shows a maximum of transmission where the other shows a maximum of absorption. With a fixed selector speed these curves represent the transmission as a function of neutron velocity measured in terms of the selector velocity as a unit. Now we may take the Maxwellian velocity distribution curves in Figs. 11D and 11H and multiply each ordinate by the corresponding ordinate of the transmission curve to get points of the transmitted velocity distribution curves. Such transmitted velocity curves are drawn in Figs. 11D and 11H for selector speeds of $2\alpha/3$ and $4\alpha/3$ where $\alpha = \sqrt{2kT/M}$, the most probable velocity of the Maxwellian distribution. Curves like these have been plotted for a number of selector speeds and the relative areas under the curves found by use of a planimeter. The areas are proportional to the numbers transmitted at the corresponding speeds out of a Maxwellian distribution of velocities. (If the detector efficiency did not vary with neutron velocity the appropriate velocity distribution curve would be $(V/\alpha)^3 e^{-(V/\alpha)^2}$ because the higher velocities are more likely to come out of the source where the density function is $(V/\alpha)^2 e^{-(V/\alpha)^2}$, but since the detecting elements Li and B show absorptions varying approximately as $1/V$ the V^2 distribution was used.)

If these areas multiplied by an appropriate constant are plotted against the selector speed we get the experimental curve to be expected if the velocity selector is operated at various speeds

with a $1/v$ detector on a neutron beam having the Maxwellian V^3 velocity distribution. Such expected curves for 300°K with the 1 to 1 ratio velocity selector running "in phase" and "out of phase" are given in Fig. 12. Two curves are shown for operation in phase, one using the V^3 velocity distribution and the other the V^2 distribution. In a Letter to the Editor of the *Physical Review*[30] the "in phase" data were given with an expected curve calculated from the V^3 distribution since at that time it was not known that the Li detector had an absorption varying as $1/v$. Much better agreement is now seen to be obtained with the V^2 velocity distribution.

The expected curves for both the in phase and out of phase conditions with the 3 to 1 ratio velocity selector and the V^2 velocity distribution are given in Fig. 13 with the experimental points obtained with the new velocity selector. The deviations of the points from the curves are within the statistical fluctuation limits except at 5000 r.p.m. At this speed the count is too high, presumably because the noise made by the velocity selector was being picked up by the slightly microphonic ionization chamber and was thus causing spurious counts.

Figs. 10 and 11 show clearly that intensity is rapidly lost as resolution is gained. The loss of intensity of the slow neutrons transmitted is especially troublesome because of the background of fast neutrons which are not absorbed by Cd. Two devices were used to help in this matter of background. A grid of copper bars 2.5 cm deep radiating from the axis with spacings like those

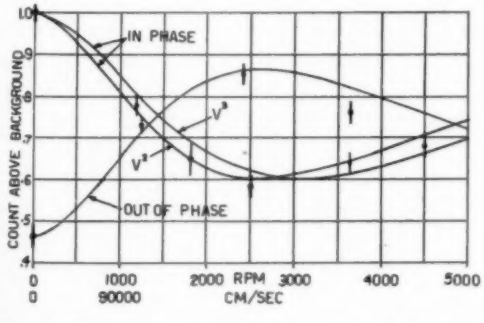

FIG. 12. Expected curves and observed points for 1 to 1 ratio velocity selector.

[30] Fink, Dunning, Pegram and Mitchell, Phys. Rev. **49**, 103(1936).

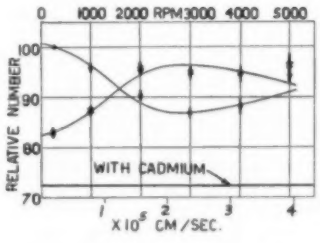

FIG. 13. Expected curves and observed points for 3 to 1 ratio velocity selector.

between the fixed Cd sectors was placed in contact with them to scatter away from the chamber the fast neutrons that would otherwise go through the fixed sectors and cause background counts. In addition this copper absorbs gamma-radiation and scatters back some of the slow neutrons that would otherwise be absorbed in the Cd, thereby increasing the intensity through the openings. At the upper end an absorbing grid is wanted in place of a scatterer and boron carbide is used in sheet copper forms. However, even with these devices the number of slow neutrons transmitted when running slowly in phase is only about 40 percent above the background. As a detector to be used with this selector an ionization chamber constructed and filled with BF_3 gas by Dr. Mitchell and Professor Rasetti of this laboratory has proved very useful. Its sensitivity to slow neutrons is about five times that of a chamber having only a lining of Li or B. Its sensitivity for neutrons which penetrate Cd is also greater so that its background ratio is about the same as that of Li and B-lined chambers. To obtain precision in absorption measurements therefore considerable time will be required. Out of phase operation, in which one end of the velocity selector is open when the other end is closed, can be used to select neutrons of known velocities for absorption measurements. Preliminary tests with Ag and Pyrex sheets can be relied on only to show that the absorption is greater with lower velocities.

The author wishes to acknowledge his indebtedness to Professors G. B. Pegram, J. R. Dunning, F. Rasetti and Dr. D. P. Mitchell for much assistance in the laboratory and helpful discussion of the problems encountered in the course of this work.

Collision of Neutron and Proton

PHILIP M. MORSE, J. B. FISK AND L. I. SCHIFF, *Eastman Laboratory, Massachusetts Institute of Technology*

(Received June 9, 1936)

An exact solution is found for the bound and free states of a neutron-proton pair under the influence of a potential field $-D[2\exp(2/r_0)(r_1-r)-\exp(4/r_0)(r_1-r)]$, where the field can be of the Majorana type and may depend on the spin coupling. Values of binding energy (for the deuteron), of elastic cross section, of capture cross section and of cross section for the photoelectric disintegration of the bound state are computed for a wide range of the parameters used. Curves of the results are shown. In order to correspond to the experimental values of binding energy and of elastic cross section for slow neutrons, the value of D for the singlet state, D_s, must be made about one-half that for the triplet state, D_t. Separate calculations are made, assuming a bound singlet state, and assuming no bound singlet state. When this is done, the capture and photoelectric cross sections check the experimental values fairly well, the computed results being practically independent of r_0 and r_1 as long as these parameters are less than 6×10^{-13} cm. Thus a proper choice of two relations between the four parameters D_s, D_t, r_0, r_1, gives agreement with four different experimental values; the other two relations needed to determine all four parameters will require further experimental data for their determination.

INASMUCH as the fundamental theory of the interactions between the particles in the nucleus has not yet been developed, it is necessary to obtain knowledge of these interactions by empirical methods. Accordingly, it is of interest to assume a number of different types of force fields between the constituent nuclear particles, to work out as accurately as possible the behavior of these particles corresponding to the assumed forces, and to see which of the behaviors corresponds best to the experimental data. This program has already been initiated in a number of papers.[1, 2] The present article continues the work by studying in some detail the interaction between proton and neutron.

The Wave Functions

A potential field which allows of exact solution and which permits a considerable variation of form, is given by the expression

$$V(r)=-2D\exp(2/r_0)(r_1-r)+D\exp(4/r_0)(r_1-r). \quad (1)$$

When $r_1=0$ the field is everywhere attractive, having a minimum at $r=0$. For r_1 larger than zero the field is attractive for large r and repulsive for small r, having a minimum at $r=r_1$. Fig. 1 shows typical shapes of the potential.

Writing energies and lengths in nuclear units: energy unit $=m_e c^2=506{,}000$ ev

length unit $=(h/2\pi c)(1/m_e m_p)^{\frac{1}{2}}=8.97\times10^{-13}$ cm,

the wave equation for the motion of a neutron and proton relative to their center of mass is $[\nabla^2+(W-V)]\psi=0$. If the wave function has spherical symmetry, $\psi=R(r)/r$, this reduces to

$$(d^2R/dx^2)+[-m^2+2ke^{(x_1-x)}-ke^{2(x_1-x)}]R=0 \quad (2)$$

where $x=(2r/r_0)$, $x_1=(2r_1/r_0)$, $m^2=-(r_0/2)^2W$ and $k^2=(r_0/2)^2D$.

The solution of this equation corresponding to the bound state is the confluent hypergeometric function

$$R_0=z^{-\frac{1}{2}}M_{k,\,m}(z)=z^m e^{-z/2}\left[1+\frac{\frac{1}{2}+m-k}{1!(2m+1)}z+\cdots\right] \quad (3)$$

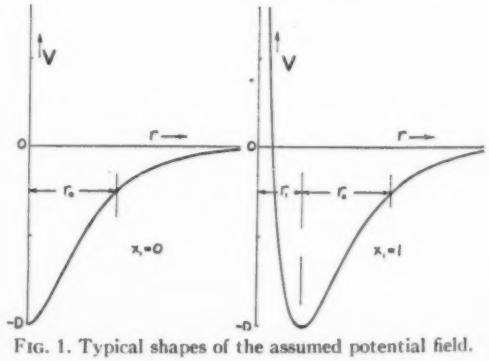

FIG. 1. Typical shapes of the assumed potential field.

[1] Feenberg and Knipp, Phys. Rev. **48**, 906 (1935); Heisenberg, Zeits. f. Physik **77**, 1 (1932); Majorana, Zeits. f. Physik **82** (1933); Massey and Mohr, Proc. Roy. Soc. **A152**, 693 (1935); Thomas, Phys. Rev. **47**, 903 (1935); Wigner, Phys. Rev. **43**, 252 (1933); Young, Phys. Rev. **48**, 913 (1935).

[2] Bethe and Peierls, Proc. Roy. Soc. **A148**, 146 (1935); Feenberg, Phys. Rev. **47**, 857 (1935); Fermi, Phys. Rev. **48**, 570 (1935); Hall, Phys. Rev. **49**, 401 (1936).

TABLE I. *Values of k for the bound state.*

x_1	$m=0$	$m=0.5$	$m=1.0$
0	0.900	1.480	2.032
0.5	.728	1.228	1.713
1.0	.608	1.070	1.540

where $z=2ke^{x_1-s}$, and where m is adjusted so that $R=0$ when $z=0(r=\infty)$ and when $z=z_0=2ke^{x_1}$ $(r=0)$. The first requirement is met when m is real and positive. The second is met by solving the transcendental equation $M_{k,\,m}(2ke^{x_1})=0$. Values of k satisfying this equation are given in Table I, for different values of m and x_1. Intermediate values can be obtained with considerable accuracy by second-difference interpolation.

The solution of Eq. (2) for the states of positive energy are obtained by setting $m=i\mu$, $\mu^2=(r_0/2)^2W$;

$$R=(i/2z^{\frac{1}{2}})[(z_0)^{-i\mu}e^{-i\delta_0}M_{k,\,i\mu}(z) - (z_0)^{i\mu}e^{i\delta_0}M_{k,\,-i\mu}(z)] \quad (4)$$

where the phase angle δ_0 is obtained by computing the real and imaginary parts of the series

$$\text{Re}+i\ \text{Im}=1+\frac{\frac{1}{2}-k+i\mu}{1!(1+2i\mu)}z_0 + \frac{(\frac{1}{2}-k+i\mu)((3/2)-k+i\mu)}{2!(1+2i\mu)(2+2i\mu)}z_0^2+\cdots;$$

$$\tan(\delta_0)=(\text{Im}/\text{Re}). \quad (5)$$

This solution is zero at $r=0(z=z_0)$, and has the asymptotic form

$$R\rightarrow\sin(w^{\frac{1}{2}}r+\delta_0), \qquad (r\rightarrow\infty,\ z\rightarrow 0).$$

The important expression for the computation of elastic scattering is $\sin(\delta_0)/\mu$. The limiting value of this as μ goes to zero will be called Δ. The quantity $\pi\Delta^2$ is plotted in Fig. 2 as a function of k and x_1.

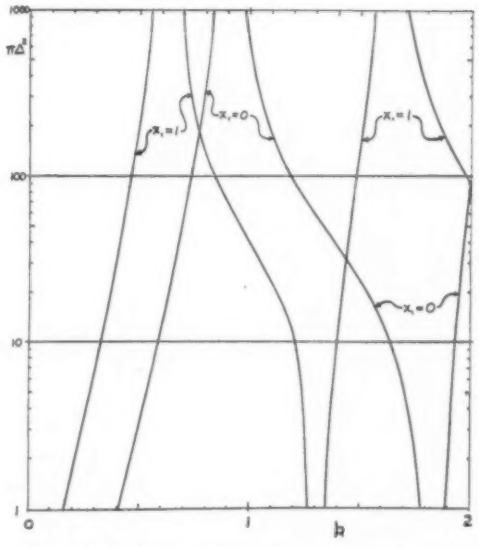

FIG. 2. Cross-section factor $\pi\Delta^2$ for slow neutrons.

NORMAL STATE OF THE DEUTERON

The potential operator for the neutron-proton interaction may have a dependence on the coupling of the two spins and it may include a permutation operator of the Majorana type.[1] The observed value of the binding energy of the deuteron gives us a relationship between the width and depth of the interaction potential for the triplet state. We have assumed that the observed value of this binding energy W_t is -4 nuclear units. The results given in the rest of this paper will not be appreciably altered if the binding energy is chosen as large as -4.4, as recent work[3] seems to indicate.

The results given in Table I can be utilized to find the relation between D and r_0 which makes $W_t=-4$. The depth D_t is plotted (solid lines) in Fig. 3 as a function of r_0 for two different values of x_1. The corresponding values of the normalizing factor

$$N_t=\left[4\pi\int_0^\infty\psi^2r^2dr\right]^{-\frac{1}{2}}=\left[2\pi r_0\int_0^{z_0}M^2_{k,\,m}(z)dz/z^2\right]^{-\frac{1}{2}}$$

are given in Table II. The shapes of two normalized wave functions, with their corresponding potential energy curves, are given in Fig. 4.

ELASTIC SCATTERING

The cross section for elastic scattering of neutrons by protons is given by the formula[4]

$$Q=(\pi r_0^2/\mu^2)\sum_l(2l+1)\sin^2(\delta_l). \quad (6)$$

[3] Oliphant, Nature **137**, 396 (1936).
[4] Allis and Morse, Zeits. f. Physik **70**, 567 (1931).

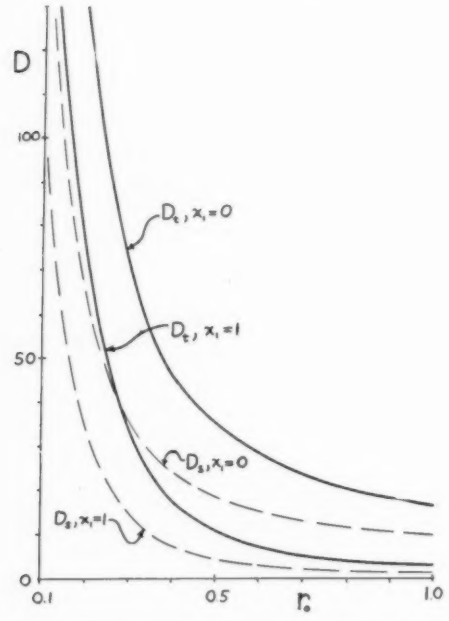

FIG. 3. Relation between depth and radius of triplet potential to give observed deuteron binding energy (solid lines), and for singlet potential to give observed elastic cross section for slow neutrons (dotted lines).

The phase angle δ_0 is obtained from Eq. (5) and the angles for larger l are obtained by numerical integration of the equation

$$R_l''+[\mu^2+2\epsilon_l k e^{x_1-x} -\epsilon_l k e^{2(x_1-x)}-l(l+1)/x^2]R_l=0, \quad (7)$$

and calculation of the phase in the usual manner.[4] The factor ϵ_l is equal to $(-1)^l$ if the potential is of the Majorana type; it is equal to unity if the potential is of the usual type.

For very slow neutrons only the term in $l=0$ is important, and the limiting value of the cross section is

$$Q_0=\pi r_0^2\Delta^2, \qquad \Delta=\lim (\sin\delta_0/\mu).$$

Fig. 5 shows a curve of Q_0 against r_0 for those values of D which give the right binding energy for H^2. The curve is for $x_1=0$, but the curves for $x_1=0.5$ and $x_1=1.0$ are practically identical, not differing by more than five percent at any part of the range shown. Since the experimental value[5] of Q_0 is about 45 square nuclear units, it is seen that the calculated cross section does not agree, except for improbably large values of r_0. Evidently the potential field must depend on spin orientation.

To study this effect we assume a singlet potential energy having the same value of r_0 as for the triplet, but having a smaller depth, D_s. The elastic cross section will then be

$$Q=(1/4)(Q_s+3Q_t). \quad (8)$$

The problem can then be worked backward, to find a value of D_s such that Q_0, computed from Eq. (8) and using the value of D_t which gives the

[5] Dunning, Pegram, Fink and Mitchell, Phys. Rev. **48**, 265 (1935). Other work, Fermi and Amaldi, Ricerca Scient. **1**, 56 (1936), indicates the possibility of somewhat smaller values for Q_0, but this will not appreciably alter the general results of this paper.

TABLE II. *Values of the constants for the deuteron.*

		$x_1=0$				$x_1=1$			
	r_0	0.2	0.4	0.6	0.8	0.2	0.4	0.6	0.8
	k_t	1.135	1.366	1.593	1.814	0.792	0.977	1.163	1.351
	m_t	0.2	0.4	0.6	0.8	0.2	0.4	0.6	0.8
Triplet	D_t	128.8	46.64	28.20	20.57	62.73	23.86	15.03	11.41
State	N_t	0.6737	0.7217	0.7103	0.6843	0.6203	0.6150	0.5660	0.4984
	Δ_t	−6.64	−3.77	−2.13	−0.01	−6.88	−3.90	−2.22	+0.79
	W_t	−4	−4	−4	−4	−4	−4	−4	−4
	k_s	0.865	0.834	0.809	0.791	0.580	0.552	0.528	0.508
Singlet	D_s	74.8	17.4	7.27	3.91	33.7	7.61	3.10	1.59
Unstable	Δ_s	36.1	17.8	12.1	9.46	35.9	17.7	12.0	9.36
	k_s	0.937	0.978	1.017	1.053	0.637	0.671	0.705	0.736
	m_s	0.031	0.066	0.099	0.130	0.031	0.069	0.105	0.139
Singlet	D_s	87.8	23.9	11.5	6.93	40.6	11.3	5.52	3.39
Stable	N_s	0.2310	0.2513	0.2634	0.2680	0.2206	0.2504	0.2544	0.2576
	Δ_s	−36.1	−17.8	−12.1	−9.46	−35.9	−17.7	−12.0	−9.36
	W_s	−0.096	−0.109	−0.109	−0.106	−0.096	−0.119	−0.123	−0.121

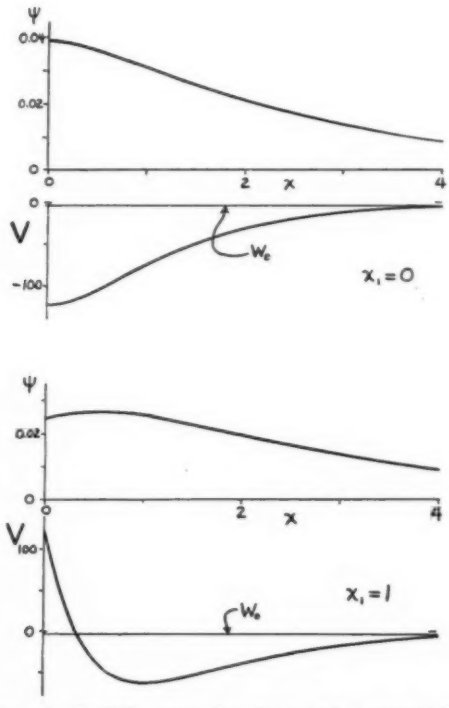

FIG. 4. Possible wave functions and corresponding potential energy curves for the deuteron. Horizontal lines on the energy plots show the deuteron energy level.

correct binding energy for H^2, comes out equal to 45. There are several values of D_e which satisfy this requirement, one having a stable singlet level very close to the top of the potential hole, and one having no stable singlet state. The constants for these two possibilities are given in Table II for different values of r_0 and x_1. In the case of the stable state the value of the allowed energy W_e is also given. It is interesting to notice that this value is practically independent of r_0 and of x_1 for a wide range of values of these parameters. The level, if it exists, is only about 60,000 ev below the top of the potential hole. The dotted curves in Fig. 3 show D_e for the case of no stable singlet state.

The variation of cross section with neutron velocity can then be computed. Fig. 6 shows curves of Q for $x_1=0$, plotted as a function of $W^{\frac{1}{2}}$, assuming a nonpermuting potential function; i.e., one where $\epsilon_l=1$. The differences between the curves are due to the increasing importance of the $l=1$ term in the series for Q as the value of r_0 is

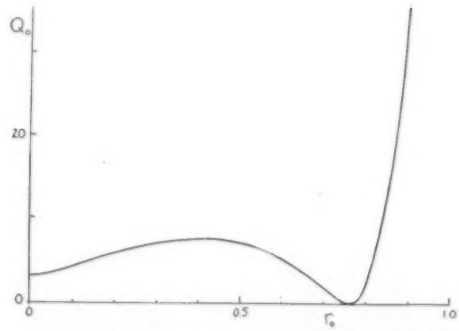

FIG. 5. Cross section for slow neutrons using the same potential as for bound state.

increased. The terms for $l>1$ are negligible for the range of r_0 studied. Fig. 7 shows corresponding curves for $x_1=1$. The chief difference is that at $x_1=1$ the term in $l=1$ becomes important for a smaller value of r_0.

When a potential of the Majorana type, $\epsilon_l=(-1)^l$, is assumed, all the terms in the series for Q are negligible except the first, and the cross-section curves for $x_1<1$ and $r_0<1$ are all practically identical with the curves shown for $r_0=0.2$.

Thus the variation of elastic cross section with neutron velocity is not a critical test for the value of r_0. If the experimental curve is similar to

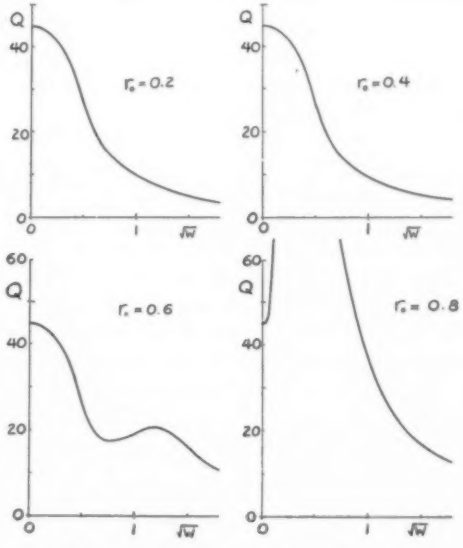

FIG. 6. Variation of cross section with neutron velocity for $x_1=0$, for different values of r_0, assuming a non-permuting type of potential. For a Majorana potential all curves would be similar to that shown for $r_0=0.2$.

the first one shown in Fig. 6, the potential can be nonpermuting with $r_0<0.4$, or it can be of the Majorana type with $r_0<1$. If, on the other hand, the curve shows a "Ramsauer effect" as in the curves for $r_0=0.8$, the potential is probably of the nonpermuting type with $r_0=0.8$ or larger.[6]

Capture Cross Section

During the collision of neutron and proton there is a finite probability that the neutron will be captured by the proton, forming a deuteron, radiating away the excess energy. The effective cross section for such a transition is given by the usual expression

$$q=(16\pi^4\nu^3/3c^3hv)M^2 \tag{9}$$

where v is the incoming neutron velocity and M is the effective moment,[7] either electric or magnetic, due to the transition. The wave function for the incoming neutron is normalized to unit amplitude at large distances. This means that the radial parts of the terms in the series for plane-plus-scattered wave must have the asymptotic form $(1/W^{\frac{1}{2}}r)\sin(W^{\frac{1}{2}}r-\delta_l-\frac{1}{2}l\pi)$.

From Eq. (9) can be derived the expression for the reciprocal of the mean life, before capture, of a neutron in paraffin, $(1/\tau)=nqv$, which can be measured experimentally.[8] The quantity n, the number of protons per cc in paraffin, is taken to be 0.72×10^{23}.

The expression for that part of $(1/\tau)$ due to electric dipole radiation is

$$(1/\tau)_e=\tfrac{3}{4}n\left(\frac{e^2h}{6\pi c^2m_p{}^2}\right)(m_e/m_p)^{\frac{1}{2}}W_r{}^3[\int\psi_0\Phi_t x\,dV]^2$$

where all lengths in the integral are in nuclear units. The constant W_r is the energy given off during the transition: it equals $W-W_t$. The function ψ_0 is the normalized wave function for the bound state and Φ_t is the unit amplitude wave for the triplet state. The factor (3/4) comes because only the triplet state takes part in this transition.

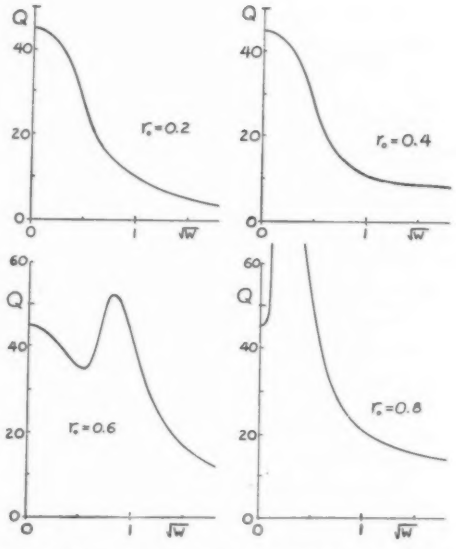

FIG. 7. Curves similar to those of Fig. 6 for $x_1=1$. Again the curves for a Majorana potential would all be similar to the first curve shown.

Values of $(1/\tau)_e$ have been computed by Breit and Condon[7] for a "square" potential hole, for a wide range of sizes. Inasmuch as our results for this quantity agree on the whole with theirs, it is not considered necessary to reproduce our curves in detail. We need only mention that the electric dipole cross section is more sensitive to changes in x_1 (i.e. in the shape of the potential curve) than any of the other quantities discussed in this paper.

This part of $(1/\tau)$ is very small for small values of $W(W<1)$, which is not in accord with experiment.[8] Therefore the part due to magnetic dipole radiation must predominate at low neutron velocities. The expression for the effective magnetic dipole for the allowed transition (singlet to triplet) is[8]

$$M_m=3^{\frac{1}{2}}(eh/4\pi m_pc)(g_p-g_n)\int\psi_0\Phi_s\,dV. \tag{10}$$

where g_p is the proton g factor, g_n that for the neutron, and c.g.s. units are used in the integral. We have used the following values[9] for the g's: $g_p=5.7$; $g_n=-4.0$.

[6] None of these curves are in agreement with the results of Goldhaber, Nature **137**, 824 (1936), who reports a cross section of 3.5 at $W=0.4$ nuclear unit. In order to check both Dunning's and Goldhaber's results, we should have to use a value of r_0 much larger than unity; in which case none of the results on inelastic collision, discussed later in this paper, would agree with experiment. This difficulty occurs whether Majorana forces are assumed or not.

[7] For a discussion of the validity of this formula, see Breit and Condon, Phys. Rev. **49**, 904 (1936).

[8] Fermi, Phys. Rev. **48**, 570 (1935).

[9] We are indebted to Professors O. Stern and I. I. Rabi on this point. Probable values of magnetic moment for the proton and the deuteron are 2.85 and 0.85 nuclear magnetons, respectively.

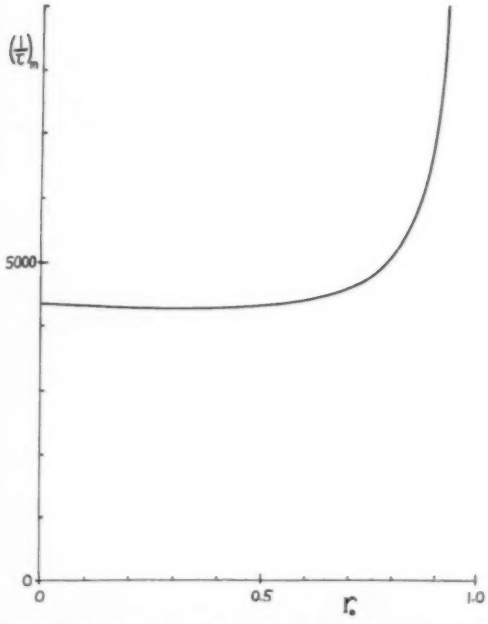

FIG. 8. Reciprocal mean life time of a neutron in paraffin. The observed value is of the order of 10^4 sec^{-1}.

If the singlet potential is equal to that of the triplet this moment will be zero, due to the orthogonality of ψ_0 and Φ_s. If the singlet field is used which gives the correct value of the elastic cross section, by Eq. (8), then M_m will not be zero. Transforming the integration into nuclear units and combining terms, the expression for that part of $(1/\tau)$ which is due to magnetic dipole radiation becomes

$$(1/\tau)_m = \tfrac{1}{4}n(e^2h/8\pi c^2 m_p^2)(m_e/m_p)^{\frac{1}{2}} \times W_\tau^2(g_p-g_n)^2[\int\psi_0\Phi_s dV]^2 \quad (11)$$

where ψ_0 and Φ_s are given in terms of the functions defined in Eqs. (3) and (4) for the proper values of k.

A curve of $(1/\tau)_m$ for very slow neutrons is shown in Fig. 8 as a function of r_0 for $x_1=0$, for the case where there is no stable singlet state. In contrast to $(1/\tau)_e$, the quantity $(1/\tau)_m$ is practically independent of r_0 for r_0 less than 0.8, and of W when W is less than unity; having a value of 4300 sec.$^{-1}$ within this range. The curve for $x_1=1$ is practically identical with the one shown. The corresponding curves for the case of a stable singlet state are also similar, the value of $(1/\tau)_m$ for the range ($W<1$, $r_0<0.8$, $x_1<1$) being 3600 sec.$^{-1}$. In this latter case one must include the probability of transition from the triplet incoming state to the stable singlet state; but this quantity is negligible due to the small value of the factor W_τ^3 in the expression corresponding to Eq. (11) for such a transition.

Therefore the magnetic dipole type of capture predominates for neutron energies below about 500,000 ev. The results obtained here indicate that measurements of slow neutron capture cross section will have to be much more accurate than is possible at present before this experiment, by itself, can decide whether the deuteron has a stable singlet state or not. The two values obtained, 4300 and 3600 sec.$^{-1}$, both check the experimental value within its probable error. Presumably other experiments can be devised which are more sensitive to the presence or absence of a stable singlet state.

PHOTOELECTRIC DISINTEGRATION OF THE DEUTERON

It can be shown[10] that the cross section for the disintegration of the deuteron by photons of frequency ν (where $h\nu = W_\tau = -W_t + W$ in nuclear units) is related to the cross section for the inverse process, the capture of neutrons, discussed in the previous section. In fact the disintegration cross section is

$$\sigma = 15.2\times10^{-6}(W_\tau+W_t)^{\frac{1}{2}} (1/W_\tau)^2[(1/\tau)_m+(1/\tau)_e],$$

in nuclear units, and where $(1/\tau)_e$ and $(1/\tau)_m$ are the quantities considered in the previous section, considered as functions of $W=W_\tau+W_t$.

We have seen that when $W\ll1$ and when $r_0<0.8$ and $x_1<1$, the magnetic dipole capture predominates. Therefore for photons of energy just above the photoelectric threshold, the disintegration cross section is

$$\sigma \backsimeq \left\{\begin{matrix}0.053\\0.064\end{matrix}\right\}(W_\tau+W_t)^{\frac{1}{2}}(1/W_\tau)^2 \quad \text{nuclear units,} \quad (12)$$

where the two constants are for the presence or the absence of a stable singlet state, respectively.

The only experimental data available[11] leads

[10] Bethe and Peierls, Proc. Roy. Soc. **A148**, 146 (1935).
[11] Chadwick and Goldhaber, Proc. Roy. Soc. **A151**, 479 (1935).

to a value for σ of the order of 10^{-3} nuclear units for $W_\tau = 5.2$, an energy outside the range of validity of Eq. (12). The results of Breit and Condon[7] show that at this energy, the part of σ due to electric dipole transition is as large as that due to magnetic dipole, or perhaps somewhat larger. Utilizing this, the computed value of σ comes out to be about 0.005 nuclear units, in fair agreement with the experimental result.

Conclusions

It has often been stated that the general characteristics of the interaction between neutron and proton are more or less independent of the shape of the field and of the size of the potential hole. We have shown, in a specific case which can be calculated by analytic means, that this is indeed the case. Once the constants are chosen so as to give the correct binding energy and elastic cross section for slow neutrons, the computed values of $(1/\tau)$ and σ (for low energy photons) are insensitive to variation of the remaining parameters r_0 and x_1 within quite wide ranges of values of these parameters. Nor are the results particularly sensitive to the presence of a Majorana exchange operator in the potential, or to whether there is a stable singlet state or not. Empirical determination of these properties will require the experimental measurement of quantities which depend more markedly on the angular momentum than do those discussed in the present paper.

The above result is a negative one, and as such is not particularly satisfying. However several positive conclusions can be drawn from our results. One is that the neutron-proton interaction must contain a term dependent on the coupling between the spins of proton and of neutron. Only in this way can be explained the large elastic cross section for slow neutrons, and the fact that the mean life of a slow neutron in the presence of protons is independent of its velocity, a property of magnetic dipole capture.

It is also apparent that the results are internally consistent: i.e., if one assumes that r_0 is less than 0.8, that x_1 is less than unity and that V_s is not equal to V_t, then a choice of parameters to fit two of the four bits of experimental data discussed above gives results which fit the other two experimental values.

OCTOBER 15, 1936 PHYSICAL REVIEW VOLUME 50

Electronic Energy Bands in Sodium Chloride

William Shockley, *George Eastman Research Laboratory of Physics, Massachusetts Institute of Technology*

(Received July 27, 1936)

The Wigner and Seitz method of cellular potentials has been applied to the calculation of wave functions in NaCl. A renormalized Hartree field has been used around the Cl and the Prokofjew field around the Na. The relative heights of the potentials are determined by use of Madelung's number. The problem of joining the functions at the cell boundaries has been treated by the Slater method of fitting ψ and ψ' at midpoints. For the outer Cl electrons a reasonable approximation is to join at Cl−Cl midpoints only. This gives rise to a face-centered lattice for which solutions of the Slater conditions have been found by Krutter. Several new solutions have been derived which allow fairly accurate energy contours in momentum space to be drawn for the Cl $3p$ band. If the joining is made at Cl−Na midpoints alone, a large number of unsatisfactory zero-width bands arise. When both Cl−Cl and Cl−Na midpoints are used, the boundary conditions can be treated only for special cases. For these they are consistent with the Cl−Cl solutions. Several attempts to calculate the ultraviolet absorption frequency are described and the difficulties involved are discussed.

I. Introduction*

THERE has been a great advance in the calculation of wave functions in solids in the last four years. The initial impetus was derived from the contributions of Wigner and Seitz.[1] From a consideration of the Pauli principle they concluded that an electron in a monovalent metal

* The writer is indebted to Dr. Seitz for discussions of this paper and that by Douglas H. Ewing and Frederick Seitz. The viewpoints of the two papers differ in that the ionic picture of the lattice has been adhered to in this paper and no attempt to obtain a self consistent field has been made.

[1] Wigner and Seitz, Phys. Rev. **43**, 804 (1933).

is surrounded by a "Fermi hole" in the charge distribution of the other electrons. This hole has roughly the volume corresponding to one atom. When the electron is on one of the atoms in the lattice, it finds that the hole produces a net positive charge on that atom, while all other atoms are neutral and produce no field. The total potential for this electron is, thus, just that which it would experience about the same atom in the case of free atoms. If the field for the free atom is known, this picture gives the field in the metal. Since the field is spherically symmetrical about any atom, the wave equation can be separated in spherical harmonics and the radial functions obtained by numerical integration. The problem of utilizing the functions so obtained to construct Bloch type functions continuous in going from atom to atom was first discussed by Slater.[2] On the basis of this picture, calculations have been carried out for metallic Na,[2] Li,[3] Cu,[4] diamond,[5] LiH and LiF.[6]

In a later attempt to improve their values, Wigner and Seitz[7] consider their method from the viewpoint of the Fock equations. The Fock equation for one of the one-electron wave functions may be written in the form

$$[-(h^2/2m)\nabla^2 - eV(r_j) - A_j(r_j)]\psi_j(r_j) = E_j\psi_j(r_j) \quad (1)$$

where $V(r_j)$ is the coulomb potential of the combined positive and negative charges and

$$A_j(r_j) = (1/\psi_j(r_j))\sum{}'i \int \psi_i^*(r) \times \psi_j(r)(e^2/|r-r_j|)dv\psi_i(r_j). \quad (2)$$

The $\sum'i$ is to be taken over all occupied states of the same spin as ψ_j. In the case of free electrons, where the ψ's are plane waves, the exchange term A_j is merely a constant which depends upon the momentum of the wave function ψ_j.[8] In the case of metallic sodium, the wave functions are near enough plane waves to warrant regarding the term as a constant there. For the case of a substance such as NaCl, the wave functions will be as near free atom Bloch functions as plane waves, and the effect of A should be considered afresh. Consider Bloch functions of the form

$$\psi_{j,\,n}(r) = (1/\sqrt{N})\sum_\alpha e^{2\pi i k_j \cdot R_\alpha}\psi_n(r-R_\alpha). \quad (3)$$

The N atoms of the lattice are located at the lattice points R_α the index n refers to the atomic level and the allowed values of k_j are determined by periodicity requirements on the boundary of a large box. For these functions the summation over i in the A term can be readily worked out. It is found that if r_j is on atom α, A vanishes unless r is on atom α also. Thus, so far as exchange is concerned, Eq. (1) reduces to the Fock equation for a single atom. This result could have been seen at once by realizing that the Bloch functions (3) are obtained from the single atom functions $\psi_n(r-R_\alpha)$ by a unitary transformation which does not mix free atom functions having different energy parameters E_n. Under these conditions the Fock equations will be satisfied in formally the same way by either set of functions.

Thus, for both the free electron functions and the atomic Bloch functions, the A term is interpretable as the potential due to a hole in the electron distribution which surrounds a given electron. For the free electrons the shape of the hole has no particular significance, but the potential due to it depends on the momentum or wave vector of the solution.[8] For the atomic Bloch functions, the hole for a given $\psi_{j,\,n}$ in the ψ_n distribution is Hartree-like about a given atom (at least insofar as the Hartree approximation represents the Fock equations for one atom) and does not depend on k. Since in NaCl the ions are not very tightly squeezed together, we should expect the Hartree hole to be preferable to the Fermi hole.

II. Calculation

The fields of the Cl^- ion have been computed by Hartree.[9] These were modified before use by renormalizing them so that all the $3p$ and $3s$ electrons were contained in a sphere whose volume was equal to the space over which these functions were expected to be large in the lattice. This was taken to be the volume belonging to a NaCl molecule less the volume of a spherical

[2] J. C. Slater, Phys. Rev. **45**, 794 (1934).
[3] J. Millman, Phys. Rev. **47**, 286 (1935).
[4] H. M. Krutter, Phys. Rev. **48**, 664 (1935).
[5] George E. Kimball, J. Chem. Phys. **3**, 560 (1935).
[6] Ewing and Seitz, Phys. Rev. (this issue).
[7] Wigner and Seitz, Phys. Rev. **46**, 509 (1934).
[8] John Bardeen, Phys. Rev. **49**, 653 (1936).
[9] D. R. Hartree, Proc. Roy. Soc. **A141**, 282 (1933).

Na^+ ion. The fields corresponding to the renormalized charge distributions were then calculated, and new s and p functions for a wide range of energy parameters were computed from them by Hartree's methods of numerical integration.[10] There are no d and f functions in Cl^-, so the Hartree field for them was taken to be the same as for the $3p$ functions, that is, the spherically averaged field of the configuration $1s^2 2s^2 2p^6 3s^2 3p^5$ and the nucleus.

Since the valence electrons of Cl were expected to have small amplitude about the Na^+ ion, the hole about the Na was considered negligible and the field and wave functions there were taken to be the same as those in metallic sodium.[11]

Since the ions in NaCl are not neutral, the field due to the neighbors of any one ion must be considered. If this field is expanded in spherical harmonics, it will contain a constant term and terms in $l=4$, 6, 8, etc., which are neglected because they are much smaller than the constant term and average to zero in the spherical approximation. The value of the constant term can be obtained from Madelung's number which gives the electrostatic energy per cell (4 molecules) and consequently the potential at a lattice point of an ionic lattice in terms of the lattice constant and the charge on the lattice points. For the NaCl lattice this gives

$$\varphi_{Cl} = (13.94e^2/a) \div 4 \qquad (4)$$

for the potential at a Cl^- ion due to the other ions.[12] In atomic units this value is 0.66 for NaCl. Hence, if a wave function were obtained in the Hartree field of a Cl^- ion less one $3p$ electron (net charge zero) for a positive energy parameter ϵ_C, then the total energy in the lattice for the same wave function would be $\epsilon_L = \epsilon_C - 0.66$. Similarly for Na^+ wave functions it would be $\epsilon_L = \epsilon_N + 0.66$.

Thus the charge distribution which produces the field in which the electron moves is that of the entire ionic lattice when the electron is on a Na ion, or else the same charge less that of one electron on the Cl ion where the electron is. Physically it does not seem very plausible that the defect of one electron in the neighborhood of a given electron should vanish entirely when the electron moves from a Cl ion to a Na ion. To investigate this the exchange potential due to a two atom type Bloch function (see Eq. (6)) was calculated. This exchange potential has decidedly nonphysical properties. It is in general complex and, when averaged spherically, gives zero fields for the wave function with $k=0$. This peculiar behavior probably indicates a deficiency of the Fock-Bloch method of dealing with this case. A more sensible behavior of the hole when the electron moves onto a sodium would be for it to distribute itself onto the six surrounding Cl ions. This results in a lowering of the sodium potential by 0.38 At.U., so that $\epsilon_L = \epsilon_N + 0.66 - 0.38 = \epsilon_N + 0.28$. It was convenient to carry out calculations for $\epsilon_L = \epsilon_N + 0.58$ at the same time, and the results for both are given in the next section.

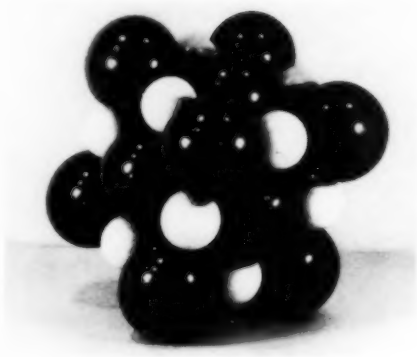

FIG. 1. Scale model of NaCl.

III. JOINING METHODS

On the basis of the ionic radii, it is seen that in NaCl the Na^+ and Cl^- ions touch and the Cl^- ions almost touch (Fig. 1). We are interested principally in the $Cl^- 3p$ band. For this the wave functions will be much larger around the Cl than around the Na. Hence, the requirements of continuity will probably be as important in going from Cl to Cl as Na to Cl. Three different sets of continuity requirements were considered in all. These are classified according to the

[10] D. R. Hartree, Proc. Camb. Phil. Soc. **24**, 89 (1928).
[11] The writer is indebted to Professor J. C. Slater for the use of his wave functions calculated in connection with reference 2.
[12] See the article by Born and Göppert-Mayer, *Handbuch der Physik*, XXIV/2, for a discussion of lattice potentials.

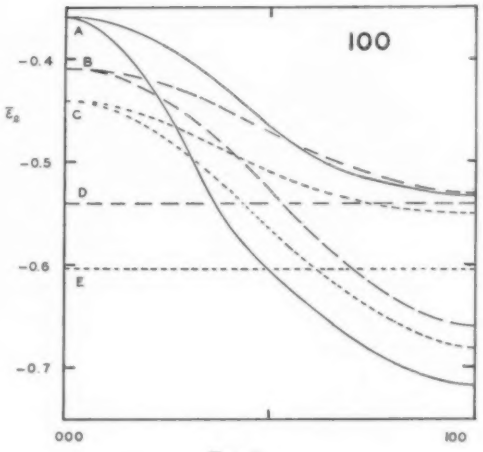

FIG. 2.

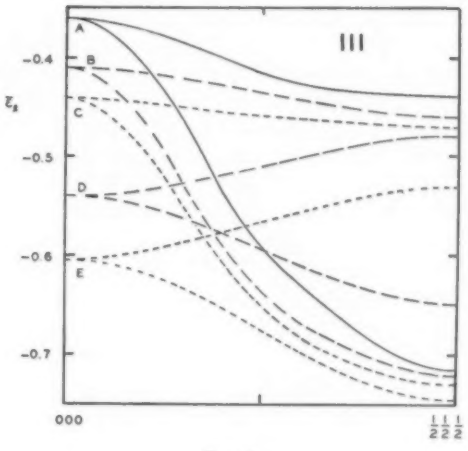

FIG. 3.

FIGS. 2 AND 3. Energy bands for the three joining conditions. (k space is body-centered and the scale has been chosen so the lattice points are 111, 200, etc.)

A. Cl−Cl
B. Cl−Cl−Na $\epsilon_L=\epsilon_N+0.58$
C. Cl−Cl−Na $\epsilon_L=\epsilon_N+0.28$
D. Na−Cl $\epsilon_L=\epsilon_N+0.58$
E. Na−Cl $\epsilon_L=\epsilon_N+0.28$

points at which the Slater conditions (continuity at the midpoint of an interatomic line of ψ and the component of $\nabla\psi$ along the line) are fulfilled.

1. Cl−Cl

Neglecting the wave functions of the Na^+ ions entirely, we are led to consider a face-centered lattice of Cl^- ions. The Slater conditions are required to be fulfilled at the Cl−Cl midpoints. For this lattice a suitable set of 12 wave functions (one s function, three p's, five d's, and 3 f's of the form $x(y^2-z^2)/r^3$) have been found by Krutter.[4] He gives solutions for the particular directions 100, 110, 111 for k. The relationship between energy and k for the 100 and 111 lines are shown in Figs. 2 and 3. A sufficient set of further solutions have been obtained to allow rough interpolations to be made to general points in k space[13] (Fig. 4).

2. Na−Cl

For one type of atom in a lattice with centers of symmetry it can be proved that the wave function should be of the type

$$\psi_k(r)=\sum_\alpha e^{2\pi ik\cdot R_\alpha}[u_g(r-R_\alpha)+iu_u(r-R_\alpha)] \quad (5)$$

where u_g is an even real function of its vector argument and u_u is odd and real. Such functions materially simplify the setting up of the Slater conditions. If there are two types of atoms at centers of symmetry, as in NaCl, then the proper function is of the form of (5) summed over one set of atoms plus a precisely similar sum over the other set.

$$\psi_k(r)=\sum_\alpha e^{2\pi ik\cdot R_\alpha}[u_g(r-R_\alpha)+iu_u(r-R_\alpha)]+\sum_\beta e^{2\pi ik\cdot R_\beta}[v_g(r-R_\beta)+iv_u(r-R_\beta)]. \quad (6)$$

If we consider a Cl^- ion as being at $r=0$, then it is surrounded by 6 Na ions at $a(\pm\frac{1}{2}\,0\,0)$, $a(0\,\pm\frac{1}{2}\,0)$ and $a(0\,0\,\pm\frac{1}{2})$. The continuity requirements at the Na−Cl midpoint $a(\frac{1}{4}\,0\,0)$ are

$$\begin{aligned} u_g+iu_u&=e^{\pi ik_x a}[v_g-iv_u],\\ u_g'+iu_u'&=e^{\pi ik_x a}[-v_g'+iv_u']. \end{aligned} \quad (7)$$

Here the functions are taken to be sums of surface harmonics times their corresponding radial functions. They are all evaluated for an argument of $a(\frac{1}{4}\,0\,0)$ and $'$ indicates $\partial/\partial r$. Separating real and imaginary parts, we see that each interface gives 4 conditions and the six interfaces would give 24 conditions in all.

[13] These new solutions are to be submitted to the *Physical Review* in the near future.

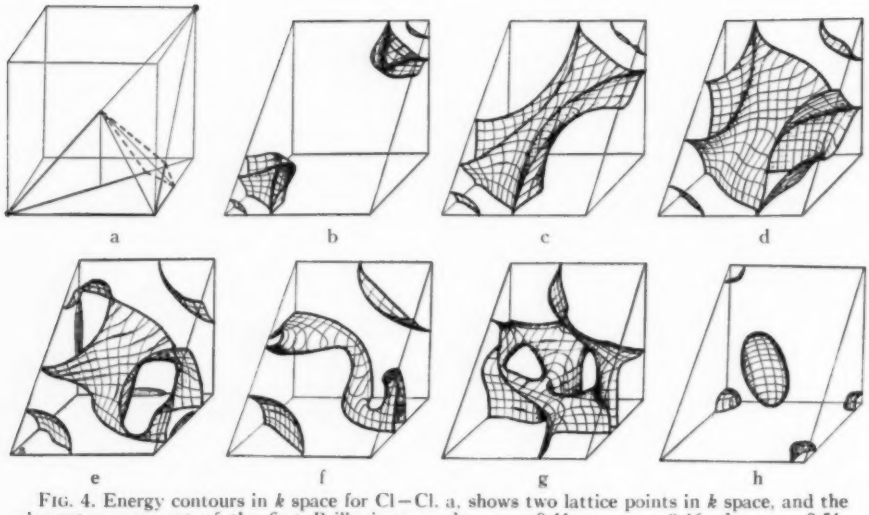

FIG. 4. Energy contours in k space for Cl−Cl. a, shows two lattice points in k space, and the elementary segment of the first Brillouin zone; b, $\epsilon_L=-0.41$; c, $\epsilon_L=-0.46$; d, $\epsilon_L=-0.51$; e, $\epsilon_L=-0.56$; f, $\epsilon_L=-0.61$; g, $\epsilon_L=-0.66$; h, $\epsilon_L=-0.71$.

However, for functions of type (6), the $a(\frac{1}{4}\,0\,0)$ and $a(-\frac{1}{4}\,0\,0)$ interfaces are equivalent and only 12 conditions are independent. Hence, if we expand the u's and v's in terms of 12 solutions of the spherical equations for the Na^+ and Cl^- ions, the 12 homogeneous equations (for the expansion coefficients) will be soluble if, and only if, the determinant of the equations vanishes. This determinant is a function of k_x, k_y, k_z and the various radial functions and their derivatives. Since the latter are functions of the energy, the vanishing of the determinant gives a relationship between energy and momentum.[14]

The natural set of twelve functions to choose is an s function, three p's, and two d's of the form $(x^2-y^2)/r^2$ for each type of atom. Even for these simple functions, the determinant derived from the Eq. (7) proves to be more difficult to handle than the corresponding 12th order determinant of the face-centered lattice. Some results for calculations in the special directions 100 and 111 are shown in Figs. 2 and 3. In Fig. 3 the upper band is double; in Fig. 2 the "zero width" band is double and there is also a third band corresponding to the single band of Fig. 3, which is not shown. The dotted curves correspond to a total defect of one electron on the Cl's which surround the electron when it is on a Na, and the dashed curve to a lesser defect (see Section II).

[14] See reference 2 for a discussion of this method.

The reason the change of 0.3 in the Na potential produces only the small change 0.05 in the results is that the values lie within the Cl^-3p band (the energy range for which $p'/p<0$). Within this band p'/p is a relatively sensitive function of the energy, while the corresponding quantities are much less sensitive for the Na^+ wave functions. Hence, a change in the energy parameter of the latter can be compensated by a much smaller change in the former.

3. Cl−Cl−Na

The set of conditions derived by considering both Cl−Cl and Na−Cl midpoints simultaneously leads to twenty-four conditions, twelve of each type. Due to the complexity of this case, no attempt was made to choose a suitable set of functions. Instead, certain directions or points were chosen in k space and sets of functions were chosen in accordance with the symmetry groups for these points. Since the point $k=0$ corresponds to full octahedral symmetry, only functions of the representation Γ_4 (that of the Cl^-3p functions) were used.[15] Similar considerations in connection with the other end points of Figs. 2 and 3 gave the results shown there. The dotted and dashed curves have the same significance as for the Na−Cl case.

[15] For a classification of spherical harmonics according to the representations of O_h, see H. Bethe. Ann. d. Physik **3**, 133 (1929).

IV. Comparison of Results

We see that for all the cases considered, the width and location of the energy band is approximately the same. The Cl−Cl and Cl−Cl−Na are very similar and are both quite different from the Na−Cl. In the absence of any criterion for testing the validity of the various methods, it appears that the width and location of the energy band is probably nearly right and that the detailed structure is more like that of the Cl−Cl and Cl−Cl−Na than the Na−Cl.

V. Concerning the Binding Energy

It does not appear practical to carry out this method far enough to calculate binding energies as is done in the case of metals. The reason for this is the presence of six valence electrons rather than one. This means that when the wave functions are calculated in the crystalline field, any change in the wave function gives a fivefold reaction on the field for which the wave function is calculated. Also, there is no adequate zero for the energy of the lattice. The energy values obtained by Hartree for the Cl^- ion may be in error (due to neglect of exchange effects and polarization of the other electrons by any one) by an amount comparable with the binding energy of NaCl. If these errors are not independent of the lattice spacing, their variation may obscure the variation which gives the binding energy.

VI. Concerning Excitation

One quantity which is generally supposed to be intimately connected with electronic bands in an insulator is the energy of excitation and the ultraviolet absorption. Under the influence of light, there will be a probability of excitation of an electron from a state in an occupied band to one in an unoccupied band. For ultraviolet light, the change in momentum of the electron will be negligible and the possible transition energies will be those for excitation without change of momentum. Absorption will become large when the energy of the light is equal to the least energy difference between states of the same momentum in an occupied and an unoccupied band.

There are rather serious difficulties in applying the Fock method discussed in Section I to the calculation of excited states. The excitation of one electron will, of course, make an entirely negligible change in the field for an unexcited electron, so that the changes in the occupied states are inappreciable. However, the field acting on the excited electron is very different from that acting on one in a filled band. This is due to the orthogonality of the excited state wave functions to the filled state wave functions. Due to this orthogonality, the exchange potential for the excited electron will be very small, and the Fermi hole for it will be nearly negligible. From this we suspect that the Fock approximation is not as good for excited states as for the ground state and should be modified by a correlation between electrons of parallel spin, which would restore some of the lost hole.

An attempt to calculate the excitation energy on the basis of the three joining conditions used in III gave unsatisfactory results. The energy difference between the bands varied from about 3 times the experimental value (0.54 At.U.), when the hole was omitted for the excited state wave functions, to about $\frac{1}{3}$, when the hole was retained.

Also, the width (0.35 At.U.) of the lower band alone is roughly five times the width expected for the first absorption band for NaCl from the data of Hilsch and Pohl[16] and O'Bryan.[17] Since it is rather unlikely that the upper band should be such as to decrease the total spread for band to band transition, it does not appear possible that the electronic energy band picture can give the right behavior for absorption. There is a possibility that the detailed structure of the bands, causing a concentration large number of transition probabilities in certain energy ranges, could be responsible for the absorption peaks.[18] However, until more accurate work is done on the bands, this cannot be determined.

The writer wishes to acknowledge his indebtedness to Professor J. C. Slater for directing this research and to Professor P. M. Morse for the theory and practice of drawing space contours.

[16] R. Hilsch and R. W. Pohl, Zeits. f. Physik **59**, 812 (1930).
[17] H. M. O'Bryan, Phys. Rev. **49**, 944 (1936).
[18] Such peaks have been computed for the energy levels of Cu. E. Rudberg and J. C. Slater, Phys. Rev. **50**, 150 (1936).

On the Electronic Constitution of Crystals; LiF and LiH

DOUGLAS H. EWING AND FREDERICK SEITZ, *Bausch and Lomb Laboratory of Physics, University of Rochester, Rochester, N. Y.*

(Received July 27, 1936)

A self-consistent solution of the Hartree-Fock system of equations for the ionic crystals LiF and LiH is attempted using approximation methods previously employed in metals. In part *A* the boundary equations which the periodic functions must satisfy in the case of a face-centered cubic lattice are examined from the group theoretical standpoint. In part *B* the Hartree system of equations is solved using ion core fields which include the $(1s)^2$ electrons in both Li and F, so that eight electrons are given periodic functions in LiF and two in LiH. These solutions, which are regarded as preliminary ones, involve the use of the "*s* sphere approximation." The final results in both cases show that the Hartree approximation allows considerable charge to be in the vicinity of the metal ion so that the classical ion model is appreciably incorrect in that the valence electrons are not localized in a definite region about the electronegative atoms. The extent to which this affects the Born-Madelung lattice energy computations is discussed from the viewpoint of a complete solution.

IT is the intention of this paper* to extend the schemes that are available at present for determining solid state electronic wave functions of the Bloch type, and to investigate the electronic structure of the ionic solids LiF and LiH. These extensions to the general procedure lie partly in the introduction of formal group theoretical methods into the schemes available for specifying the one-electron states, and partly in the use of particular simplifying steps in carrying through an approximate solution of Hartree's equations for solids. These developments are applied to the cases of the crystals mentioned above in order to obtain a better understanding of their constitution and to attempt to throw more light upon some of their characteristic optical and electronic properties.

Ionic crystals have been made the subject of a considerable amount of investigation from the classical atomic standpoint by Madelung, Born and others using semi-empirical methods, and this work has been successful in tying together various properties of these crystals such as compressibility, density and binding energy. On the other hand, there is convincing evidence to indicate that the simple ion model which forms a starting point for this development greatly oversimplifies the actual condition, and for this reason an investigation of such substances from the purely theoretical standpoint seems particularly appropriate. This topic will be discussed in later paragraphs, and we shall proceed with the discussion of the construction of wave functions after outlining the formal background.

PART A. GROUP THEORETICAL FOUNDATION

1. Reduction of space groups

The symmetry properties of crystals[1] are primarily characterized by the presence of a translation group (i.e., lattice structure). That is, the crystal is sent into itself by a set of translations of the type

$$l = n_1\tau_1 + n_2\tau_2 + n_3\tau_3 \qquad (1)$$

where τ_1, τ_2, τ_3 are the primitive translations, which define the fundamental cell of the crystal, and the n's are integers. In addition, however, the crystal may have other symmetry operations which instead of being of the simple translational form

$$x_1' = x_1 + t_1, \quad x_2' = x_2 + t_2, \quad x_3' = x_3 + t_3, \qquad (2)$$

corresponding to (1), where x_1', x_2', x_3' are the coordinates of the points x_1, x_2, x_3 after translation by means of $t = (t_1, t_2, t_3)$, are of the type

$$\begin{aligned} x_1' &= a_{11}x_1 + a_{12}x_2 + a_{13}x_2 + a_1, \\ x_2' &= a_{21}x_1 + a_{22}x_2 + a_{23}x_3 + a_2, \\ x_3' &= a_{31}x_1 + a_{32}x_2 + a_{33}x_3 + a_3. \end{aligned} \qquad (3)$$

In this the crystal is to be regarded as rotated as well as translated, the rotation being de-

* We wish to thank Dr. W. Shockley for valuable discussions in connection with his work on NaCl, which accompanies this paper, and ours.

[1] R. W. G. Wyckoff, *Structure of Crystals* (1931); F. Seitz, Zeits. f. Krist. **88**, 433 (1934), et seq.

scribed by means of the matrix

$$\alpha=\begin{pmatrix} a_{11} & a_{12} & a_{13} \\ a_{21} & a_{22} & a_{13} \\ a_{31} & a_{31} & a_{22} \end{pmatrix} \tag{4}$$

and the translation by means of the vector

$$a=\begin{pmatrix} a_1 \\ a_2 \\ a_3 \end{pmatrix}. \tag{5}$$

The complete symmetry of the crystal will be described by a group of transformations of type (3), and since the Hamiltonian operator will have this symmetry, it follows that all its eigenfunctions will belong to irreducible representations of this group in accordance with the fundamental theorem of Schur.[2] Since the total wave function of the normal state will belong to the unit representation, practically speaking (i.e., have the same symmetry as the crystal), we may conclude that the one-electron functions of the Hartree-Fock approximation will belong to particular representations of the space group.[3] This means, essentially, that the Hartree-Fock field acting on a given electron will have the symmetry of the lattice which is a self-consistent assertion.

Bloch[4] has shown that the translation group will be reduced if the coordinate system in the Hilbert space is defined by means of the set of functions

$$\psi_k=\chi_k e^{ik\cdot r} \tag{6}$$

where χ_k is invariant under the translation group, and, using periodic boundary conditions,

$$k=\frac{n_1}{N}\frac{\tau_2\cdot\tau_3}{(\tau_1\tau_2\tau_3)} \tag{7}$$

where n_1, n_2, n_3 are integers, N is the number of cells along an edge of the crystal block for which the periodic conditions are satisfied, and $(\tau_1\tau_2\tau_3)$ is the volume of the unit cell. Actually, the reduction of the translation group is never necessary since the complete group is always larger. This is true even in the triclinic case because of the time reversal symmetry of the Schrödinger equation.[5] Nevertheless it is convenient to use (6) because of its inherent simplicity. In this connection we may introduce the concept of a three-dimensional k space in the usual way. This is defined by the practically continuous set of points (7).

Regarding the problem of reducing the space groups, this has been formally carried through by one of us for all types of crystals.[6] In the present paper, however, we shall consider only those results of this investigation that refer to the simple type of space group in which all elements are of such a type that that a in (3) is a member of the group of translations (1). The simple face centered lattice of the NaCl type belongs to this set. Under these conditions the irreducible representations may be found as follows.

In k space, all of the functions of type (1) going with points k that are sent into one another by the g-order group G of the crystal class[7] acting at the origin of coordinates, $k=0$, will belong to a g-dimensional irreducible representation, unless two of the equivalent k's differ by a vector of "type K," where

$$K=l_1\frac{\tau_2\cdot\tau_3}{(\tau_1\tau_2\tau_3)}+l_2\frac{\tau_3\cdot\tau_1}{(\tau_1\tau_2\tau_3)}+l_3\frac{\tau_1\cdot\tau_2}{(\tau_1\tau_2\tau_3)}, \qquad (l_1, l_2, l_3=0, 1, 2\cdots). \tag{8}$$

When this condition is met with, as it will be when one of the k's lies along a symmetry axis or plane or at a distance $K/2$ from a symmetry plane, etc., the irreducible representations are not g dimensional, but are generally lower. If we consider the set of $r=g/n$ equivalent k's which differ by vectors of type K (which belong to equivalent representations of the translation group) and the subgroup R of G which send these into one another, the theory asserts that only those linear combinations of this set which belong to an irreducible representation of R belong to an irreducible representation of the space group. The full set of g equivalent k's divide themselves

[2] E. P. Wigner, *Gruppentheorie*, Vieweg (1931); H. Weyl, *Group Theory and Quantum Mechanics*.
[3] F. Seitz, Phys. Rev. **47**, 400 (1935).
[4] F. Bloch, Zeits. f. Physik **52**, 555 (1928).
[5] E. P. Wigner, Nach Gött. Geo. (1932).
[6] F. Seitz, Annals of Math. **37**, 17 (1936).
[7] i.e., the factor group of the space group in which the translation group corresponds to the unit element, etc. g is 48 for crystals of type O^h.

into n sets containing r points which, like the foregoing set, go with $r\psi$'s that belong to equivalent representations of the translation group and which are sent into one another by an r-dimensional subgroup of G that is equivalent to R. If the first set of r functions is reduced with respect to R into irreducible representations, D_i, of dimensionality l_i (i runs over all irreducible representations of R), those functions in the other $n-1$ sets which belong to the equivalent irreducible representations of the corresponding group will join with the l_i functions of the first, going with D_i to form an nl_i-dimensional irreducible representation of the space group.

To summarize, if the $g\psi$'s equivalent to a given one do not all belong to different representations of the translation group, it is not sufficient that it be of the form (1) if it is to belong to an irreducible representation of the space group, but it is also necessary (and sufficient) that it belong to an irreducible representation of the group R which connects it into those $r-1$ of the g functions which belong to equivalent representations of the translation group.

It is to be emphasized that this statement is valid only for the simple types of space group specified above. The situation is more complicated for crystals of the beryllium and diamond type in which screw motions occur.

From this standpoint it is possible to draw several important conclusions[8] concerning the nature of the energy surface in K space, and for the purpose of the discussion we shall employ the reduced zone scheme in which points of k space which differ by a vector K are regarded as identical, so that we view the energy function as a many-valued function in the first zone, that is as a set consisting of many three-dimensional surfaces. At most points in this first zone the energy surfaces will be separated because the functions going with the point k will belong to different or equivalent representations of the space group, and the energies of these tend to repel one another. At certain points along symmetry axes or at the point $k=0$, however, some of the surfaces will touch one another because several functions which belong to equivalent representations of the translation group belong to the *same* representations of the space group, for reasons we have outlined above, and must have the same energy. We shall consider practical cases of this later in connection with the face centered cubic crystals.

If one goes to an extended zone picture, instead of the reduced one, in which the energy surface is taken to be single valued, the existence of contact between some of the surfaces in the multiple surface picture of the latter scheme will reflect itself in the absence of discontinuities of the energy surface at certain points of some of the zones or even at entire lines. In the zone space of the face-centered lattice, the eight cube corners

$$\begin{pmatrix} \pm 1/2a \\ \pm 1/2a \\ \pm 1/2a \end{pmatrix}$$

are of this character, where $2a$ is the length of the edge of the fundamental cube of the crystal lattice.

A very interesting behavior occurs when we get far enough from the origin so that there is an equivalent point which differs by a K vector that is not zero. (Such points will only occur at the boundary of the zone if the Brillouin construction has been used.) We may regard the g-dimensional representation as breaking up into a number of smaller dimensional ones (if a symmetry plane or the time reversal operator has caused this, the number will be two) which insures us that there will be a gap at this point between the different surfaces. If this occurs at all points of the surface of the first zone it may be said to be specified by symmetry.[9] This is true of the cube of the simple cubic lattice, the rhombic dodecahedron of the body centered

[8] L. P. Bouckaert, R. Smoluchowski and E. Wigner, Phys. Rev. **50**, 58 (1936), have considered similar problems from essentially the same viewpoint.

[9] It is to be kept in mind that we have adopted the convention that the points of k space are so chosen that those going with the same representation are equidistant from the origin, that is, are of equal length, and are sent into one another by the symmetry operation in such a way that k space undergoes a *rigid rotation* (i.e., there are no dilatations or other distortions). If only this restriction is made, the Brillouin zone scheme is not unique in the specification of zones, but rests only upon a perturbation scheme in which free waves are used in the starting approximation. If another starting scheme is used, a different set of zones will generally be met with, even when the foregoing convention is used. A small number of zones are uniquely specified by symmetry, however, and all schemes of construction will lead to these.

lattice, or the hexagonal prism of the hexagonal lattice Γ_h, in cases in which the symmetry class is D_6^h. On the other hand, only the center points of the hexagonal faces of the truncated octahedron of the face-centered lattice are specified by symmetry (the square faces are completely specified). This means that it is not necessary to use these plane surfaces as zone boundaries, but any other (curved) surfaces which join the center point and the square faces could be employed as long as surfaces on opposite sides of the figure are parallel and the cubic symmetry is maintained. Actually, of course, the Brillouin construction is the simplest to use in this particular case, but this is not always true, particularly in crystals of low symmetry. (The second zone in the hexagonal lattice in such a case.)

2. The construction of solid state wave functions

The plan which we shall use in specifying solid state wave functions will be essentially that employed heretofore in other cases[10] with the addition of the concepts discussed in Section 1. We shall assume that the potential field within the lattice is spherically symmetric about each atom and use such a field within the polyhedron surrounding each atom which is determined by planes that cut the lines joining nearest neighbors orthogonally. In the case of LiF, we may choose these planes in a number of independent ways because the Li and F atoms are not symmetrically equivalent as in most of the simple monoatomic lattices. Nevertheless, we shall select them so as to bisect the lines joining neighbors, thus giving a system of space filling cubes which are of equal size and surround each atom. The reason for this choice lies in the fact that closed shell electrons of the Li ion[11] just fit into such a cube without extending outside appreciably, while a smaller cell about these atoms would not be able to contain all of this charge distribution. On the other hand, it seems reasonable to use as large a region for the F atom since the fluorine field is very strong near the nucleus, so that the use of cubes seems to be a reasonable choice. Similar comments cover the LiH case.

[10] E. Wigner and F. Seitz, Phys. Rev. **43**, 804 (1933); **46**, 509 (1934); J. C. Slater, Phys. Rev. **45**, 794 (1934), etc.
[11] Hargreaves, Proc. Camb. Phil. Soc. **25**, 75 (1928).

Within these cubes, we shall assume that the eigenfunctions may be expanded into a series of surface harmonics $\theta_m{}^l$ with radial-function coefficients $f_l(r)$ which satisfy the Schrödinger equation in which the spherically symmetric part of the field going with the polyhedron occurs. That is,

$$\psi_k{}^{(0)} = \sum_{l,\,m} a_{lm}{}^{(0)} f_l(r) \theta_m{}^l \tag{9}$$

within the polyhedron where the a s are constants. Not all surface harmonics will necessarily appear in this expansion, but only those which are compatible with the representation of the space group to which the function ψ_k belongs. To be more explicit, we shall discuss the LiF lattice. Suppose that we choose the origin of coordinates so that an F atom is situated there. We may then choose the phase of the wave function under discussion so that

$$\psi_k = \psi_{e(o)} + i\psi_{o(o)} \tag{10}$$

where $\psi_{e(o)}$ is a real even and $\psi_{o(o)}$ a real odd function relative to an inversion in the origin, t_o. If the k vector going with ψ belongs to a 48 rowed representation, there will be no limitation upon the surface harmonics which enter in (9) and ψ_e and ψ_o in (10) will contain all even and odd harmonics, respectively. If, however, the k goes with a representation of lower order, the harmonics which appear are restricted to the set belonging to a particular representation R (see Section 1) which sends the equivalent k's that differ by K vectors into one another. At the point $k=0$, for example, the only functions which appear in a given case must belong to the same representation of O^h. In other words, (9) must be of the form

$$\psi_k{}^{(0)} = \sum_l b_l{}^{(0)} f_l(r) A_j{}^l \tag{11}$$

where $A_j{}^l$ is a harmonic of order l going with a particular representation of R. If the phases are chosen in accordance with (10), the b's going with even l will be purely real numbers, and those going with odd l will be imaginary. We shall determine the b_l's which occur in (11) by the conditions, (a), that this ψ_k join on continuously with the similar function in each of the neighboring polyhedra and (b) that at points on opposite sides of the unit cell which are

separated by primitive translation distances τ_i $(i=1, 2, 3)$, the phase of ψ_k differs by $e^{ik\cdot\tau_i}$.

If the neighboring cell is centered about the atom at a point r_n, the corresponding function will not be an even function plus i times an odd one as long as (10) is taken as the basis for choice of phase referring to inversion ι_n at the point r_n, but will be a constant times this. We know, however, that

$$\iota_o = \iota_n - 2r_n \tag{12}$$

where $2r_n$ a translation of magnitude twice the distance r_n which is always an allowed translation, so that the form must be

$$\psi_k{}^{(n)} = e^{ik\cdot r_n}(\psi_{e(n)} + i\psi_{o(n)}) \tag{13}$$

where $\psi_{e(n)}$ and $\psi_{o(n)}$ are even and odd real functions relative to the inversion ι_n.

In a similar way, using equation of type (12), we may find the representation of the group R, operating about r_n, to which ψ_k must belong if it belongs to a given representation of the group R acting about the origin. We shall discuss practical examples of this later. Knowing this representation, we may determine the allowable harmonics which enter into the expansion in the polyhedron about r_n, so that we have

$$\psi_k{}^{(n)} = e^{ik\cdot r}\sum_l b_l{}^{(n)} f_l A_j \tag{14}$$

where the $b_l^{(n)}$ are purely real or purely imaginary depending upon whether l is even or odd.

Since all F atoms are equivalent; as are all Li atoms, the b's going with a given function will be the same for all F cells and for all Li cells, so that we need consider but two independent sets. Actually, we shall not consider an infinite number of these, but will only deal with a finite number going with the lowest order coefficients, using the conditions (a) and (b) discussed in a preceding paragraph of this section. This restriction to a finite number of terms rests, of course, upon practical limitations since we have not felt it feasible to solve determinants of higher than the eighth order. This procedure would be accurate only if independent methods of determining the coefficients led to essentially the same results. Actually, the error involved in the case of LiF is not negligibly small for the excited states.

In addition to using a small number of coefficients, we have introduced the "s sphere simplification" into the present paper. In this the fundamental polyhedron (a cube in our case) is replaced by a sphere of equal volume and the boundary conditions are satisfied at the surface of this rather than at the surface of the actual polyhedron. The approximation is not as good in this case as in that of the alkali metals, where its use could be rigorously justified, but the error it introduces is undoubtedly smaller than others, such as that discussed in the last paragraph, so we shall not hesitate to use it in this semi-quantitative investigation. In later work with LiH, in which we intend to strive for quantitative accuracy, we shall avoid its use and obtain a comparison with the present results.

We shall now proceed with a discussion of the determination of the boundary equation.

3. Boundary equations

No fixed rules regarding the points at which boundary conditions were satisfied were made. Generally speaking, points situated at prominent symmetry positions were used, except in cases in which these did not lead to a satisfactory specification (i.e., the secular equation vanished identically or leads to too simple an equation). Such cases indicate that the series (9) do not converge rapidly at these points so that new points were used. The equations derived in the following paragraphs cover k values in the three prominent symmetry directions, namely the (100), (111) and (110) directions, which will be discussed separately. Only two or three points on each of the energy surfaces going with these directions were determined and enough equations were obtained to discuss the filled and first empty band in LiF. Only one band is filled in LiH, so that all of the equations are not important for this case. We shall refer only to LiF in the discussion, but with the understanding that the results will be used for LiH as well.

I. $k=0$

For the case $k=0$, the basic symmetry requirement on the functions going with both of the polyhedra is that they belong to irreducible representations of the group[12] O^h. Since the lowest valence electron levels are s levels (considering the $(2s)^2$ $(2p)^5$ configuration on F and

[12] We are here employing Bethe's notation, Ann. d. Physik **3**, 133 (1929).

the 2*s* on Li and H), it is obvious that the lowest lattice function will be determined by Γ_1. The next will be Γ_4 because this is the analog of the *p* representation of spherically symmetric fields. This representation is triply degenerate, whence we may expect three energy surfaces to come in contact at $k=0$ to give a band capable of holding six of the eight electrons going with each unit cell of LiF. The other two electrons in this case, and the only two for LiH, will occupy the low "Γ_1 band." As we shall show later, the third, unoccupied band, is also Γ_1 at $k=0$.

(a) Γ_1. The prominent spherical harmonics which belong to Γ_1 are the *s* and *g* functions

$$1, \quad x^2y^2+y^2z^2+z^2x^2-(1/3)(x^4+y^4+z^4),$$

respectively. The angular functions which enter into both the Li and F expansions are the same in this case because $e^{ik\cdot\tau}=1$ for all τ's. It turns out that the use of the *s* sphere approximation excludes the appearance of the *g* function if prominent points are employed. The equations *s* functions must satisfy are

$$F(s)=L(s), \quad F'(s)=-L'(s) \tag{15}$$

where $F(s)$, $L(s)$ are the values of the radial *s* functions for F and Li at the boundary of the *s* sphere. The compatibility equation for (15) is

$$\frac{F'(s)}{F(s)}=-\frac{L'(s)}{L(s)}. \tag{15a}$$

(b) Γ_4. For Γ_4 the most important spherical harmonics are the *p* and *f* functions

$$p: \quad x, \; y, \; z$$

$$f: \quad x\left(x^2-\frac{3}{2}(y^2+z^2)\right), \quad y\left(y^2-\frac{3}{2}(z^2+x^2)\right), \quad z\left(z^2-\frac{3}{2}(x^2+y^2)\right)$$

of which we may select *x* and $x\left(x^2-\frac{3}{2}(y^2+z^2)\right)$ as belonging to the same row of equivalent representations. The boundary conditions were satisfied at the points (100) and (−100) for neighboring Li and F atoms, and for neighboring F atoms in the (110) direction at the points $(1/\sqrt{2},\ 0,\ 1/\sqrt{2})$ and $(-1/\sqrt{2},\ 0,\ 1/\sqrt{2})$. In addition, the derivative in the *x* direction was made continuous at the points (001) and (00−1) for neighboring Li and F atoms in the (001) direction. The equations are

$$\begin{aligned} F(p)+F(f)&=-L(p)-L(f)\\ F'(p)+F'(f)&=L'(p)+L'(f)\\ -F(p)+\frac{1}{2}F(f)&=0\\ F(p)-\frac{3}{2}F(f)&=L(p)-\frac{3}{3}L(f) \end{aligned} \tag{16}$$

in the order mentioned above. The compatibility equation is

$$\frac{5}{2}\frac{F'(p)}{F(p)}+5\frac{F'(f)}{F(f)}+\frac{13}{2}\frac{L'(p)}{L(p)}+\frac{L'(f)}{L(f)}=0. \tag{16a}$$

II. Limiting point of (100) direction

The group *R* (see Section 1) going with the point $(k)=1/2a$ at the boundary of the zone in the (100) direction is D_4^h which has five even and five odd representations. The character system of the classes of rotations of determinant 1 is as follows.

	E	C_2	C_4	C_2'	C_2''
Γ_1	1	1	1	1	1
Γ_2	1	1	1	−1	−1
Γ_3	1	1	−1	1	−1
Γ_4	1	1	−1	−1	1
Γ_5	2	−2	0	0	0

where

E is the unit element
C_2 is the twofold rotation about the *x* axis
C_4 is the fourfold rotation about the *x* axis
C_2' and C_2'' are twofold axes at right angles to these.

It is readily seen that the representation about the Li and F atoms will be identical by considering nearest neighbors in the *x* direction. The rotation about the *x* axis leaves both centers fixed, while the reflection planes ρ_F and ρ_{Li} and the twofold rotations δ_F and δ_{Li} satisfy the relation

$$\rho_F=\rho_{Li}+\tau, \quad \delta_F=\delta_{Li}+\tau,$$

where τ is the primitive translation in the *x* direction of magnitude $2a$, for which

$$K\cdot\tau=2\pi.$$

Since there is no possibility that the widely separated lower bands of the halides will cross one another, it seems natural to expect that the lowest will have a point going with the unit representation (Γ_1) at this limit point. Similarly, it seems natural to expect the second band to split into Γ_2 and the doubly degenerate Γ_3, because Γ_4 of O^h contains these two. We shall consider each of these cases.

(a) Γ_1. The simplest functions belonging to Γ_1 are

$$s: 1, \quad d: (y^2+z^2-2x^2)$$
$$g: x^2y^2+y^2z^2+z^2x^2-\tfrac{1}{3}(x^4+y^4+z^4).$$

Boundary conditions were satisfied between Li and F polyhedra neighboring in the x direction at the points (100) and (−100) and between neighboring cells in the y and z directions at (010), (0−10) and (001), (00−1), respectively. Only the s and d functions are needed for this and the resulting equations are

$$\begin{aligned} F(s)-2F(d)&=-L(s)-2L(d),\\ F'(s)-2F'(d)&=L'(s)-2L'(d),\\ F(s)+F(d)&=L(s)+L(d),\\ F'(s)+F'(d)&=L'(s)-L'(d). \end{aligned} \tag{17}$$

The secular equation reduces to

$$9\left(\frac{F'(s)}{F(s)}\frac{F'(d)}{F(d)}+\frac{L'(s)}{L(s)}\frac{L'(d)}{L(d)}\right)+8\left(\frac{F'(s)}{F(s)}\frac{L'(s)}{L(s)}+\frac{F'(d)}{F(d)}\frac{L'(d)}{L(d)}\right)+\left(\frac{F'(s)}{F(s)}\frac{L'(d)}{L(d)}+\frac{F'(d)}{F(d)}\frac{L'(s)}{L(s)}\right)=0. \tag{17a}$$

(b) Γ_2. Γ_2 is represented by

$$p: x, \quad f: x\left(x^2-\frac{3}{2}(y^2+z^2)\right).$$

The function and derivatives were taken to be continuous at the (100) and (−100) points for unlike neighbors in the x direction, and neighboring F functions were made continuous at $(1/\sqrt{2}\ 0\ 1/\sqrt{2})$ and $(-1/\sqrt{2}\ 0\ -1/\sqrt{2})$. In addition, the tangential gradients at (010) and (0−10) for unlike neighbors in the (010) direction were made equal. The resulting equations are

$$\begin{aligned} F(p)+F(f)&=L(p)+L(f),\\ F'(p)+F'(f)&=-L'(p)-L'(f),\\ F(p)-\frac{1}{4}F(f)&=0,\\ F(p)-\frac{3}{2}F(f)&=L(p)-\frac{3}{2}L(f). \end{aligned} \tag{18}$$

The secular equation is

$$\frac{5}{4}\frac{F'(f)}{F(f)}\frac{F'(p)}{(Fp)}+\frac{1}{4}\frac{F'(f)}{F(f)}\frac{L'(p)}{L(p)}+\frac{F'(p)}{F(p)}\frac{L'(f)}{L(f)}=0. \tag{18a}$$

(c) Γ_3. For the doubly degenerate state Γ_3, we took

$$p: z, \quad f: z\left(z^2-\frac{3}{2}(x^2+y^2)\right)$$

and joined these, with continuous slope and derivative, to unlike neighbors in the z direction at the center of the square faces. In addition, the tangential gradient at the centers of the other faces were made continuous with those of the other unlike neighbors. These equations are

$$\begin{aligned} F(p)+F(f)&=L(p)+L(f),\\ F'(p)+F'(f)&=L'(p)+L'(f),\\ F(p)-\frac{3}{2}F(f)&=L(p)-\frac{3}{2}L(f),\\ F(p)-\frac{3}{2}F(f)&=-L(p)+\frac{3}{2}L(f) \end{aligned} \tag{19}$$

$$\text{or}\quad \frac{3}{2}\frac{F'(p)}{F(p)}+\frac{F'(f)}{F(f)}=-\left(\frac{3}{2}\frac{L'(p)}{L(p)}+\frac{L'(f)}{L(f)}\right). \tag{19a}$$

III. Midpoint of (100) direction

The group R associated with the point

$$k=\begin{pmatrix}114a\\0\\0\end{pmatrix}$$

midway from the origin to the boundary of the

zone in the (100) direction is amply C_4^v which is generated by a fourfold axis in the x direction and a plane passing through this. There are five representations for which the character system is

	E	C_2	C_4	R_v	R_v'
Γ_1	1	1	1	1	1
Γ_2	1	1	−1	−1	1
Γ_3	2	−2	0	0	0
Γ_4	1	1	1	−1	−1
Γ_5	1	1	−1	1	−1

R_v and R_v' stand for the two classes of reflecting planes which pass through the x axis. The representation will be the same for both atoms in a given case since the line joining nearest neighbors is either parallel to the symmetry axis or perpendicular to it.

Just as in the preceding case, we may conclude safely that the function associated with the lowest energy surface goes with Γ_1. The representation Γ_4 of O^h contains both this and Γ_3, which is doubly degenerate, so that it may be expected that the former will go with the same surface as Γ_2 of D_4^h and the latter will go with the same two surfaces corresponding to Γ_5 of this group. In other words, two of the three energy surfaces of the second band remain in contact along the entire (100) axis.

(a) Γ_1. Functions which belong to Γ_1 are

$$s: 1, \quad p: x, \quad d: 2x^2-(y^2+z^2),$$
$$f: x\left(x^2-\frac{3}{2}(y^2+z^2)\right)$$

and all of these were used for either one state or the other. The boundary conditions employed were:

(A) Lowest band, using s, p, d functions

(1) Continuity of functions and derivative at the center of the square face joining neighboring unlike atoms in the x direction. The equations obtained from this are

$$\begin{aligned} F(s)+2F(d)-iF(p) &= -i[L(s)+2L(d)+iL(p)], \\ F'(s)+2F'(d)-iF'(p) &= i[L'(s)+2L'(d)+iL'(p)]. \end{aligned} \tag{20}$$

(2) Continuity of function and derivative at center of square face between nearest neighbors in the y (and z) directions

$$\begin{aligned} F(s)-F(d) &= L(s)-L(d), \\ F'(s)-F'(d) &= -L'(s)+L'(d). \end{aligned} \tag{20a}$$

The secular equation associated with these equations may be reduced to

$$\begin{vmatrix} \dfrac{F'(s)}{F(s)}+\dfrac{L'(p)}{L(p)} & 2\left(\dfrac{F'(d)}{F(d)}+\dfrac{L'(p)}{L(p)}\right) & 0 \\ \dfrac{L'(s)}{L(s)}+\dfrac{F'(p)}{F(p)} & 2\left(\dfrac{L'(d)}{L(d)}+\dfrac{F'(p)}{F(p)}\right) & 3\left(\dfrac{F'(p)}{F(p)}+\dfrac{L'(s)}{L(s)}+\dfrac{2L'(d)}{L(d)}\right) \\ \dfrac{F'(s)}{F(s)}+\dfrac{L'(s)}{L(s)} & -\left(\dfrac{F'(d)}{F(d)}+\dfrac{L'(d)}{L(d)}\right) & \dfrac{L'(s)}{L(s)}-\dfrac{L'(d)}{L(d)} \end{vmatrix} = 0$$

(B) Second Band, using s, p and f functions

(1) Continuity at same point as in (1) of A:

$$\begin{aligned} F(s)-i[F(p)+F(f)] &= -i\{L(s)+i[L(p)+L(f)]\} \\ F'(s)-i[F'(p)+F'(f)] &= i\{L'(s)+i[L'(p)+L'(f)]\}. \end{aligned} \tag{21}$$

(2) Continuity of the tangential gradient at the point mentioned in (2) of A:

$$F(p)-\frac{3}{2}F(f) = L(p)-\frac{3}{2}L(f). \tag{21a}$$

(3) Continuity of the function at the point $(0\ 1/\sqrt{2}\ 1/\sqrt{2})$ and $(0\ -1/\sqrt{2}\ -1/\sqrt{2})$ for nearest like

neighbors in the (011) direction.

$$\begin{vmatrix} \frac{F'(s)}{F(s)}+\frac{L'(p)}{L(p)} & -\frac{3}{2}\left(\frac{F'(s)}{F(s)}+\frac{L'(p)}{L(p)}\right) & \frac{5}{2}\frac{F'(s)}{F(s)}+\frac{3}{2}\frac{L'(p)}{L(p)}+\frac{L'(f)}{L(f)} \\ \frac{F'(p)}{F(p)}+\frac{L'(s)}{L(s)} & \frac{F'(f)}{F(f)}+\frac{L'(s)}{L(s)} & 0 \\ 1-\frac{1}{\sqrt{2}} & \frac{1}{4\sqrt{2}}-\frac{3}{2} & \frac{5}{2} \end{vmatrix}=0 \tag{21b}$$

(b) Γ_3. Three functions belonging to Γ_3 are

$$p: y; \quad d: xy; \quad f: y\left(y^2-\frac{3}{2}(z^2+x^2)\right).$$

The conditions a linear combination of these was made to satisfy were

(1) Continuity, with unlike neighbors in x direction at the point $(1/\sqrt{2}\ 1/\sqrt{2}\ 0)$:

$$\frac{i}{\sqrt{2}}F(p)+\frac{1}{2}F(d)-\frac{i}{4\sqrt{2}}F(f)=\left(\frac{i}{\sqrt{2}}L(p)-\frac{1}{2}L(d)-\frac{i}{4\sqrt{2}}L(f)\right). \tag{22}$$

(2) Continuity of the gradient in the x and y directions at the same points

$$\begin{aligned} &\frac{1}{\sqrt{2}}\left(i\frac{F'(p)}{\sqrt{2}}+\frac{F'(d)}{2}-i\frac{F'(f)}{4\sqrt{2}}\right)-i\frac{F(p)}{2}-\frac{9}{8}iF(f) \\ &\qquad=-\frac{i}{\sqrt{2}}\left(i\frac{L'(p)}{\sqrt{2}}-\frac{L'(d)}{2}-i\frac{L'(f)}{4\sqrt{2}}\right)+i\left(i\frac{L(p)}{2}+\frac{L(d)}{\sqrt{2}}-\frac{3}{8}iLf\right), \\ &\frac{1}{\sqrt{2}}\left(i\frac{F'(p)}{\sqrt{2}}+\frac{F'(d)}{2}-i\frac{F'(f)}{4\sqrt{2}}\right)+i\frac{F(p)}{2}+\frac{9}{8}iF(f) \\ &\qquad=\frac{i}{\sqrt{2}}\left(i\frac{L'(p)}{\sqrt{2}}-\frac{L'(d)}{2}-i\frac{L'(f)}{4\sqrt{2}}\right)+i\left(i\frac{L(p)}{2}+\frac{L(d)}{\sqrt{2}}-\frac{3L(f)}{8}\right). \end{aligned} \tag{22a}$$

IV. Endpoint of (111) direction

The group R going with

$$k=\frac{2\pi}{4a}\begin{pmatrix}1\\1\\1\end{pmatrix}$$

at the endpoint of the (111) axis is D_{ι}^{3}, and the irreducible representations have the character system

	E	C_3	C_2
Γ_1	1	1	1
Γ_2	1	1	−1
Γ_3	2	−1	0

C_3 and C_2 correspond to the classes of threefold rotations about the (111) axis and twofold rotations at right angles to this respectively. Since the inversion is present, it is implied that the three classes of operators of determinant −1 have either an even or an odd character system.

If we consider two neighboring unlike atoms in the x direction, say an F at the origin and a Li at $-a$, the phase of the latter, relative to the former, is $-i$. A simple computation shows the following correction between the representations of the classes E, C_3, C_2 and I (inversion) for the two atoms.

$$E_L = E_F, \quad C_{3L} = C_{3F}, \quad C_{2L} = -C_{2F}, \quad I_L = -I_F$$

where the subscript indicates the atom involved. In other words, if the representation going with the F polyhedron is Γ_1, even, that about Li will be Γ_2 odd; if that about F is Γ_3 even, that about Li will be Γ_3 odd; etc.

It seems reasonable to expect the lowest state to be Γ_1 even for F and Γ_2 odd for Li (and similarly for H and Li in LiH) since the F plays the most important role in the states of the lowest band. Γ_4 of O^h breaks into Γ_2 and Γ_3, the latter being doubly degenerate, and we have drawn the conclusion that the two (111) endpoints in the second band are:

$$\text{F}: \Gamma_2 \text{ odd}, \quad \text{Li}: \Gamma_1 \text{ even},$$

$$\text{F}: \Gamma_3 \text{ odd}, \quad \text{Li}: \Gamma_3 \text{ even}.$$

(a) F: Γ_1 even, Li: Γ_2 odd.

The Γ_1 even functions used were

$$s: 1; \quad d: xy+yz+zx$$

$$g: x^2y^2+y^2z^2+z^2x^2-\tfrac{1}{3}(x^4+y^4+z^4)$$

while the Γ_2 odd were

$$p: x+y+z,$$

$$f_1: x\left(x^2-\frac{3}{2}(y^2+z^2)\right)+y\left(y^2-\frac{3}{2}(x^2+z^2)\right)+z\left(z^2-\frac{3}{2}(x^2-y^2)\right),$$

$$f_2: xyz.$$

(1) The continuity condition at the point (100) and (-100) between neighbors in the x direction give

$$F(s)-\tfrac{1}{3}F(g)=L(p)+L(f_1), \quad F'(s)-\tfrac{1}{3}F'(g)=-L'(p)-L'(f_1). \tag{23}$$

(2) Continuity of the y (and z) gradient for the point considered in (1) yields

$$-F(d)=L(p)-\frac{3}{2}L(f_1). \tag{23a}$$

(3) Continuity between the same neighbors at the points $(-1/\sqrt{3}\ 1/\sqrt{3}\ 1/\sqrt{3})$ and $(1/\sqrt{3}\ 1/\sqrt{3}\ 1/\sqrt{3})$:

$$F(s)+F(d)+\frac{2}{9}F(g)=-\frac{1}{\sqrt{3}}\left(L(p)-\frac{2}{3}L(f_1)-\frac{1}{3}L(f_2)\right). \tag{23b}$$

(4) Continuity of the x and y gradient at the same point.

$$\begin{aligned}
\frac{1}{\sqrt{3}}\left(F'(s)+F'(d)+\frac{2}{9}F'(g)\right)&=\frac{1}{\sqrt{3}}\left(\frac{1}{\sqrt{3}}L'(p)-\frac{2}{3\sqrt{3}}L'(f_1)-\frac{1}{3\sqrt{3}}L'(f_2)\right)-\left(\frac{4}{3\sqrt{3}}L(p)-\frac{4}{3\sqrt{3}}L(f_1)\right),\\
\frac{1}{\sqrt{3}}\left(F'(s)+F'(d)+\frac{2}{9}F'(g)\right)&=\frac{1}{\sqrt{3}}\left(\frac{1}{\sqrt{3}}L'(p)-\frac{2}{3\sqrt{3}}L'(f_1)-\frac{1}{3\sqrt{3}}L'(f_1)\right)-\left(\frac{2}{3\sqrt{3}}L(p)-\frac{2}{3\sqrt{3}}L(f_1)\right).
\end{aligned} \tag{23c}$$

The resulting determinant may be reduced to

$$\begin{vmatrix} \frac{F'(s)}{F(s)}+\frac{L'(f)}{L(f)} & \frac{1}{3}\left[\frac{F'(g)}{F(g)}+\frac{L'(f)}{L(f)}\right] & \frac{L'(f)}{L(f)}-\frac{L'(p)}{L(p)} \\ \frac{2L'(f)}{L(f)}-\frac{1}{3} & \frac{5}{18}\frac{L'(f)}{L(f)}+\frac{1}{9} & \frac{5}{2}\frac{L'(f)}{L(f)}-\frac{2}{3}+\frac{1}{\sqrt{3}}\frac{L'(p)}{L(p)}-\frac{L'(f)}{L(f)} \\ \frac{2F'(s)}{F(s)}+\frac{3F'(d)}{F(d)}-2 & \frac{4}{9}\frac{F'(g)}{F(g)}+2-\frac{F'(d)}{F(d)} & \frac{5F'(d)}{F(d)}-4 \end{vmatrix}. \tag{23d}$$

(b) F: Γ_2 odd; Li: Γ_1 even.

The equations corresponding to this case may be derived from (a) by interchanging F and Li.

(c) F: Γ_3 odd; Li: Γ_3 even.

In this case the odd functions selected were

$$p: x+y-2z,$$
$$f_1: x\left(x^2-\frac{3}{2}(y^2+z^2)\right)+y\left(y^2-\frac{3}{2}(x^2+z^2)\right)-2z\left(z^2-\frac{3}{2}(x^2+y^2)\right)$$

and the only even function was

$$d: x^2+y^2-2z^2.$$

(1) Continuity at (100) and (-100) for nearest neighbors in x direction

$$F(p)+F(f)=L(d), \quad F'(p)+F'(f)=L'(d). \tag{24}$$

(2) Continuity of z gradient at same point

$$-2F(p)+3F(f)=0. \tag{24a}$$

The secular equation yields

$$\frac{F'(p)}{F(p)}+\frac{5}{3}\frac{L'(d)}{L(d)}+\frac{2}{3}\frac{F'(f)}{F(f)}=0. \tag{24b}$$

V. (110) endpoint

The group R going with

$$k=\frac{3\pi}{4a}\begin{pmatrix}1\\1\\0\end{pmatrix}$$

is C_2^v which has the character system

	E	C_2	C_v	C_v^1
Γ_1	1	1	1	1
Γ_2	1	1	−1	−1
Γ_3	1	−1	−1	1
Γ_4	1	−1	1	−1

where C_v and C_v^1 represent the two reflecting planes which pass through the (110) axis.

If we consider two neighbors in the x direction, the relative phases of Li and F, assuming the latter to be at the origin and the former at $-a$, is $e^{-i(3\pi/4)}$. The representatives of the group are the same for both polyhedra.

We may expect Γ_1 to go with the lowest surface again, while Γ_1, Γ_3, and Γ_4 go with the next band which is not degenerate at this point.

(a) Γ_1. The functions of type Γ_1 that were used are

$$s: 1, \quad p: x+y; \quad f: x^3+y^3-\frac{3}{2}(x+y)(xy+z^2).$$

(1) Continuity at (100) between nearest x neighbors

$$\begin{aligned} F(s)+i(F(p)+F(f)) &= e^{i(3\pi/4)}[L(s)-i(L(p)+L(f))], \\ F'(s)+i(F'(p)+F'(f)) &= -e^{i(3\pi/4)}[L'(s)-i(L'(p)+L'(f))]. \end{aligned} \tag{25}$$

(2) Continuity of y gradient at same point

$$F(p)-\frac{3}{2}F(f)=e^{i(3\pi/4)}\left(L(p)-\frac{3}{2}L(f)\right). \tag{25a}$$

These will furnish a point in both the first and the second band.

(b) Γ_3. The functions used in treating Γ_3 are

$$p: z, \quad d: z(x+y), \quad f: z\left(z^2-\frac{3}{2}(x^2+y^2)\right).$$

(1) Continuity at (001) and (00−1) for neighbors in z direction

$$F(p)+F(f_1)=-(L(p)+L(f)), \quad F'(p)+F'(f)=L'(p)+L'(f). \tag{26}$$

(2) Continuity of z gradient at (100) and (−100) for neighbors in x direction

$$\left[i\left(F(p)-\frac{3}{2}F(f)\right)-F(d)\right]=-\frac{1}{\sqrt{2}}(1+i)\left[i\left(L(p)-\frac{3}{2}L(f)\right)+L(d)\right]. \tag{26a}$$

(3) Continuity of neighbors in x direction at $(1/\sqrt{2}\ 0\ 1/\sqrt{2})$ and $(-1/\sqrt{2}\ 0\ 1/\sqrt{2})$.

$$\frac{1}{\sqrt{2}}i\left[F(p)-\frac{1}{4}F(f)\right]-\frac{1}{2}F(d)=-\frac{1}{\sqrt{2}}(1+i)\left[\frac{i}{\sqrt{2}}\left(L(p)-\frac{L(f)}{4}\right)+\frac{1}{2}L(d)\right]. \tag{26b}$$

(c) Γ_4. Functions employed:

$$p: (x-y), \quad d: z(x-y), \quad f_1: (x^3-y^3)-\frac{3}{2}(xy(x-y)+z^2(x-y), \quad f_2: x(y^2-z^2)-y(x^2-z^2).$$

(1) Continuity at $(1/\sqrt{2}\ 0\ 1/\sqrt{2})$ and $(-1/\sqrt{2}\ 0\ 1/\sqrt{2})$ for neighbors in x direction:

$$\left[i\left(\frac{F(p)}{\sqrt{2}}-\frac{1}{4\sqrt{2}}F(f_1)-\frac{1}{2\sqrt{2}}F(f_2)\right)+\frac{1}{2}F(d)\right]=-e^{3\pi i/4}\left[i\left(\frac{1}{\sqrt{2}}L(p)-\frac{1}{4\sqrt{2}}L(f_1)=\frac{1}{2\sqrt{2}}L(f_2)\right)+\frac{1}{2}L(d)\right]. \tag{27}$$

(2) Continuity of x, y and z gradients at same point

$$\begin{aligned} &\frac{1}{\sqrt{2}}\left[i\left(\frac{F'(p)}{\sqrt{2}}-\frac{1}{4\sqrt{2}}F'(f_1)-\frac{1}{2\sqrt{2}}F'(f_2)\right)+\frac{F'(d)}{2}\right]+\frac{1}{2}\left[i\left(\frac{F'(p)}{\sqrt{2}}+\frac{9}{4\sqrt{2}}F(f_1)+\frac{1}{2\sqrt{2}}F(f_2)\right)\right. \\ &\quad =e^{(3\pi/4)i}\left[\frac{1}{\sqrt{2}}\left\{i\left(-\frac{L'(p)}{\sqrt{2}}+\frac{1}{4\sqrt{2}}L'(f_1)+\frac{1}{2\sqrt{2}}L'(f_2)\right)-\frac{L'(d)}{2}\right\}\right. \\ &\qquad \left.\left.+\frac{1}{2}\left\{i\left(\frac{L(p)}{\sqrt{2}}+\frac{9}{4\sqrt{2}}L(f_1)+\frac{1}{2\sqrt{2}}L(f_2)\right)\right\}\right], \end{aligned} \tag{27a}$$

$$i\frac{1}{\sqrt{2}}F(p)+\frac{1}{2}F(d)=e^{(3\pi/4)i}\left(i\frac{L(p)}{\sqrt{2}}+\frac{L(d)}{2}\right), \tag{27b}$$

$$\frac{1}{\sqrt{2}}\left[i\left(\frac{F'(p)}{\sqrt{2}}-\frac{1}{4\sqrt{2}}F'(f_1)-\frac{1}{2\sqrt{2}}F'(f_2)\right)+\frac{F'(d)}{2}\right]-\frac{1}{2}i\left(\frac{F(p)}{\sqrt{2}}-\frac{9}{4\sqrt{2}}F(f_1)+\frac{1}{2\sqrt{2}}F(f_2)\right)$$
$$=e^{(3\pi/4)i}\left[\frac{1}{\sqrt{2}}\left\{i\left(\frac{-L'(p)}{\sqrt{2}}+\frac{L'(f_1)}{4\sqrt{2}}+\frac{L'(f_2)}{2\sqrt{2}}\right)-\frac{L'(d)}{2}\right\}+\frac{1}{2}i\left(\frac{L(p)}{\sqrt{2}}+\frac{9}{4\sqrt{2}}L(f_1)+\frac{L(f_2)}{2\sqrt{2}}\right)\right]. \tag{28}$$

Part B. Application to LiF and LiH

4. The self-consistent field

In order to obtain the Hartree self-consistent field for the system of filled bands, it would be necessary to obtain the charge distribution arising from all electrons by summing $|\psi_k|^2$ over all bands at each step of the conventional Hartree procedure. Instead of doing this, we have taken the set of eight wave functions for $k=0$ going with the two filled bands of LiF, normalized each of these to 1 within the unit cell and used the spherically symmetric part of the sum of $|\psi_k|^2$ for these as the charge distribution within each of the polyhedra in terms of which the field is computed. In the case of LiH, the two states for $k=0$ going with the single filled band were used. This procedure seems entirely justifiable for the present purposes since the work on monovalent metals shows that the function going with $k=0$ always gives a good representation of the charge distribution and the same may be expected here.

Using this scheme, we have obtained a self-consistent charge distribution for the lattice, treating eight valence electrons in the case of LiF and two in that of LiH. We employed Hartree's potential for the $(1s)^2$ configuration of F^-,[13] the ion core field for Li^+ developed by one of us,[14] and, of course, the Coulomb field for H. We first selected what seemed to be a reasonable charge distribution for the valence electrons, basing our judgment upon the atomic wave functions, and then computed an effective potential for this distribution. This was added to the ion core field and the potential to obtain the potential field within each of the polyhedra arising from the enclosed charge. The spherically symmetric part of the Madelung potential from all of the external ions was added to the field within a given polyhedron in the cases in which the polyhedra were not electrostatically neutral, in order to obtain the total field. Using this and the results of Section 3, the wave functions going with $k=0$ were computed and a new charge distribution was obtained. This was then compared with the previously assumed one and a new choice of

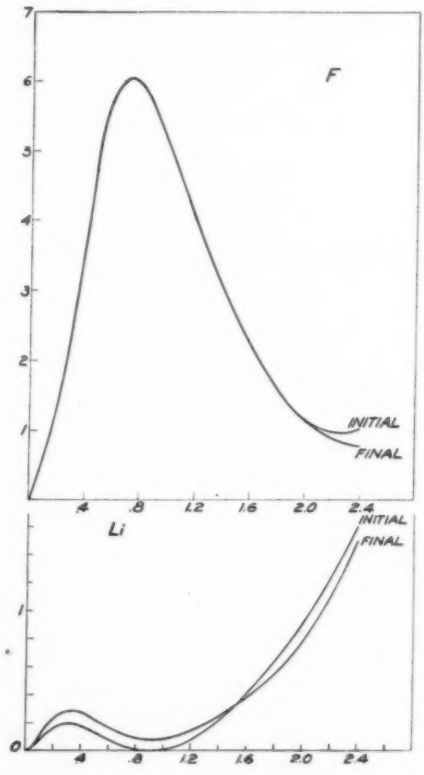

Fig. 1. The initial and final radial charge distributions for F and Li in LiF are plotted on a relative scale of ordinates. The abscissas are in Bohr units and the critical radius r_s of 2.4 corresponds to the radius of the s sphere that was used. These results are valid for the Hartree, not the final, approximation.

[13] D. Hartree, Proc. Roy, Soc. **A151**, 96 (1935).
[14] F. Seitz, Phys. Rev. **47**, 400 (1935).

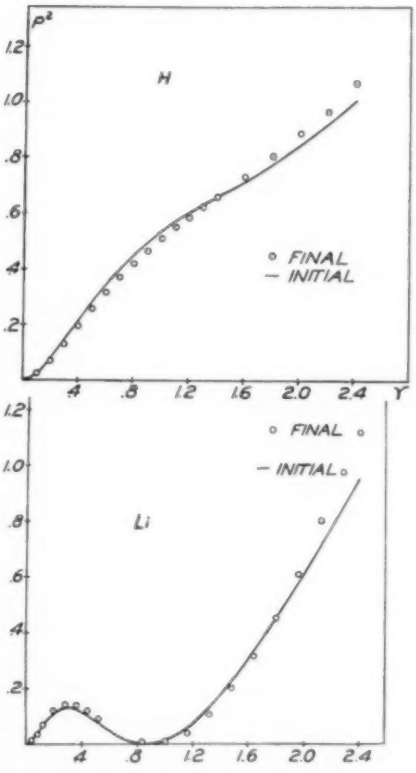

FIG. 2. Same as Fig. 2 for LiH.

starting field was made on the basis of the agreement.

The procedure is actually rather a tedious one to carry through, mainly because one may not use some simple mean between the initial and final charge distribution of one trial in order to obtain a good starting distribution for the next. This lack of stability arises from the fact that wave functions in neighboring cells do not affect one another only because of their potential interaction, but also because of the continuity conditions which they must satisy.

The charge distributions, from the "*s* sphere approximation" standpoint, which lead to a practically self-consistent solution are shown in Figs. 1 and 2 for LiF and LiH, respectively. In the first case, the initial distribution was taken to be of such a type that the Li and F spheres were electrostatically neutral, and the final distribution was such as to give the F sphere a charge of $-0.2e$ and the Li sphere the negative of this. Actually the self-consistent solution is much nearer the starting one, and were the normalization carried through in such a way that the total charge on the F sphere were $-0.05e$ and that on the Li $+0.05e$, the field would be self-consistent. We have used the starting field going with this case in the following because the neglect of exchange in the computations is greater than the error made in not using the exact Hartree self-consistent field. The case of LiH is much easier to handle because the situation is inherently simpler, and in this case the initial and final distributions form a self-consistent solution in which the H has an excess of 0.35 electron and the Li a deficit of the same amount.

The total potential in each of the spheres is shown in Fig. 3 for LiF. The way in which these have been joined at $r=2.4a_h$ is a consequence of the *s* sphere approximation and has no significance other than that it shows, roughly, how the potential varies in going from one ion to its nearest unlike neighbor.

The neglect of the Fock terms in the self-consistent equations is, without question, not quantitatively justifiable. Nevertheless, it may be made clear that these will not lead to a justification of the classical concepts by use of the following arguments.

In the first place, the classical picture would be valid only if there were a self-consistent solution of the Heitler-London type in which the

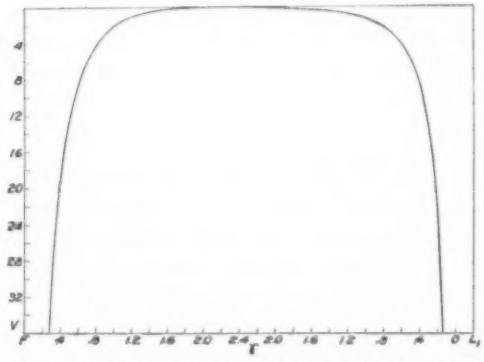

FIG. 3. The Hartree potential in LiF is schematically represented. The ordinates are in Rydberg units and the abscissas in Bohr radii. The junction at 2.4 is connected with the use of the spherical approximation so that the illustrated internuclear distance is not the observed one. Actually the (100) distance is less than this by a factor of 2/2.4.

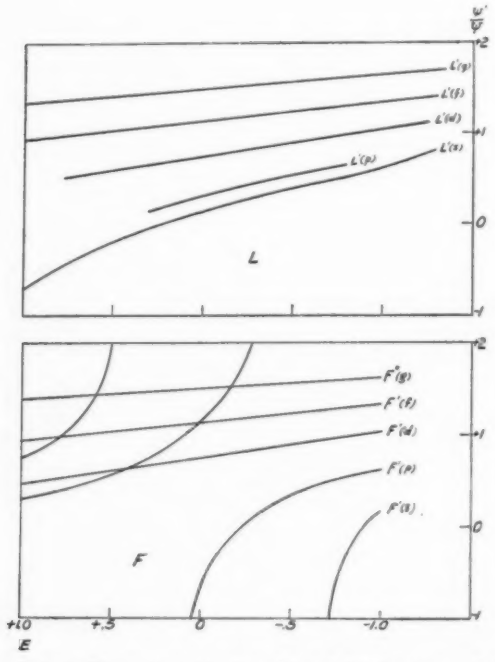

FIG. 4. The ratios x'/x (i.e., L′ and F′) for the radial functions of interest at the point $r_s = 2.4a_0$ are plotted as a function of the energy, in Rydberg units.

valence electron wave functions used are localized about the F (we shall use the case of LiF as an example), and have zero amplitude wherever the Li field is appreciable (e.g. within our Li sphere). This is clearly not possible since the F^- solution of Hartree has a charge of 0.9 outside of our s sphere. This charge is in the region of the Li fields and will distribute itself symmetrically about the Li nuclei. We may expect the charge distribution to be pulled toward the F atoms when one uses Fock's equations, but this will not lead to completely ionized Li since the Fock and Hartree fields for the Na^+ are very similar.[15] Correlation effects will change this by only a small amount if the case of He may be used as an example. We estimate that the negative charge excess of the F sphere, over a neutral value, will lie between 0.25 and 0.5 electron. In the case of LiH, exchange and correlation effects will not be nearly as important since there are fewer electrons, and an examination of the H^- solution of Bethe shows clearly that the Li atom cannot be completely ionized in this case either. That is, Heitler-London functions which are centered about H and have zero amplitude on the Li region will not form a self-consistent solution.

Since the Madelung-Born computations for both LiF and LiH agree very closely with the experimental values,[16] and the present work shows that the necessary conditions for the justification of the ionic crystal model are not met with, we are inclined to the belief that the agreement of the former is purely fortuitous and that a large part of the heat of sublimation of ionic crystals arises from the same source as the binding energies of metals and valence crystals. That is, the binding energies are not primarily connected with the fact that the Li ion is left in a region where no valence electrons reside; but is mainly dependent upon the fact that the electrons in a crystal may be at regions of favorable potential (the Li and F nuclei, etc.) in a correlated way. This does not mean that the electrostatic field of the Li ion does not play an extremely important role, but rather that the change in the electronic wave functions in going from the gaseous to the solid state plays at least as important a role. We hope to verify this aspect of the situation more completely by a quantitative computation on LiH, which is the most ideally suited substance. In order to do this, it is absolutely essential to take into account exchange and correlation effects since these are of the same order of magnitude as the heat of sublimation in this case, just as in that of metals.[17]

5. The distribution of energy bands

A. LiF

Using the equations of Section 3, we have determined the energy bands of both LiF and LiH with the field corresponding to the Hartree approximation. The ratios ψ'/ψ at $r_s = 2.4a_h$ as a function of energy for each of the important

[15] V. Fock and M. Petraschen, Physik. Zeits. Sowjetunion **6**, 368 (1934). See also Hartree, Proc. Roy. Soc. **A150**, 9 (1935) for case of Be.

[16] J. Sherman, Chem. Rev. **11**, 93 (1932).

[17] The Hartree solution for Cl^- (Proc. Roy. Soc. **A141**, 282 (1933)) shows that these remarks will be just as true for the alkali chlorine compounds as for the fluorides. About 1.5 electrons lie byeond the radius corresponding to half the minimum distance in NaCl, for example, and, as a result, overlap into the closed shell region of the Na ions.

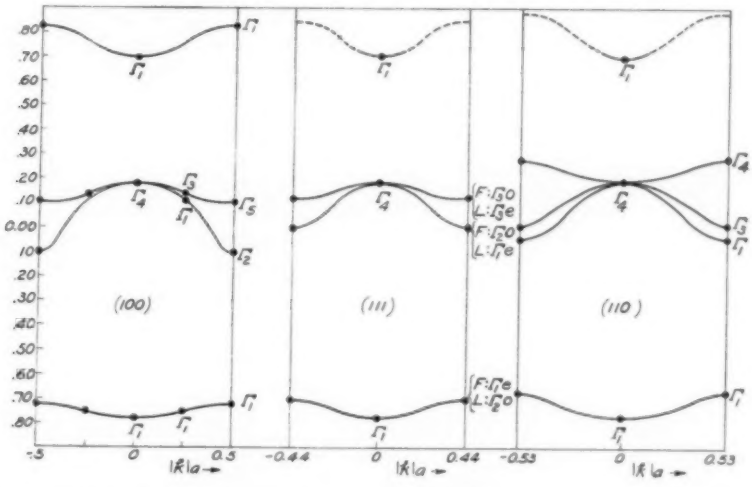

FIG. 5. $E(k)$ plots for three prominent crystallographic directions. The ordinates are Rydberg units. It is to be emphasized that these results are only approximate.

radial functions are shown in Fig. 4. This choice of the radius of the s sphere is valid in both LiF and LiH. It is to be emphasized that only the relative positions of the bands in a given solid have significance because of the neglection of exchange and correlation effects.

The energies going with the various wave functions are tabulated in Table I for LiF, and the probable positions of the bands are shown in Fig. 5. The wave functions for $k=0$ going with the first three bands are shown in Fig. 6. These have been joined at r_s instead of the actual midway point, in accordance with the s sphere approximation, but the general form is representative. The difference in energy between center points of the second (filled band) and the upper band correspond to the long wave-length limit of the absorption band of LiF and is found here to be about 1500A, as compared[18] with the observed value of about 1200. We would naturally expect to get too low a value for the energy difference since exchange effects are more important for electrons of the same type as those giving rise to the field than for others, as Bardeen[19] has shown, so that the lowest band will be pushed down more than the upper, unfilled band.

TABLE I. $E(k)$ *for particular points in LiF.*

Band	I	II	III	IV	V
$k=0$	−0.77	+0.18	0.18	0.18	0.7
(100) Limit	−0.73	0.10	0.10	−0.11	0.82
(100) Midpoint	−0.75	0.15	0.15	0.12	
(111) Limit	−0.76	0.12	0.12	0.03	
(110) Limit	−0.68	0.01	0.05	0.07	

[18] F. H. Melvin, Phys. Rev. **37**, 1230 (1931); E. G. Schneider, Phys. Rev. **49**, 341 (1936).

It is to be observed that the wave function going with the unfilled band is much more like that for a free electron than are the other functions.

B. LiH

The ψ'/ψ ratios for LiH are shown in Fig. 7 and the positions of the bands for the (100) direction of propagation is shown in Fig. 8. Only the lowest band is filled in this case, and the wave function going with $k=0$ is illustrated in Fig. 9. The energy difference of the end points of the first and second bands corresponds to an absorption wave-length of 1900A which is in agreement with the value of 1900A found by Bach and Bonhoeffer.[20] The accuracy of agreement is, of course, not particularly significant and, as a matter of fact, these workers observe

[19] J. Bardeen, Phys. Rev. **49**, 653 (1936).

[20] F. Bach and K. F. Bonhoeffer, Zeits. f. physik. Chemie **23**, 256 (1933). In connection with the remarks made in the text, it is worth emphasizing the fact that a stoichemical excess of one substance in a compound (or an impurity) will give rise to localized electronic states which lie between the bands. These will undoubtedly possess sharper absorption peaks than the band to band transitions do.

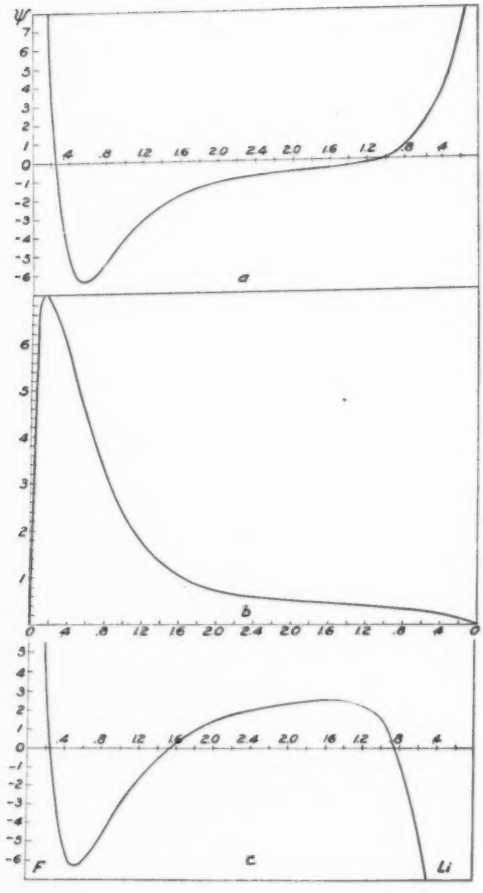

FIG. 6. Relative scale plots of the three prominent wave functions for $k=0$. a and b go with the first and second filled hand and c goes with the first unfilled one.

another absorption peak at 2500A. This is so narrow that it seems improbable that it is connected with a volume effect, but more likely that it is either a surface absorption of the same type met with in photoelectric effect, or is connected with the presence of an excess of Li. For this reason we feel inclined to make the present assignment. As we have stated above, we are in the process of extending this work on LiH in order to obtain more quantitative results.

6. Critique of viewpoint

In cases such as the present one in which F^- and Li^+ form closed shell configurations, it is always preferable to use Bloch type of eigenfunctions rather than a Heitler-London scheme in which the valence electrons are viewed as being centered about one type of atom (F), but to extend into the region of the other (Li), at least as long as aperiodic phenomena are not considered. This is true since one can always take an appropriate linear combination of the rows or columns of given spin in the total determinantal eigenfunction, if Heitler-London functions are used, in such a way as to obtain a new determinant in which the elements are of Bloch form. A suitable linear combination of atomic orbitals would be

$$\psi_k=\sum_\alpha e^{ik\cdot r_\alpha}\Big(\sum_i a_i\psi(r_{\alpha,\,i})\Big) \tag{29}$$

where ψ_k is the Bloch eigenfunction, $\psi(r_{\alpha,\,i})$ is the Heitler-London function for the electron centered about the ith atom of the αth unit cell, and the a's are constants. In the case of LiF, for example, the ψ's might appropriately be centered about the F atom, though they would extend into the Li region. Since the best Bloch function which would satisfy Fock's equation, would generally be different from (29) (except for the case of x-ray electrons in which case they would be the same), they would yield a better binding energy than the Heitler-London scheme would. For this reason the use of Bloch eigenfunctions is

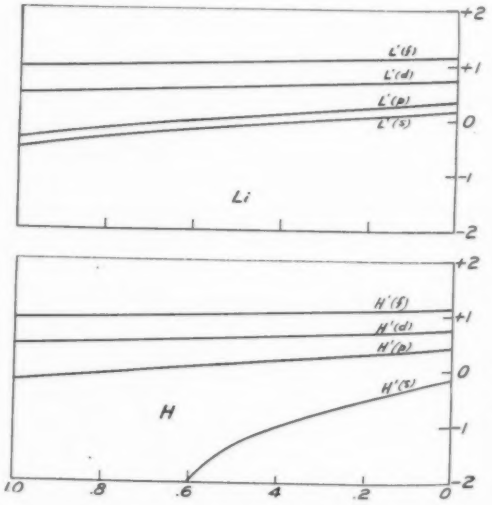

FIG. 7. Same as Fig. 4, but for LiH.

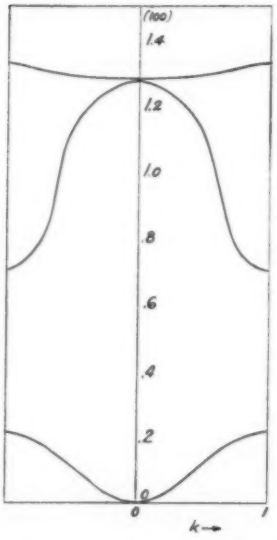

FIG. 8. Same as Fig. 5, but for LiH.

justifiable as long as it is implied that there are correlational modifications.[21]

One now approaches the question of whether one should use Heitler-London or Bloch eigenfunctions in the description of a situation in which one electron is in an excited state and the filled band is left with a dearth of one electron (as usual we shall refer to this as an anti-electron). In the case of both LiF and LiH it seems unquestionable that one should use the Bloch functions for the excited electron since these functions are essentially those of free electrons and differ markedly from the states of the filled band. Even in the case of the anti-electron, however, we believe that it is more appropriate to consider a Bloch rather than a Heitler-London eigenfunction to be absent, simply because the energy of these electrons is such that the electron may jump from one atom to the next with ease. That is, there is no question of a very small probability

[21] In a recent paper (Physik. Zeits. Sowjetunion **9**, 158 (1936)) Frenkel attempts a criticism of the use of the Bloch picture in such cases as the present one. We believe that this criticism is not justifiable to the extent this author presses it for the reasons mentioned here.

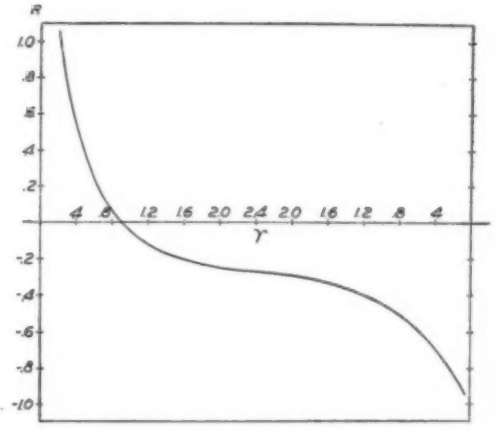

FIG. 9. Same as Fig. 6, but for LiH.

of leakage through a barrier as in the case of x-ray electrons, simply because the wave function has an appreciable amplitude at all points. It is probably true, however, that the anti-electron is conducted through the lattice at a much slower rate than the electron in the excited state.

On the other hand, there are unquestionably states in which the electron is strictly localized to a definite position such as those corresponding to the U centers in ionic crystals or to surface states. When an electron makes a transition from such a state to a free state, the anti-electron created may very well be localized in certain cases. For example, if the U center arises from an electron bound to an excess Li ion which is an open space in the lattice, the locality of this ion may remain positively charged when the electron is removed by light absorption, simply because the other electron present which will be in the upper filled band will not be able to extend over the open space sufficiently well to completely neutralize it. That is, one may regard the situation as if a Li ion were attached to the "surface" of a hole. We do not feel justified in entering into more speculations of this type in the present paper, though it is felt that the viewpoint emphasized here is capable of explaining most of the conduction properties of halide crystals, and intend to return to this on another occasion.

Quartet States in Diatomic Molecules Intermediate Between Cases *a* and *b*

W. H. BRANDT,* *Laboratory of The Cold Metal Process Company, Youngstown, Ohio*

(Received July 13, 1936)

The determinantal equation given by Hill and Van Vleck for the energies of diatomic molecules intermediate between Hund's cases *a* and *b* has been set up for quartet states and solved by a series method. The solutions are similar in form to those given by Budo for triplet states and the same methods of rotational analysis apply.

THE solutions for the doublet case of Eq. (20) of Hill and Van Vleck[1] are simple and satisfactory for rotational analysis. The triplet case does not yield simple closed formulas, but suitable series solutions have recently been given by Budo[2] and applied successfully to two $^3\Pi$ states of N_2. The purpose of this paper is to develop series solutions for quartet states.

The equation to be solved is

$$\omega^4-\{(10/4)\Lambda^2Y(Y-4)+(9/2)+10J(J+1)\}\omega^2+\{8\Lambda^2Y(Y-1)-4-16J(J+1)\}\omega$$
$$+(9/16)\Lambda^4Y^2(Y-4)^2+(9/2)\Lambda^2Y(Y-4)J(J+1)+9J^2(J+1)^2-(11/2)J(J+1)$$
$$-(13/2)\Lambda^2Y-(35/8)\Lambda^2Y^2-(15/16)=0, \quad (1)$$

where σ_k, j and λ of Hill and Van Vleck are replaced by Λ, J and Y and

$$\omega=[W+B\Lambda^2-B\{J(J+1)+5/4\}]/B. \quad (2)$$

If we make

$$y_1=\Lambda^2Y(Y-4)/4, \quad (3)$$

Eq. (1) becomes

$$\omega^4-\{10[y_1+J(J+1)]+9/2\}\omega^2+\{8\Lambda^2Y(Y-1)-4-16J(J+1)\}\omega+9[y_1+J(J+1)]^2$$
$$-(11/2)[y_1+J(J+1)]-3\Lambda^2Y^2-12\Lambda^2Y-15/16=0. \quad (4)$$

This is a fourth-order equation of the type,

$$x^4+bx^2+cx+d=0, \quad (5)$$

which has solutions,[3]

$$x=\{-b/2+\tfrac{1}{2}(b^2-4d)^{\frac{1}{2}}\}^{\frac{1}{2}}-c/2(b^2-4d)^{\frac{1}{2}}+\cdots\{-b/2-\tfrac{1}{2}(b^2-4d)^{\frac{1}{2}}\}^{\frac{1}{2}}+c/2(b^2-4d)^{\frac{1}{2}}+\cdots,$$
$$-\{-b/2-\tfrac{1}{2}(b^2-4d)^{\frac{1}{2}}\}^{\frac{1}{2}}+c/2(b^2-4d)^{\frac{1}{2}}+\cdots,\ -\{-b/2+\tfrac{1}{2}(b^2-4d)^{\frac{1}{2}}\}^{\frac{1}{2}}-c/2(b^2-4d)^{\frac{1}{2}}+\cdots. \quad (6)$$

Now $(b^2-4d)^{\frac{1}{2}}=\{64[y_1+J(J+1)]^2+112[y_1+J(J+1)]+49+12\Lambda^2Y^2+48\Lambda^2Y-25\}^{\frac{1}{2}}$

$$=8[y_1+J(J+1)]+7+\{(6\Lambda^2Y^2+24\Lambda^2Y-25/2)/(8[y_1+J(J+1)]+7)\},$$

* Now with the Research Laboratories of the Westinghouse Electric and Manufacturing Company, East Pittsburgh, Pennsylvania.

[1] Hill and Van Vleck, Phys. Rev. **32**, 261 (1928). See Eq. (20).

[2] Budo, Zeits. f. Physik **96**, 219 (1935).

[3] These solutions may be derived as follows:

Assume that in Eq. (5) $x=\sum_{i=0}^{\infty}x_iy^i$, $b=b_0+b_1y$, $c=c_0+c_1y$, $d=d_0+d_1y$. Substitute these values in Eq. (5) and set the sum of the coefficients of each y^i equal to 0 giving the infinite set of equations,

$$x_0^4+b_0x_0^2+c_0x_0+d_0=0$$
$$\{4x_0^3+2b_0x_0+c_0\}x_1+b_1x_0^2+c_1x_1+d_1=0.$$
$$\cdot \quad \cdot \quad \cdot \quad (I)$$

Set $y=1$ so that $b=b_0+b_1$, $c=c_0+c_1$ and $d=d_0+d_1$. Choose b_0, c_0 and d_0 so that the first of Eqs. (I) can be solved and use further Eqs. (I) to determine x_1, x_2 etc. Specifically make $b_0=b$, $b_1=0$, $c_0=0$, $c_1=c$, $d_0=d$ and $d_1=0$ which reduces the first of Eqs. (I) to a quadratic in x_0^2. The solutions given by Budo for the triplet case may be derived in a similar manner.

neglecting higher terms in the expansion. If we set[4]

$$\delta=\{6\Lambda^2Y^2+24\Lambda^2Y-25/2\}/\{8[y_1+J(J+1)]+7\},$$

$$(b^2-4d)^{\frac{1}{2}}=8[y_1+J(J+1)]+7+\delta.$$

Solutions (6) become,

$$\begin{aligned}
\omega_4&=\left\{9[y_1+J(J+1)]+\frac{23}{4}+\frac{\delta}{2}\right\}^{\frac{1}{2}}-\frac{\Lambda^2Y(Y-1)-\frac{1}{2}-2J(J+1)}{2y_1+7/4+\delta/4+2J(J+1)}+\cdots,\\
\omega_3&=\left\{y_1+J(J+1)-\frac{5}{4}-\frac{\delta}{2}\right\}^{\frac{1}{2}}+\frac{\Lambda^2Y(Y-1)-\frac{1}{2}-2J(J+1)}{2y_1+7/4+\delta/4+2J(J+1)}+\cdots,\\
\omega_2&=-\left\{y_1+J(J+1)-\frac{5}{4}-\frac{\delta}{2}\right\}^{\frac{1}{2}}+\frac{\Lambda^2Y(Y-1)-\frac{1}{2}-2J(J+1)}{2y_1+7/4+\delta/4+2J(J+1)}+\cdots,\\
\omega_1&=-\left\{9[y_1+J(J+1)]+\frac{23}{4}+\frac{\delta}{2}\right\}^{\frac{1}{2}}-\frac{\Lambda^2Y(Y-1)-\frac{1}{2}-2J(J+1)}{2y_1+7/4+\delta/4+2J(J+1)}+\cdots.
\end{aligned}\tag{7}$$

Neglecting the constant, $-B\Lambda^2+B5/4$, in the energy and terms beyond the second in ω,

$$\begin{aligned}
W=F_4(J)&=B\left[J(J+1)+\{9y_1+9J(J+1)+23/4+\delta/2\}^{\frac{1}{2}}-\frac{\Lambda^2Y(Y-1)-\frac{1}{2}-2J(J+1)}{2y_1+7/4+\delta/4+2J(J+1)}\right],\\
F_3(J)&=B\left[J(J+1)+\{y_1+J(J+1)-5/4-\delta/2\}^{\frac{1}{2}}+\frac{\Lambda^2Y(Y-1)-\frac{1}{2}-2J(J+1)}{2y_1+7/4+\delta/4+2J(J+1)}\right],\\
F_2(J)&=B\left[J(J+1)-\{y_1+J(J+1)-5/4-\delta/2\}^{\frac{1}{2}}+\frac{\Lambda^2Y(Y-1)-\frac{1}{2}-2J(J+1)}{2y_1+7/4+\delta/4+2J(J+1)}\right],\\
F_1(J)&=B\left[J(J+1)-\{9y_1+9J(J+1)+23/4+\delta/2\}^{\frac{1}{2}}-\frac{\Lambda^2Y(Y-1)-\frac{1}{2}-2J(J+1)}{2y_1+7/4+\delta/4+2J(J+1)}\right].
\end{aligned}\tag{8}$$

When J becomes large the solutions approach the values, $B(J^2+4J+10/4)$, $B(J^2+2J-2/4)$, $B(J^2-6/4)$ and $B(J^2-2J-2/4)$, i.e., if we add the term $+(5/4)B$ which was dropped from the energies, they approach the values, $BK(K+1)$, where $K=(J+3/2)$, $(J+\frac{1}{2})$, $(J-\frac{1}{2})$ and $(J-3/2)$, respectively.

The second differences are

$$\begin{aligned}
\Delta_2F_4(J)&=4B(J+\tfrac{1}{2})\left[1+9/2\{9y_1+23/4+\delta/2+9J(J+1)\}^{-\frac{1}{2}}\right.\\
&\qquad\left.+\frac{3\Lambda^2Y^2-6\Lambda^2Y+5/2+\delta/2}{\{2y_1+7/4+\delta/4+2(J+1)(J+2)\}\{2y_1+7/4+\delta/4+2(J-1)J\}}\right],\\
\Delta_2F_3(J)&=4B(J+\tfrac{1}{2})\left[1+\tfrac{1}{2}\{y_1-5/4-\delta/2+J(J+1)\}^{-\frac{1}{2}}\right.\\
&\qquad\left.-\frac{3\Lambda^2Y^2-6\Lambda^2Y+5/2+\delta/2}{\{2y_1+7/4+\delta/4+2(J+1)(J+2)\}\{2y_1+7/4+\delta/4+2(J-1)J\}}\right],
\end{aligned}\tag{9}$$

[4] This term is carried as δ since it may have an appreciable value for small J. It can easily be computed from the value of Y determined by first approximation.

$$\Delta_2 F_2(J)=4B(J+\tfrac{1}{2})\Big[1-\tfrac{1}{2}\{y_1-5/4-\delta/2+J(J+1)\}^{-1}$$

$$-\frac{3\Lambda^2Y^2-6\Lambda^2Y+5/2+\delta/2}{\{2y_1+7/4+\delta/4+2(J+1)(J+2)\}\{2y_1+7/4+\delta/4+2(J-1)J\}}\Big],$$

$$\Delta_2 F_1(J)=4B(J+\tfrac{1}{2})\Big[1-9/2\{9y_1+23/4+\delta/2+9J(J+1)\}^{-1}$$

$$+\frac{3\Lambda^2Y^2-6\Lambda^2Y+5/2+\delta/2}{\{2y_1+7/4+\delta/4+2(J+1)(J+2)\}\{2y_1+7/4+\delta/4+2(J-1)J\}}\Big],$$

when $\{C+(J+1)(J+2)\}^{\frac{1}{2}}+\{C+(J-1)J\}^{\frac{1}{2}}$ is set $=2\{C+J(J+1)\}^{\frac{1}{2}}$. ($C=9y_1+23/4+\delta/2$ or $y_1-5/4-\delta/2$). In determining the constant, B, the mean of the $\Delta_2 Fs=4B(J+\frac{1}{2})$ should be used. This may be seen from Eqs. (9) or more rigorously from the fact that the sum of solutions for $\omega=0$ for all values of J since the coefficient of the cubic term $=0$ in Eq. (4). It is probably necessary to add a term $DK^2(K+1)^2$ to Eqs. (8) and $8D(K+\frac{1}{2})^3$ to Eqs. (9) in order to get well fitting curves. This point and other details of analysis are ably discussed by Budo.

Thanks are due Professor F. W. Loomis and Professor G. M. Almy of the University of Illinois for many helpful suggestions.

LETTERS TO THE EDITOR

Prompt publication of brief reports of important discoveries in physics may be secured by addressing them to this department. Closing dates for this department are, for the first issue of the month, the eighteenth of the preceding month, for the second issue, the third of the month. The Board of Editors does not hold itself responsible for the opinions expressed by the correspondents.

Communications should not in general exceed 600 words in length.

The Disintegration of Nitrogen by Fast Neutrons

In a paper in the *Physical Review*[1] we have reported on a number of nitrogen disintegration forks which were observed in a Wilson cloud chamber and which were attributed to the reaction

$$_7N^{14}+{}_0n^1\rightarrow{}_5B^{11}+{}_2He^4+Q_1.$$

Our original interpretation of the data indicated the disappearance of kinetic energy in most of the disintegrations. This gave support to the radiative capture theory proposed by Kurie.[2] He postulated the capture of the neutron by a radiative transition to a virtual level of $_7N^{15}$ and the subsequent disintegration of the unstable $_7N^{15}$ into $_5B^{11}$ and $_2He^4$.

The value of Q_1 used in our original interpretation of the experimental data was 2.1 Mev. Since then we have shown that Q_1 is approximately -0.3 Mev.[3] Since such a large change in the value of Q_1 alters materially the interpretation of the results, we have thought it advisable to reconsider the data. For convenience we have listed the relevant data on the disintegration forks in Tables I and II.

When the nitrogen disintegrations are produced by the neutrons from Be+H², the maximum amount of energy which should appear in the forks is Q_1+4.5 Mev, or 4.2 Mev. This value is now in good agreement with the experimental data and one no longer has to account for the disappearance of kinetic energy when nitrogen is disintegrated by neutrons with an energy of 4.5 Mev or less.

TABLE I. *Data on nitrogen disintegration forks with neutrons from Be+H². This source gives neutron groups with energies of 4.8, 4.0, 2.8, and 1.4 Mev.*[4] *E_n is the calculated neutron energy, E_f is the energy appearing in the forks (both in Mev).*

E_n	E_f	E_n	E_f	E_n	E_f
4.9	2.38	7.5	4.40	6.6	3.94
4.4	3.28	1.7	2.00	6.3	3.61
4.8	3.36	4.2	3.17	3.3	1.55
3.1	2.37	4.6	4.35	0.8	2.55
3.0	2.54	4.2	2.98	6.8	3.38
2.9	3.17	4.4	3.72	5.9	3.14
6.4	3.27	3.3	3.37	3.2	3.52
3.6	2.79	0.8	2.07	5.6	3.61
3.8	3.62	5.5	3.52	6.5	2.97
2.1	2.33	3.0	2.92	4.8	3.90
3.3	2.18	3.9	3.37	5.7	4.40
5.3	3.49	7.7	4.31	2.4	2.64
2.9	2.99	5.8	4.48	6.2	3.47
5.9	4.09	8.9	3.95	6.1	4.40
6.5	1.93	7.1	3.58	7.4	3.79
4.0	2.71	7.2	3.65	6.6	4.55
4.1	3.60	5.6	3.62	4.7	4.07
5.5	4.38	7.6	3.15	6.3	4.21

TABLE II. *Data on nitrogen disintegration forks with neutrons from Li+H². This source gives a neutron group with an energy of 13.5 Mev and a continuous distribution below this value.*[5] *E_n is the calculated neutron energy, E_f is the energy appearing in the forks (both in Mev).*

E_n	E_f	E_n	E_f	E_n	E_f
11.3	4.43	7.1	4.43	4.1	2.94
4.4	3.08	12.3	3.98	3.3	1.92
8.7	2.43	18.5	3.67	4.9	5.02
3.6	3.01	1.5	2.33	8.9	3.24
5.8	2.69	4.8	2.98	5.2	2.09
3.7	3.28	4.1	3.03	13.0	6.87
2.7	2.52	10.3	3.05	2.7	1.92
16.5	5.00	3.7	2.09	4.7	3.36
3.3	4.26	9.5	5.79	7.7	3.38
8.7	5.07	7.2	3.54	11.1	2.71
21.8	5.23	5.6	3.54	19.8	4.90
				4.4	4.49
				6.4	2.08

When the higher energy neutrons from Li+H² are used to disintegrate nitrogen, there still appears to be a number of well-established cases where kinetic energy disappears. The analysis of the data is made difficult because of the uncertainty in the energy of the neutron which produced the disintegration. Since we know that the maximum energy of the neutrons from Li+H² is 13.5 Mev, we see that errors of 30 or 40 percent are made in the calculation of the neutron's energy from the disintegration fork.

In Table II there appear to be 9 cases where roughly 6 Mev of kinetic energy disappears. These cases of disintegrations by high energy neutrons may now be simply explained by assuming that the B^{11} nuclei were left excited to either of the known excitation levels (4.5 or 6.8 Mev) in these cases.

Thus it seems that it is no longer necessary to explain the disintegrations of nitrogen with fast neutrons by the radiative capture theory.

T. W. BONNER

Rice Institute,
Houston, Texas.

W. M. BRUBAKER

Ohio State University,
Columbus, Ohio,
September 30, 1936.

[1] Bonner and Brubaker, Phys. Rev. **49**, 223 (1936).
[2] F. N. D. Kurie, Phys. Rev. **47**, 97 (1935).
[3] Bonner and Brubaker, Phys. Rev. **49**, 778 (1936).
[4] Bonner and Brubaker, Phys. Rev. **50**, 308 (1936).
[5] Bonner and Brubaker, Phys. Rev. **48**, 742 (1935).

The Piezoelectric Properties of Rochelle Salt

In a recent paper,[1] I tested the hypothesis that the piezoelectric deformation of Rochelle salt is proportional to the inner field F. A satisfactory check was found at temperatures above the Curie point and for frequencies above 100 cycles/sec. Below the upper Curie point the piezoelectric modulus d_{14} increases with the applied field which I thought to be contrary to Mueller's[2] theory.

Dr. Mueller has called to my attention that this conclusion is wrong. Mueller's theory predicts that d_{14} should have the same value above and below the Curie point when the applied field is small compared to the inner field. An error was made in the calculation of curve B of Fig. 13 in my paper.[1] The corrected curve B of Fig. 13 should have approximately the same slope but should be displaced 0.6 to larger values of $d_{14}\times 10^{10}$. The new intersection of curves A and B is almost at zero voltage. Hence this point of the theory is verified.

The permanent inner electric field F_0 can have the values $+F_0$ and $-F_0$. For a.c. measurements both directions are equivalent and we may therefore assume that one-half the crystal has the field $+F_0$ and the other half $-F_0$. If a field E is applied, the inner field during the first half-cycle becomes F_0+F_1, in the other half-cycle $-F_0+F_2$. The experiment records the average $\frac{1}{2}(F_1+F_2)$. In the first approximation F_1 and F_2 are equal and proportional to E. This approximation leads to Eq. (15)[1] and is correct if E is very small in comparison with the field F_0. Near the Curie point the field F_0 is about 100 volt/cm. The experiments were carried out with applied fields up to 47.2 volt/cm. For such large fields F_1 and F_2 are not equal. This may be seen from Fig. 3 of Mueller's paper.[2] Eq. (14)[1] in my paper is incorrect for large applied fields because it was derived on the assumption that F_1 and F_2 were equal. F_1 increases very slightly slower than const.$\times E$, but F_2 increases considerably faster than const.$\times E$. Hence the average of both fields increases faster than the applied field E, which explains the observed increase of d_{14} with voltage. The order of magnitude of the observed increase is in good agreement with the theory, but we cannot expect an accurate check since the observed hysteresis curves differ from the theoretical ones.

OSCAR NORGORDEN

University of Minnesota,
Minneapolis, Minnesota,
September 19, 1936.

[1] Oscar Norgorden, Phys. Rev. **49**, 820 (1936).
[2] Hans Mueller, Phys. Rev. **47**, 175 (1935).

Effects of Chemical Combination on X-Ray Emission Spectra

The discrepancy noted between the wave-lengths determined by Tanaka and Okuno[1] and McDonald[2] for the Fe $K\beta_1$ from FeS_2 raised a question as to the origin of this difference. With the idea of checking the Japanese results further, the $K\beta$ lines of 26 Fe, 25 Mn, and 24 Cr in Fe_2O_3, $KMnO_4$, and $K_2Cr_2O_7$ were photographed with the focusing crystal spectrograph heretofore described.[3] The results in iron are again contrary to those of Tanaka and Okuno. In Cr and Mn, results checking theirs, as well as those of Yoshida[3] and Wetterblad,[4] for the wave-lengths from Cr_2O_3 and divalent Mn, were obtained. Evidently the $KMnO_4$ and $K_2Cr_2O_7$ decomposed rapidly under the fairly high power which was used because of the limited time at the writer's disposal.

TABLE I. *Wave-lengths in X.U. of the Kβ lines of 24 Cr, 25 Mn, and 26 Fe from various compounds.*

	$K\beta'$	$K\beta_1$	$K\beta_5$
Cr		2080.39±5	
Cr_2O_3	2086.1±1	2080.41±5	2067.5±1
Mn[2]	1910.3±1	1905.97±5	
Fe_2O_3	1756.9±1	1753.01±5	1741.7±1

The results are listed in Table I. In the light of the report of Roseberry and Bearden,[5] who found by direct bombardment of Fe_2O_3 no change in width or asymmetry from the pure metal, the shift shown by the $K\beta_5$ of Fe is interesting.

Tanaka and Okuno also report the $K\beta_1$ in pure Cr at about 0.2 X.U. shorter wave-length than the value of about 2080.6 X.U. given by Eriksson[6] and Bearden and Shaw.[7] This would seem to show that the surface of the Cr becomes oxidized very rapidly from the residual vapors present in the tubes. Parratt[8] mentions the possibility of such oxidation as an explanation of the difference between his work and that of Bearden and Shaw on the widths of the $K\alpha$ lines of Cr and Ti.

If the positions of the K edge of Cr and Fe in Cr_2O_3 and Fe_2O_3, as measured by Coster[9] and Lindh,[10] are used in conjunction with the wave-lengths of the $K\beta_5$ line for calculating the term values of the MIV, V shell, we get values, in Rydberg units, of 1.41 and 1.35, respectively, much larger than the corresponding values for the metals of 0.2 and 0.4.

Preliminary results have been attained in an extension of Valasek's work[11] on the potassium halides. Using the K $K\beta_1$ as a standard, the wave-lengths of the K $K\beta''$ and $K\beta_5$ in KCl were found at 3442.7±2 and 3435.1±2 X.U., respectively. The characteristic violet coloration of KCl obtained on exposure to x-rays was noted. If the $K\beta''$ is not considered a spark line, and the second ionization potential of K is computed from it in the way Valasek used the $K\beta_1$ for the same purpose, a value of 28.1 volts, lower than the true value of 31.7 volts, is obtained. Even if the mean of this value and that gotten from the $K\beta_1$, 33.1 volts, or a mean of 30.8 volts, is considered, we see that it differs by more than the experimental error from the true value. The $K\beta''$ may be a spark line, however.

With KI, wave-lengths of 3447.11±5 X.U., and 2142.1 X.U. for the K $K\beta_1$ and I $L\alpha_1$, respectively, were found.

JOHN C. MCDONALD

University of Minnesota,
Minneapolis, Minnesota,
September 15, 1936.

[1] Tanaka and Okuno, Jap. J. Phys. **9**, 75 (1934); **10**, 1 (1935).
[2] McDonald, Phys. Rev. **50**, 694 (1936).
[3] Yoshida, Inst. Phys. Chem. Res. Tokyo **20**, 298 (1933).
[4] Wetterblad, Zeits. f. Physik **49**, 670 (1928).
[5] Roseberry and Bearden, Phys. Rev. **50**, 204 (1936).
[6] Eriksson, Zeits. f. Physik **48**, 360 (1928).
[7] Bearden and Shaw, Phys. Rev. **48**, 18 (1936).
[8] Parratt, Phys. Rev. **50**, 1 (1936).
[9] Coster, Zeits. f. Physik **25**, 83 (1924).
[10] Lindh, Zeits. f. Physik **31**, 210 (1925).
[11] Valasek, Phys. Rev. **47**, 896 (1935).

Spin-Orbit Coupling in Nuclei

In considering the spin-orbit coupling of a proton or a neutron in a nucleus, we may accept as a first approach the classical model of a spinning particle, in terms of which the analogous atomic problem was first understood.[1] The part of the energy dependent on the relative orientation of the orbital angular momentum $\mathbf{L}$ and spin $\mathbf{S}$ consists of two terms. The magnetic term, which is the more important in the atomic case, may be described as $\boldsymbol{\omega}_L \cdot \mathbf{S}$, $\boldsymbol{\omega}_L$ being the Larmor precession of the spin axis in the coordinate system of the particle. The relativistic term may similarly be described as $\boldsymbol{\omega}_T \cdot \mathbf{S}$, $\boldsymbol{\omega}_T$ being the Thomas precession, the angular velocity, in the nuclear coordinate system, of the coordinate system (and spin axis) of the particle due to its velocity $\mathbf{v}$, acceleration $\mathbf{a}$, and the finite speed of light. It was shown by Thomas[1] that $\boldsymbol{\omega}_T = -\mathbf{v} \times \mathbf{a}/2c^2$. In the atomic case, due to the circumstance that the magnetic field causing $\boldsymbol{\omega}_L$ arises from a transformation, to the electron coordinate system, of the same electric field which makes the acceleration (and due also to the normal spin gyromagnetic factor, $g=2$, of the electron) there is a remarkably simple relation $\boldsymbol{\omega}_T = -\frac{1}{2}\boldsymbol{\omega}_L$. The partial cancelation of the magnetic term by the relativistic term leaves the sign determined by the magnetic term, which gives rise to *regular* doublets. The relativistic term alone is *inverted*.

Studies[2] in nuclear stability indicate that a proton or neutron in a nucleus experiences short range binding forces, probably of an exchange nature and not electromagnetic in any simple way, which are so strong as to leave the electric forces comparatively unimportant, and especially so in the lighter nuclei. The relativistic term, which is proportional to the acceleration, is the weaker by only a factor $\frac{1}{2}$ in the atomic case, and may therefore be expected to dominate in the nuclear case, leading to rather wide *inverted* doublets (and other multiplets) for *protons and neutrons alike*.

In this comparison of nuclei with atoms, both terms have been reduced by the mass ratio 1/1840, which enters $\boldsymbol{\omega}_T$ in $\mathbf{a}$ and $\boldsymbol{\omega}_L$ in the magneton. An electric field sufficiently strong to cause the acceleration of a proton would transform into a magnetic field, in the proton coordinate system, strong enough to preponderate over the relativistic effect; in actual nuclei, however, the electric field is both weak and repulsive. We assume that the nuclear binding forces in effect do not transform into such a magnetic field. For the proton, $\boldsymbol{\omega}_L$ is enhanced by an anomolous[3] gyromagnetic factor, $g \approx 6$; the excess of the binding forces over electric forces may be expected to enhance $\boldsymbol{\omega}_T$ even more (at least in light nuclei). The magnetic term strengthens the coupling for protons, weakens it for neutrons (g of the neutron being apparently negative). Even without exact knowledge of the effectiveness of the strong binding forces *in accelerating the particle*, it seems very unlikely that the actual exchange forces would lead to an expected acceleration of smaller order of magnitude than would be had by substituting an effective central potential, adjusted to give the correct size of the nucleus and average potential energy per particle. Introducing as a rough approximation such an effective potential energy $V(r)$, we may put $\mathbf{a} = -\mathbf{r}(dV/dr)/Mr$. The average of the spin-orbit energy, considered as a perturbation term in the Hamiltonian, is then roughly $\boldsymbol{\omega}_T \cdot \mathbf{S} = -\overline{(dV/dr)/r}\mathbf{L} \cdot \mathbf{S}/2M^2c^2$.

Feenberg and Wigner have indicated theoretically (in press) that Li^7 should have a ^2P as lowest states. Although it involves a mixture of configurations, the important spin-orbit coupling is that of the "extra" proton. A preliminary estimate of the relativistic term for this proton gives $^2P_{1/2} - {}^2P_{3/2} \approx 0.2$ Mev (neglecting antisymmetry, the size of the one-particle wave function $(x+iy)e^{-\nu r^2}$ being taken from a perturbation calculation[4] of the binding energy of Li^6, and V being the quadratic potential appropriate to the wave function). This agrees in sign and order of magnitude with the experimental result, 0.4 Mev, of Rumbaugh and Hafstad for Li^7 from proton ranges in the reaction $Li^6 + H^2 \rightarrow Li^7 + H^1$ (also in press). A similar estimate of the corresponding magnetic term is 0.03 Mev.

Although there appears to be some difficulty with the anomalous magnetic moments of protons and neutrons, the Dirac equation does contain implicitly the transformation properties of their spin angular momenta, and these lead to the relativistic term discussed above. If, in a classical limit, the velocity of a proton (a "Dirac proton" with $g=2$) were known, we could derive the term thus: Consider three equally strong fields; (a) electric, attractive, (b) electric, repulsive, and (c) nonelectric, attractive; assuming additivity of their contributions to the instantaneous energy of the proton. If $\Delta\nu$ is the result of the usual Dirac method for the doublet splitting in (a), we find for (b)+(c) a magnetic splitting, $-2\Delta\nu$, by considering the Pauli spin in the proton coordinate system, which is not accelerated in this case. Adding, the splitting for (c) alone is $-\Delta\nu$, the nonelectric nature of the force reversing the sign. An elegant and direct derivation of the result from the Dirac equation will be discussed by Dr. W. H. Furry.

Professor Gregory Breit, to whom I am also indebted for generous discussion, and for acquaintance with the experiment mentioned, has pointed out that one may obtain the Thomas result (without any question of the properties of a classical model) by requiring that Pauli spin wave functions transform between Lorentz frames of different velocity in such a way as always to be derivable by reducing the Dirac wave functions to two components. If they are also to satisfy, to order v^2/c^2, a Pauli wave equation, it must be corrected by addition of the relativistic term of Thomas to the Hamiltonian.

D. R. Inglis

University of Pittsburgh,
Pittsburgh, Pennsylvania,
September 17, 1936.

[1] Thomas, Phil. Mag. **3**, 1 (1926); Frenkel, Zeits. f. Physik **37**, 243 (1926); see following letter.
[2] Heisenberg, Wigner, Majorana, Feenberg, Young, *et al.*, see Rev. Mod. Phys. **8**, 226 (1936).
[3] Estermann, Frisch and Stern, Zeits. f. Physik **85**, 17 (1933); Rabi, Kellogg and Zacharias, Phys. Rev. **46**, 163 (1934); **50**, 396 (1936).
[4] As outlined in Inglis, Phys. Rev. **50**, 399 (1936).

On the Thomas Precession of Accelerated Axes

The Thomas precession theorem, which is of interest in the study of atomic spectra and also finds a new application in the preceding note, may be derived with less algebra or more elementary concepts than heretofore,[1] as follows: We consider a coordinate system P, in which the center of gravity of a "planetary" particle remains at rest. P has a velocity and an acceleration $\mathbf{a}$ in another system N, in which a nucleus or laboratory is at rest. Because of the acceleration, we cannot by means of special relativity transform from P to N, but the rotation (or "Thomas precession") of P in N may be demonstrated by considering two nonaccelerated coordinate systems P' and P'' with which P coincides at times t and $t+\delta t$, respectively.

We orient the axes in such a way that P' and N have their x axes (which we call x' and x, respectively) parallel to their relative velocity $\mathbf{v}$, and that x'' and x' make the same angle with the relative velocity $\mathbf{u}'$ of their systems P'' and P', $\mathbf{u}'$ being in the xy planes. Thus a Lorentz transformation without space rotation will serve between P'' and P', and between P' and N. We wish to show that the transformation between P'' and N does involve a rotation nevertheless (or, in other words, that observers in P'' and N would agree that their axes are not parallel, although each agrees with an observer in P' on parallelism with his axes). We do this by showing that the axes x'' and x make different angles ϕ'' and ϕ with the relative velocity $\mathbf{u}$ of P'' and N.

From the familiar Lorentz transformation

$$dx=(dx'-vdt')/(1-v^2/c^2)^{\frac{1}{2}}, \quad dy=dy',$$
$$dt=(dt'-vdx'/c^2)/(1-v^2/c^2)^{\frac{1}{2}},$$

is had by division the usual rule for relativistic velocity addition:

$$u_x=(u_x'+v)/(1-vu_x'/c^2),$$
$$u_y=u_y'(1-v^2/c^2)^{\frac{1}{2}}/(1-vu_x'/c^2).$$

For infinitesimal δt and finite acceleration, $\mathbf{u}'$ is infinitesimal, and we have for the angle between $\mathbf{u}$ and x

$$\phi=\tan\phi=u_y/u_x=u_y'(1-v^2/c^2)^{\frac{1}{2}}/v.$$

To get the components of $\mathbf{u}$ in P'', in terms of $\mathbf{v}$ and $\mathbf{u}'$, we have to transform $\mathbf{v}$, known in P', to P'', the relative velocity $\mathbf{u}'$ being infinitesimal. The infinitesimal relativistic correction to ordinary velocity addition may be neglected ($\mathbf{u}'$, although oblique, being analogous to v above), and we have

$$\phi''=\tan\phi''=u_y'/v.$$

We see that ϕ'' and ϕ are, indeed, not the same, their difference being the angle through which P has turned in N about the z axis during δt:

$$\delta_T\delta t=\phi-\phi''=u_y'\{(1-v^2/c^2)^{\frac{1}{2}}-1\}/v\approx-u_y'v/2c^2.$$

Substituting $u_y'=a_y'\delta t'\approx a_y\delta t$ (neglecting higher powers of v/c), we have the angular velocity of the Thomas precession of P in N:

$$\boldsymbol{\omega}_T=-\mathbf{v}\times\mathbf{a}/2c^2.$$

Any directed quantity, such as an angular momentum, which is constant in the coordinate system of an accelerated and moving particle, has this rotation in a "stationary" coordinate system. In the well-known atomic case, there is a magnetic field $\mathbf{H}$ in P corresponding to the electric field $\mathbf{E}$ in N, and a classical electron spin would be constant in a Larmor coordinate system having a precession $\boldsymbol{\omega}_L$ in P or $\boldsymbol{\omega}=\boldsymbol{\omega}_L+\boldsymbol{\omega}_T$ in N. (This summation assumes that P has a time scale differing from that of N only in higher order in v/c, as do the Lorentz frames P' and P''.) Using $\mathbf{a}=-\mathbf{E}e/m$, we have

$$\boldsymbol{\omega}_L=\mathbf{H}(\mu/S)=-[\mathbf{v}\times\mathbf{E}/c](e/mc)=\mathbf{v}\times\mathbf{a}/c^2=-2\boldsymbol{\omega}_T.$$

The term $\boldsymbol{\omega}\cdot\mathbf{S}$ (which we may ordinarily consider as a perturbation term) in the Hamiltonian of any classical model of an atomic electron with spin $\mathbf{S}$, consists of two terms, the magnetic term $\boldsymbol{\omega}_L\cdot\mathbf{S}$ being half canceled by the relativistic term $\boldsymbol{\omega}_T\cdot\mathbf{S}$, which thus introduces the familiar "Thomas factor" $\frac{1}{2}$ in the atomic spin-orbit energy.

SIDNEY DANCOFF,
D. R. INGLIS

University of Pittsburgh,
Pittsburgh, Pennsylvania,
September 17, 1936.

[1] L. H. Thomas, Nature 514 (1926), Phil. Mag. **3**, 1 (1926); Frenkel, Zeits. f. Physik **37**, 243 (1926); Goudsmit and Uhlenbeck, Physica **6**, 276 (1926); Ruark and Urey, *Atoms, Molecules, and Quanta*, p. 162; Sommerfeld, *Convegno di Fisica Nucleare* (Rome, 1932); Kramers, Physica **1**, 825 (1934); see also Zeeman Verhandelingen, 405 (1935).

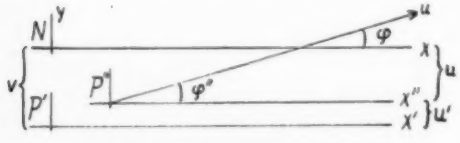

FIG. 1. The brackets indicate relative velocities.

On the Introduction of Nonelectric Forces into Dirac's Equations

The doublet separations of nuclear energy levels have been discussed by Inglis,[1] who assumed that on account of the nonelectric character of the forces the main contribution to the splittings comes from the Thomas relativistic effect. In this note we shall see how such a result follows from Dirac's equations. Although it is not generally supposed that these equations actually hold for a heavy particle, they still represent our only way of treating the relativistic quantum mechanics of a particle with spin, so that it is interesting to see what their application gives. The addition of extra terms[2] in order to obtain agreement with observed values of the magnetic moments would not affect these results.

The Dirac equations for a particle subject to an electrostatic force are

$$c\{p_0-(H_0+V_e)/c\}\psi=c\{p_0-V_e/c+(\boldsymbol{\alpha}\cdot\mathbf{p})+\beta mc\}\psi=0, \quad (1)$$

where $V_e=$(charge)$\cdot$(electrostatic potential)$=$potential energy due to the electrostatic force. It is evident that if we try to introduce a nonelectric potential energy V_n by adding it to the Hamiltonian as V_e is here added, the new

term will be indistinguishable from V_s in all its effects on the behavior of the wave function. Adding a term in this way really corresponds to introducing a four-vector whose space components vanish in the particular Lorentz frame used. On the other hand if we introduce a term proportional to V_n in such a way that it transforms like the Lagrangian, which is a scalar invariant, it can just as reasonably be called a potential energy as can a term added to the Hamiltonian; and the scalar so introduced will differ in its effects from a nonscalar such as the term in V_e. Accordingly, for a particle subject to both an electrostatic force and a nonelectric force we write

$$c\{p_0 - V_e/c + (\boldsymbol{\alpha}\cdot\mathbf{p}) + \beta(mc + V_n/c)\}\psi = 0. \quad (2)$$

The various relativistic quantities[3] which can be formed from the Dirac matrices offer only these two possibilities for introducing quantities which may reasonably be regarded as potential energies, and which have a suitable effect on the behavior of ψ in the lowest order in v/c.

If in (2) we introduce the usual convenient notations,

$$\boldsymbol{\alpha} = \begin{pmatrix} 0 & \boldsymbol{\sigma} \\ \boldsymbol{\sigma} & 0 \end{pmatrix}, \quad \beta = \begin{pmatrix} 1 & 0 \\ 0 & -1 \end{pmatrix}, \quad \psi = \begin{pmatrix} \chi \\ \varphi \end{pmatrix}, \quad (3)$$

where the σ's and 1 are two-rowed matrices and χ, φ are two-component functions, we get

$$c\{(p_0 + mc - V_e/c + V_n/c)\chi + (\boldsymbol{\sigma}\cdot\mathbf{p})\varphi\} = 0 \quad (4a)$$

$$c\{(p_0 - mc - V_e/c - V_n/c)\varphi + (\boldsymbol{\sigma}\cdot\mathbf{p})\chi\} = 0. \quad (4b)$$

On carrying out the elimination of the "small components" χ in the usual way,[4] we obtain an equation for φ of the form $(cp_0 - mc^2 - \bar{H})\varphi = 0$, valid to order $(v/c)^2$, with

$$\bar{H} = p^2/2m + V_e + V_n + \{(\hbar/4mc)(\boldsymbol{\sigma}\cdot[(\mathbf{p}/mc)\times\text{grad}\,(V_e - V_n)])\} + \{(i\hbar/4mc)((\mathbf{p}/mc)\cdot\text{grad}\,(V_e - V_n))\}. \quad (5)$$

Thus, although V_n and V_e appear in the same way in the lowest order in v/c, they appear with opposite signs in the spin-orbit terms of the first bracket, in agreement with our expectations from Inglis' argument about the Thomas effect. They also oppose each other in the second bracket, in terms of a type first discussed by Darwin.[5]

The introduction of a scalar potential energy added to the proper energy corresponds closely to Nordström's special-relativistic theory of gravitation.[6] Since the forces in nuclei are surely not gravitational, the fact that astronomical observation decides for general relativity and against Nordström's gravitational theory does not impair the interest of this way of discussing the action of nonelectric forces.

W. H. Furry

Physics Laboratories,
Harvard University,
Cambridge, Massachusetts,
September 17, 1936.

[1] D. R. Inglis, this issue, p. 783.
[2] W. Pauli, *Handbuch der Physik*, XXIV/1, p. 233.
[3] W. Pauli, reference 2, p. 221.
[4] Originally done by Darwin, reference 5; for brief treatment in a notation more like that used here, cf. reference 2, p. 237.
[5] C. G. Darwin, Proc. Roy. Soc. **A118**, 662 (1928).
[6] G. Nordström, Ann. d. Physik **42**, 540 (1913).

Mutual Reactions of Metals and Salts

When a metal is heated in contact with a salt one or more of the following phenomena may take place: (1) solution of the metal in the salt; (2) dissociation of the molecules of the salt; (3) diffusion of the dissociated metallic atoms of the salt into the metal; (4) formation of chemical compounds of liberated metalloids with the metal.

We shall describe an experiment made with a copper bar heated in cadmium chloride. At a temperature below the melting point of $CdCl_2$ the copper dissolves in the salt, which becomes colored (reddish) after about one hour of heating. At a temperature above the melting point of $CdCl_2$ copper dissolves rapidly in the liquid $CdCl_2$ and after cooling the faces of the crystals of the salt are covered with a thin sheet of metallic copper alloyed with cadmium (thickness of a few microns).

In this experiment dissociation of $CdCl_2$ and formation of chemical compounds with copper take place. The reaction is:

$$\alpha_1\text{Cu} + \alpha_2\text{CdCl}_2 \rightleftarrows \beta_1\text{CuCl} + \beta_2\text{CuCl}_2 + \beta_3\text{Cd}.$$

The values of α and β depend upon the temperature. The heat evolved in the reaction (U_v) has a negative value. Consequently from the van't Hoff law ($\partial \lg R_v/\partial T = U_v/RT^2$) the value of the equilibrium constant (R_v) of the mass action law decreases when the temperature rises

$$R_v = \frac{C^{\alpha_1}(\text{Cu})\cdot C^{\alpha_2}(\text{CdCl}_2)}{C^{\beta_1}(\text{CuCl})\cdot C^{\beta_2}(\text{CuCl}_2)\cdot C^{\beta_3}(\text{Cd})},$$

where the C's are the concentrations of the reacting substances and their products. This law shows that the concentrations of the products of the reaction increase with the temperature. Hence a rapid lowering of the temperature of the reacting bodies causes metallic copper to be separated out of the salt. This phenomenon is only possible in the exothermic reactions (thermit). The liberated metals: cadmium and copper are dissolved in the melted salt. The concentration of dissolved metals is greater in the liquid than in the solid state of $CdCl_2$ and so on crystallization of that salt the metal excluded from the salt during the solidification is deposited on the faces of the crystals.

Analogous phenomena occur also in the case of metals (copper) heated in an atmosphere of vapors of subliming chlorides such as $NiCl_2$ and $CdCl_2$.[1] The metals of the dissociated chlorides diffuse into the copper. This phenomenon is analogous to the phenomenon of diffusion of two metals in contact. (A theory of this phenomenon by Mr. J. Cichocki is to be published in the Journal de physique.)

Copper heated in $MgCl_2$ for 24 hours at a temperature of 640°C contains after the heating 3 atoms per hundred of magnesium. The metal liberated in these reactions is deposited on the copper and on the walls of the vessel and form porous deposits or metallic crystals.

Thaddeus Peczalski

University of Poznan,
Poland,
September 1, 1936.

[1] Comptes rendus **181**, 463 (1925).